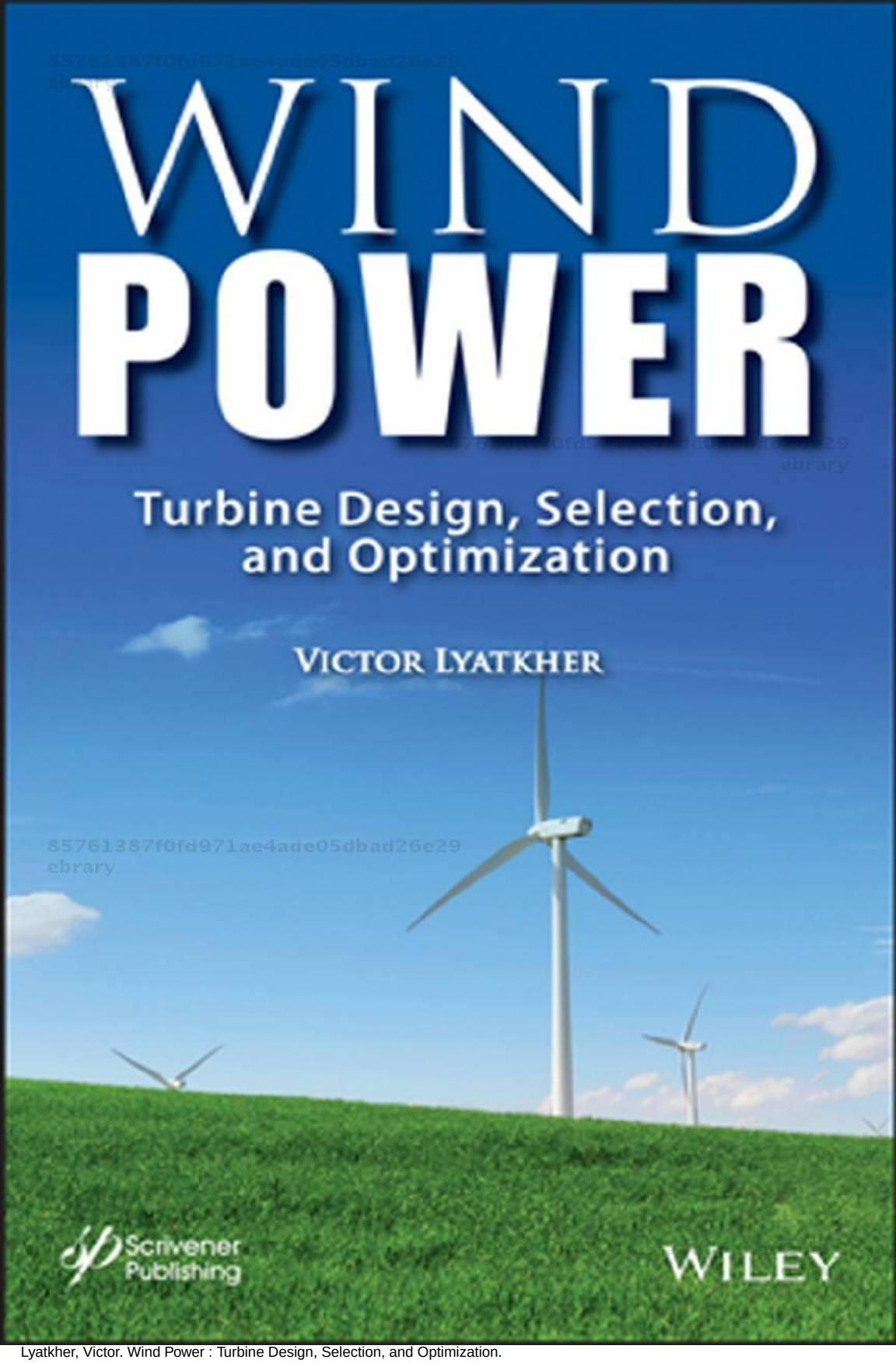

Wind Power

Scrivener Publishing
100 Cummings Center, Suite 541J
Beverly, MA 01915-6106

Publishers at Scrivener
Martin Scrivener (martin@scrivenerpublishing.com)
Phillip Carmical (pcarmical@scrivenerpublishing.com)

Wind Power

Turbine Design, Selection, and Optimization

Victor Lyatkher

Co-published by John Wiley & Sons, Inc. Hoboken, New Jersey, and Scrivener Publishing LLC, Salem, Massachusetts.
Published simultaneously in Canada.

Cover design by Kris Hackerott

Library of Congr ess Cataloging-in-Publication Data:
ISBN 978-1-118-72092-9

Printed in the United States of America

10 9 8 7 6 5 4 3 2 1

Contents

Preface

The proposed wind power units are intended for the conversion of wind energy into electric power of alternating current in regions with moderate and high winds. The installations are used as part of an electrical network, which includes other generating sources of considerably larger capacity. The units may be located on the surface of the water, thereby using more strong winds without the environmental impact. The assembly of the general wind power unit (Chapter 5) is nontraditional. Working blades of aerodynamic profile are fixed vertically and move in opposite directions along the ring routes, located one above another and connected by the forces of electromagnetic interaction. The idea of the unit consists in the use of the pull force of the wing, arising at its flow around, with attack angles smaller than the critical one; the effect of the turbulent mixing of air flows providing the recovery of wind energy at the approach to the rear order of the blades; and the effect of the mutual compensation of torques and transverse forces acting on the blades, which move in opposite directions. The indicated ideas, reflected in the construction of the unit, allow for qualitatively increasing its economic effectiveness and reliability. The general problems of the small wind speed power system (Chapter 6) and the high wind speed power system in atmospheric jet streams (Chapter 7) are discussed.

1

Transformation of Flow Power

The systems transforming the energy of wind currents can be either those employing mechanical action in combination with electric, pump, frictional or thermal units, or those employing non-mechanical action, using, for example, an effect of ionization and conductivity of the stream passed through an electric or magnetic field. All mechanical systems, called - power installations (PI), use the action of the forces arising at a flow of mobile elements of the installations which are structurally united into power rotors (PR). The PI's working elements, PR, move on the closed routes, sweeping some surfaces where the axis of symmetry can be either parallel (collinear), or perpendicular (orthogonal) to the stream. Respectively, PR are classified into two groups:

- Collinear, at which the axis of symmetry is approximately parallel to the stream, and
- Orthogonal, at which the axis of symmetry lies in the orthogonal plane to the stream direction.

The PR elements are able to move more slowly or quickly than the stream on the way to the PR. Respectively, they are called low-speed

(action turbine) or high-speed (reaction turbine) machines. The collinear high-speed units (see Figure 1.1) are the most popular at present. Other types of units are not even included in the modern handbooks [1].

The orthogonal units may have a horizontal or a vertical axis (see Figure 1.2).

Comparing various types of power installations of even one class causes certain difficulties as it is necessary to take into account some criteria measured in different equipment: specific material consumption (per a power unit and an output), quality of developed energy, degree of simplicity and factory readiness, convenience and reliability in operation, labor input of construction and operation, ecological safety. The combination of these criteria defines

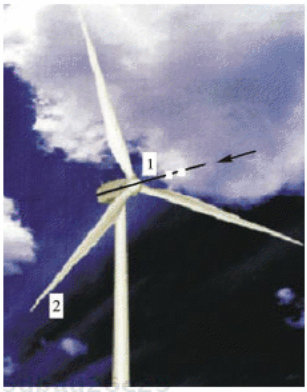

Figure 1.1 Modern collinear wind turbine. The rotation axis (1) is parallel to the stream. The blades (2) move in a plane perpendicular to the stream.

Figure 1.2 Orthogonal high-speed units with the rotation axis (1) perpendicular to the direction of the current. The blades (2) move by the ring routes. Left: a horizontal unit which is effective at invariable directions of the streams (for example, in a mountain valley or on a seashore); right: a vertical wind turbine.

the multidimensional quality characteristics of PR. Comparing PR quality is especially difficult for machines of various classes. Therefore, the choice of perspective schemes is conditional. The cost change (the social importance) of some points in view of the quality may change the conclusions. However, the economic, power, and ecological indicators currently accepted as the main points, should preserve the value for many years.

Since the wave aerodynamic resistance and acoustic radiation greatly increases when the body movement speeds approach the speed of sound, the wind unit elements should be designed so that air flows around them at speeds significantly less than sound speed (with small Mach numbers). Thus, the air can be considered almost incompressible, or squeezed under any law (adiabatically or isothermally); and all the results of aerodynamic calculations become suitable for recalculation by the movement conditions of incompressible liquids with any other density. In particular, all results can be directly applied to the analysis of river or oceanic power installations of similar configurations. Thus, one should keep in mind that for quiet water streams with small Froude numbers, the role of the stream free surface is somewhat close to the role of a firm smooth wall. [2]

Therefore, the analogy, for example, between land wind and river (oceanic) installations can be twofold – applying both to the arrangement of units at the water surface or at the bottom of a reservoir. Certainly, the designs of the units, applied materials, strength and technical and economic estimates for power units can vary significantly in air and in water.

In any scheme of stream power selection it makes sense to replace, as the first approximation, the unit which is carrying out this process with some hypothetical flat permeable figure with contours which are projections of the borders of a body, swept around by the rotor, on the figure plane, perpendicular to the stream direction on the way to the unit (Figure 1.3).

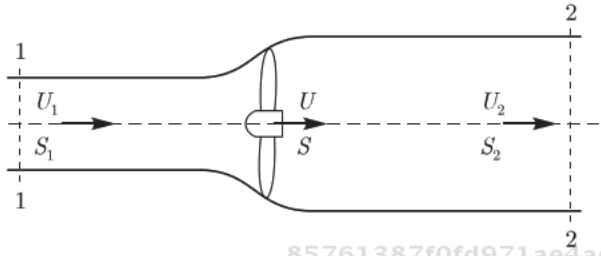

Figure 1.3 Scheme of currents in the turbine zone.

In the case of traditional, collinear units, a circle or a ring will be such a figure; in the case of orthogonal units it can be a strip (as in the pictured model), a rectangle, a trapeze, an ellipse figure (Darrieus unit section) or a triangle. Whatever this figure is, at some distance in front of it, the stream speed U and pressure p keep an non-indignant value:

$$U = U_1 \; p = p_0 \tag{1.1}$$

and at some distance downstream, where the pressure distribution across the stream is leveled and returns to a reference value p_0, the speed in the current tube leaning on the allocated figure has a smaller value $U_2 = (U_1 - u)$. If the current speed through the allocated figure is designated as U, and the pressure from the frontal and back parts of the figure as p_1 and p_2, respectively, the Bernoulli equations for the front and back parts of the current tube will take the following form:

$$p_1 + \rho U^2/2 = p_0 + \rho U_1^2/2 \tag{1.2}$$

$$p_2 + \rho U^2/2 = p_0 + \rho (U_1 - u)^2/2 \tag{1.3}$$

If the stream speed and the surface pressure upon of the allocated current tube are accepted as constant, the equation of change of the movement quantity for the allocated volume is:

$$Q\rho u = \Delta p \; S \tag{1.4}$$

$$Q = U \; S \tag{1.5}$$

- Discharge of the medium moving in the considered current tube, S - the surface area imitating a turbine,

$$\Delta p = p_1 - p_2$$

- Difference of pressure on the allocated flat figure replacing the power unit is calculated by subtraction of equalities (3) from equality (2) taking into account (4) and (5):

$$\Delta p = \rho u (U_1 - u/2) = \rho 2 (U_1 - U) U \tag{1.6}$$

From the equations (2)-(5), we find:

$$U = U_1 - u/2 \text{ or } u = 2(U_1 - U) \tag{1.7}$$

The capacity lost by the stream and transferred to the turbine, is equal to:

$$P=U\Delta p\ S = \rho u(U_1 - u/2)^2\ S = \rho 2(U_1 - U)U^2\ S \qquad (1.8)$$

The found solution (6), (8), presented as a resistance coefficient:

$$C_D = 2\Delta p\ /\ \rho U_1^2 \qquad (1.9)$$

and a power factor:

$$C_P = 2P\ /\ \rho U_1^3 S \qquad (1.10)$$

appears depending on one parameter only - the relative stream speed in the unit zone U/U_1.

$$C_D = 4\ (1 - U/U_1)\ U/\ U_1 \qquad (1.11)$$

$$C_P = 4\ (1 - U/U_1)(U/\ U_1)^2 \qquad (1.12)$$

The maximum value of power observed at $U/U_1 = u/U_1 = 2/3$ makes:

$$P_{max} = 16/27\ S\ \rho U_1^3/2, \qquad C_{Pmax} = 16/27 = 0.593 \qquad (1.13)$$

The obtained ratios (6), (8), (13) are usually associated with the works of N.E. Zhukovsky (1912) and A. Betz (1919), giving a sense of certain limit laws to these ratios [4].

However, the reality is different. The initial equations (2) – (5) are not precise and reflect some model of the phenomenon only. In particular, the equation (3) obviously is not true at $U \to 0$. If this limit case is real (an impenetrable unit), the pressure p_2 behind the unit will obviously be less than the pressure p_0 at a distance from the unit, rather than greater, as follows from (3). However, the idea of replacing the unit with one or several permeable flat or other figures where a rupture of pressure and a concentrated power selection occur appears very productive.

Let us consider a characteristic example in which the speed U is set on a permeable flat figure modeling the power unit. This speed is constant at all points of the figure and perpendicular to the plate surfaces. The non-stationary hydrodynamics equations (Euler equations) are solved by the method of final remainders. The solution

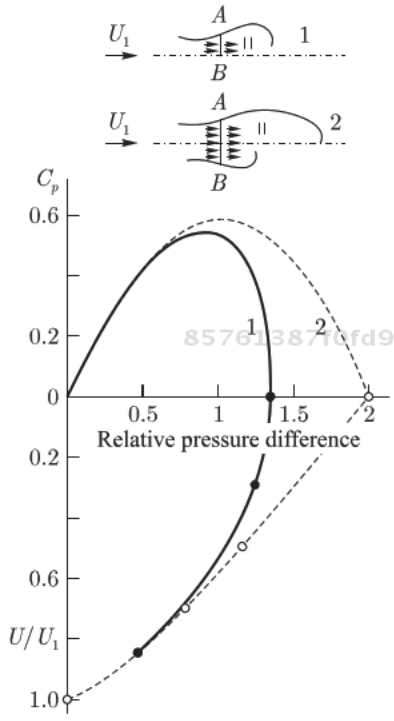

Figure 1.4 Efficiency of the power unit C_p, simulated by a flat permeable plate, depending on the relative stream speed through the plate U/U_1 at a symmetric flow hypothesis (1) and without any additional hypotheses (2).

for a strip plate figure (two-dimensional non-stationary objective) is different with the introduction of a current symmetry condition and without the introduction of such a condition (Figure 1.4). This distinction is demonstrated in the picture of currents and pressure distribution only behind the plate. It is essential to the definition of loadings. It is curious that, though the difference in loads of a permeable plate in different statements is quite great (especially at small values of U), the maximum power factor differs slightly, being within the limits:

$$(C_P)_{max} = 0.55 \div 0.59 \qquad (1.14)$$

The calculation supposes the relative stream speed through the plate U/U_1 to be set, and we obtain the relative pressure difference $2\Delta p/\rho U_1^2$ and the power factor (efficiency) $C_p = 2\Delta pU/\rho U_1^3$.

Unlike the theory of Betz-Zhukovsky, the resistance coefficient of a flat impenetrable plate calculated this way (without an additional condition of the current symmetry behind the plate) appears to be precisely equal to the experimental value $C_D = 2$ at an infinite plate length. At a symmetric flow off the plate, the pressure decline behind the plate is less (due to the influence of the formed return stream), and the settlement result corresponds to the experimental data of a rectangular plate where the long part is 15-fold greater than the short one ($C_D = 1.38$). The pressure difference on the permeable plate modeling the power unit can be found, for example, by a generalization of the Kirchhoff problem (Kirchhoft, 1869, 1876) [5]) of jet flow off] the plate with the presence of filtration through the plate (GGS model [6]). The pressure coefficient obtained for an impenetrable plate in Kirchhoff's model and GGS, naturally, is almost identical: 0.88 and significantly smaller than the real experimental value. This is caused by the pressure decline behind the plate and is not considered in both of these models in actual practice.

The maximum power factor 0.301 is so small in the GGS model only because it is neither the real pressure decline behind the plate, nor the filtration condition through the plate formulated at the statement of problem actually taken into account in the solution.

The obtained picture, as well as Kirchhoff's solution, has to be close to the truth at a cavitational flow of the turbine when the pressure behind the plate does not depend on the current speed. For usual, not cavitational conditions, the result would be closer to the experimental values, if the pressure decline behind the barrier is considered. For an impenetrable plate, such option is provided by the scheme of D.A. Efros (1946) [5], for example, in which the jet stream from the plate returns back to the plate. The models of Ryabushinsky with two plates (one behind another) are widely known. A successful example of a permeable plate is M.A. Lavrentyev's model (1958) [7], in which two rotating water rings are located behind the plate.

Other models providing other estimates and correct results in the known limit points ($U = 0$ and $U = U_1$) are also possible.

If, for example, instead of the equations (1.3) and (1.4) we use simply a parametrical representation of the plate resistance coefficient:

$$C_D = C^0_D (1 - (U/U_1)^m) \qquad (1.15),$$

true at the specified limit points at $C^0_D = 2$, the power factor expression becomes:

$$C_P = 2(1 - (U/U_1)^m)\,(U/U_1), \tag{1.16}$$

and the maximum power factor is equal to:

$$(C_P)_{max} = C^0_D\, m/(m+1)^{1+1/m} \text{ at } (U/U_1) = (1+m)^{-1/m} \tag{1.17}$$

In particular, at $C^0_D = 2$ and

$$m = 0.5,\ 1.0 \text{ or } 2.0 \tag{1.18}$$

the maximum power factor is equal to:

$$(C_P)_{max} = 0.30,\ 0.50 \text{ or } 0.77 \text{ at } U/U_1 = 0.444,\ 0.5 \text{ or } 0.577 \tag{1.19}$$

respectively.

If we accept other parametrical representation, for example:

$$C_D = 2(1 - U/U_1)^m \tag{1.20},$$

then the maximum power factor $(C_P)_{max} = 2m^m(1+m)^{-(m+1)}$ is obtained at $U/U_1 = 1/(1+m)$, that gives the same parameter values m by (1.18)

$$(C_P)_{max} = 0.296,\ 0.5 \text{ and } 0.577 \text{ at } U/U_1 = 0.333,\ 0.5 \text{ and } 0.667 \tag{1.21}$$

respectively.

It is clear that the widely applied Betz-Zhukovsky limit provides no reliable assessment. The primitive representations (1.15) or (1.20) can be closer to reality if we introduce the empirical values of resistance coefficients of impenetrable plates depending on a ratio of the parts, rather than the coefficient 2:

Relation of the parts =	20:1	10:1	4:1	1:1
$(C_D)_{max}$ =	1.45	1.29	1.19	1.10

Considering these ratios instead of the estimates (19) or (21) for the turbine with a rectangular cross section with a ratio of parts 4:1, we obtain the maximum efficiency, about 45.8÷34.3% (for linear interpolation at m =1 $C_{Pmax} = 0.298$), which is close to the empirically

reached results. If we apply the same reasoning to an assessment of the maximum efficiency of the collinear units replaced in zero-dimensional consideration with a permeable round disk, then at the impenetrable disk resistance of 1.25, the maximum efficiency of the collinear turbine (or any axis-symmetric system), can be expected to be within 48÷36%.

According to the GGS model mentioned above, the best achievable efficiency of free flow turbines makes 30.1% at the current speed via the turbine 0.613 from the running stream speed. The problem has been set by the authors for equation of continuity of an incompressible liquid stream which is flowing around a flat permeable plate, located perpendicular to the stream speed at a distance from the plate. On the plate surface, the liquid filtration condition through the plate is supposed - formula (1.5) of the original. In the rectangular system of coordinates associated with the plate, this condition takes the form:

$$[p] = r\, V_x \qquad (1.22)$$

Here, as in the original, [p] is the pressure difference on the plate which at the end of this article is accepted to be equal to a simple pressure on the front part of the plate; the liquid density is accepted to be equal to 1; V_x is the longitudinal component of the stream speed on the plate (filtration speed through the plate); r is the coefficient of filtration resistance of the plate.

At the creation of a kinematic picture, the condition (1.22) was not used. The picture of the flow was made by synthesis of the known Kirchhoff scheme in which the streams of constant speed equal the speed of a stream at a distance from the plate descending from the end points of the plate, and permeability of the plate was set by some angle φ in the speed potential plane, i.e. the current speed through the plate was given by a kinematic ratio:

$$V_x = V \sin \varphi \qquad (1.23),$$

not connected to the condition (1.22). This parameter (angle) φ defines the solution, in particular, a relative liquid consumption through the plate, i.e. the average speed of "filtration" through the plate and the whole picture of currents in front of the plate.

The pressure on the plate is defined fairly by the Bernoulli formula (formula (16) of the original), and this record is used for calculation of efficiency of the turbines, which can be presented in the function

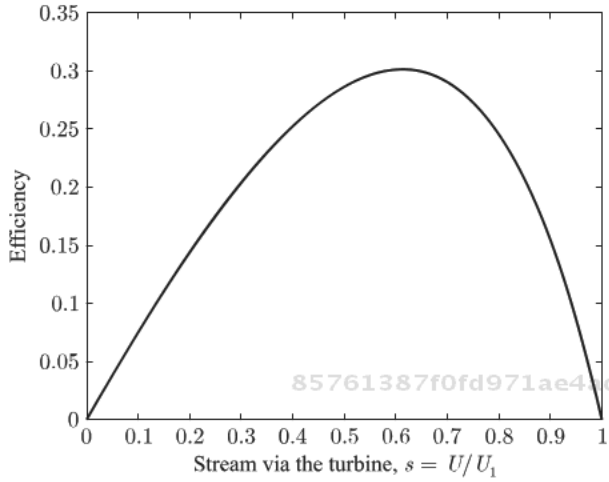

Figure 1.5 Efficiency of the turbine as a function of the "filtration" speed. GGS model.

of "filtration" speed through the plate (Figure 1.5). However, the pressure has to meet the condition (1.22). Thus, the parameters φ and r on the plate surface have to satisfy the equation:

$$\tfrac{1}{2}\,(1 - V^2) = r\,V_x \qquad (1.24)$$

or

$$V^2 + 2\,r\,V \sin\varphi - 1 = 0 \qquad (1.25)$$

We obtain from the above, that the speed module on the plate, the resistance coefficient r, and the parameter φ have to be connected by the formula:

$$V = \sqrt{(1 + r^2 \sin^2\varphi)} - r \sin\varphi \qquad (1.26),$$

in which the values of r and φ do not vary along the plate, and the speed module V obviously changes from the minimum value on the plate axis to the maximum value on the plate edge. Thus, equation (1.26) and, therefore, condition (1.22) at constant r and φ (along the plate), are not satisfied in the constructed solution. The average pressure upon the plate is measured in fractions of the high-speed pressure at a distance from the plate; and then defined from the original data as a limit of efficiency of the relation of the current speed $s = U/U_1$ through the plate at $s \to 0$ is 0.77, that is much lower

than Kirchhoff's result (0.88), though these results are likely to coincide. The difference is explained by the influence of the weight function where the pressure on the plate is averaged at the efficiency calculation. Such function is the current speed through the plate.

Nevertheless, the resultant assessment of efficiency of the turbines, obtained by the GGS model, makes sense, but it is related to some kinematic scheme (1.23), which in some conditions (at variable r) is able to correspond to the reality, rather than to the physically clear condition (1.22).

It is possible to try to specify the GGS model, having entered an additional addend into the calculation formula of pressure difference on the plate, as a function of the stream speed through the plate. In the elementary representation we consider the pressure decline behind the plate in the form of additional difference, which is naturally accepted by a linear function s:

$$\Delta C_D = \Delta p = A(1 - s) \qquad (1.27),$$

where the coefficient A is a difference between the real pressure difference on the impenetrable plate and the pressure determined by the Kirchhoff scheme or the GGS model. Both models actually characterize the pressure upon the front part of the plate.

Figure 1.6 shows the pressure coefficient C_D calculated by the efficiency and speed data through the plate, taken from the original for the GGS model (line 1), and correct ed by the ratio (1.27), taking the empirical value of the impenetrable plate resistance (line 2) into account.

The increments of power factor corresponding to the formula (1.27) are given by:

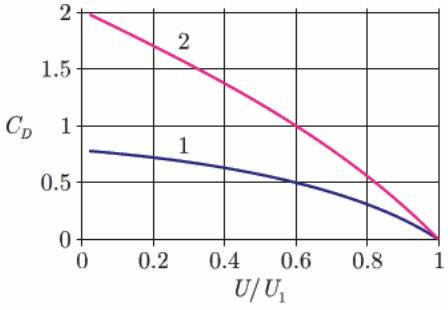

Figure 1.6 Pressure ratio $C_D = C_P/s$ by the original (1) and modified (2) GGS models.

$$\Delta(C_p) = A(1 - s)s \tag{1.28}$$

The increment maximum takes place at s = 0.5:

$$\text{Max } \Delta (C_p) = 0.25\ A \tag{1.29}$$

Where the coefficient A depends on the plate form:

The ratio of the rectangle parts	∞	20:1	10:1	4:1	1:1	Circle
C_D	= 2.0	1.45	1.29	1.19	1.10	1.25
A	= 1.23	0.68	0.52	0.42	0.33	0.48
Max $\Delta(C_p)$	= 0.307	0.17	0.13	0.105	0.082	0.12

The GGS model specified in such a way for real orthogonal turbines with a rectangular cross-section with the relation of sides 4:1, provides the greatest possible efficiency, about 40% at a relative current speed through the turbine of about 0.55.

If we consider the solution of GGS precisely corresponding to the Kirchhoff's model, i.e. the pressure upon the plate equal to 0.88 at s = 0, the coefficient A values in the provided Table have to be reduced at 0.11, and the comparison of our numerical model and the modified GGS model for an infinite strip is:

U/U_1	1	0.8	0.6	0.4	0.2	0.0
C_D	0	0.562	0.945	1.332	1.665	2
C_P	0	0.450	0.567	0.533	0.333	0
C_D (GGS modified)	0	0.527	0.947	1.302	1.595	2
C_P (GGS modified)	0	0.422	0.568	0.521	0.319	0

The difference of the results is quite small.

Using the modified GGS model for the orthogonal turbine with the length 2.5-fold greater than the diameter (A = 0.265), we obtain the following values of efficiency and resistance of the turbine (Figure 1.7):

U/U_1	1	0.8	0.6	0.4	0.2	0
C_P (GGS modified)	0	0.285	0.363	0.317	0.182	0
C_D	0	0.356	0.605	0.792	0.910	1.145

The maximum efficiency value (0.363) is close to the one observed in experiments.

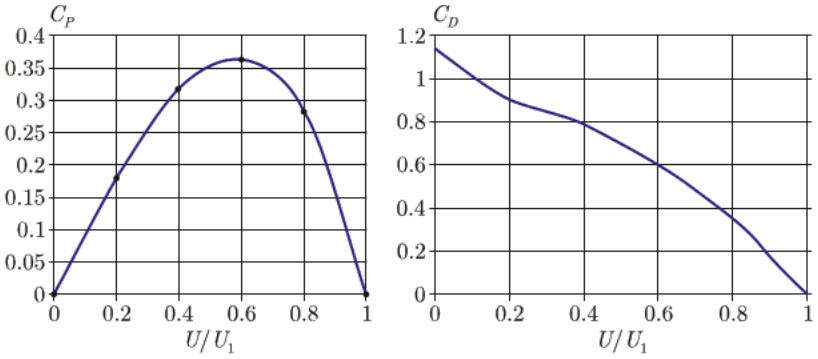

Figure 1.7 Efficiency and resistance of the orthogonal turbine with the turbine length 2.5-fold greater than the diameter. The modified GGS model.

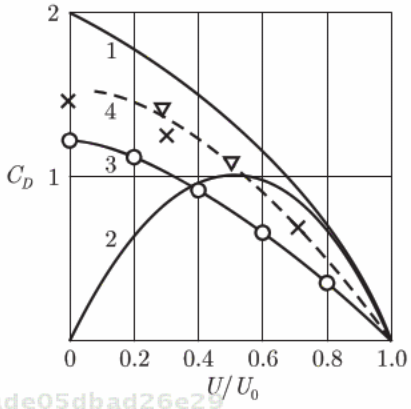

Figure 1.8 Coefficient of pressure upon the permeable round disk. 1- model of G.H. Sabinin, 2 – model of Betz-Zhukovsky, 3 - numerical modeling for unlimited space (dots), approximation (1.16) at m=1.6 and C^0_D=1.2 (line), 4 – the same as 3, but for conditions of a wind tunnel at a shadowing of 16%.

The calculations for a permeable circle modeling an "ideal" collinear unit are of particular interest. The pressure coefficients determined by the models created by Betz-Zhukovsky and G.H. Sabinin [8], present the greatest difference at the small disk permeability (Figure 1.8). The numerical model of the disk flowing with a uniform distribution of speed through the disk yielded intermediate results with an exact compliance to the experiment data at U = 0.

According to this model, corresponding to one assumption only – a uniform distribution of speeds in the stream through "ideal

unit", the pressure coefficient is approximated by the expression (1.15) with the parameters C^0_D=1.2 and m = 1.6, that determines the collinear unit efficiency in a boundless stream having the size:

$C_P = 1.2(1 - (U/U_1)^{1.6})U/U_1$ with the maximum value:

$$\mathbf{(C_p)_{max} = 0.41 \text{ for } U/U_1 = 0.55.} \quad (1.30)$$

It is important to mention a significant role of the external boundary conditions – the calculation for aerodynamic pipe conditions in which the wind wheel model would occupy 16% only, that gives a resistance coefficient value (and the turbine efficiency, accordingly) at 20% more than in the unlimited stream conditions.

Both the elementary theory and more sophisticated calculations do not yet reflect the specifics of the power unit which can be revealed by consideration of the hydro aerodynamics of the rotor which is flowed around with a speed of U. Using some mathematical model of the rotor, it is possible to construct a function of the pressure difference on the rotor depending on the speed U. Uniting this solution with the one modeling the unit by a permeable figure and a jump of pressure on it, we find the relative stream speed in the unit zone U/U_1 and all its characteristics. Such approach became a basis for many works searching for the optimum designs of power units. Now there are mathematical models allowing complex hydro aerodynamic calculations of the power units, taking the currents both in the unit zone and beyond its limits into account without use of the permeable plate model.

By consideration of the turbines in an open boundless stream, the problem parameters are represented by the relative geometric characteristics of the turbine as a whole and the blades separately, and the relative movement speed of the blades $V/U = 2\pi nR/60U$. By consideration of the external problem, the stream characteristic speed U is replaced with the set speed outside the turbine influence U_1 or U_0. An essential impact can be rendered by the Reynolds local number made by the blade chord b and by its linear movement speed V.

$$Re_v = Vb/\nu \quad (1.31)$$

The turbine capacity P depending on the running stream speed U_0 and the linear speed of blades $V = \pi Dn/60$ can be given in two forms:

$$P = C_P \rho U_0^3 S/2 \quad (1.32)$$

$$P = C_N \rho V^3 S\sigma/2, \text{ here } \sigma = ib/D \quad (1.33)$$

where S = D H - area of axial cross-section of the body swept around by the blades, (S σ) - area of the median (chord) surface of working blades, σ - solidity, i - number of blades, b - length of the blade chord, D - diameter of the route of blades, ρ - environment density (air). The coefficients C_P and C_N, depending on the turbine outlines, ratio of speeds V/U_0, quality of blades, and Reynolds number are connected by identities as follows:

$$C_N = C_P (U_0/V)^3/\sigma \quad (1.34)$$

$$C_P = C_N (V/U_0)^3\sigma \quad (1.35)$$

In the American literature the expression (1.33), connecting the unit capacity with the movement speed and the surface area of blades, is written differently, keeping the axial section area of the swept around surface in consideration:

$$P = K_P \rho V^3 S/2 \quad (1.36),$$

where the coefficient K_P is connected with the coefficient C_P by the identity:

$$C_P = K_P (V/U_0)^3 \quad (1.37)$$

Figures 1.9 and 1.10 present an example of the power characteristic of a modern collinear unit with fixed blades, presented depending on the "rapidity" ("tip speed relation") of the wind wheel $C_P(V/U_0)$ or the relative wind speed $K_P(U_0/V)$. The points A, B, C, D mark the identical modes in different coordinates.

The characteristic speed of the blades in all cases is accepted as the speed of the blade ends.

$$V = \omega R \quad (1.38).$$

The capacity P and torque M on the turbine shaft are connected as follows:

$$M = P/\omega \quad (1.39).$$

The relative value of the torque of $C_M = M/(\rho U^2_0 SR/2)$ is defined by the coefficient C_P and the turbine rapidity $-\lambda = V/U_0$ (in the

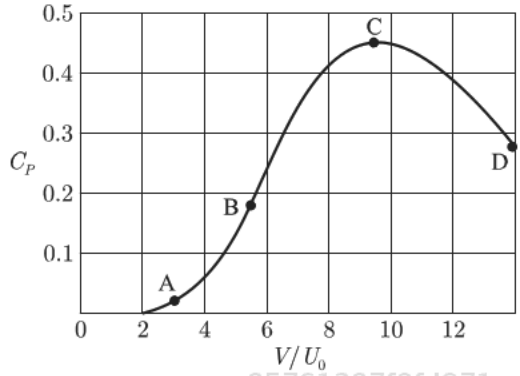

Figure 1.9 Example of the power characteristic of the high-speed wind wheel with a horizontal axis and a fixed turn of the blades.

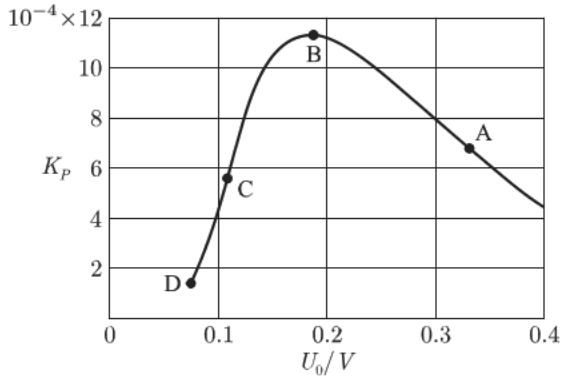

Figure 1.10 The same as in Figure 1.9, but with coordinates of wind speed of power factor K_P.

Russian literature, λ is sometimes called the "number of modules"; in the English literature, the "tip speed relation"):

$$C_P = C_M \lambda \qquad (1.40).$$

The choice of a record form (1.36) from positions of the similarity theory is incorrect, as the uniformity principle of the group of initial dimensional parameters is not satisfied. We use the area value S = DxH not connected directly with geometry of blades, rather than area of blades as in (1.33). It is reflected in the results – in all modes the parameter K_p is strongly dependent on the solidity σ, and is not applied to the wind unit analysis (note that in the extensive

book [9] by Prof. R.E. Wilson, the quantitative data on coefficient K_P are provided on the charts having errors in scales). The use of representation (1.36) is convenient in the analysis of collinear units in which the shadowing varies along the turbine radius. It is clear that the capacity taken from the stream on a permeable figure modeling the unit and the turbine capacity differ at a value of energy of the additional turbulence generated by the stream in the rotor.

The representation (1.32) establishes a direct connection between the initial energy $\rho U_0^3/2$ carried through the area unit of the stream cross section and transformed by the equipment to the mechanical capacity P of the rotating rotor. The equipment takes energy from the stream, thus slowing it down. Therefore, the stream speed in the power unit zone U is always less than the stream speed U_0 at a distance, or far away. The maximum capacity which can be taken from the stream corresponds to a certain value of the relation U/U_0. The elementary theory of Betz-Zhukovsky, as it has been noted above, gives the maximum possible value $C_P = 16/27 = 0.5926$ at $U/U_0 = 2/3 = 0.67$ - formula (1.13). The calculation of currents through the permeable "plate" modeling the power unit (theories of "ideal unit") yields different results depending on the conditions applied to the "plate". If we accept a uniform distribution of speeds on the plate, two different solutions are obtained for a rectangular plate - for a symmetric trace and without this restriction (Figure 1.4).

In both options the maximum unit efficiency is within $C_P = 0.55 \div 0.58$ at $U/U_0 = 0.55 \div 0.60$.

If we do not demand a uniform distribution of speeds on the permeable plate surface modeling the power unit, set a proportionality condition of the current local speed through the plate to the speed module near the plate (filtering plate), and consider the pressure reduction behind the plate (modified GGS model), the maximum efficiency appears almost the same.

The actual efficiency of the units significantly depends on their design and may be considerably different from the given estimates, both towards smaller values that are explained by the non-optimality of the design or the mode and energy losses, and towards greater values that can be connected with the attraction of some stream energy which is not passing through the unit cross-section.

The representation (1.33) may seem physically less evident. However, it makes sense as the actual taking of wind energy happens when flowing around the unit blades. The arising forces are proportional to the square of the relative speed of the blade flowing

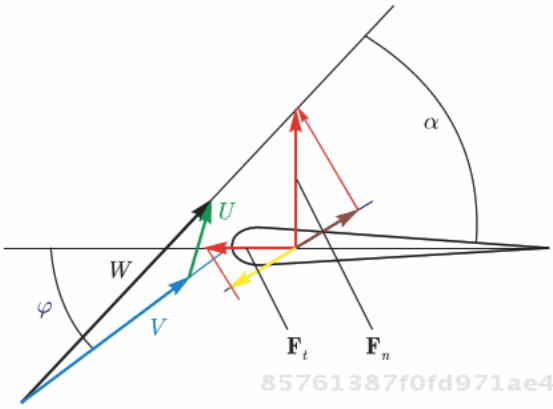

Figure 1.11 Scheme of the power unit blade flowing

and its area, and the local capacity is proportional to the blade speed. Let us consider the wind power unit blade flowing in the plane, which is perpendicular to the blade median surface and parallel to the stream speed in the wind power unit zone (Figure 1.11).

The relative speed of the blade flowing W is defined as a vector remainder of the local wind speed U and the blade end linear speed V. The force operating per unit length of the blade can be presented in the form of the vector sum of pulling force F_t operating along the blade chord, and normal force F_n operating perpendicular to the blade chord.

$$F_t = C_t \rho W^2 b/2 \quad (1.41)$$

$$F_n = C_n \rho W^2 b/2 \quad (1.42)$$

Each of these forces is proportional to a high-speed pressure of relative stream speed and aerodynamic coefficients C_t, C_n depending on the attack angle α, blade profile shape, blade relative lengthening ("aspect ratio" $A = L_b^2/S_b$, where L_b – blade length, S_b – blade surface area. For rectangular "plan" $A = L_b/b$) blade surface roughness, Reynolds number, and level of stream turbulence.

The coefficients C_t and C_n can be expressed by the carrying power coefficient C_L (lift) and the resistance coefficient C_D (drag), marked in the Russian literature as C_Y and C_X:

$$C_t = C_L \sin\alpha - C_D \cos\alpha \quad (1.43)$$

$$C_n = C_L \cos\alpha + C_D \sin\alpha \quad (1.44)$$

In Figures 1.12 and 1.13, the influence of the lengthening and thickness of the blade profile are shown. At great attack angles below the "critical" value corresponding to lift off of a stream, the dynamic effects of prolongation of the lift off moment are observed at the increase of the attack angle, and prolongation of the continuous flow recovery at the reduction of the attack angle. This is especially noticeable on comparatively thick and short blades.

The influence of the Reynolds number and the roughness of profiles is great, especially at the near-critical attack angles (Figures 1.14, 1.15).

A special profile developed in the Langley research center (USA) for low-speed planes of noncommercial aircraft shows high and steady aerodynamic characteristics. This profile is named General Aviation-Witcomb-1 (GAW-1) (Figure 1.16). This profile, with relative thickness 17%, provides a dramatically high value of the pulling force coefficient: $C_t = 0.356$ at $\alpha = 16°$ and $Re = 1.9\ 10^6$ (Figure 1.17).

By scalar multiplication of the forces (1.41, 1.42) at the speed of the blade aerodynamic center V and summarizing the result, we obtain the capacity taken from the wind by the wind turbine generator from the length unit of one blade. In a common collinear power unit, the direction and value of the stream speed in the unit zone U almost does not depend on the blade position in the course of rotor rotation, but is able to change on different distances from

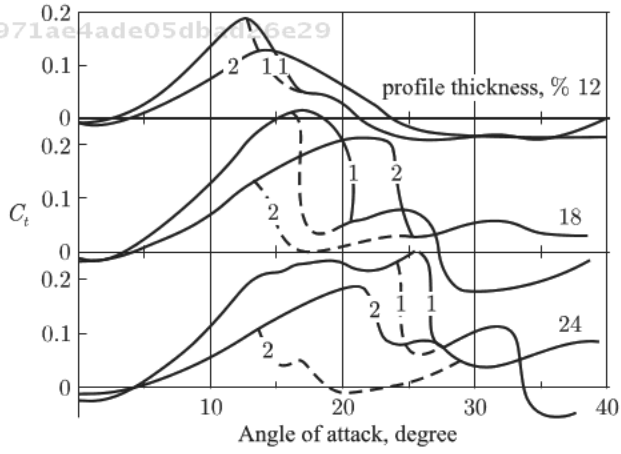

Figure 1.12 Coefficient of the pulling force for the NACA 00XX profiles with an infinite length of the blade (1) and A = 5 (lines 2) [10]. Reverse motion (dotted line) – reduction of the attack angle. Re = 0.59 10^6

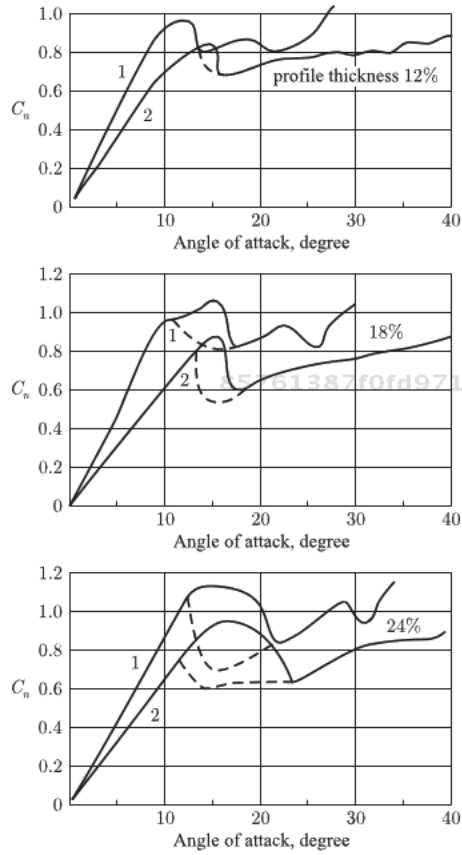

Figure 1.13 Coefficient of normal force for the NACA 00XX profiles with an infinite length of the blade (1) and A = 5 (lines2). Reverse motion (dotted line) – reduction of the attack angle. Re = 0.22 10^6

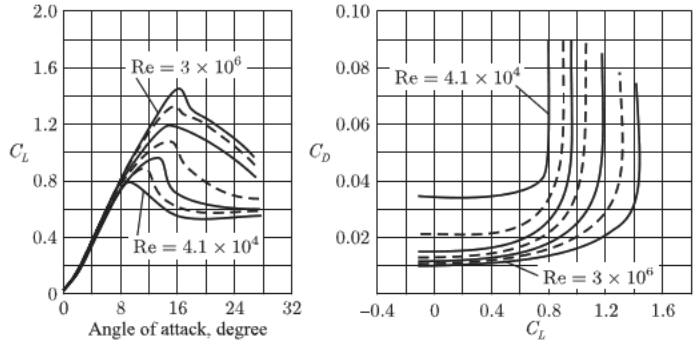

Figure 1.14 NACA 0018

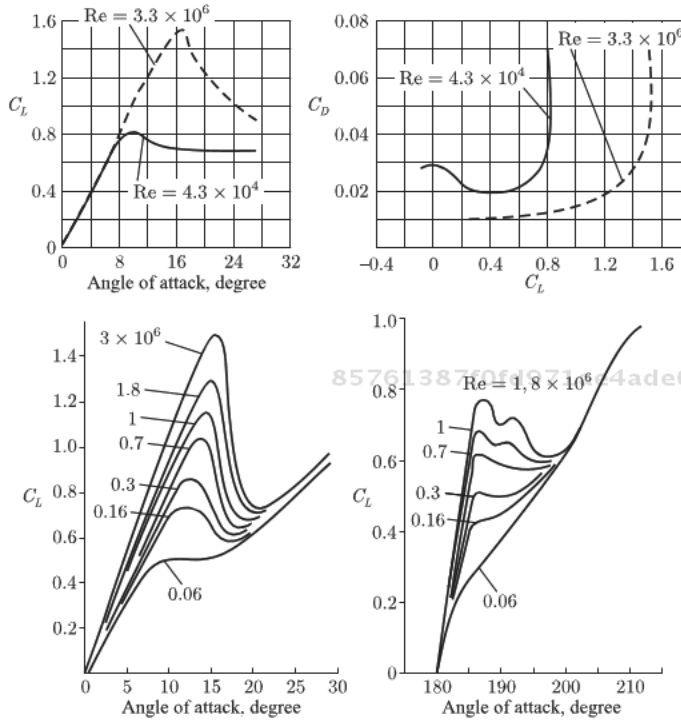

Figure 1.15 NACA 0015

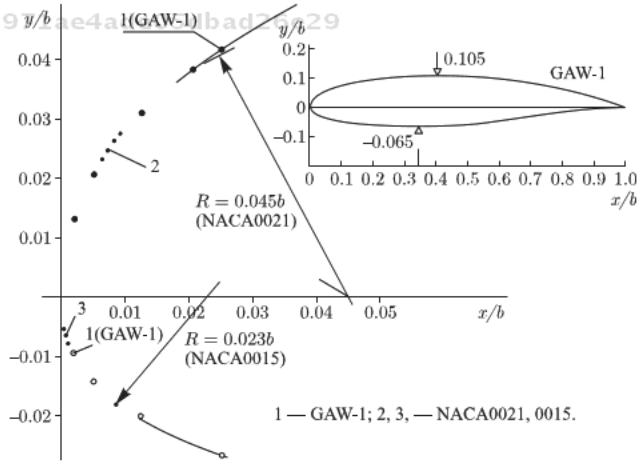

Figure 1.16 Comparison of shape sock profiles GAW-1 and NACA.

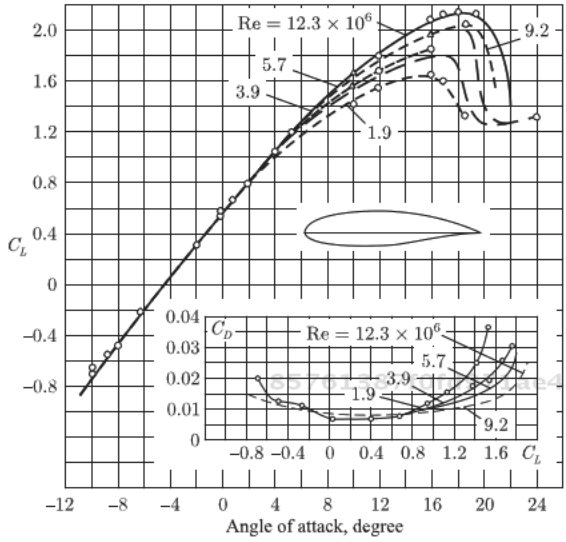

Figure 1.17 GAW-1

the rotation center and for different time instances (non-stationary wind).

In the orthogonal machines, on the contrary, values and directions of the stream speed concerning the blade vary for each point along the route of the blades, but are almost identical for different sections of the unit with direct blades. The number of blades, relative chord length b/D, mutual influence of the blades, and the design features are demonstrated by the relative values and distributions of the stream speed U inside the equipment.

The power characteristics of high-speed orthogonal and collinear units are qualitatively different (Figure 1.18). Though the power efficiency maximum in both cases is approximately identical (in orthogonal machines of new type with direct blades and optimum solidity $\sigma = 0.3$; as seen in Figure 1.18, it can even be much higher), the type of characteristics is different.

The collinear unit has rather big movement speeds of the blades. A failure of the brake system and loss of electric loading of such a wind generator, even at a low wind speed, practically means acceleration and destruction of the equipment. On the contrary, in the orthogonal machine, the movement speed of the blades is only 3-4-fold greater than the stream speed, and the runaway speed does not greatly exceed the optimum speed. The collinear wind generator produces a strong noise – the ends of blades move too quickly,

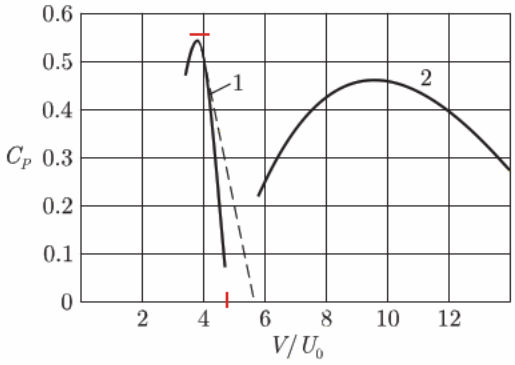

Figure 1.18 Characteristics of the best orthogonal and collinear units at the fixed turn of the blades. 1 - orthogonal unit, 2 – collinear unit.

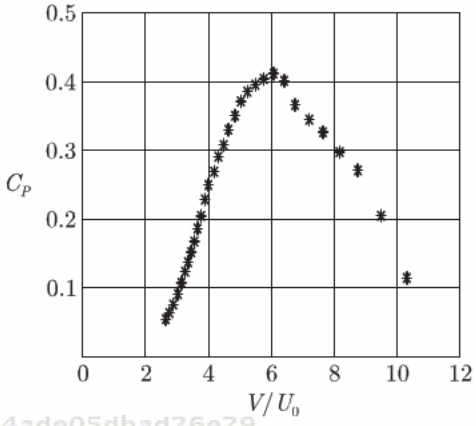

Figure 1.19 Efficiency of the two-bladed orthogonal turbine Sandia. Solidity σ from 0.05 to 0.12. Rotation frequency is 34 rpm.

and the hydraulic unit is subject to the danger of cavitation on the blades. On the other hand, the flat form of the efficiency maximum of the collinear units makes the requirement to speed regulation of the movement of blades less rigid.

The orthogonal unit of Darrieus type ("a jump rope – troposken") at a small shading can have the characteristic with an expanded high efficiency zone and high runaway speeds (Figure 1.19). [11]

These units, as noted above, demand a preliminary spinup; they are subject to considerable unbalanced aerodynamic loadings, which cause dangerous vibrations.

D = 34.2 m, H=41.9 m. Clean blades.

The turbine power characteristic $C_p(V/U_0)$ significantly depends on the turbine design and the operation conditions. In the same boundary conditions, the influence of the turbine form – number and shapes of cross-section of the blades and traverses, stream speeds and turbulence are great. According to the calculations and experiments, the power factors C_N or K_p with the fixed blades in the operation range of the turbines are approximately described by the following linear functions:

$$C_N = B\,(U_0/V - B_0),\ \text{if}\ B_0 < U_0/V < B_{lim} \qquad (1.45)$$

$$K_p = K\,(U_0/V - K_0),\ \text{if}\ K_0 < U_0/V < K_{lim} \qquad (1.46)$$

Actually, (1.45) and (1.46) mean that at a constant speed of blades (V = constant) the turbine capacity is directly proportional to the first (rather than the third!) stream speed. This has been revealed by the trials of collinear and orthogonal turbines of different types (Figures 1.20 – 1.22).

Thus, the turbine power characteristic can be approximately set by three parameters only. The parameter $1/B_0$ is the maximum relative speed of the blades reached by the turbine without braking, or, on the contrary, the parameter B_0 is the minimum relative wind speed at which the turbine starts working. The parameters B and B_0 define the turbine efficiency:

$$C_P = B\,(U_0/V - B_0)(V/U_0)^3\sigma \text{ – for orthogonal machines} \qquad (1.47)$$

$$\text{Or } C_P = \kappa\,(U_0/V - \kappa_0)(V/U_0)^3 \text{ - for collinear machines} \qquad (1.48)$$

The maximum efficiency is equal to, respectively:

$$(C_P)_{max} = 4B\sigma/27\,B_0^2 \text{ at } V_{opt} = 2\,U_0/3B_0 \qquad (1.49)$$

$$\text{Or} \qquad (C_P)_{max} = 4\kappa/27\kappa_0^2 \text{ at } V_{opt} = 2\,U_0/3K_0 \qquad (1.50)$$

In review of Irvin E. Vas [13], 17 innovative schemes, some of which have been practically developed, are considered. The offers connected with air ionization and direct transformation of the electroconductive stream energy are not yet developed. The use of aeroelastic effects, and thermodynamic and phase transitions is possible, though their practical assessment and development is still intended for the future. Within one mechanical principle of wind power transformation, the most varied constructive schemes are known. Many proposals concern forms of diffusers and confusers

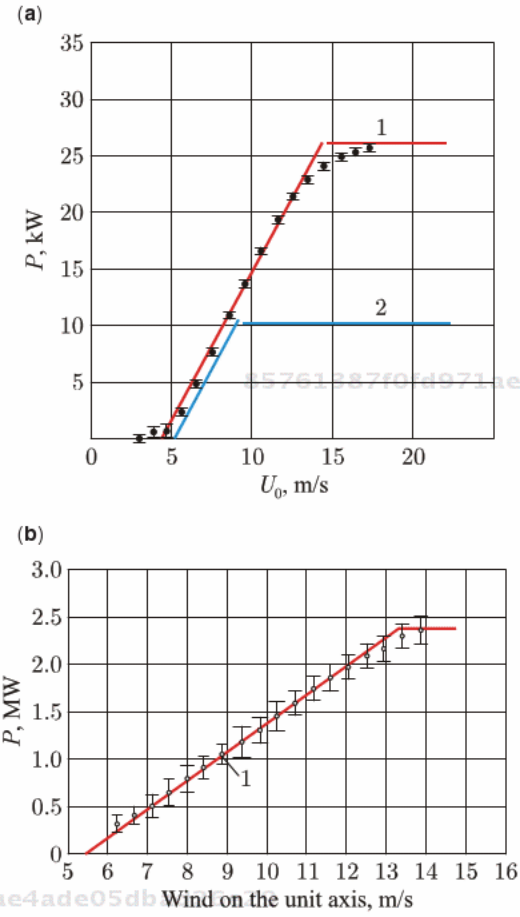

Figure 1.20 Natural tests of collinear units with diameters 10 m and 91.4 m. 1 – clean blades, 2 – blades covered with dust, insects, seeds of plants (after long operation).

for collinear units. The main idea of these proposals involves attracting the energy of air streams which is not passing directly through a hypothetical cylinder leaning on the turbine driving wheel, such as various concentrators and stream-directing systems, as well as the devices providing pressure decline behind the driving wheel, the so-called the ejection effect. These devices have to accept the influence of strong (storm) winds that reduces their economic efficiency. The ejector systems can be positioned at a distance from the driving wheel. For example, the scheme of combined ejector BPR with descending and ascending air streams is shown in Figure 1.23.

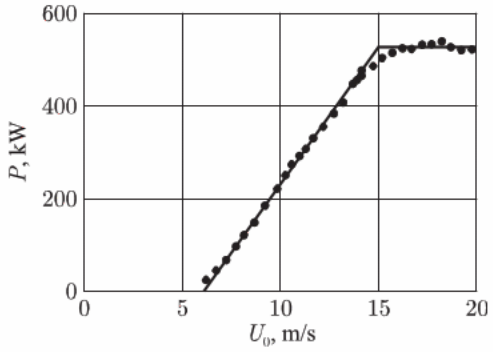

Figure 1.21 Capacity of two-bladed orthogonal wind power unit (Darrieus type) depending on the wind speed on the rotor equator (Sandia, D=34.2 m, N=41.9 m, σ_{min}=0.053, rotation frequency 34 rpm. The natural measurements with cleared blades, January-April, 1989)

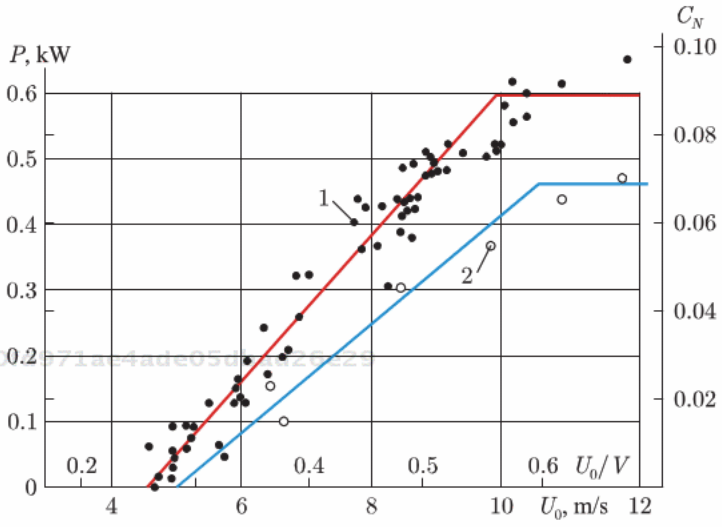

Figure 1.22 Trials of orthogonal wind power unit with straight blades on IFA polygon of the Academy of Sciences of the USSR (1) and in the wind tunnel of TSAGI (2) [12].

In this scheme, the motionless cylindrical ferroconcrete tower with inclined columns on the base forms a bearing framework of the installation. Inside the tower there is a vertical pipe leaning on the base by the vertical columns, bearing aerodynamic profile shutters which carry out the functions of the directing device for the unit working by the ascending air stream. The mobile top nozzle,

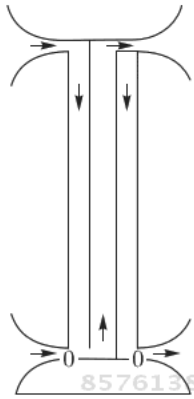

Figure 1.23 Ejector power installation with ascending and descending streams.

independently established by the wind direction (for creation of the ascending air stream in the internal pipe, and the descending air stream in the ring space between the pipe and the tower), includes confuser and diffuser parts.

The confuser part, when catching a head wind, creates a pressure in the top section of the descending stream; the diffuser part provides a smooth expansion of the ascending stream and its connection to the discharging zone behind the diffuser.

The mobile confuser at the tower base, independently established towards the wind stream in the ground layer, serves to create an upthrust in the bottom section of the ascending stream. The mobile diffuser at the tower basis is established independently by the wind stream in the ground layer discharging in the bottom section of the descending stream. Simultaneous installation of confusers and diffusers is carried out by the power impact of the wind stream on their surfaces, due to a special constructive solution supposing a discrepancy of the rotation centers and the curvature centers of these surfaces. The air turbine can be placed horizontally, as shown in the figure, or vertically, but on the bottom marks.

It is clear that the external bearing tower of this sophisticated design is able to perform several functions: to bear television antennas, a solar power station boiler, etc. One of advantages of the described, quite sophisticated BPR design is a small specific material capacity of machine-building and electrotechnical products, such as rotors and generator, and the technological availability of installation.

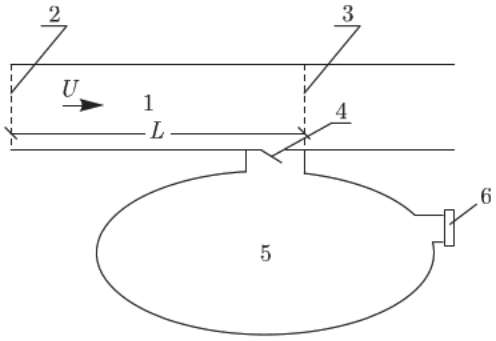

Figure 1.24 Air shock unit.

The mechanical and electric equipment can be made more compact by an increased operation air pressure on the turbine. The pressure increase on the turbine pressure side and its reduction on the turbine local side are provided due to non-stationary shock phenomena. The application principle of such phenomena is the following [14]. At the initial stage of work, air freely moves in pipe 1 with speed U (Figure 1.24). At some moment lock 3 is closed, causing the shock wave to run from right to left (towards the current), behind which front the pressure makes $p_3 = \rho U c$, and the speed is equal to zero. After the shock wave achieves lock 2, this lock is closed. Finally, the energy $\rho U^2 L \Omega / 2$ is concentrated in the pipe, where L – pipe length, Ω –its cross section area.

Further, lock 4 opens, and a part of this energy passes to tank 5 - this part depends on the pressure maintained in tank 5. After that, lock 4 is closed, locks 2 and 3 are opened, and free air movement is restored in the pipe. Turbine 6, which develops the power, is installed at the output of tank 5.

$$P = \Delta p \, Q_T \qquad (1.51),$$

Where Δp - pressure difference between tank 5 and the atmosphere, Q_T - air consumption via the turbine.

Let us estimate the possible capacity of turbine 6. After closing locks 2 and 3, the air density in the pipe is incremented at:

$$\Delta \rho = \rho \, U / c \qquad (1.52)$$

If the pressure is maintained in tank 5:

$$p_5 = \alpha\rho Uc, \text{ where } \alpha<1, \tag{1.53}$$

then, after opening lock 4 the following weight comes to the tank:

$$\Delta M = (1 - \alpha)\rho\, UL\, \Omega/c \tag{1.54}$$

The time of inflowing of this weight is short – about:

$$t_{in} = \alpha_{in}\, L/c \sim L/c \tag{1.55}$$

The current recovery time in pipe 1 after opening locks 2 and 3, according to the experiments performed by U.R. Liyv, makes about:

$$t_{out} = \alpha_{out}\, L/U \sim 0.5\, L/U >> t_{in} \tag{1.56}$$

The average volume expense via turbine 6 makes:

$$Q_T = (1-\alpha)(U\, L\, \Omega/c)\ /(t_{in} + t_{out}) \tag{1.57}.$$

The turbine power calculated by (1.51) – (1.57) is written as:

$$P = \alpha\rho Uc\,(1-\alpha)(U\, L\, \Omega/c)\ /(t_{in} + t_{out}) = \alpha(1-\alpha)\,\rho U\,(U\, L\, \Omega)\ /(t_{in} + t_{out}) \tag{1.58}$$

will make the maximum at $\alpha = 0.5$:

$$P = 0.25\, \rho U^2 \Omega/(\alpha_{in}\ /c + \alpha_{out}\ /U) \sim \rho U^3 \Omega/2 \tag{1.59}.$$

Thus, the air shock unit appeared approximately 3-fold more effective, than a free wind-driven generator with swept around surface which is equal to the pipe cross section area.

The BPR construction design can be implemented with counter-streams (descending and ascending) (Figure 1.23). Instead of air turbines in the flowing part, the air shock BPR has locks closing the air stream channels. The locks have to be equipped with a special automatic drive of remote programmed control for periodic opening and closing of the air stream channels to form shock aerodynamic waves in these channels.

The air shock scheme can be designed to use both a compression phase, and a discharging phase. For this purpose two tanks with

a turbine between them are established. Air in the compression phase is forced into the increased pressure tank, and during the same periods it is evacuated from the lowered pressure tank. VES units, containing an air turbine and a generator, operate due to the pressure difference in the tanks of increased and lowered pressure.

The air shock scheme is capable of mitigating the wind speed pulsations, performing functions of a small accumulator. The pressure difference in the turbine in this scheme can make about:

$$\Delta p = 4\ \rho c U_0 \tag{1.60}$$

where c - sound speed in air, U_0 - wind speed at approach to BPR. The material capacity of the turbine and the generator here obviously has to be approximately 10-fold less than in other designs. As proved by calculations, the area of the flowing part of the air shock unit Ω can be about 0.2 from the cross-section area of the concentrator Ω_0, and the maximum capacity of an optimum system with concentrator, diffuser, and locks in the feeding and evacuation lines makes:

$$P = 3.4\ \rho\ U_0^3 \Omega_0 \tag{1.61}$$

The assessment (1.61) exceeds by an order those limit ratios obtained at the beginning of this chapter (border of "Betz-Zhukovsky"). What is it - a new quality of an essentially non-stationary system or a consequence of inexact intermediate hypotheses? This problem should finally be resolved by practical experiment with a real product.

The air shock system is characterized by an ability to operate at any wind speeds. Its compact power and electrotechnical equipment is placed on the ground and is able to comprise several groups of the turbines' generators intended for 2–3 ranges of pressure. Since the pressure in the tanks is proportional to the stream speed (rather than to the high-speed pressure), at the change of the wind speed by an order that blocks energetically a significant range, the pressure difference in the turbines will change by an order too, that significantly expands the capabilities of power regulation and considerably increases the output and the power usage time. It is important that the air shock unit, in principle, allows foreffective use of the deep low-frequency pressure fluctuations arising behind the concentrator, to strengthen these fluctuations by a choice of the

corresponding maneuvering rhythm by the working locks, to use these fluctuations for attraction of energy of the streams passing by VES, and increasing the capacity and output of the system.

Another special type of the mechanical transformation scheme of current energy is the use of energy of fluctuations, excited at aeroelastic or hydroelastic interaction of the stream and the design. A well-known accident with Takomsky Bridge, caused by aeroelastic fluctuations, attracts attention to the analysis of application conditions of this scheme. Figures 1.25 – 1.26 show two aeroelastic converters studied experimentally with a well streamlined profile and with a badly streamlined "balance beam". In both cases a positive power effect has been reached. However, quantitatively the application efficiency of these schemes is low. The trials of a fluctuating wing [15] with the NACA 0012 profile, the chord of 20 cm, and the span of 105 cm were carried out with an amplitude of vertical wing

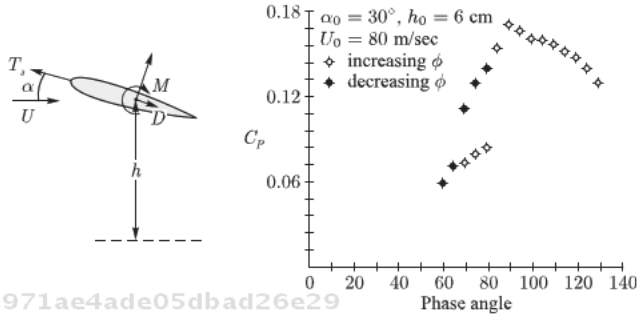

Figure 1.25 Scheme and results of the trials of the shaking wing in the air stream.

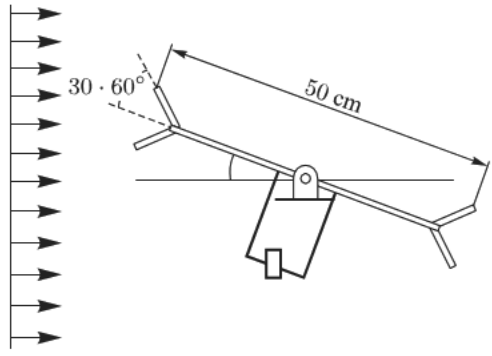

Figure 1.26 Trials of a fluctuating balance beam with whirlwind generators.

movements h_0=6 cm and the attack angle amplitude α_0 = 25° and 30°. The phase angle ψ in the shift formulas $h = h_0 \sin \omega t$ and the attack angle $\alpha = \alpha_0 \sin(\omega t+\psi)$ of 6.2 and 8 m/s are the main object of attention.

The average power taken by such an oscillatory system is commonly proportional to the swept around area and the initial energy stream, but significantly depends on the phase ψ. The maximum efficiency of the system is reached at ψ = 90–100°, if the phase increases. The maximum obtained efficiency value made $C_P = 0.283 \times 16/27 = 0.168$.

The possibility of usinga single fluctuating wing as a stream energy converter was confirmed in 1976 by the experiments of E.P. Grebeshov and O.A. Sagoyan who demonstrated the efficiency of such a propeller not conceding to an ordinary propeller or a rowing screw [16].

The trials of the "balance beam" in Figure 1.26 were carried out [17] at the entrance to the wind tunnel with a cross-section of 45×45 cm. The model at which the length of the "balance beam" made 2b = 50 cm, and the width – 45 cm, almost blocked the pipe. The end sites had angles (from the axis) of 30° or 600°.

The distance between the extreme points of these sites made 15 or 30 cm. The balance beam was counterbalanced by a weight under the central hinge. The weight varying from 4.4 to 11 kg was fastened on the end of a steel core 37 cm long and weighing 5.6 kg.

The stream speed U varied from 5.5 to 11.6 m/s. The power generated by this system was normalized by the wind power stream through all cross-sections of the pipe. At such normalization, the system effectiveness, generally depending on the parameter $k=b\omega/U$, never exceeds 1% at k = 0.05–0.07.

The practical realization of a fluctuating wing idea was carried out in 2004 in the Stingray project, according to the US Patent 6731018. The unit with one pair of wings produced the maximum power of 150 kW at the stream speed over 3 m/s, and at the period of compelled fluctuations of the wings, about 30 sec.

Figure 1.27 shows one of the possible power use schemes of the flexible cylindrical tower fluctuations raised by wind or water. Inside the tower the electromagnet 2 covering the coil 3, fixed on a motionless internal rack 4 is established. The base of the fluctuating tower 1 and the motionless rack 4 are separated. However, for strengthening of the effect, it is possible to create a device providing counterphase fluctuations. It is also possible to create several

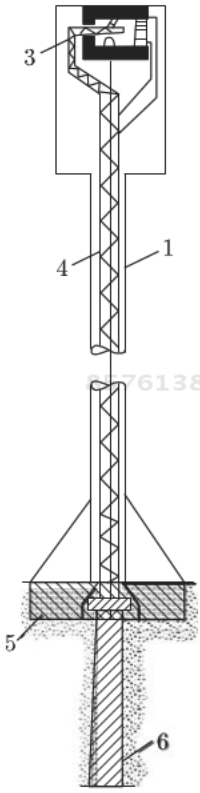

Figure 1.27 The tower shaking under the influence of the wind. The tower frequency is adjusted by the wind speed due to change of the water weight in the tank above. 1 - vibrating cylinder, 2 - magnetic system ("rotor"), 3 - motionless winding system (stator), 4 - stator supporting framework, 5 – seismic emitting base of the shaking tower, 6 - stator base.

towers on the general elastic basis, transferring fluctuations and providing self-synchronization of fluctuations. The feature of this design is availability in the tower top part of a tank for liquid to be filled or emptied depending upon the wind speed, so that the frequency of its own tower oscillation corresponds to the conditions of "capture" and generation of self-oscillations with the maximum amplitude. The power efficiency of such schemes calculated by the cross-section areas of the swept around fluctuating design is able to reach 25 ÷ 30%.

The aeroelastic fluctuations in the most different forms are discussed in the book of Prof. Edward Naudacsher and Donald Rockwell [18]. Almost all examples provided in this book as sources

of danger, in our understanding, can be used as energy transformation mechanisms from liquid to oscillatory system and further into electricity, into mechanical or other accumulative system (tank with liquid, pressure head tank, heat or cold storage, hydrogen).

Numerous publications written by A.A. Krasovsky and M.Sh. Misrikhanov [19] cover the oscillatory type energy converters, formed by several wings which are elastically fixed in the frames perpendicular to the stream.

Also, the options of energy mechanical transformation are represented by the schemes including thermodynamic cycle elements. In La Mancha (Spain), 100 kW solar and wind power installation constructed by Germany engineers hasoperated since 1982.

This installation includes a vertical steel pipe 200 m high, (weight 250 tons) with a diameter of 10 m, fixed by seven extensions on the basic ring including a wind rotor. The ring is supported by eight steel columns. The transparent "sunhouse" roof with a diameter of 250 m consisting of cells of 6 x 6 sq.m of transparent film 0,1 mm thick is also attached to the ring. The height of the "sunhouse" is 2 m. Due to air (and land) heating under the film, a draft is created in the pipe providing the wind turbine power output.

According to the actual data, the wind speed in the pipe makes not less than 4 m/s (at night or in the afternoon without sunlight), and about 12 m/s in usual conditions. Due to the soil thermal inertia, this unit possesses certain heat-accumulation ability. Lifting of air can be accompanied by vapor condensation. If we consider this process and enter an additional element of air compression, expansion (the installation efficiency) can be increased. The installation of this kind for the conditions of Punta Tuna (Puerto Rico) at the power of 10 MW and 4 ÷ 5 thousand hours of operation per year can cost about 16 million dollars (1600 dollars/kW); that is comparable with expenses of a traditional VPR. El Segundo company developed some designs of return action installations in which rather cold, for example, sea water is applied to the tower top. With evaporation, drops of this water reduce the air temperature, directing down the tower trunk.

First in Spain, and now in Australia, the project of a combined solar and wind power station is realized. According to this project, a considerable part of the territory is covered by a transparent material under which the air is heated up by the Sun. In the center of the site covered with such material, is positioned a high tower with a high speed air stream inside (Figure 1.28). High-speed, and

Figure 1.28 Solar - wind power station, 50 kW. (1982 - 1989, Manzanares, Spain).

therefore very effective and economic, wind power units are placed in this tower.

In this case, the central pole can carry out the function of an exhaust pipe with some additional units in the base. The same pole can be included in the air shock unit scheme.

A real assessment of possible energy development by a wind power unit or a group of wind power units (wind power station – WPS), as well as definition of a possibility to ensure the required demanded power in the set mode (by the set production schedule) is determined by the characteristic of WPS and the wind mode.

A complete description of wind or water flow as a space-time casual process demands introduction of an unrealistically huge volume of data. For practical purposes, it is important to allocate a volume of data which can be actually obtained (at modern setup of observations), and which can be used for analysis of power installations as:

- Power objects, capable of producing power at fixed instances with a certain probability at the restrictions relating to dispersion and fluctuation in the range of power;
- Construction objects, possessing a certain durability and reliability.

The detalization degree and particular contents of information can be different for the stages of design, construction and operation of the installations. At the operational phase (without research

purposes) continuous data on module and direction of the stream speed at one or several fixed points, mitigated by a set time interval depending on the unit design are necessary. These data are used for control of the power object. At the construction stage, only the particular data of a short-term forecast on the maximum stream speed during the planned installation period of the equipment are important. The fullest data are required at the design stage.

The meteorological basis of a choice of the location of future wind power station (WPS) is a map of average (annual and seasonal) wind power streams, and maps of average (annual and seasonal) wind speeds at the heights of 100 and 500 m (in earlier works the heights of 10 and 50 m were considered characteristic) from an average surface on the ground. These two sets of maps for different heights provide a general understanding of seasonal and annual development of separate wind turbines or the wind power stations of any type. Now, similar maps and detailed atlases are available for all regions of the world. A general idea of wind potential distribution on the ground is provided in the map shown in Figure 1.29, World Meteorological Organization (1981).

The wind speeds obtained by a standard technique of term supervision, mitigated by an interval of 10–60 minutes both in seasonal, and in annual realization, follow well the Weibull probability distribution law [20] (Figure 1.30):

$$\text{Probability}\left\{\xi \le U\right\} \equiv F(U) = 1 - \exp - \left(\frac{U}{C}\right)^{\chi} \qquad (1.62)$$

As probability distribution of the wind speed values U – $F(U)$, the parameters χ and C are connected with the average value $\langle U \rangle$ and mean square (standard) deviation of the wind speed U' ratios:

$$C = \frac{\langle U \rangle}{\Gamma\left(\frac{1}{\chi}\right)} \qquad (1.63)$$

$$U' = C\sqrt{\frac{2}{\chi}\Gamma\left(\frac{2}{\chi}\right) - \frac{1}{\chi^2}\Gamma^2\left(\frac{2}{\chi}\right)}, \qquad (1.64)$$

where $\Gamma(z)$ – gamma function.

The values of constants in (1.62) for some areas are shown in Table 1.1.

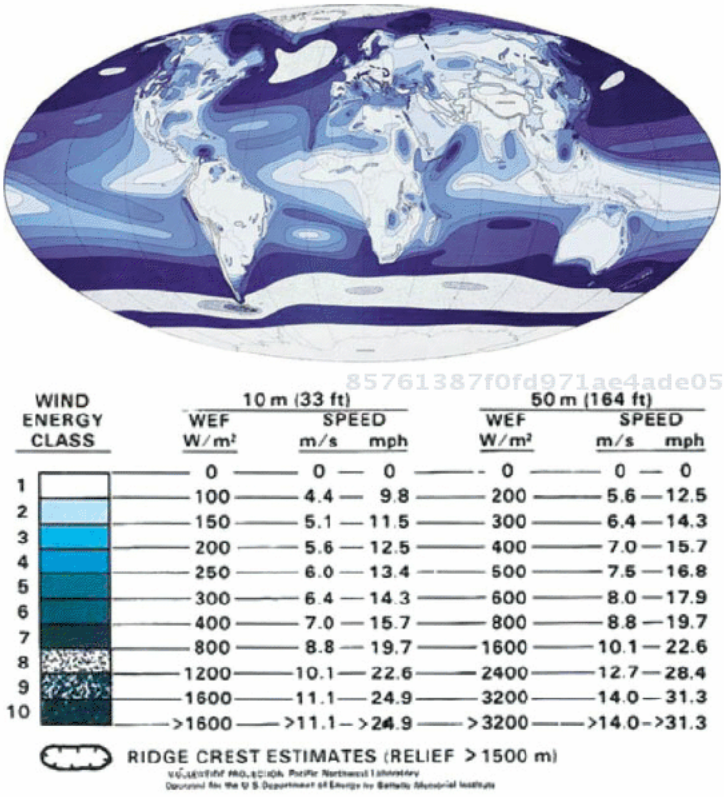

Figure 1.29 Classes of wind energy flux (WEF).

Approximately, the values of parameter χ in the polar areas and on sea coasts can vary from 1 to 2, and in the continental zones – up to 3.

The maps of average annual (seasonal) wind power streams show the zones of the greatest power efficiency of WPS, and in combination with the maps of average wind speeds, allow us to find parameters χ and C in the probability distribution (1.62). The ratio between an average cube of wind speed $\langle U^3 \rangle$ and the average speed $\langle U \rangle$ in the third degree, following of the law (1.62) is used for this purpose:

$$\frac{\langle U^3 \rangle}{\langle U \rangle^3} = \frac{3\chi^2 \Gamma\left(\frac{3}{\chi}\right)}{\Gamma^3\left(\frac{1}{\chi}\right)}. \qquad (1.65)$$

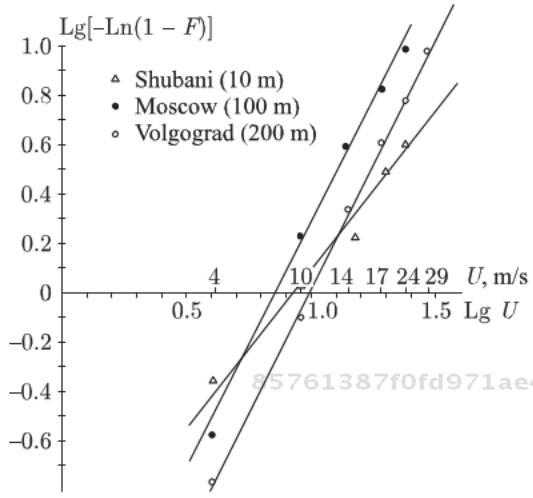

Figure 1.30 Probability distribution functions of wind speeds in different areas and at different heights. Straight lines show the Weibull law (1.62).

Table 1.1.

Observation points	Pelworm, (Germany)		New Zealand	Shubani (Apsheron)	Moscow	Volgograd
Parameter	h = 5,7 m	h = 45 m	h = 10 m	h = 9 m	h = 100 m	h = 200 m
C, m/s	5,7	8,6	5,9	8,32	7,08	9,77
χ	1,88	2,15	1,8 – 2,3	1,28	2,00	2,00

The solution of the equation (1.65) by means of Figure 1.30 allows to find a value of parameters χ and C for the considered region, and at the set power characteristic of the unit to calculate its mean monthly, seasonal or annual output. Processing of the observation data proves that the parameter χ rather slightly changes with the height change over the ground and with the change of the calculation procedure of average values – by one (seasonal or annual) realization or a set of realization of different years. In contrast, the average speed (or parameter C) is able to change considerably.

The choice of a wind mode as a basis of the maps at the heights of 100 and 500 m is caused by a need to abstract from the local conditions of data acquisition by separate meteorological stations at the first stage. These local conditions may greatly distort the overall picture. Despite attempts by many meteorologists to enter the individual correction coefficients considering conditions of an

arrangement of meteorological stations, there is no concrete and reasonable technique of introducing such amendments.

The data of particular meteorological stations and the observations performed by the local experts become necessary upon transition to the following stage – microdivision into districts of the selected area by the wind conditions. By means of simultaneous measurements for various directions and speeds of the wind, a plan of isolines of average wind speeds at the weather vane height (10 m) or at the height of the axis of projected wind power units is construction on the basis of measurements or calculations. This is the major stage of search of "wind rivers" which can be carried out in some substages with the subsequent integration of scale, if necessary (especially in mountain areas). Not only natural plotting, but also mathematical or physical modeling can be applied. An average (by probability) distribution of speeds by height for different seasons of year has to be set for the selected point of VES placement. The quasiperiodic components of the wind speed and spectral characteristics of the casual component at different heights are specified. Special attention is paid to spatial (by height and plan) correlations of speed variations (module and direction) at the distances of an order of dimensions of the equipment and WPS as a whole. This is necessary both for calculation of the power equipment, and for specific durability calculations of the units. It is important to identify the borders of the maximum and the minimum correlations among all variety of meteorological situations. The distribution functions of the wind speeds with small mitigation (below 3 sec) and continuous registration are studied for the same purposes. Currently, the equipment giving out the corresponding results (Figure 1.31) [21] immediately in the course of measurements is available; thus the observer has no need to study the wind speed realization.

The distribution of speeds by a vertical (average on probability, standards and mutual correlations) is necessary, not only for an assessment of the power efficiency of a particular unit, but also for a forecast of the mutual shading of the units, and the aerodynamic loads of their elements. Even in the conditions of stabilized uniformity in length current, such major current characteristic as, for example, length of separation zone behind a dead obstacle, strongly depends on the unevenness of the average speed curvature on the way to an obstacle, from the intensity of the turbulence of a running stream. For example, a whirlpool length significantly increases with the reduction of unevenness of the speeds and intensity of turbulence in the stream on the way to an obstacle.

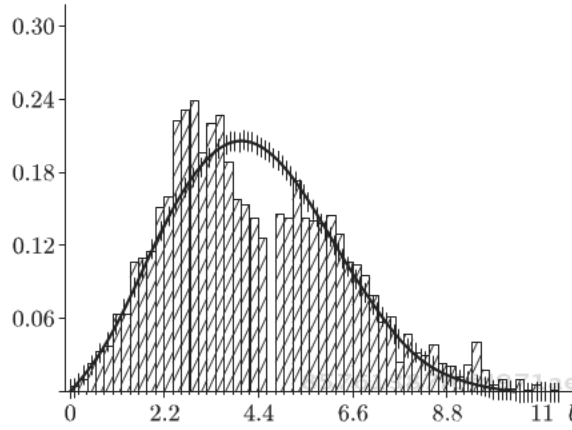

Figure 1.31 Probabilities distribution density of the wind speed module. Measurements performed in summer near Vung-Tau (Vietnam). The Weibull distribution is shown by a line.

There are the data on the essential influence and scale of the turbulence. As for characteristics of flowing of the blades and power parameters of the units, their dependence on the structure of turbulence can be especially strong.

The distribution of average on probability speeds by a vertical depends on the conditions of stratification of the atmosphere and can be very diverse. (A description of the phenomena can be found in many books and articles on atmospheric turbulence.) For the neutral conditions which usually are not the average per year or other climatic period (!), over a smooth district with a uniform roughness, a logarithmic law is considered fair:

$$\frac{U(Z)}{U_*} = 2,5 \ln \frac{Z + Z_0}{Z_0}, \qquad (1.66)$$

where: $U_* = \sqrt{\frac{|\tau|}{\rho}}$ - "friction speed" (dynamic speed), calculated by the average tangent tension of wind τ at the ground surface; z_0 - height of roughness of mm - over a quiet reservoir, cm - in rural areas, m - over a city building (Figure 1.32), Table 1.2.

The instant profiles of speeds and the profiles of speeds averaged in days, months, seasons, or years, as a rule, do not follow the ratio (1.66). In the "instant" (with averaging from 2 to 10 minutes) profiles of speeds in the ground layer, the local maxima at the height of about 100 m (mesostream) are often observed. In some areas (for

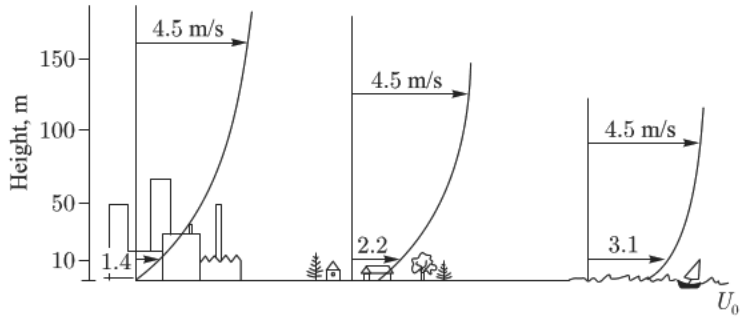

Figure 1.32 Distribution of speeds over surfaces with different roughness.

Table 1.2 Height of roughness for different conditions.

z_0, m	Height of roughness
10	Hilly and mountain areas
	City areas with high buildings
	Big cities
1	Wood
	Small cities
	Suburbs
	Land with sparse population
10^{-1}	Rural areas
	Many fences
	Separate trees (summer)
	High grass, agricultural fields
10^{-2}	Runways
	Rare trees (winter)
	Mowed grass
10^{-3}	Natural snow cover on the flat hill district
	Flat coastal areas
	Smooth desert
10^{-4}	Large reservoirs
	Quiet water surface
	Natural snow cover on the open flat district
10^{-5}	Smooth open ice

example, Odessa, Kustanay) the wind maximum in the ground layer and by the profiles of speeds, the average during a season or a year (Figure 1.33) are observed.

The wind speeds, the average for a climatic interval, in the bottom hundred-meter layer will follow a degree formula:

$$U(Z) = U(10) \cdot \left(\frac{Z}{10}\right)^m . \qquad (1.67)$$

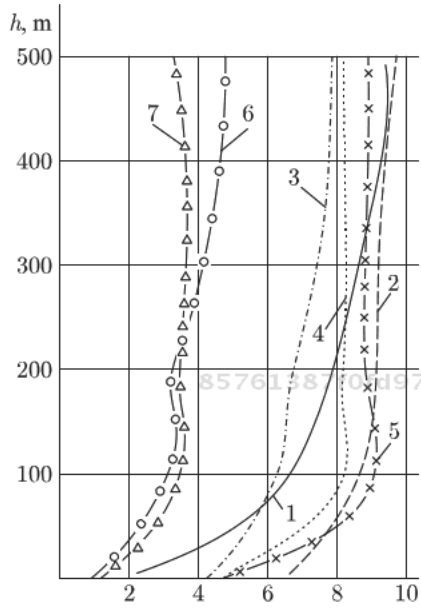

Figure 1.33 Distribution of mean annual wind speeds (m/s) by height in different areas: 1 - Moscow, 2- Volgograd, 3 - Blagoveshchensk, 4 - Odessa, 5 - Kustanay, 6 - Verkhoyansk, 7 - Yerevan

Where $U(10)$ – the wind speed at the height of 10 m from the ground, $U(z)$ - the same at height of z meters.

The exponent depends on a season, topography and a geographical arrangement of the district. According to some information, an absolute value of average speed influences that too. In this list of influencing variables, there is no contradiction of modern methods of the similarity theory, operating with dimensionless complexes. The recognition of legitimacy, for example, of such empirical recommendation [22], as:

$$m = 0.6\,(U_{mean}) - 0.77 \qquad (1.68),$$

means only that in the climatic conditions for which data have been collected, the thermal mode and the wind speed are correlated so that the average influence of stratification was generalized by a ratio (1.68). Certainly, it would be wrong to apply similar communications to other regions or climatic periods. For different climatic periods this is usually ranging from m = 0,17 to 0,24. At the tops and front slopes of flat hills, the parameter "m" should be reduced 1,5-fold, since the speeds increase at the ground (Figure 1.34).

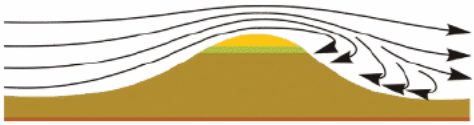

Figure 1.34 Wind speeds at the ground considerably increase on the flat height top.

The greater the ground roughness and the measure of the atmosphere stability, the greater is the parameter m, increasing from 0,05 to 0,7.

The turbulence intensity parameter is the standard (mean square deviation) of speed pulsations, measured in shares of the local average speed or friction speed. This value makes different sense and value at a different interval of the wind speed mitigation smoothing and different duration of the period by which the average speed is calculated:

$$U'_{\tau,\mathrm{T}} = \sqrt{\frac{1}{T}\int_{T_0-T}^{T_0}\left(U_\tau - \tilde{U}_\tau\right)^2 dt}. \qquad (1.69)$$

Here $U_\tau = \frac{1}{\tau}\int_{t-\tau}^{t} U dt$ - the wind speed mitigated within the interval τ, $\tilde{U}_\tau = \frac{1}{T}\int_{T_0-T}^{T_0} U_\tau dt$ - the speed, average in the period T.

Let us note that in the conditions of general wind nonstationarity the results of averaging by a set of climatic uniform measurements have a special value. For example, the mean annual speed and its standard of variation in January are given by:

$$\langle U\rangle = \frac{1}{N}\sum_{i=1}^{N} U_i;\ U' = \sqrt{\langle (U - \langle U\rangle)^2\rangle}, \qquad (1.70)$$

mean speed i January in the i-th years, the sign average calculation by a set or by a probability (in this case, the independence of wind speeds in January is provided in different years, therefore averaging by a set and by a probability provides the same value as usually supposed). The average (by a set) speed at a certain hour of January, etc. can be calculated similarly.

The average values of speeds do not depend on the mitigation interval; the standards of pulsations at different τ and T can significantly differ, and the correlations between the speeds mitigated at different intervals can be quite low!

In the ranges of turbulent pulsations of the wind speed it is possible to allocate a range of local and isotropic turbulence, where almost only one parameter is the average speed of dissipation of turbulence energy ε:

$$S_U = C_U \kappa^{-5/3} \varepsilon^{2/3} \tag{1.71}$$

$$S_V = S_W = 4/3 C_U \kappa^{-5/3} \varepsilon^{2/3} \quad \kappa = \omega / U \tag{1.72}$$

and the low-frequency range in which sharp changes of the range form are possible. One of the main parameters of the low-frequency part of the range is the integrated scale of turbulence L. Usually, the value L determined by autocorrelated function of the wind speed $R(\tau)$, having excluded quasiperiodic component $R_{\Pi}(\tau)$ from it:

$$L = \frac{1}{R(0) - R_{\Pi}(0)} \int_0^{\infty} \left[R(\tau) - R_{\Pi}(\tau) \right] d\tau. \tag{1.73}$$

The conditions of local isotropy are usually satisfied for the fluctuation periods less than $(1/5 \div 1/10)L/U$. The form of the low-frequency part of the range is usually accepted as the simplest, but such to satisfy the asymptotic ratios (1.71) - (1.72). The corresponding formulas are provided in the books on atmospheric turbulence, in the reviews and books with engineering appendices [23]. Let us consider the modern opportunities for modeling the low-frequency part of the range by means of numerical experiments (item 3).

The non-stationary phenomena, rushes, are specially characterized. At the preliminary stages, the maps of general division into districts of the maximum wind speeds with different repeatability - once in 5, 20, and 50 years (with averaging of the wind speed in 10 minutes) are used, and the maximum rushes of various degrees of repeatability (with averaging of 3 sec.) [24] However, considering that these maps for the mountain areas actually are unavailable, practically in any point of design of large VES the organization of continuous observation over the wind is necessary for at least one year. In the presence of such observation, the maximum rushes of small security are found by extrapolation with the use of one of the Gumbel limit distributions [25] (mainly, distributions of the first type). According to these observations, the probability distribution functions for quasistationary periods in characteristic meteorological situations are specified.

The probability distribution function of intervals of excess by the wind of certain values can be an important characteristic of

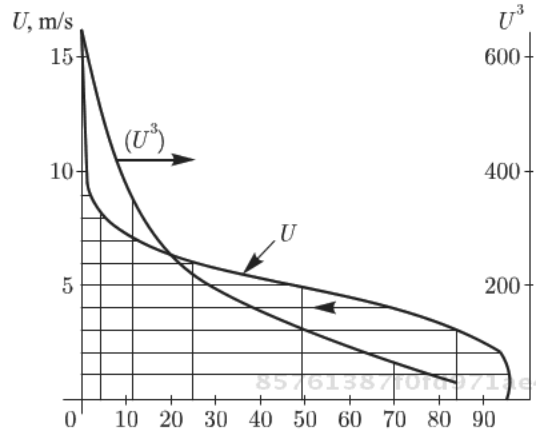

Figure 1.35 Relative duration of winds and wind power streams

the wind. For the wind speeds mitigated by 10-minute and longer intervals of time, this function is important for an assessment of the power qualities of the generators operating from wind. The probability distribution function of the wind speeds, presented in the form of communication of relative time of wind action below a certain value, considerably differs from the same function for a cube of the speed of the wind characterizing the wind power stream (Figure 1.35).

From comparison of these functions, it is evident that strong winds are observed for a short time, but bear big streams of energy that justifies some overestimate of settlement wind speeds at the design of wind power units.

For the wind speeds mitigated by intervals of less than 3 ÷ 4 s, this function is an important load characteristic, allowing the estimate of a fatigue resource of the designs. In the case of a normal process, the required information is given by Rice known ratios. Usually, however, it is not possible to use these ratios, and it is necessary to carry out the corresponding processing of a continuous record of the wind.

The local orographical conditions can sharply distort the overall picture. Despite the attempts of many meteorologists to enter individual correction coefficients considering the conditions of the arrangement of meteorological stations, a rather concrete and reasonable technique introducing such amendments is unavailable.

The data of particular meteorological stations and the observations of local experts become necessary at transition to the next

stage - microdivision into districts of the wind conditions of the chosen area. By means of simultaneous measurements for the various directions and speeds of the wind, a plan of isolines of average wind speeds at the height of a weather vane or at the height of an axis of the designed wind power units is made by measurements or calculations. This major stage of search for "the wind rivers" if necessary (especially in the mountain areas) can be carried out by some substages with the subsequent integration of the scale. The topography on the site, mathematical or physical modeling, or even comparative observation of the form of the trees, can be applied (Figure 1.36). Detailed tables connecting the observed deformations of trees with the average wind speed are available. [26]

The wind-driven generators should not be placed close to buildings (Figure 1.37). Denmark used to have a relevant royal decree regulating placement of wind turbines and production constructions.

Figure 1.36 Strong wind with primary direction deforms bushes and trees

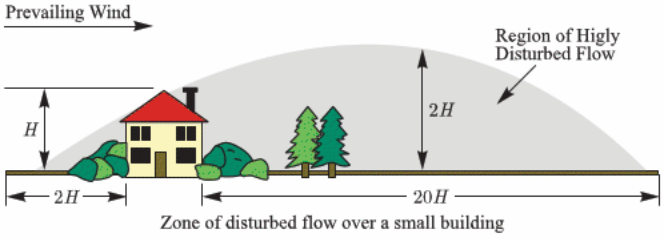

Figure 1.37 Wind-driven generators in the rural areas should not be placed closer than 20 times their height from the buildings.

For the selected site of WPP (Wind Power Plant) placement, an average (by probability) distribution of speeds by height for different seasons of the year must be set. Quasiperiodic components of the wind speeds and spectral characteristics at different heights are specified. Special attention is paid to spatial (by height and in the plan) correlations of speed pulsations (module and direction) at distances of an order of dimensions of the units and the WPP as a whole. This is necessary both for calculation of the power equipment, and for specific strength calculations of the units. Finding the limits of the maximum and minimum correlations among all variety of meteorological situations is important. For the same purposes, the distribution functions of the wind speeds with small mitigation (no more than 3 s) and continuous registration are studied. These functions, at different heights from the ground, differ mainly in the zone of small speeds of the wind. The winds of big force usually cover very thick layers of air – a relative duration of strong winds at different heights differs not too considerably (Figure 1.38).

The wind speed is a stochastic function of time and coordinates with very wide frequency and wave range. Even by consideration of the average monthly speed of the wind, this value preserves the essential features of a casual process, though with significantly smaller dispersion (Figure 1.39). This "smoothed" process accurately shows a climatic periodic component. At the reduction of the mitigation time and the duration of the period included in

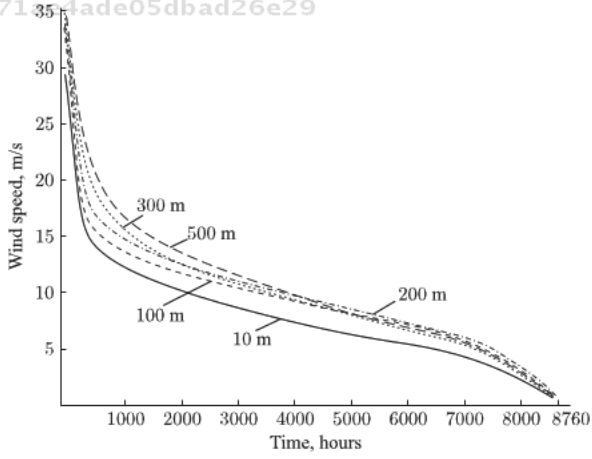

Figure 1.38 The total duration of winds within a year at different heights near Volgograd.

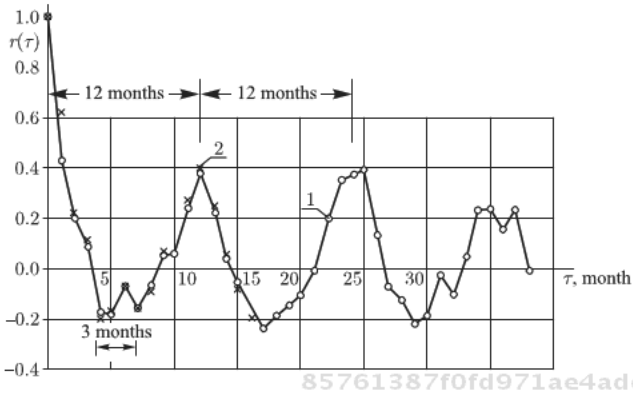

Figure 1.39 Autocorrelated functions of average monthly energy streams (1) and speeds (2) of the wind for the 11-year period over Moscow at the height of 128 m. The annual cycle (period of 12 months) is clearly visible, the seasonal cycle (period 3 of months) is less expressed. $\langle U^3 \rangle = 199$ m^3/s^3, $(u^3)' = 94$ m^3/s^3, $\langle U \rangle = 5.74$ m/s, $u' = 0.76$ m/s.

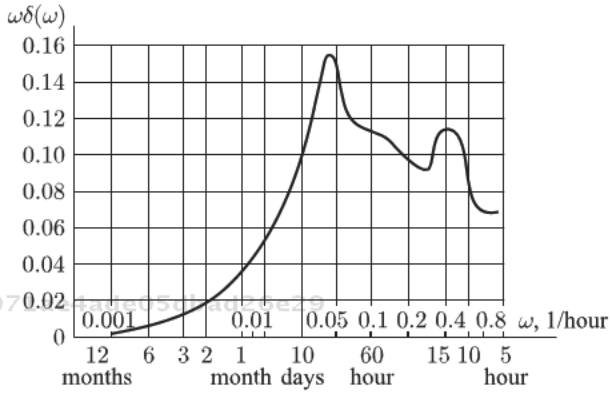

Figure 1.40 Rated spectral density of the wind speed by the measurements in Moscow within a year at the height of 128 m. Disturbances with the period of 5–6 days and 12–16 hours give the maximum contribution to the dispersion.

processing, the lines of the quasiperiodic process are naturally erased. At mitigation, the wind speed within an hour and processing of record of one year, the autocorrelated function allocates a very weak periodic component, demonstrated only in the spectral analysis (Figure 1.40).

The forms of the wind speed ranges at ten-minute and three-second mitigation in the comparable (low-frequency) part are rather close. As for the ratio of the speed dispersions, defined by the relative

duration of the mitigation intervals measured in shares of integrated turbulence scale, it is very varied in practice. An assessment of the contribution of the high-frequency components of the wind speed has been carried out by the selective analysis of the three-hour record of rather stable wind at the height of 15 m around the Volgograd dam (June 08, 1983 from 2PM to 5 PM). The measurements were conducted by a standard revolving object with various intervals of mitigation - 30, 300 and 600 *s*. The average values of the wind speed were naturally close (9,4; 9,1 and 9,0 m/s). The standards of pulsations and correlation coefficients are provided in Table 1.3.

The given example shows that, though reduction of a mitigation interval according to known regularities increases the relative value of the standard of pulsations (approximately up to u'/<U> = 0,2), the absolute value of the variation coefficient of high-frequency pulsations is insignificant, and, taking into account possible mitigation introduced due to inertia of the wind power units, will be even less.

The relative variation of the wind speed and the power on the plugs of the wind power unit considerably decreases at an increase in speed (Figure 1.41).

For one of the sites of the Northern coast of Germany, a systematic analysis of the influence of the averaging interval on the energy stream assessment has been carried out. The relation of the energy streams calculated by average monthly, average daily, or average hourly values of the wind speed to the energy stream, calculated by the average annual value of the wind speed made 1,34, 2,34 and 2,87, respectively. This relation (for one observation point) is not dependent on average (daily or monthly) wind speeds, and that proves the stability of the probability distribution function of the wind speed determined by hourly averaging. Further reduction of the mitigation interval, as well as the transition from annual to two years' averaging, changes the results a little (Figure 1.42).

Table 1.3 Standards of pulsations of the speed (m/s) (diagonal) and the correlation coefficients (*italics*) between pulsations with various intervals of mitigation.

Mitigation interval, s	30	300	600
30	1,81	*0,40*	*0,47*
300		1,68	*0,87*
600			1,18

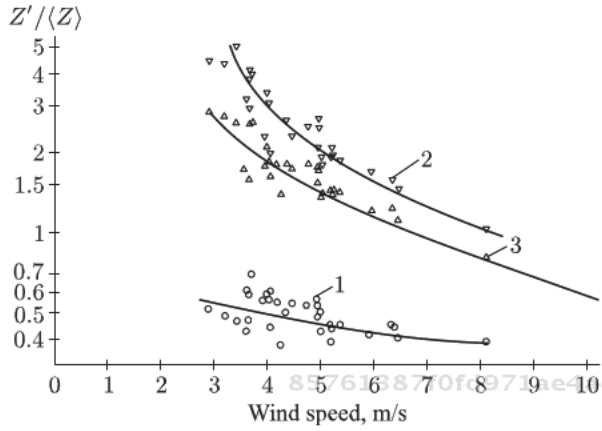

Figure 1.41 Dependence of coefficient of the wind speed variation (1) and power on the wind generator plugs (2, 3) from the average daily wind speed. 1 – wind speed, 2 – power of a traditional collinear wind power unit (Howden-750), 3 – power of orthogonal two-bladed wind power unit (VL-130).

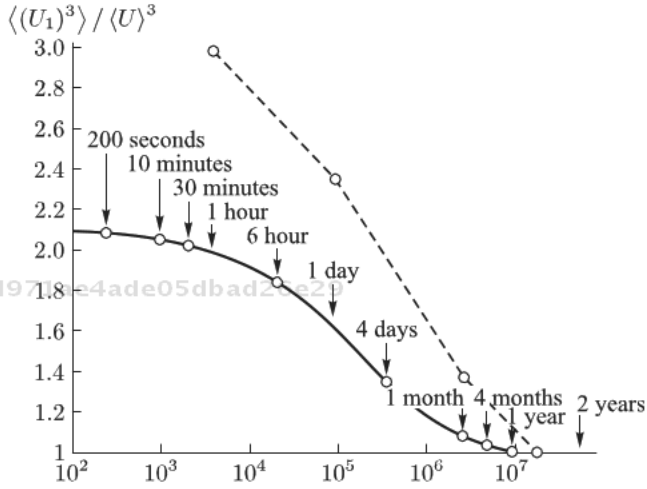

Figure 1.42 Influence of pulsations of various scale on electric energy development.

If to reduce the averaging interval of speeds to T = I s with duration of registration of the process of 10–60 min., a standard wind speed variation can increase considerably, for example, from U′/<U>= 0,063 at T = 200 s to U′/<U> = 0,15 at T = I s.

Consideration of wind pulsations with mitigation less than 30 s from positions of a power system is not of interest. However, it can

matter for calculations of durability of elements of VPR designs. It appears that the transition from mitigation in 30 s to 1 ÷ 3 s at strong winds is able to give a noticeable increase in the standard speed pulsation, especially if the averaging interval does not exceed the minimum characteristic climatic cycle which is easily allocated for records of the wind speed. Thus, according to Richardson, who doubted the possibility of determining the average wind speed, it is possible to offer a system of local "integrated" scales of turbulence for characteristic spectral ranges of the wind turbulence.

These features of the wind mode have been considered when forming the modern meteorological practice according to which the wind speed measured with 10-minute mitigation is considered a little different from the wind speed averaged by 3 hours. Based on the vast meteorological material collected by such a scheme, it is possible to estimate the variability of the wind mode by a set of the data relating to the same climatic (geographical) terms, but in different years.

The results of statistical processing of the set of 26 simultaneous wind measurements in Moscow (h = 85 m), Murmansk (h = 140 m) and Nizhny Novgorod (h = 104 m) are presented in Tables 1.4 and 1.5. The wind measurements results taken in the winter months

Table 1.4 Average value of the wind speed (m/s) determined by a set of measurements within 5 years.

Observation site	$\langle U \rangle$				Per day, m/s
	0h	6h	12h	18h	
Moscow	5,72	5,15	6,00	6,76	5,93
Murmansk	8,88	8,81	7,82	9,55	8,96
Nizhny Novgorod	5,44	5,00	5,64	5,00	5,24

Table 1.5 Coefficient of the wind speed variation in the measurements within 5 years.

Observation site	$u'/\langle U \rangle$				Total, m/s	For average daily speed
	0h	6h	12h	18h		
Moscow	0,38	0,49	0,39	0,42	0,42	0,34
Murmansk	0,48	0,44	0,51	0,51	0,47	0,38
Nizhny Novgorod	0,67	0,64	0,55	0,72	0,65	0,56

Table 1.6 Relative parameters of the wind power average stream.

	$\langle U^3\rangle/(\langle U\rangle)^3$					$(U^3)'/\langle U^3\rangle$
Observation site	0h	6h	12h	18h	For average daily speed	For average daily speed
Moscow	1,47	1,72	1,50	1,57	1,39	1,12
Murmansk	1,73	1,63	1,76	1,83	1,45	1,06
Nizhny Novgorod	2,47	2,46	2,02	2,71	2,04	1,45

(from December 15 to February 15), for 5 years (1975–1979), at the same time - midnight, 6 AM, midday and 6 PM approximately , and at the identical height (about 100 m) are chosen for processing.

Table 1.6 contains the calculation results of the variation of the energy streams measured in the site's points over the same period of time.

As proved by the data in the Tables, the exception of intra daily variation of the wind speed slightly changes the statistical characteristics of the data set as a whole– the coefficients of the data relating to one term of observation are slightly different from those for all data sets. However, mitigation of the data (consideration of average daily speeds of the wind) considerably reduces the variation coefficient (the values in the last column of Tables 1.5 and 1.6 are smaller than in the second column from the right).

In Table 1.6, the relations $\langle U^3\rangle/(\langle U\rangle)^3$ are shown for the periodic observation, and separately for the average daily values. Normally, for urgent observation, the relation $\langle U^3\rangle/(\langle U\rangle)^3$ makes 1,56; 1,74 and 2,42 for Moscow, Murmansk and Nizhny Novgorod, respectively. If considering only the average daily speeds of the wind, the influence of pulsations on the average capacity is naturally less (second right column in Table 1.6). However, the variation coefficient even for the average daily streams of energy is very great – for all three sites it is more than one unit (see the last column in Table 1.6).

A transition from the average daily to the average monthly wind speeds introduces qualitative changes. The data processing of 11 years of observations for Moscow (height 128 m) provides the following for the average monthly speed values:

$$\langle U\rangle = 5{,}74 \text{ m/s};$$

$$\frac{\langle U^3 \rangle}{\langle U \rangle^3} = 1,05;$$

$$\frac{\langle U^3 \rangle'}{\langle U^3 \rangle} = 0,42.$$

As we see, the influence of pulsations of the average monthly speed values on the average energy stream is insignificant.

As proved by the provided analysis, the main increment of an average energy stream in comparison with the energy stream calculated by the average speed, is connected with disturbances of an intra-annual to an intra-daily scale, and probably to scales of higher frequency. Actually, not all variations of the wind power can be perceived by the unit and power loading. Both the unit inertia, and its power characteristic matter. Besides a quantitative assessment of the wind, the quality of wind power in various zones has a great value. The guaranteed total power of the wind streams in different parts of the country or the region is a very important indicator of the wind power mode. At calculations of the output with considerable mitigation intervals of the wind speed (month, year), the actual phase ratios of the wind speeds in different areas are usually not considered. This makes no difference for assessment of an average energy stream. However, for variation of the total power of possible wind power units and estimates of the guaranteed minimum of this power, the specified ratios are very important. The calculation results of correlation coefficients between streams of energy (power) of wind in three points located in the European part of Russia, calculated in winter months for the sets of the wind speeds recorded at the same time, are presented in Table 1.7. Table 1.8 provides the same data for average daily streams of energy. The values $\frac{\rho\langle U^3 \rangle}{2}$ and $\frac{(\rho U^3)'}{2}$ (kW/sq.m) for midnight (00 o'clock) and for 6 AM (top numbers) or for midday (12 o'clock) and for 6 PM are shown on the main diagonal in the top and bottom parts of the table 1.7. The bottom table provides the same data for midday (12 o'clock) and for 6 PM (top numbers).

The diagonal cells of the Tables contain average (by sets) and standard variations of the energy stream (kW/sq.m). The correlation coefficients are specified in the cells over the diagonal. As we

Table 1.7 The parameters of the wind power stream in Moscow, Murmansk, Nizhny Novgorod in the fixed time of a day.

Observation site	Moscow	Murmansk	Nizhny Novgorod
Moscow	0,17/0,21 0,15/0,13	0,17	0,63
Murmansk	0,4	0,76/0,91 0,70/0,88	–0,03
Nizhny Novgorod	0,63	–0,22	0,25/0,41 0,19/0,36

Top part of the Table (above the diagonal) – midnight
Bottom part of the Table – 6 AM

Observation site	Moscow	Murmansk	Nizhny Novgorod
Moscow	0,20/0,27 0,30/0,32	–0,07	0,63
Murmansk	0,50	0,53/0,55 1,00/1,27	–0,10
Nizhny Novgorod	0,29	0,26	0,23/0,35 0,31/0,32

Top part of the Table – midday
Bottom part of the Table – 6 PM

Table 1.8 The correlation parameters of the wind power stream in Moscow, Murmansk, Nizhny Novgorod at daily mitigation (winter months).

Observation site	Moscow	Murmansk	Nizhny Novgorod
Moscow	0,18	0,22	0,48
Murmansk		0,65/0,69	–0,07
Nizhny Novgorod			0,18/0,27

see, the correlation coefficients are rather small and are even negative in several cases. That means, that the total power has to vary significantly less than that of separate stations. For example, if we unite the wind power streams in the considered points (Moscow, Murmansk, Nizhny Novgorod) at 6 AM Moscow time, the average

value of the wind power stream would make 0,34 kW/sq.m at mean square deviation of 0,32 kW/sq.m, i.e., the variation coefficient is about 1,3-fold less, than for one station. If we average the energy streams (for example, in 100 points of the European part of Russia) the variation coefficient of an average energy stream will decrease to approximately 0,1 ÷ 0,2. That means, that the guaranteed (90%) capacity will make 0,88 ÷ 0,76 from the average power for the appropriate time. At the possibility of daily averaging of the power (for example, due to energy accumulation) a low correlation between the wind power streams in different points of the territory of Russia remains (Table 1.8), the variation coefficient of an average energy stream becomes even less, and the share of the guaranteed power is even higher. The arrangement of data on the diagonal in Table 1.8 is the same as in Table 1.7.

The time-space correlation of the wind speed and the streams of its energy in the certain region have been studied in the example of Estonia [27]. It is necessary to emphasize that this example gives the most conservative estimates of the guaranteed average (in space) wind power streams and the corresponding power return of the wind turbines in the region. In the mountain district, for example, in Dagestan or the mountain part of Ural, the spatial correlations have to fade more sharply (at smaller distances); that increases relative values of the guaranteed wind power streams on the average over the region territory.

In Estonia the wind characteristics are rather steady (Figure 1.43)

The variation coefficient of average monthly wind speeds defined within a time period from 1936 to 1980 does not exceed 0,2.

The statistical stability of these observations makes it possibleto track the existence of connections between the average monthly wind speeds in different locations of Estonia. As proved by the correlation analysis, even at such considerable averaging (per month), the wind speeds in rather close locations of Tallinn and Pakri are not connected. The functional and maximum correlation coefficient does not rise over 0,76. The minimum correlation is observed in the summer and makes about 0,5 (Table 1.9). The average values and mean square deviations of the average monthly wind speeds are specified by diagonals of Table 1.9 for the same months - July and January in the same period of observations. If considering hourly observations (with standard ten-minute averaging) during a shorter term (for example, one month) the results turn out a bit differently.

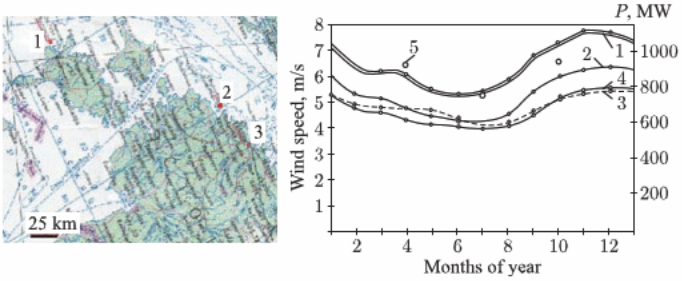

Figure 1.43 Average monthly wind speeds at the level of a weather vane in separate points (1-3) and normally in Estonia (4) in comparison with average power P of the power supply system (5) in the year 1980. 1 – Vilsandi, 2 – Pakri, 3 – Tallinn

Table 1.9 Mutual correlation between the average monthly values of the wind speeds in three locations in Estonia in July (above the diagonal) and in January (below the diagonal).

Measurement site	Vilsandi	Tallinn	Pakri
Vilsandi	5,4/0,74 *7,6/1,15*	0,54	0,51
Tallinn	*0,75*	4,5/0,81 *5,6/1,1*	0,56
Pakri	*0,76*	*0,69*	4,8/0,8 *6,6/0,94*

Table 1.10 presents the autocorrelation values of the wind speeds in Vilsandi (above the diagonal) and in Pakri, calculated by the sets of the data of urgent measurements within 30 days in January, 1980.

The average values and standard changes of the wind speed in the corresponding periods of measurements are specified on the diagonal.

The results of the same calculations, but performed for the stream of the wind power proportional to the cubed wind speed, are presented in Table 1.11. The data of both

Tables shows that on the islands (Vilsandi) a rather high correlation remains, at least within 6 hours. In the continental coastal zone (Pakri), the wind changes more quickly – a high correlation remains for a shorter time.

Table 1.10 Autocorrelation of the wind speeds at different times of day in January, 1980.

Time of day	0	3	6	9	12	15	18	21
0	5,3/2,9 *4,8/4,2*	.65	.82	.66	.61	.56	.36	.31
3	*.91*	5,2/2,7 *4,7/4,2*	.62	.53	.44	.32	.15	.21
6	*.87*	*.88*	5,6/2,8 *5,2/4,1*	.88	.76	.71	.55	.56
9	*.73*	*.72*	*.82*	5,8/3,0 *5,6/3,2*	.86	.78	.64	.61
12	*.54*	*.56*	*.62*	*.88*	5,6/3,0 *5,7/3,8*	.83	.61	.49
15	*.25*	*.30*	*.30*	*.58*	*.84*	5,8/3,1 *5,8/3,9*	.81	.62
18	*.30*	*.36*	*.32*	*.56*	*.82*	*.95*	5,4/2,9 *5,7/4,5*	.77
21	*.27*	*.36*	*.28*	*.50*	*.74*	*.88*	*.94*	5,8/2,8 *5,4/4,2*

The diagonal contains average values of the wind speed cube and the deviation standard of this value from the average value.

The data of Tables 1.10 and 1.11 allow an integral estimation of the proximity degree of the wind speed probability distribution measured in fixed terms to the Weibull law. The ratios between an average speed cube and the average speed cube $\frac{\langle U^3 \rangle}{\langle U \rangle^3}$, and also the variation coefficients of the wind speeds $\sigma_U = \frac{U'}{\langle U \rangle}$ and the energy streams $\sigma_{U^3} = \frac{\left(U^3\right)'}{\langle U^3 \rangle}$, shown in Table 1.12, serve as material for comparison.

The settlements of Vilsandi and Pakri belonging to one geographic zone are located rather close to each other. However, the

Table 1.11 Autocorrelations of wind power streams at different time of a day in January, 1980 in Pakri.

Time of day	0	3	6	9	12	15	18	21
0	293/399 *493/1461*	.54	.72	.61	.48	.64	.53	.26
3	.98	255/285 *480/1442*	.73	.71	.69	.54	.40	.49
6	.88	.98	325/429 *537/1477*	.86	.85	.77	.65	.65
9	.86	.79	.86	379/527 *373/650*	.93	.85	.78	.63
12	.48	.45	.50	.69	368/593 *454/642*	.81	.69	.60
15	.08	.09	.09	.19	.77	382/618 *503/897*	.93	.62
18	.14	.16	.24	.23	.81	.93	321/507 *634/1210*	.69
21	.06	.09	.07	.16	.71	.82	.96	5,8/2,8 *5,4/4,2*

Table 1.12 Probability distribution parameters of the wind speeds and the wind power streams by measurements at different times of day.

Site	Parameter	0h	3	6	9	12	15	18	21h
Vilsandi	$<U^3>/<U>^3$	1,97	1,81	1,85	1,94	2,10	1,96	2,04	1,70
	σ_U	0,53	0,52	0,50	0,52	0,54	0,53	0,54	0,48
	σ_U^3	1,36	1,12	1,32	1,39	1,61	1,62	1,58	1,22
Pakri	$<U^3>/<U>^3$	4,46	4,62	3,82	2,12	2,45	2,58	3,42	3,32
	σ_U	0,88	0,89	0,79	0,57	0,67	0,67	0,79	0,78
	σ_U^3	2,96	3,00	2,75	1,74	1,41	1,78	1,91	2,04

wind power parameters in these two places appeared significantly different. Variability of the wind over the continental coast was significantly higher. If judging by the ratios $\frac{\langle U^3 \rangle}{\langle U \rangle^3}$, in Vilsandi the parameter χ in the Weibull distribution changes from 1,85 to 2,3, on

average at 2,0. In Pakri this parameter changes from 1,15 to 1,86, on average $\chi \approx 1.3$.

Though in Pakri the average wind speed is less than in Vilsandi, the average energy stream in Pakri appears greater. However, this does not mean, that the wind power mode in Pakri is more favorable. On the contrary, a big variability in the wind will demand overestimation of the relative power of electric equipment and will cause some rise in the price of energy and decrease in its quality. Mutual correlations between speed and power of the wind streams in different locations of Estonia at a characteristic hour of the maximum of power loading on the system (9 AM) are shown in Table 1.13.

The average values of the wind speeds and variation standards are shown above the diagonal, and the average values and variation standards of the speed cube – below the diagonal. As we see, all correlations are positive; however, their values, especially the correlations between the energy streams are insignificant. That is, creation of the joint wind power system even in such a small territory as Estonia is able to provide an essential decrease in power pulsations and guarantee delivery of a certain power (Figure 1.44).

Table 1.13 shows that the distance between Tallinn and Pakri (40 km) is critical in this case, since a closer relative positioning of the wind power stations is inexpedient. The characteristic schedules of change of the wind speed by days and by seasons testify to the possibility of the guaranteed participation of the wind power plants

Table 1.13 Mutual correlation between the wind speed (above diagonal) and the wind power streams (below diagonal) in the characteristic locations of Estonia by the measurements at 9 AM in January, 1980.

Locations	Vilsandi	Pakri	Tallinn	Kunda
Vilsandi	5,83/3,04 *379/528*	.66	.49	.46
Pakri	*.35*	5,61/3,17 *373/650*	.70	.48
Tallinn	*.18*	*.63*	3,61/2,24 *110/194*	.34
Kunda	*.31*	*.10*	*.09*	4,13/2,35 *151/246*

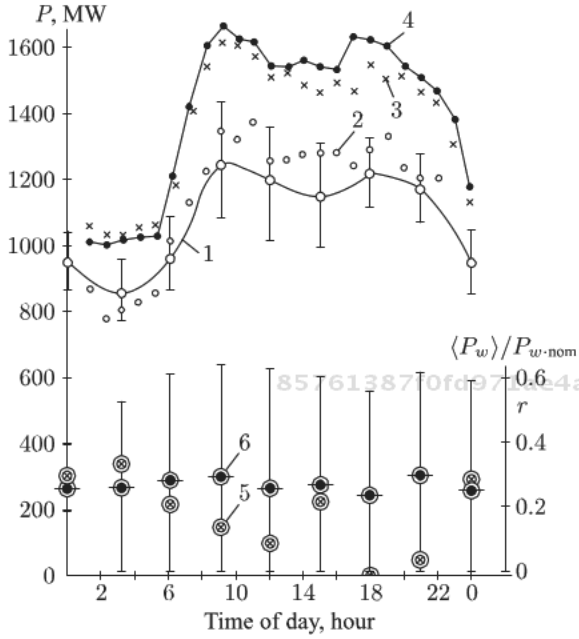

Figure 1.44 Loading of the power system of Estonia, average (line 1) for January, 1980, in comparison to the real production schedules recorded on January 15, 1980 (points 2), January 15, 1986 (points 3) and December 16, 1986 (points 4). The relative average capacity of the wind power stations in January, 1980 which could operate on Vilsandi (+/−the standard of pulsations) – points 6, and the correlation coefficient r (point 5) between the wind power station capacity and the power supply system loading.

in covering of the loading schedule of the power supply systems. Such calculations have been performed for different regions of the European part of Russia (Figure 1.45).

Still, great opportunities for inclusion of the wind power stations into the production schedule of the power supply systems are provided by connection of WPS to hydroelectric power stations, even to the ones with small reservoirs. Possible power return of WPS and small hydroelectric power stations usually have maxima in different seasons of the year (Figure 1.46), that increases efficiency in the use of these objects in a complex.

The above examples show the importance of detailed micro-wind power division of a location into districts. Within micro-division into districts, it is necessary to study in detail the instant distribution of the wind speeds by a vertical, the statistical characteristics of flaws. The examples of such research for conditions in the Moscow

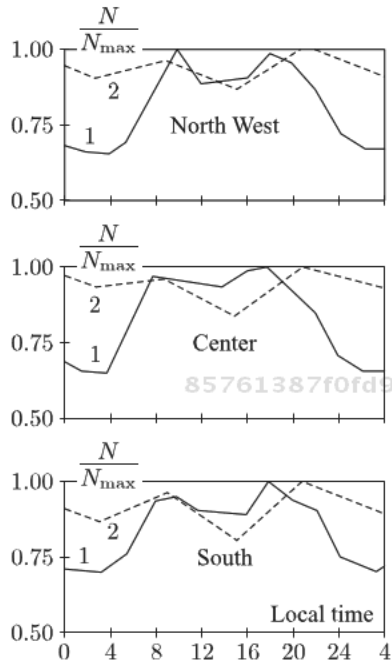

Figure 1.45 The relative daily production schedule of the power supply systems of the European part of Russia (1) and the average distribution for the long-term period of the relative wind power in winter, averaged by the system territory (2).

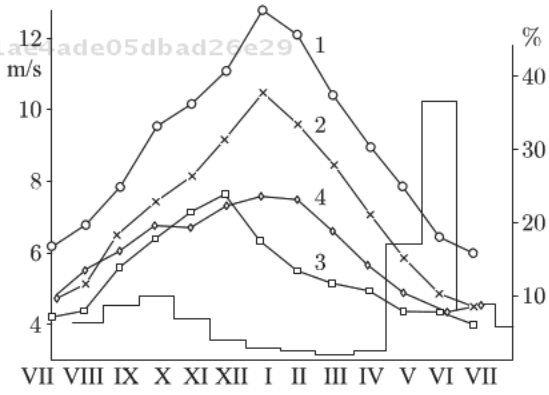

Figure 1.46 Change of the average monthly wind speeds in different points and the relative river drains of the Kola Peninsula within one year.

region (Obninsk) show that the distribution of the wind speeds by height, even in 10 minutes on average, may be very various, including a local maximum. The gradient of the wind speed by height greater by the module 0,14 1/s us quite common. The assessment of probabilities of big gradients of speed is one of problems of microdivision into districts.

The integrated assessment of the wind power potential of particular regions is of interest. It is clear that in these estimates it is impossible to base only on the data of the wind mode existing before construction of WPS – availability of wind-driven generators will change the wind situation.

The author has proposed [28] to estimate the wind power potential on the dissipation speed of mechanical wind power in the mass of the atmosphere over the respective territory. The role of wind power converters at such treatment of the wind potential is that, in some volume W_A, the speed of dissipation of energy decreases by $\Delta\varepsilon$ (usually at the expense of the current speed reduction in the wind power unit zone - a similar effect of the dissipation speed reduction at the expense of the current speed reduction takes place in reservoirs of hydrostations). In global estimates, such an approach does not yield contradictions, but in the local estimates it is less convenient, as the energy transfer processes are able to play an essential role.

Believing the dissipation speed for the atmosphere as a whole to be in the range 2,3 ÷ 10,4 cm^2/s^3 (the most reliable assessment 7,1 cm^2/s^3), we find the wind power potential of all the atmosphere of the Earth (weight $5{,}3\ 10^{18}$ kg) = $1{,}2 \div 5{,}4 \cdot 10^{12}$ kW (the most reliable $3{,}8 \cdot 10^{12}$ kW) [29]. This exceeds, by more than 2 orders, the full energy potential of the rivers of the whole world, as the wind closes the water circulation cycle in the nature, supporting the existence of rivers and lakes. Here the capacity of the wind power stations should be understood as an average value for a long period – for example, in a year, that is 3-4-fold less than the rated capacity.

The land area of the countries, for example, in the territory of the former USSR makes $2{,}2 \cdot 10^{13}$ m^2, the weight of the atmosphere over this territory is $2{,}3 \cdot 10^{17}$ kg. If we accept that the dissipation speed here is the same as the average for the whole Earth 7,1 cm^2/s^3, the wind potential of these territories is estimated by $1{,}6\ 10^{11}$ kW or $1{,}4\ 10^6$ billion kW·hour/year. This energy exceeds the needs of all mankind 10-fold, provided that the population number reaches 8 billion people, and energy consumption per capita will increase twice in comparison with the modern level in the most developed countries.

Certainly, the dissipation speed of mechanical wind power cannot be reduced to zero, as it practically takes place in hydroelectric power station reservoirs. The expedient value of wind power selection is defined by technical and ecological conditions. For example, if we consider a single wind power unit, choosing its operation mode to obtain the maximum capacity at a preset wind speed at a distance from the unit, the relative change of dissipation speed in the unit zone is given by:

$$\Delta\varepsilon/\varepsilon = (1 - u^3/U^3) = 0.80 \div 0.88 \qquad (1.74)$$

Where $u = (0{,}5 \div 0{,}55)U$ - stream speed in the unit zone in the operation conditions with the maximum power efficiency. At mass construction of wind power units, such strong reduction of the wind speed (1,8 ÷ 2-fold) practically can not be accepted owing to ecological restrictions. Therefore, a real wind potential of particular regions has to be determined not only by the stream of wind power proportional to the third degree of the local wind speed, but also taking into account the particular technical means of its use, real topographical and ecological restrictions.

According to representations (1.33) and (1.45), the unit capacity at a fixed speed of blades is either constant at small and high wind speed ($U<U_1$, $U>U_N$), or linearly depends on the wind speed. If the speed of the wind power unit blades with the fixed geometry changes in proportion to the wind speed providing the maximum power efficiency of the unit, its capacity in an interval:

$$U_1<U<U_N$$

is proportional to U^3 and constant outside this interval. Thus, the energy developed by the unit is defined by its rated capacity, the wind mode, and the speed parameters U_1, U_N, and U_M,
where

U_1 – wind speed corresponding to the conditional beginning of power delivery,

U_N – wind speed corresponding to the rated (established) unit power,

U_M – storm wind speed at which the unit stops.

It is expedient to appoint the speed of U_M to make the loads to the design such that the wind load is below that of a parked car at the greatest possible (standard) wind for a particular region in which

the unit placement is planned. The parameters U_1, U_M poorly influence the average annual maximum possible output of the unit. The main role is played by the ratio $U_N/\langle U\rangle$ and the function of distribution of the wind speeds. For distribution of probabilities of wind speeds F(U) by the Weibull law (1.62), the average capacity <p> is given by:

$$\langle P\rangle/P_N = C/(U_N - U_1)\,\psi(x,y) + F(U_M) + U_1/(U_N - U_1)$$
$$F(U_1) - U_N/(U_N - U_1)\,F(U_N) \qquad (1.75)$$

$$\psi(x,y) = \int z^{1/\chi} \exp{-z}\, dz_y^x \qquad (1.76)$$

$$x = U_N/C,\ y = U_1/C \qquad (1.77)$$

The characteristic values relating to Weibull distribution are given in the table 1.14.

In actual practice, when standard wind power units are used, the average capacity produced by a wind power unit within one year is practically defined by the average annual wind speed (Figure 1.47),

Table 1.14 Speed ratio and power generation with different parameter Weibull distribution.

χ	1	1.5	2	2.5	3
$C/\langle U\rangle$	1	1.11	1.13	1.13	1.12
$U'/\langle U\rangle$	1	0.68	0/53	0.42	0.36
$\langle U^3\rangle/\langle U\rangle$	6.00	2.71	1.92	1.57	1.36

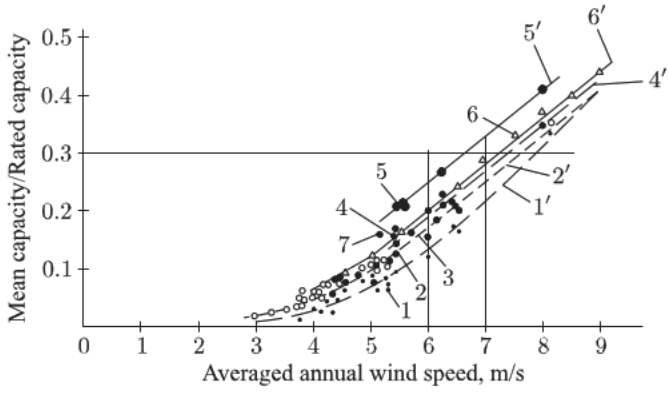

Figure 1.47 Average annual capacity of a wind turbine in rated capacity shares (Relative mean power) as the average annual speed of a wind for various areas and units of various type.

and at the average wind speed 6–7 m/s does not exceed 25–30% from the rated capacity.

References

1 T.Burton, D.Sharpe, N.Jenkins, E.Bossanyi, Wind Energy. Handbook, John Willey&Sons, Ltd, 2005, 617p.
2 V.M. Lyatkher, A.M. Prudovsky. Hydraulic simulations, Moscow, Energoatomizdat, 1984, 392 pp.
3 V.M. Lyatkher, A.M. Prudovsky. Researches of open streams on pressure head models, Moscow, Energy, 1971, 288 pp. On page 3 must be [2, 3].
4 Gijs A.M. van Kuik, The Lanchester–Betz–Joukowsky Limit, Wind Energ. 2007; 10:289–291. A.Betz, Schraubenpropeller mit geringstem energieverlust. Gottinger Nachr., 1919, Germany, B.B.Kazhinsky, Windpower installation. GIZ. M-L, 1928, 311 pp, Le Gourieres, Wind Power Plants, Pergamon Press, 1982, 285p., E.E. Schpilrein, Renewables and their prospects for Russia, collected works: Power engineering of Russia. Problems and prospects, M. "Science", 2006, p. 284 - 292.
5 M.I. Gurevich, Theory of streams of true liquid, Fizmatgiz, M, 1961, 496 pages.
6 Gorban' A.N., Gorlov A.M., Silantyev V.M. Limits of the Turbine Efficiency for Free Fluid Flow, Journal of Energy Resources Technology, ASME, 2001, v. 123, pp.311–317.
7 M.A.Lavrentyev, B.V.Shabat. Problems of hydrodynamics and their mathematical models, "Science", M. 1977.
8 G.H. Sabinin, Theory of an ideal wind-driven generator, TSAGI, issue 32, No. 200, M, 1927.
9 Wind Turbine Technology. Fundamental Concepts of Wind Turbine Engineering. Editor David A. Spera, ASME Press, 1994, 638 p.
10 Stolyarov G.I., Tabachnikov V. G. Some features of aerodynamic of wings of big lengthening at small Reynolds numbers, Works of TSAGI, M. 1985, issue 2290, M. 1974, issue 1621.
11 Ashwill T.D. Measured Data for Sandia 34-meter Vertical Axis Wind Turbine, SAND91–2228, Unlimited Release Printed July 1992.
12 N.G.Gvazava, S.L.Zubkovsky, V.M.Lyatkher, et al. Impact of air turbulent flow on wind power installation, News of Academy of Sciences of the USSR, Power engineering and transport, 1990, No. 2, p. 116-124.
13 A Review of the Current Status of the Wind Energy Innovative System Projects, Solar Energy Research Institute (SERI), 1980, Washington.
14 V.Lyatkher, Dam-Free Hydro-Power Plant, Patent US 8177477 B2, May 15, 2012.
15 William McKinney and James De Laurier (Inst. Aerospace Studies, Univ. of Toronto, Canada), The Wingmill: An Oscillating-Wing Wind turbine, 1980.

16 Grebeshov E.P. Sagoyan O.A. hydrodynamic characteristics of the fluctuating wing functioning as a bearing element and the propulsion unit, Tr. TSAGI, issue 1725, M 1976, p. 3–30.
17 Goodarz Ahmadi, Performance of an Angular Flange Aeroelastic Wind Energy Converter, J. Energy, TN vol.7, NO.3, 1983, pp.285–288
18 E.Naudascher, D. Rockwell, Flow-Induced Vibrations. An Engineering Guide. Dover Publications, Inc., Mineola, N-Y., 2005, 414 p.
19 Krasovsky A.A., Misrikhanov M. Sh., Bases of the theory and technique of creation hydro and wind power installations of a new class, M. Energoatomizdat, 1995. A.A. Krasovsky, M. Sh., Misrikhanov. Modular wind power installations with operated oscillating movement, Power systems, 2003, No. 1.
20 In Russian works, four-parametrical distribution is often used, which differs a little from (1.62).
21 The equipment is developed and made in the IFA Russian Academy of Sciences by M.M.Fedorov.
22 Minin V.A. Basic elements of the wind power inventory of the North European part of the USSR. Problems of a power engineering of Murmansk region and neighboring areas. Academy of Sciences of the USSR, Kola branch, Apatity, 1980.
23 Monin A.S. Yaglom A.M. Statistical hydromechanics. H. I. M: Science, 1965, h. 2, 1967; V.M. Lyatkher, Turbulence in hydroconstructions, 1968, M. "Energy", 408 pages.
24 Byzova N. L. Volkovitsky Z.I. Mazurin N. F. Sergeyeva I.A. Statistical characteristics of wind speed in relation to wind load capacities. VNIIGMI-MTSTS, issue 2. Obninsk, 1983.
25 Gumbel J., Statistics of Extremes. — New York: Columbia University Press, 1958.
26 Hewson E.W., et al., Vegetation as an indicator of high wind velocity. RLP/2227-T24–79/1, Oregon State University, Dept.Atm.Sci., 1979.
27 V.M. Lyatkher, I.Ya.Roos. Transfer and energy distribution in regions of the North, 1989, p. 25–34.
28 V.M. Lyatkher. Wind power stations of big power. - M: Information power, 1987. - 72 p.
29 Monin A.S. Shishkov Yu.A. Climate history. L. : Hydrometeo publishing, 1979.

2

Collinear Wind Turbines (Horizontal-Axis Wind Turbines-HAWTs)

The collinear units with parallel spin axis (Figure 2.1) [1] are represented by the following equipment: high-speed with narrow blades of asymmetrical aerodynamic profile (1), and low-speed with a large number of rather wide blades (2). Sometimes these units have shutters (for reduction of loading on the blade in storms). The high-speed units are usually preferable for electric power generation, and the low-speed units are better aggregated with various mechanical devices (for example, wind or water-mills).

Low-speed units of the old design develop a high torque previously used for driving water pumps (Holland), or grain grinding millstones (Russia).

The wind power generators appeared rather recently (Figure 2.2).

The modern low-speed units (Figure 2.3) are convenient for driving pumps in a complex, in particular, in water treatment systems designed by the membranous technologies demanding rather high pressure. The effectiveness of these machines is good enough. Besides, they have a low runaway speed (Figure 2.3).

The Russian tragopogon, hint mills of the last century, multiblade slow "Americans" mills, and the modern huge one or three-blade wind mills with horizontal or slightly inclined spin axis

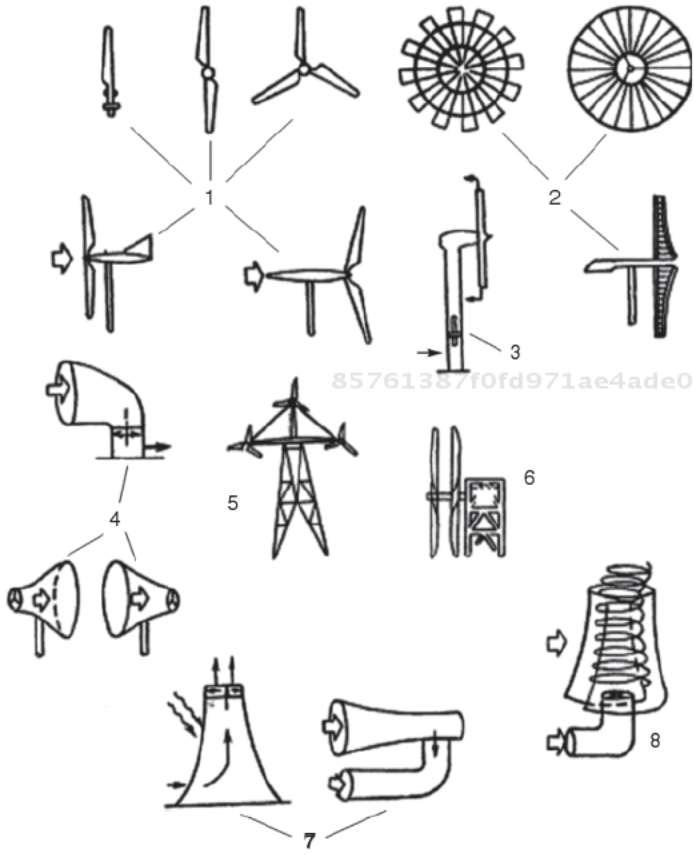

Figure 2.1 Designs options of collinear power units.

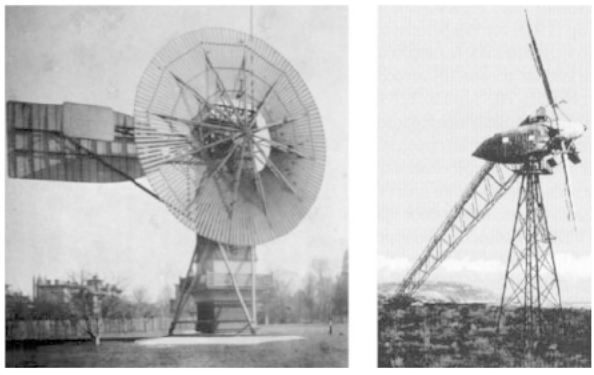

Figure 2.2 Brush wind power generator. Cleveland, USA, 1888 (left). Wind power high-speed unit. 100 kW. Balaklava, Crimea, USSR, 1931 (right).

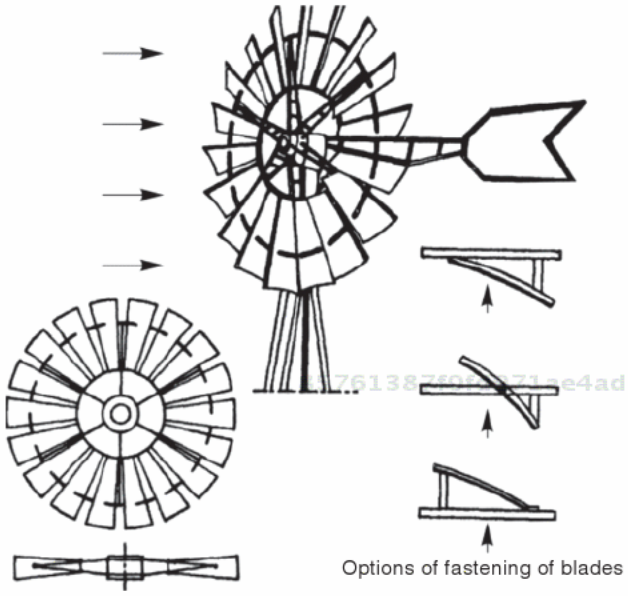

Figure 2.3 Modern low-speed wind power unit ("American").

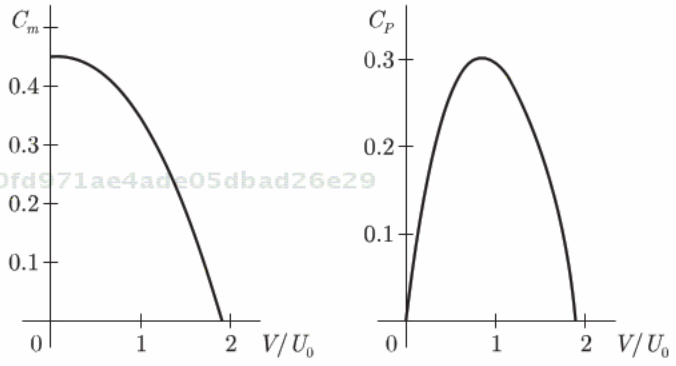

Figure 2.4 Moment coefficient (left) and effectiveness of the unit of Figure 2.3.

operate by the one power principle. According to this principle, a wind unit creates resistance to wind within a circle swept around by the blades, thus causing a concentrated pressure drop Δp on this imaginary (swept around) circle, and reduction of a longitudinal component of the air speed to value U, less than the wind speed

U_0 away from the wind unit. Thus, the airflow loses a particular capacity of P in the borders of the wind unit. All this capacity is transferred, in an "ideal" case, to the wind unit. In actual practice, it partly turns into energy of the turbulent pulsation movements arising for the wind turbine, including into energy of the screw movement, characteristic of collinear units. Very productive estimates are given in part 1, leaning on the zero-dimensional ratios allowed to estimate the maximum value of the efficiency of the unit, depending on various additional conditions which the zero-dimensional problem definition allows [2].

The equation of the momentum quantity preservation, written for a stream tube formed by the streams passing through the circle swept around by the ends of the unit working blades, is given by (Figure 2.5):

$$\rho U_0 Q + p_0 \Omega_0 - (\rho U_2 Q + p_2 \Omega_2) + [\beta_1(p_- - p_0) + p_0](\Omega - \Omega_0) + [\beta_2(p_+ - p_2) + p_2](\Omega_2 - \Omega) = (p_- - p_+)\Omega; \quad (2.1)$$

where U – flow rate of the environment through the disk surface imitating the unit; U_0, U_2, – wind speed in front of and behind the unit respectively; p – p + – pressure in front of and behind the unit, respectively; Ω_0, Ω, Ω_2 – stream tube area in the respective cross-sections 0, BA and 2 shown in Figure 2.5.

The equation (2.1), as usual, does not consider the tangential stress operating on the allocated volume surface, but unlike the traditional schemes, the coefficients β_1 and β_2 consider the pressure change on this surface.

Let us add to the equation (1) a moment-of-momentum equation, imposing restriction on tangential components of the flow rate in front of the unit $U_{\varphi-}$ and behind it $U_{\varphi+}$.

$$\rho \int (U_{\varphi+} - U_{\varphi-}) U r d\Omega = -M, \quad (2.2)$$

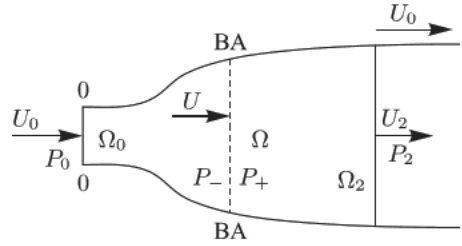

Figure 2.5 Scheme of the unit flowing around.

where $M = P/\omega$ –torque operating on the unit; ω –circular rotation frequency; P –capacity received by the unit.

Bernoulli equations are written separately for the current sites in front of and behind the unit. Having selected the values U_0 and $\rho U_0^2/2$ as scales of speed and pressure, we obtain the following set of equations:

$$2u - 2u_2 u + \beta_1 p_- (1 - u) + \beta_2 p_+ (u/u_2 - 1) = p_- - p_{+;} \quad (2.3)$$

$$u_{\varphi-}^2 + u^2 + p_- = 1; \quad (2.4)$$

$$u_{\varphi+}^2 + u^2 + p_+ - u_2^2 = 0; \quad (2.5)$$

$$2/3(u_{\varphi+} - u_{\varphi-})z = -[u_{\varphi-}^2 + p_- - u_{\varphi+}^2 - p_+], \quad (2.6)$$

where $z = \omega R/U_0$; R – radius of the swept-around disk.

The ratio between the stream rotation speeds in front of and behind the unit

$$\beta_3 = U_{\varphi-}/U_{\varphi+}; \quad (2.7)$$

as well as values of coefficients $\beta_{1,2}$ cannot be found from the given zero-dimensional equations; they are defined by solution of the complete aerodynamic problem.

The possible range of values of these parameters, defined from physical restrictions is:

$$0 \le \beta_{1,2} < 1;$$
$$-1 \le \beta_3 < 1$$

For example, at $\beta_1 = \beta_2 = 0$ and $U_{\varphi-} = U_{\varphi+} = 0$ we obtain the result of A. Betz and N.E. Zhukovsky.

$$C_D = p_- - p_+ = 4(1 - u)u \quad (2.8)$$

Introduction of a "vortex solenoid" with hypothetical properties into the system consideration is actually equivalent to some express hypotheses concerning β_1, β_2, u_{q-} and u_{q+}, allowed to obtain another ratio of C_D [3]

$$C_D = 4(1 - u)/2 - u \quad (2.9)$$

The ratio (2.8) yields the underestimated results at $u \to 0$ (impenetrable disk). On the contrary, the ratio (2.9) overestimates the

pressure difference on the low-permeable disk. In the range u>0,7 the difference of calculations by (2.8) and (2.9) is insignificant. It can be interpreted as a weak influence of the stream twist in the specified range of the relative speeds.

Having set the values β_1, β_2, β_3 and z, it is possible to construct by (2.3) – (2.6) a series of dependences $C_D = C_D(u)$, corresponding to different conditions (Figure 2.6).

In conditions when it is possible to neglect the flow twist, the prime model in which a real wind power unit is replaced with a disk with the sources evenly distributed on its surface (right) and the drains (left) seems the most natural. Numerically solving a corresponding problem for the Euler equations [4], it is possible to find a dependence of $C_D = C_D(u)$ and, in particular, to define the coefficient values β_1, β_2, corresponding the accepted model.

This solution (Figure 2.6) is matched with the test data on flowing of an impenetrable disk ($u \to 0$). However, this solution considerably differs from the results by (2.8) – (2.9) in all range u. The obtained result means that the assumption of pressure invariance on the tube surface of type ($\beta_1 = \beta_2 = 0$) – the ratio (2.8) – contradicts the assumption of uniform distribution of longitudinal speeds in the unit zone.

The results of the numerical experiment shown in Figure 6 can be generalized by the formula:

$$C_D = C_D^{\,0}(1 - u^m), \qquad (2.10)$$

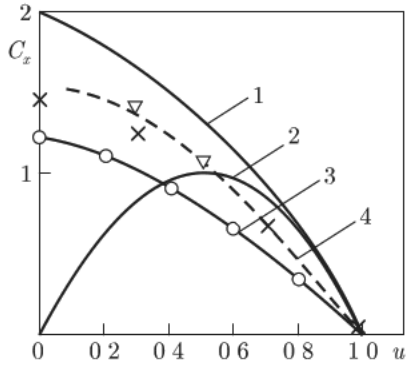

Figure 2.6 Dependence of the relative pressure drop on the unit from the relative traveling speed of the medium in the unit. The models: 1 - G. H. Sabinin, 2 - Betz-Zhukovsky, 3 - calculation for free stream, 4 - calculation for wind tunnel conditions.

where $C_D^0 \sim 1{,}2$; $m \sim 1{,}6$.

The power selected by the unit from the stream, at a small twist influence, is given by:

$$P_0 = \Delta p U \Omega, \tag{2.11}$$

where $\Delta p = p_- - p_+$.

Usually this power is associated with the power perceived by the unit, given by:

$$P = C_P(\rho U_0^3/2)\,\Omega, \tag{2.12}$$

where $C_P = C_D u$ – the capacity factor of the stream power (in the Russian works on wind power the designation ξ or C_N is used).

If we accept:

$$P = P_0,$$

then:

$$C_P = uC_D(u) \tag{2.13}$$

In actual units there are no bases for the assumption (2.13), since a part of the flow energy will be transformed into a large-scale turbulence and is not used by the unit. The equality (2.13) can be accepted as a definition of an "ideal" unit in which all energy lost by the stream (2.11) is transferred to the unit (2.12).

The ratios $C_D = C_D(u)$ (or $C_P = C_P(u)$) do not yet allow us to find the particular values C_D and C_P depending on the design data of the units. However, by these ratios it is possible to estimate the maximal speed values $(C_P)_{max}$ and the rates corresponding to them $(u)_M$ (Table 2.1).

Table 2.1 Maximal values of electrical power factors.

Coefficients	Model		
	Betz-Zhukovsky	Sabinin	The author
$(C_P)_{max}$	0,59	0,69	0,41
$(u)_m$	0,67	0,59	0,53

The maximal values of the electrical power factor by the author model are much lower, than those by models of Betz-Zhukovsky and especially G.Kh. Sabinin. The extensive experimental data gives the values $(C_p)_{max}$, close to the calculations of the author: no values greater than $C_p = 0{,}42$ (usually $(C_p)_{max} = 0{,}31–0{,}38$) have been recorded in the free stream in the experiments. In the wind tunnels the maximal values of C_p reached 0,47 [5], that can be partly explained by the influence of the pipe walls. The mitigated results of field tests of the actual large turbines yielded the effectiveness values reaching 42%. In small machines C_p did not exceed 30% (Figure 2.7).

Apparently, the results of Betz-Zhukovsky and Sabinin do not give actual asymptotic estimates for parameters of collinear units.

For the complete solution of the problem and determination of the physical value (u), in the scope of the zero-dimensional model of the elementary ratios of the wing theory, defining the load components of the blade, operating perpendicular to (q_n) and parallel to (q_L) the chord of the blade profile (Figure 2.8):

$$q_n = \tfrac{1}{2}[C_y(\alpha)\cos\alpha + C_x(\alpha)\sin\alpha](r^2\omega^2/U^2 + 1); \quad (2.14)$$

$$q_L = \tfrac{1}{2}[C_y(\alpha)\sin\alpha - C_x(\alpha)\cos\alpha](r^2\omega^2/U^2 + 1); \quad (2.15)$$

$$q_{n,L} = 2q_{n,L}/\rho U^2; \quad (2.16)$$

$\alpha = \text{arctg}\,(U/\omega r) - \varphi_0$

where α – an angle of attack on the blade element located at distance r from the spin axis; φ_0 – angle of the profile chord turn in relation to the blade speed.

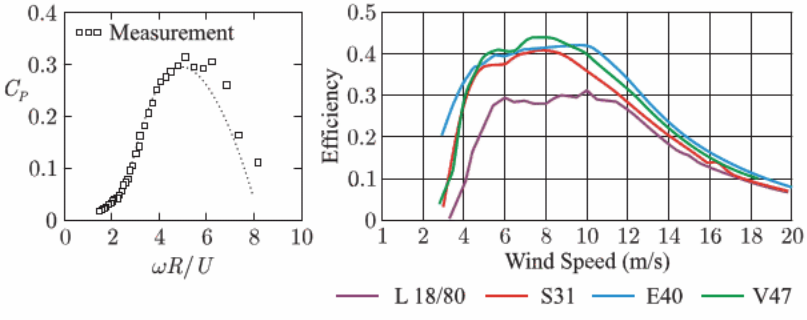

Figure 2.7 Results of field trials of small turbines (left) [6] and serial turbines of diameter to 47 m. [7]

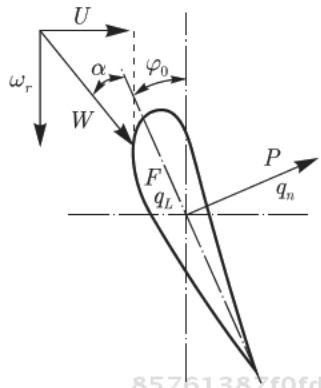

Figure 2.8 Scheme of the blade flowing around.

At known loadings, q_n and q_L the average (for a turn) pressure force operating on the unit is calculated, and the pressure coefficient is defined as:

$$C_D = i[P \cos \varphi_0 - F \sin \varphi_0] u^2; \quad (2.17)$$

$$P = 1/\Omega \int b q_n dr; \quad (2.17a)$$

$F = 1/\Omega \int b q_1 dr$

where the integrals in the right member are calculated by all lengths of the blade; i - the number of blades.

The equation (2.17) together with the equation (2.10) (accepted with the equation (2.8) or (2.9) before) close the system and allow us to find the speeds (u) in the unit zone.

The capacity developed by the unit is defined by the moment of pulling forces operating on the blade and the unit rotation frequency:

$$C_P = iz_u[M_p \sin \varphi_0 + M_F \cos \varphi_0]u^3; \quad (2.18)$$

$$M_p = 1/R\Omega \int b q_n r dr; \quad (2.18a)$$

$M_F = 1/R\Omega \int b q_L r dr;$

$z_u = \omega R/U$

The values P and M_p characterize the dimensionless value of the shear force and the moment in the blade basis, operating off the blade plane; F and M_r – the same in the blade plane (Table 2.2). For obtaining the dimensional values of forces (moments) the

Table 2.2 Maximum values of forces and moments acting on the blades ( ).

	Rapidity $z_u = \omega R/u$													
	2		**4**			**6**		**8**			**10**		**12**	
(10CP)	5	5	13	13		29	29	50	50		78	75	114	102
	6	6	15	15		33	31	55	50		82	72	113	95
	5	5	11	11		24	23	42	37		64	49	88	60
(100 | M_P |)	3	3	10	10		21	21	37	36		57	53	83	72
	4	4	11	11		24	22	40	36		59	51	81	67
	3	3	8	8		17	17	31	26		47	34	63	41
(100 | F |)	9	9	13	8		25	25	52	52		89	80	140	99
	7	6	25	25		54	47	88	67		125	82	161	93
	2	2	7	6		20	20	42	38		73	47	107	53
(1000 | M_F |)	7	7	13	8		22	22	44	44		70	56	108	70
	6	5	20	19		40	34	63	46		88	55	113	61
	2	2	7	6		18	18	36	30		61	34	83	35

Notes:

1. The data in Table 2.2 are related to the profiles "Espero", NACA 4415, NACA0012.
2. The first column of figures in each cell – at a change of turn corner of the blades (φ_0) in the range from "-4" to "+10°"; the second column – at (φ_0) from 0 to 6°.

values P, F (or M_P, M_F) should be multiplied at $\rho(u^2U_0^2/2)\ \Omega$ (or $\rho u^2U_0^2\ \Omega\ R/2$).

The calculations have been carried out for the units with relative geometrical dimensions of the AVEU-6 model, serially produced by the scientific and production association Vetroen, with variable chord length of the blade profile, that is, with variable blade width from b/R=0,083 at $r=r_0$ to b/R=0,05 at r=R. For the Espero profile, the relative profile thickness varies from c/b=0,22 at the blade basis to c/b=0,13 on the end [8]. The NACA profile coordinates with the identical relative profile thickness by radius and values of aerodynamic coefficients are taken according to the publications [9]. In the root part ($r<r_0$), the blade is considered to be a cylinder with the diameter 0,011R. It has been demonstrated (Table 2.2) that the blade chord length becomes less with removal from the spin axis, equally effective loads of the blade located at 2/3–3/4R from the spin axis. Decrease of the angle range change, especially for the NACA 4415 profile (Table 2.2), and the turn of the blades (φ_0) considerably reduces loadings.

The explained approach differs from the traditional one by determination of dependence $C_p = C_p(u)$. The calculation procedure accuracy has been verified with use of the experiments performed in NPO Vetroen (headed by V.E. Fedotov) in the wind tunnel with the working part by diameter of 3 m. The model AVEU-6 wind unit with a diameter of 1,2 m, with two blades of Espero profile (r_u = 0,2R). Filling of working cross-section of the pipe with model did not exceed 16%.

The test conditions differed from the natural by the availability of impenetrable pipe walls that has been considered in the calculation. The impermeability condition has been set on the pipe walls (r=D/2).

$$U_{r\,(r=D/2)} = 0 \tag{2.19}$$

The calculation result provides pictures of currents at different (u) and the dependence $C_p(u)$, which is much above the corresponding curve for the boundless environment (Figure 2.9).

By the empirical data on elevation coefficients and profile resistance for the Espero profile, the values of integrals defining functions $C_D(u)$ are calculated; with use of dependence $C_D(u)$ by Figure 2.6 the function $u=u(\omega R/U_0)$ is determined, and by (2.17), (2.18) the wind unit characteristics are defined. The calculation

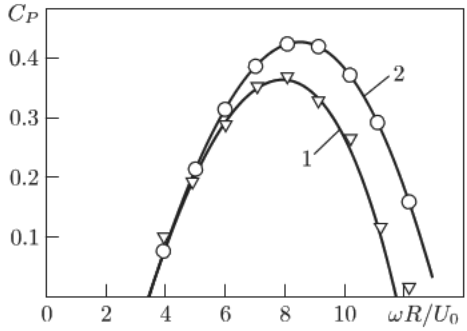

Figure 2.9 Comparison of calculation results of the wind unit power characteristics in a free stream (1) and in a wind tunnel with shadowing of 16% (2). Espero profile, $r_0/R=0,2$, $\varphi_0=2°$.

results for experimental conditions in the wind tunnel differ from the results obtained for the free wind-driven generator, since the aerodynamic loadings and power factor, even at a small relative shadowing of the pipe (16%), are nearly at 20% higher than in an open stream (Figure 2.9). This is confirmed by the publication data where, at 12% shadowing of the pipe, the trials provide values C_p at 15–20% higher than in reality.

A difference between the calculation data and the test results obtained in the corresponding conditions is insignificant (Figure 2.10). The same result is obtained when comparing the calculations for the NACA 4415 profile and the measured data [10]. Thus, for practical calculations of wind-driven generators and hydrounits of traditional configuration, the developed model with the uniform distribution of longitudinal speeds on the swept around surface is satisfactory.

The calculations demonstrate that the pressure difference on the unit (2.17), and, therefore, the relative speed and the power factor C_p by (2.11) do not depend on the pulling force ($P \cos \varphi_0 > F \sin \varphi_0$); that is, they almost do not depend on the aerodynamic features of the blade profile. On the contrary, the values $M_F \cos \varphi_0$ and $M_p \sin \varphi_0$ are commensurable, and at a greater rapidity ($z_u>10$) and an optimum turn angle of the blades, the pulling force contribution is the greatest, and the unit power factor C_p has to depend on aerodynamic features of the blade.

The Espero profile provides higher value of the maximal values of C_p, but only in a rather narrow range of change of the relative rotation frequency $z = \omega R/U_0$ (Figure 2.11). The NACA profiles provide smaller maximal values C_p, but the change of C_p depending on

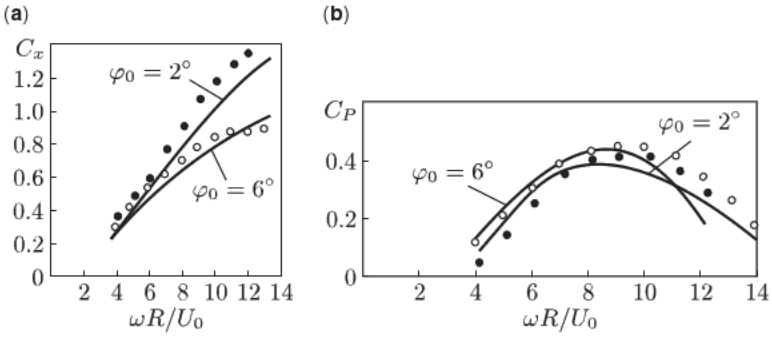

Figure 2.10 Comparison of calculation results (line) and experiments (dots) for conditions of a wind tunnel: a – coefficient of pressure on the unit; b – power factor.

z happens more smoothly. Therefore, with "soft" regulation which does not provide a strictly optimum rotation frequency, the NACA 4415 profile is able to provide larger output, than the Espero profile. The specified feature remains in the unit characteristics with the NACA 0012 profile; however, the decrease in the maximal C_p here is very great and the unit effectiveness is lower.

The developed technique can be used for comparison of the unit configurations differing from the traditional way. In particular, the influence of the length of the root part and the flow existence in the form of a hemisphere with a radius of 0,4R was revealed. It is established that the maximal values of C_p and the left branches of the characteristics change slightly (Figure 2.12). The right branch of the characteristic in the presence of fairing is much lower. At rather rigid regulation, this factor does not influence the energy development.

The effect of the root part length (at $0{,}2 \le r_0/R \le 0{,}40$) – Figure 12 appeared slightly. This can be explained in that the root part of the blades in general poorly influences the output. Besides, at $r_0/R=0{,}40$ at a larger distance from the spin axis, a relatively larger length of the blade chord than at $r_0/R=0{,}2$ is found. This result indicates the expediency of detailed optimization of the form of the blades.

For nonconventional schemes, a problem sophistication for the purpose of the accounting of nonuniformity of the velocity distribution on the disk or the ring imitating the unit may be necessary. The following step of the approach to real conditions considers all three components of non-stationary movement, including the important vortex (tangential) component [11]. The only simplification entered

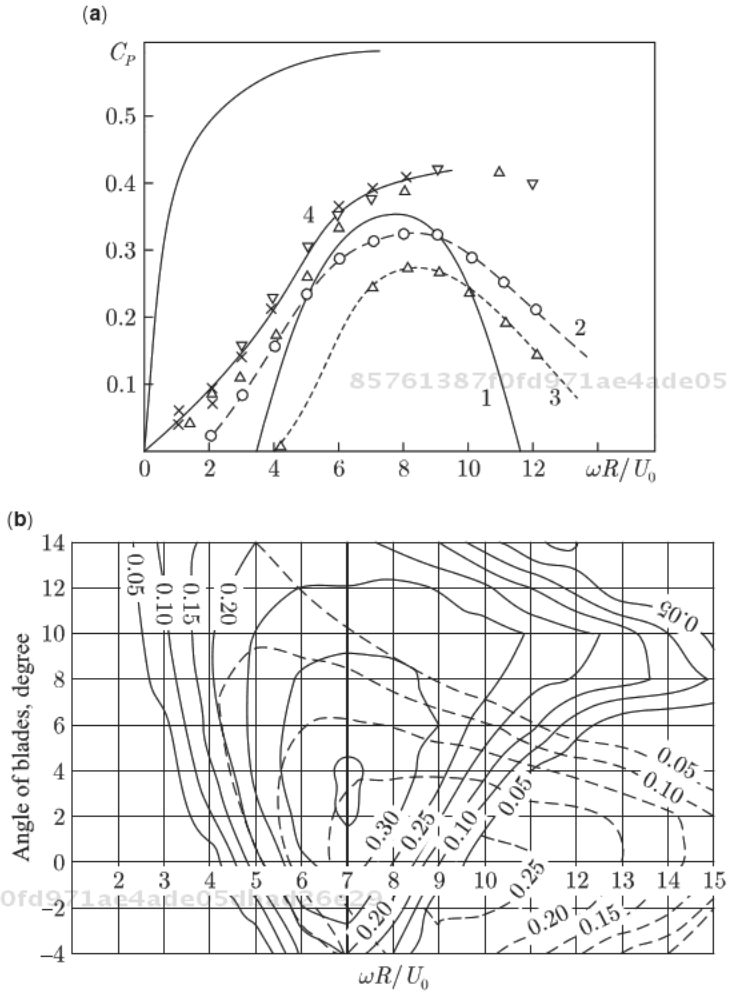

Figure 2.11 Influence of cross-sectional profile of the blades.a) – r_0=0,40R: 1 –"Espero", $\varphi_0=2^0$; 2 – NACA 4415, $\varphi_0=2^0$; 3 – NACA 0012, $\varphi_0=-2^0$; 4 –average characteristic of the "ideal" unit; b) – isolines of the power factor C_p (r_0=0,2R): _____ - –"Espero"; ---------- - NACA 0012.

in this task, consisted of an assumption of full axial symmetry of currents.

In the developed model, the unit is replaced with an axisymmetric fixed figure, the local pressure drop in which is defined by the ratio (2.17) in which, however, a longitudinal speed component U_x is supposed to be unknown and changing along the coordinate r:

$$\Delta p = \lambda(r\omega/U_x, \varphi_0)(\rho U_x^2/2) \qquad (2.20)$$

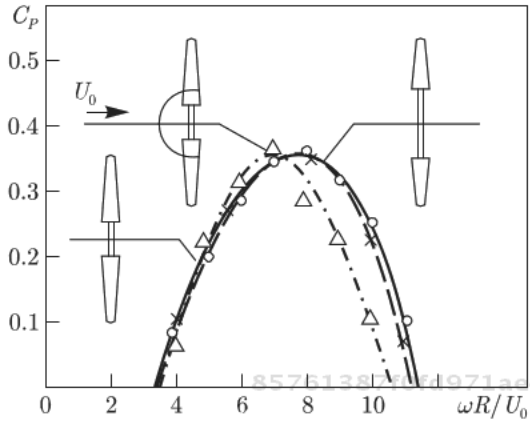

Figure 2.12 Influence of the design scheme of two-bladed units.

Here, the parameter λ is close by meaning to the parameters p and q_n

$$\lambda \approx (iq_n b/2\pi r)\cos\varphi_0 \qquad (2.21)$$

where q_n is defined by (2.14).

In this model, the problem is also split into two: solution of the hydrodynamic problem for Euler equations with the condition (2.20) on the surface replacing the unit; definition of $u_x(r)=U_x/U_0$ and torque and power calculation by the formula similar to (2.18), but with the relative speed u_x, entered under the integrals:

$$C_P = iz[m_p \sin\varphi_0 + m_F \cos\varphi_0] \qquad (2.22)$$

where: $m_p = 1/R\Omega \int bq_n u_x^2 dr$;

$m_F = 1/R\Omega \int bq_1 u_x^2 dr$

If the spin angle φ_0 changes depending on r, the corresponding functions as well as in (18) have to be entered under the integrals.

If, for simplification of the analysis, we enter the value λ averaged by the weight function r on the surface swept around by the blades, then the following equality is apparent:

$$\lambda \approx iP\cos\varphi_0 \approx iP \qquad (2.23)$$

where P is defined by (2.17a).

In the maximum zone C_p is usual $P \approx 0{,}5$, at the greatest z_u $P \approx 1$, at small z_u and $C_p \neq 0$ $P \approx 0{,}2$–$0{,}3$. In Figure 2.13 the distributions of

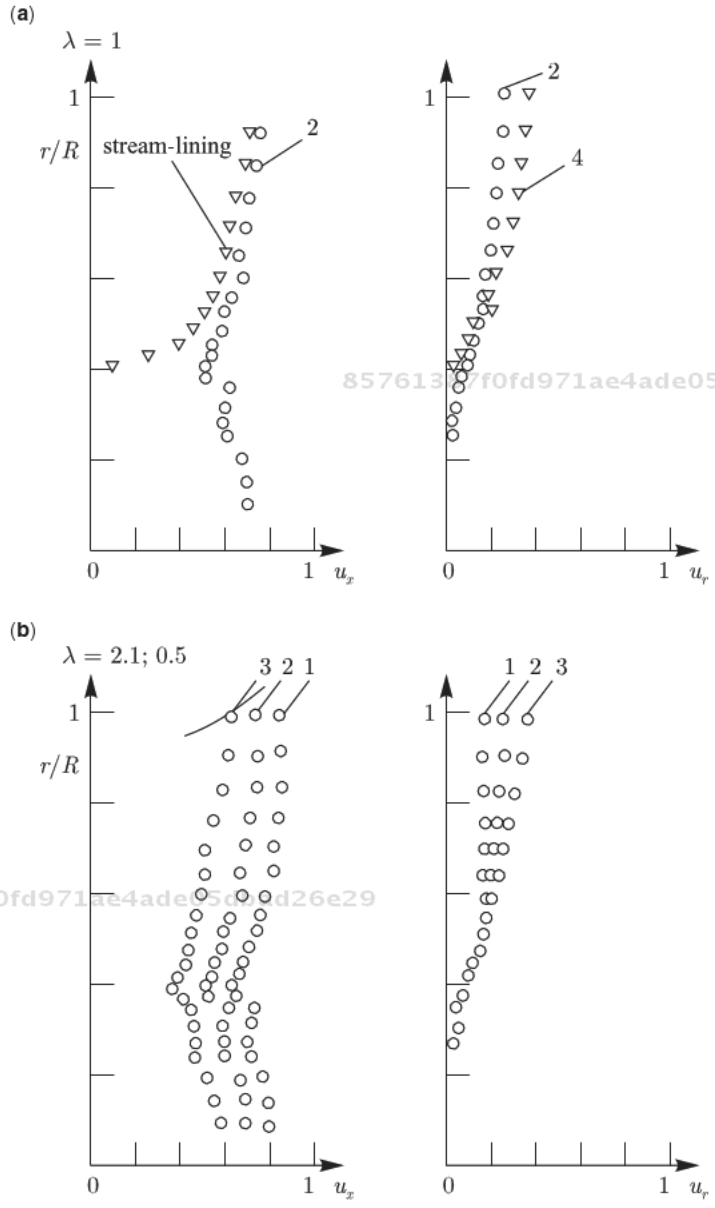

Figure 2.13 Distribution of longitudinal ($u_x=U_x/U_0$) and radial ($u_r=U_r/U_0$) of speeds in the unit plane with a fairing (1) and without a fairing (2) at λ=1:a) – influence of the parameter λ on velocity distribution; b) – 1,2,3- λ=0,56; 1,0; 2,0.

longitudinal and transversal speeds are compared at $0,5 \le \lambda \le 2$ so that for a two-bladed wind-driven generator, (i=2) covers the range of possible values. The parameter λ, naturally, influences considerably the relative speed value u_x. Thus, however, the velocity distribution nonuniformity

is insignificant. At a larger λ, the radial speed components are rather great which justifies use of the terminal devices. At the availability of a speed fairing near it, these values decrease a little. However, at the ends of the blades these values increase; that provides preservation and even some increase of the capacity factor of the wind power. Figure 2.14 shows vectors of speeds and isolines of the relative pressure ($\rho U_0^2/2$) at λ=1 and the availability of a fairing. This indicates, in particular, the expediency of turn of the blades towards the stream at approximately 10–20°. The developed technique can be efficiently used for estimates of aerodynamic loadings and power characteristics of horizontal units of various types.

As follows from the above, the classical estimates of the maximal power of units are based upon inconsistent hypotheses of constancy of pressure on the stream tube surface covering the unit, about uniform distribution of speeds in the unit plane. If keeping only one assumption of the uniform distribution of speeds (the first model), it is possible to calculate the hydro- or aerodynamic loadings and the power factors which are matching the experimental data. The maximal power factor of the units with a horizontal axis in the free stream without concentrators according to this model cannot exceed 0,41; that is 1,44-fold less than the distribution of Betz-Zhukovsky assessment.

The hypothesis of uniform distribution of the speeds in the unit plane does not allow investigation of nonconventional configurations of horizontal units. For elimination of these restrictions, the full axisymmetric numerical model is used.

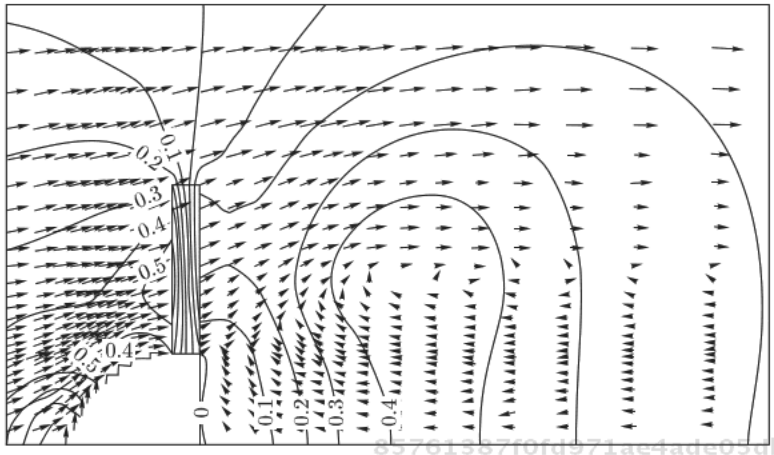

Figure 2.14 Vectors of flow rates in the plane passing through the unit spin axis.

By means of this model of the distribution of speed and pressure, power characteristics of units with the central fairing and without it have been compared. It is established that introduction of the fairing, with a diameter of up to 0,8R, as well as the corresponding shortening of blades with aerodynamic profile at preservation of the external diameter swept around by a circle (2R), practically does not cause deterioration of the unit power characteristics.

The influence of aerodynamic characteristics of the blades profile has been studied. It is established that two-bladed units with the Espero or NACA 4415 profiles have the best indexes. The maximal value of the power factor for these profiles in an open stream makes 0,35–0,36. At the trials of hydro- and wind units in the wind tunnels or trays, an uprating of the loadings and the power factor of the units are possible in comparison with the free, steady flow conditions. In particular, at a blockage of a wind tunnel section by the unit at 16%, the maximal power factor can be exaggerated over 20%.

The calculations show that for the machines with the rotor diameter up to 100 m and the power up to 3 MW, a single-blade scheme with very high rapidity could be quite competitive. It makes sense to compare the machines with different number of blades i at the preservation of the shadowing degree $\sigma = ib/D = idem$. If we compare the units with different numbers of identical blades, the three-lade machines (Figure 2.15) appear to be the most efficient according to the calculations.

Large single-blade machines produced in Italy and Germany with the optimized blade, show a good power characteristic.

The single-blade powerful machines, however, have not become popular. On the contrary, such wind-driven generators of 0.2, 0.5, 1 and 1.5 kW with a hinge-joined blade (Figure 2.16) are being produced, or used to be produced, by the Research Center VINDEK (Moscow), JSC Elektroveter (Safonovo, Smolensk Region).

The acoustic radiation of the blades in a natural wind stream and, especially in places where crossing turbulent air by the blades behind the basic tower, can be an additional restriction of the rotation speed of the blades. The example is known, that when by the ecological requirements to the acoustic infrasonic radiation, the rotation speed of a large unit was reduced, and its capacity was reduced, too. Crossing rough air behind the tower by the wind unit blades also causes additional dynamic loadings on the blade; therefore, in the modern large units the rotor is usually positioned

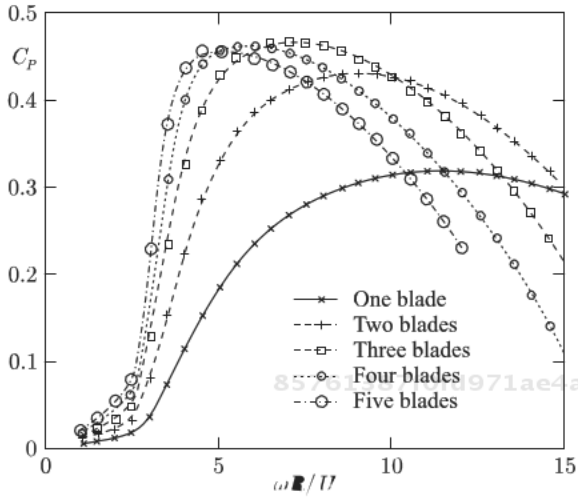

Figure 2.15 Change of the rotor effectiveness with different numbers of identical blades. Picture from Handbook of T.Burton, D.Sharpe, N.Jenkins, E.Bossanyi, Wind Energy [6]).

Figure 2.16 Single-blade self-established unit. The rotation speed changes in proportion to the flow rate.

in front of the basic tower (Figure 2.17), though the arrangement behind a tower can be preferable for small and average units, since this removes a need for special devices providing orientation by a stream.

The optimum design of a wind-driven generator with two blades behind the tower, serially produced in the 90s by Advanced Wind

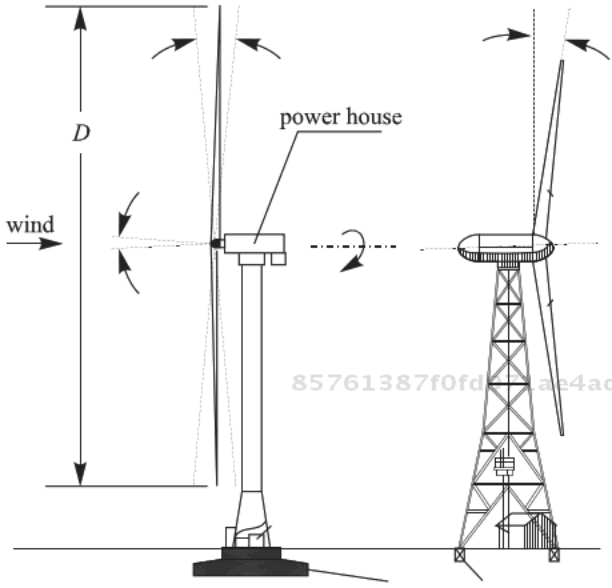

Figure 2.17 Arrangement of the rotor in front of the tower (upwind) – at the left and behind the tower (downwind).

Turbines (USA), provided the lowest power costs for that time (Figure 2.18).

In order to avoid low-frequency noise, the blade system of large modern machines is positioned in front of the basic tower, and the unit is orientated by an additional drive by a command from the wind direction sensors.

The increase in simple power of the wind units, significantly reduces specific operational expenses. At an identical relative distance between the units in the wind power station (for example, 2D), the area related to a power unit or the output of the station with large units decreases due to the wind of greater speeds at larger heights. All this proves the increase of simple capacities of the wind units which now are almost limited to the durability of the modern aviation materials, the technological capabilities of the enterprises, and also the ecological requirements to lower noise, limiting the speed of blades. A wind unit meeting the specified requirements Mod-5B-107 (Figure 2.19) has the two-bladed rotor, diameter 97,5, with the maximal speed of 89 m/s at the ends of the blades at, and the power of 3200 kW. The same company designed the installation Mod-5B-105 with the diameter rotor 126 m and the power 7300 kW.

Figure 2.18 AWT turbine behind the basic tower, diameter 26.2 m, power 275 kW at the wind 15.3 m/s, initial wind 5.4 m/s, maximal for the work – 24.6 m/s, hurricane 59 m/s. The tower height - 47.3 m.

Figure 2.19 Wind unit Mod 5B.

The ecological restrictions are probably one of the main reasons for making the modern mass production large wind units more low-speed and with three heavy blades, though the largest and most economic machines are designed and constructed with two blades.

The optimum dimensions of the units are defined by the influence of two counter tendencies. The specific material capacity and the capital investments per a power unit (or output) of the wind units tend to increase with the increase of the height and capacity of the units. This is because the mass of the power material of the rotor and all of the unit increases in proportion to the third degree of the linear dimension, and the capacity and output in the homogeneous height stream increase in proportion to a square of the linear value. Thus, theoretically the weight of the power material associated with a power unit (output) has to increase with the increase in dimensions of the unit. However, in practice this is observed only in small ($P < 1$ kW) and very large ($P > 1000$ kW) wind units. In the wind units of average dimensions, the larger share of the material weight is made by the design elements rather than the power elements. Therefore, the specific material costs depending on the unit dimensions do not change monotonically. For example, for Howden units (Figure 2.20) of 60, 330 and 750 kW with three-blade rotors with diameter 15, 31 and 45 m, the unit weight makes 112, 135 and 107 kg/kW at calculation per a power unit, or 0,052; 0,089 and 0,073 kg/kW•hour at calculation per a development unit in a year for the average annual wind speed 6 m/s on the unit axis.

The power characteristics of the units change slightly at an increase in length of the root part of the blades or the introduction of the central fairing (radius up to 0,4R). This allows us to consider

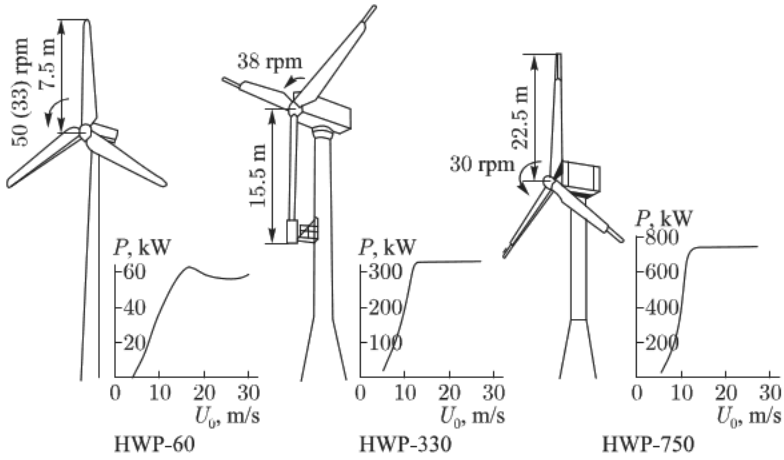

Figure 2.20 Series of optimized wind units from Howden (England).

configurations of units with the central machine house and rather short blades that help to increase (in the long term perspective) a simple capacity of collinear wind units to 20 MW at preservation of the maximal length of the console of the blades reached in the modern wind units.

Availability of a fairing allows us to change the configuration qualitatively, having placed the generator poles on the fairing diameter and, having kept the blade maximal length 64 m, to provide the radius of the swept around circle 07 m and the maximal capacity of the wind unit $P_{max}=7{,}2(107/64)^2 \sim 20$ MW at the same design implementation of the blades which are designed for the machines 7,2 MW.

The increase in the simple power of the wind unit can be reached at preservation of the maximal length of the blades 45 ÷ 60 m. This is possible due to the introduction of the central machine house closed by a profiled fairing (Figure 2.21).

Still larger technical and economic effect can be gained by use of the central torus or hollow cylindrical supporting framework displaced with respect to the vertical support axis. Two options are possible: arrangement at the torus or on the cylinder of the blades fixed on the rim of the electric generator rotor are possible. Or (the second option) arrangement on a support of two rows of the blades rotating in opposite directions (Figure 2.22).

The use of counter-rotation of the blades facilitates the electric generator design, but increases the lump of the rotating parts. Since the rotation plane of the blades is displaced in the wind direction

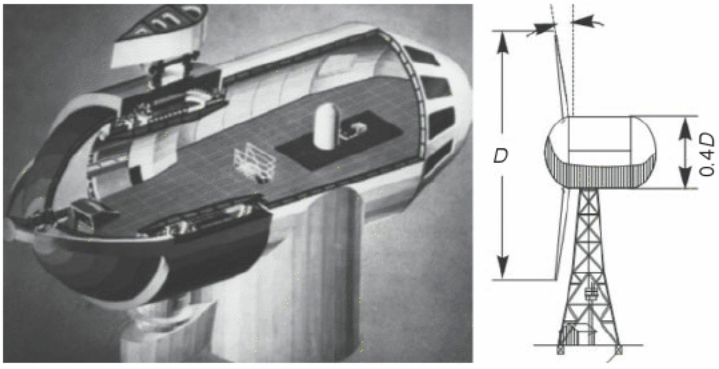

Figure 2.21 Central machine hall (right) of the wind unit of big power with truncated blades.

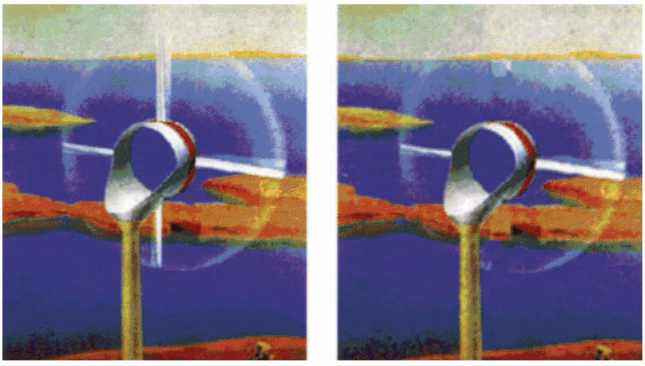

Figure 2.22 Wind units without multiplicators, with the central ejecting stream and the linear (arc) or multipolar asynchronous generator. Right - the simplest scheme, with one row of blades fixed on a short-circuited rotor of the generator, left - counterrotor version, with two rows of blades moving in opposite directions. [12].

from the vertical support axis, the unit is independently guided in the wind direction, choosing the most efficient energetic situation. This unit favorably differs from the traditional machines by the central air stream causing an ejecting action which promotes increase in power.

As proved by the calculations, availability of the machine house or an opening with diameter 0,4D in the center of the unit does not deteriorate the power characteristics in the maximum zone of the power factor C_P and small rapidities corresponding the most important strong winds (Figure 2.12).

For decrease of the unit material capacity, but preservation of the principle of counterrotor machines, the second system rotor can be located in the central opening of the design (Figure 2.23). The winding of inductors with an access via a collector in the system center is located on the rim of this internal rotor. The short-circuited rotor of the generator is positioned on the internal rim of the external wheel.

Such a configuration does not increase the unit power, but can appear useful to improving characteristics of the electric generator. The availability of the central machine "hall" of some form (cylinder or torus) of rather big diameter allows us to change the configuration qualitatively, having placed the generator poles on the external diameter of the "hall" and having kept the maximal length of the blade equal, e.g., to 63 m. Thus, the diameter

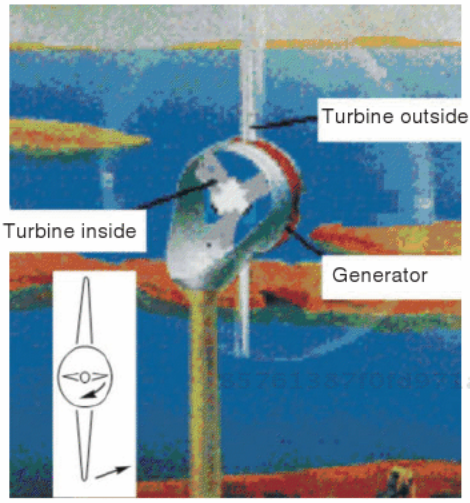

Figure 2.23 Counterrotor wind unit without multiplicator with the linear (arc) generator between turbines.

of the swept around circle will be equal to $D = 0{,}4D + 2{\cdot}63$ m; i.e. $D = 210$ m, and the possible rated capacity (at the same relative characteristics, as at Mod-5B-105 unit) is equal to $7300{\cdot}(210/126)^2 = 20300\ 7300 \bullet (210/126)\ 2 = 20300$ kW. If by restriction conditions of acoustic radiation we keep the speed of the ends of blades the same as at Mod-5B-105, i.e. 89 m/s, the rotor traveling speed in the linear (arc) generator according to Figures 34, 35 makes 35.6 m/s. Crossing the magnetic fields at such speeds in the asynchronous generator with short-circuited rotor is sufficient to create the high performance electric machine weighing no more than 2.35 kg/kW. There is no need to make the second row of counter-rotating blades in the wind unit.

Thus, the use of the configurations in Figures 2.22, 2.23 allows us to increase the simple capacity of the wind units to approximately 20 MW, at preservation of the dimensions of the blades mastered by the industry and tested in practice.

All units of the considered type with the spin axis parallel to the stream have an essential lack of the traditional designs, consisting of the impossibility of considering non-complanarity of the stream (air or water) by height. Distinction of the wind direction at different heights, unnoticeable in the units with a small span of blades, in large units is able to seriously reduce their power effectiveness and become a reason for destruction of the blades. This adverse

feature of the units can be partially compensated for by the blade design providing a possibility of turning different sites of the blade entirely or its flaps at a different corner in relation to the rotation plane. Such a solution, however, complicates the design even more and reduces its reliability.

The power characteristics of the wind units presented as dependencies of the effectiveness ratio C_p from the rapidity $z = \omega R/U_0$ are the most various. However, the actual dependence of the power normalized by the maximal (calculated) value P_p from the speed wind on the unit axis for various high-speed collinear units with constant rotation speed does not go beyond the variability of the data, obtained at tests of the same machine in different meteorological conditions (Figure 2.24):

$$\begin{aligned} P/P_p &= 0 \qquad \text{at } U<U_н \\ P/P_p &= (U - U_н)/(U_p - U_н) \text{ at } U_н < U < U_p \\ P &= P_p \qquad \text{at } U > U_p \end{aligned} \tag{2.24}$$

The initial velocity $U_{н,}$ at which the capacity is output, usually makes 5 ÷ 6 m/s. The calculated wind speed U_p at which the wind unit comes to the rated (maximal) power makes 12 ÷ 15 m/s, on the average 13 m/s. The maximal capacity taken from a unit of swept

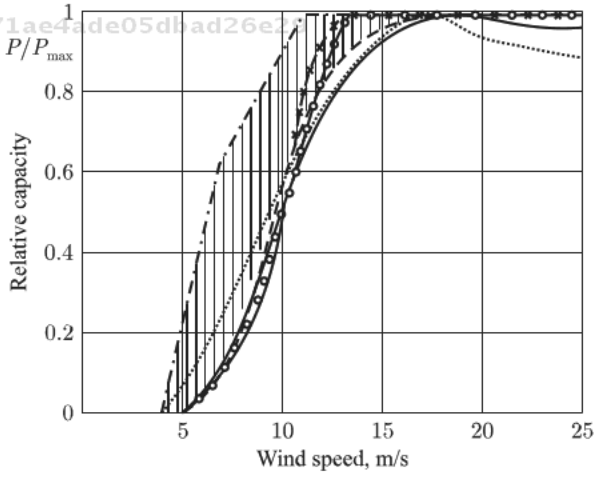

Figure 2.24 Relative capacity of head samples of serial collinear wind units P/P_{max}. The variablestrip of results at different wind structures is shaded.

around surface in the modern machines also changes in rather narrow limits:

$$\frac{4P_P}{\pi D^2} = 0,35 \div 0,47 \frac{kBT}{M^2} \qquad (2.25)$$

This power value of the wind units correspond to a quite low capacity factor of the wind power: at $U = U_p$ $C_p \le 0{,}33$, that actually reflects the influence of the above listed negative factors. At $U > U_p$ the wind power capacity factor, naturally, is even lower. Therefore, the best modern wind units transform, on the average, no more than 25 ÷ 30% of the wind flow energy through a swept around surface. At the speed of streams less than the design value, the power effectiveness of the actual units increases, aspiring to a limit for "the ideal unit", defined in item 1. In the most perfect machines the initial velocity is reduced to 4 m/s, that, however, adds only an outer effect of the machine working at a light breeze, practically without increasing the energy development. The introduction of variable rotation speed and variable turn corner of the blades by these machines, slightly curves the characteristic. For Vestas units, this characteristic can be set by three linear sites:

$$\begin{aligned} &P = 0 \text{ at } U < U_н \\ &P = B\,(U - U_н) \text{ at } U_н < U < U_1 \\ &P = B_1(U - U_1) + P_1 \text{ at } U_1 < U < U_p \\ &P = P_p \text{ at } U_p < U < U_{max} \quad P = 0 \quad \text{at } U_{max} < U \end{aligned} \qquad (2.26)$$

Vestas machines have the following values of parameters:

Unit type	V 90–3	V 90 – 1.8&2	V 52 – 850
P_p, kW	3000	1800/2000	850
P_1, kW	500	500	500
$U_н$, m/s	4	3.5	4
U_1, m/s	6	6	6
$U_н$, m/s	14(15)	11(12)/12(13)	15(16)
U_{max}, m/s	25	25	25

(The speed values corresponding to the specifications are given in brackets.)

The proposals directed on increase of the technical and economic effectiveness of collinear wind units are known. One of the prime ways of decreasing the influence of non-complanarity and

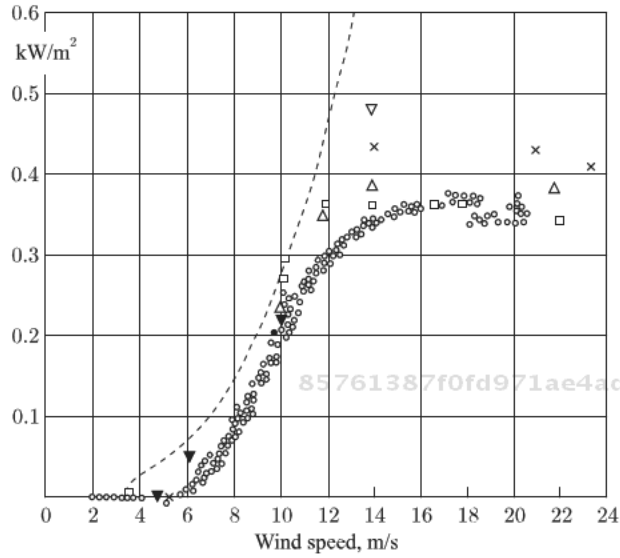

Figure 2.25 Energy obtained by different wind units from a unit area of swept around circle (the dots correspond to different machines). Line – energy by the condition of the greatest possible effectiveness of collinear machines in a boundless stream $C_p = 41\%$.

turbulence of the stream and at the same time increasing the simple power of the unit is by using confusers – a short confuser and a diffuser (scheme 4 in Figure 1). The experiments and calculations show that the effectiveness of the convergent-divergent scheme can be rather high. The optimum increase in power for this wind turbine diameter can be in 6 ÷ 8-fold. However, the total assessment of the material capacity of such systems carried out on the basis of the pilot studies in TSAGI and abroad did not yield positive results. This is bound to the use of the lengthiest diffusers in which the friction losses against the walls reached 30% of the total losses. At the same time, it was established that in the presence of confusers and diffusers the stream angle does not affect the power at the angles up to 30 ° (a difference below 10%). The capacity of a common wind-driven generator in the free stream at the 30° angle decreases 1,7-fold.

In the modern designs of concentrators at the expense of management of a boundary layer in the diffuser, its length can be rather small (bell angle to 80° at a ratio of the areas at the output and input about 4) [13]. The optimization estimates executed by the author yielded approximately the same results – in the concentrator it is desirable to have a ratio of sections about 2,8. The concentrator

operation principle consists of the creation of a zone of positive pressure in front of the turbine, and decompression sections behind it. As established by numerical and physical experiments, the air delivery in the vacuum zone (behind the concentrator) in particular conditions does not reduce, but increases, vacuum depth behind the concentrator. This result, similar to the ejection action of the central stream, is bound to the development of additional vortex surfaces in the zone behind the concentrator. In the sense of power, the introduction of the concentrator means engaging due to the intensified turbulent exchange of energy of mass of the air which is not passing immediately through the impeller of the wind unit. The maximal capacity of the unit with the concentrator by Figure 2.26 is determined by the larger coefficient C_P, defined by a formula:

$$C_P = 0,385\frac{(C_D + 0,64)^{3/2}}{\sqrt{0,066+\xi}} - \frac{\Omega}{\Omega_c} \qquad (2.27)$$

where C_D – relative pressure difference on the concentrator.

$\frac{\Omega}{\Omega_c} = 2,8$ we obtain $C_P = 0,75$.

For a single concentrator or a pairs of axisymmetric concentrators $C_D \approx 0,8$. For the system of concentrators forming flat flow

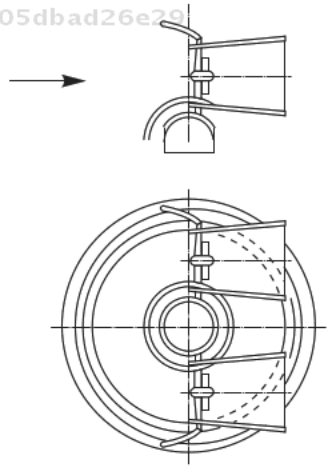

Figure 2.26 Scheme of the concentrators, including a confuser in front of the impeller and diffuser behind it.

conditions (Figure 2.28) $C_D \approx 1{,}2$ (see chapter 3); ξ – a resistance coefficient of the wind unit absorbing pipe; Ω, Ω_C – calculated and oblate sections of the power path. Accepting $\xi = 0{,}05$; $C_D = 1{,}2$.

The scheme created by the French engineer Andreau and Enfild company (UK) has some fundamental differences in which the wind stream on the turbine built in a vertical well, is created due to a vacuum at the ends of the hollow wings of the wind-driven generator located on the tower. This scheme was implemented in 1955, in nature, with the generator 100 kW (span of blades 24,4M, Up = 13,5 m/s) – Figure 2.27 and demonstrated a very low effectiveness that was confirmed with additional theoretical analysis. [14]

The cylinders can be placed as rotors on the ends of the blades, and all systems works due to the Magnus effect – Figure 2.28.

An essential deficiency of this scheme, deserving careful analysis, is the need to transfer the considerable power through the collector, with large centrifugal loads on cylinders and the related electromechanical systems. However, some important aerodynamic advantages are inherent in this scheme, too. The systematic research of the wind units with the diffusers truncated due to the stream supply to the boundary layer and without confusers, are carried out by the Vortec Energy World Power company. This company already

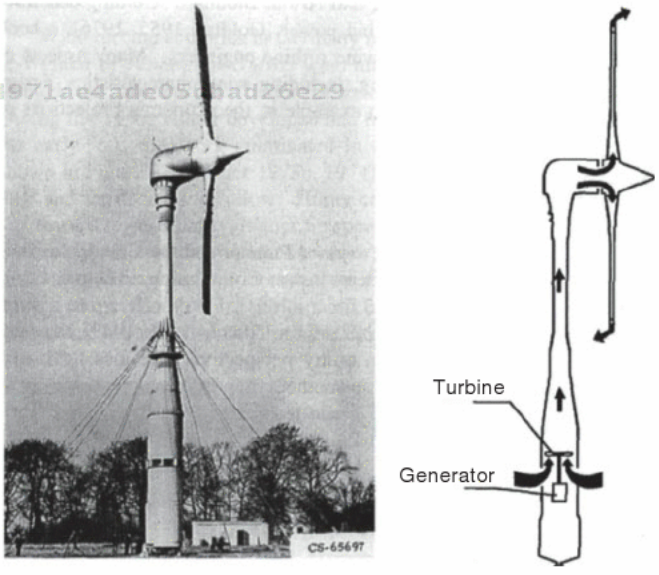

Figure 2.27 Andreau – Enfild wind unit.

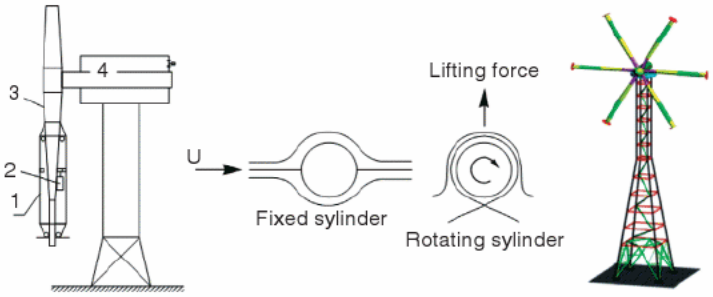

Figure 2.28 Wind unit with the cylinders (1), rotated by electric motors (2), fastened on the ends of blades (3) of the rotor with a traditional gondola (4). Rotation of the rotor is provided with the body force arising at a flow of the rotating cylinder (Magnus effect).

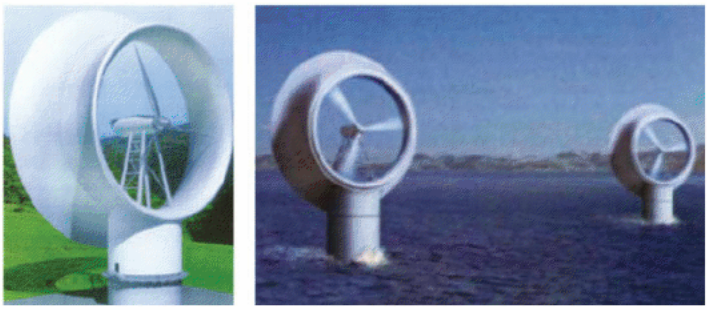

Figure 2.29 Vortec wind units with the self-orientating downwind diffusers, rotor diameter 66 m, power 5 MW (project).

constructed and tested some wind units with the power up to 1 MW, and names a universal unit of land and sea basing 5 MW with the rotor diameter 66 m only a perspective machine (Figure 2.29). By the estimates of the developers (Emily Rudkin, Derek Phillips), the cost of energy from these machines will be 20% lower than at the best installations of traditional configurations. Similar machines of small power have been successfully tested in France (Figure 2.30) and in Germany.

The idea of the use of aerodynamic interaction of several units to increase effectiveness in each unit appears promising. Having arranged two wind units nearby, we can expect greater pressure reduction behind them and, therefore, larger system effectiveness. According to the idea of A.G. Ufimtsev and V.P. Vetchinkin [15], developed in many patents and author certificates of the

Figure 2.30 Wind unit with the diffuser concentrator, power 30 kW. France.

USSR, some high-speed wind units can be located on one support, sometimes even with partial relative overlapping of the blades.

Such configuration causes operational difficulties - repair of one of the units complicates operation of the others. This circumstance becomes less essential at a large number of units. The working blades can be grouped on two or more coaxial shafts rotating in one or in counter directions. In the latter case, there is an additional gain in facilitation of the electric equipment which, however, appears more sophisticated and less reliable (additional collectors). The prospect of preliminary concentration of the wind stream directed on the wind wheel is very attractive. Special attention is drawn by an idea of a tower type unit in which a vortex motion with a deep pressure reduction in the whirlwind center is created by the operated shutters, where the evacuation pipe of a common wind unit rotating in the horizontal plane is positioned.

In all these schemes, the wind unit impellers are more high-speed, the electric equipment is rather light due to the increase in the simple power of the units, and the specific consumptions decrease by operation. However, generally, the material capacity, specific investments, and power costs, usually do not decrease. The unit (item 8 in Figure 2.1) favorably differs from others by a possibility of the creation of installations with larger dimensions and rather small relative frame masses. However, as well as in other cases, even at the optimum aerodynamics providing the power factor related to the area

in the tower dimensions equal to 0,2, the power costs in the unit 2,5 MW are much higher than those of Mod-2, for example.

The ideas of a many-tier arrangement of the wind units pairwise on one bearing tower (Figure 2.31) or as an element of a city architecture between the buildings (Figure 2.32), appear repeatedly.

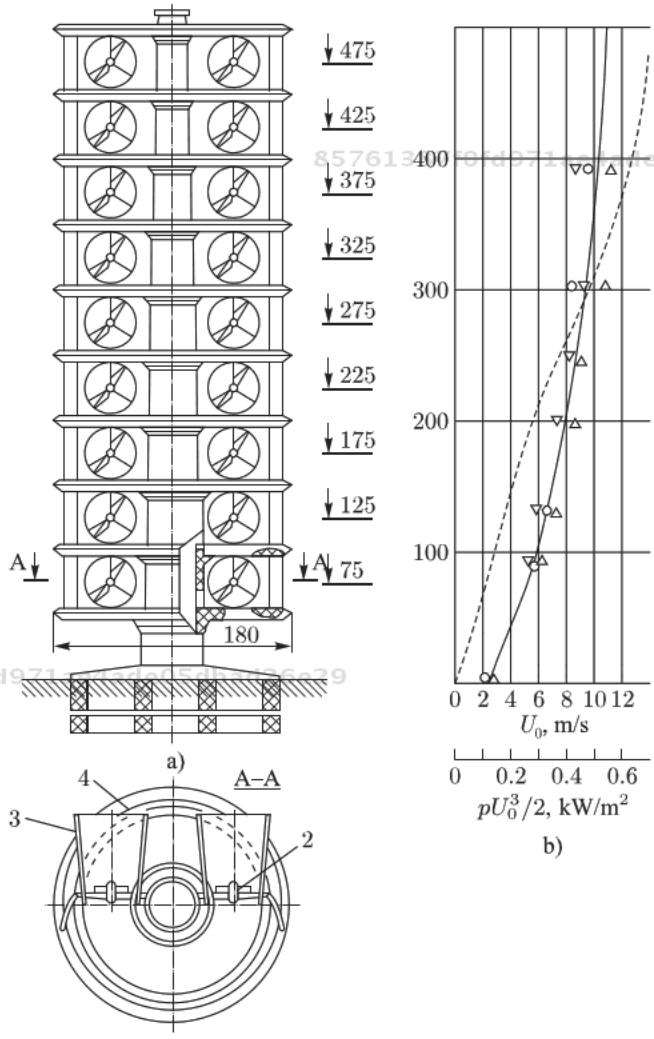

Figure 2.31 Scheme of a multi-unit VES with horizontal units and concentrators. 1 - reflector concentrator, 2 - rotor with diameter 35 m, 3 - absorbing pipe, 4 - dividing disks allowing independent turn, 5, 6, 7, 8 - wind speed distribution in Moscow in January, 1975–1978, 9 – distribution of average wind power stream in Moscow.

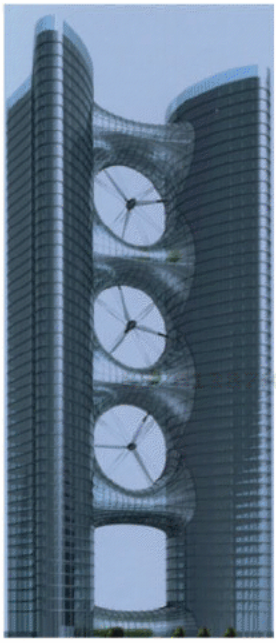

Figure 2.32 Many-tier wind power station between the houses concentrators. Vortec Energy project. The elementary version with two directing devices and one unit between them, constructed and tested in New Zealand.

The system rated capacity of the wind units with concentrators according to Figure 2.31 mounted on the ferroconcrete tower 500 m high, for example, for meteorological conditions of Moscow, turns out about 65 MW, and twice more for the district of Volgograd. Thus the wind rotor diameter accepted is 40 m, and the calculated wind speed is 13 m/s. The disks between levels of units are not an obligatory structural element. The rotors can be placed on a tower pairwise without concentrators.

The capability of downwind self-orientation of such system also matters; for this purpose the bearing point of horizontal traverses is positioned in front of the units, and the units are turned slightly outwards. Having placed the pairs of self-established wind units, for example, with diameter 126 m, with mechanical and electric equipment Mod-5B-105 on the ferroconcrete tower 500 m high, we obtain a compact wind power station 7,3 · 8 = 58,4 58,4 MW (Figure 2.33). The output of such a station for Moscow conditions will be defined from the following estimates. The average annual stream of energy at the height of 100, 200, 300 and 400 m makes 357, 599, 802 and

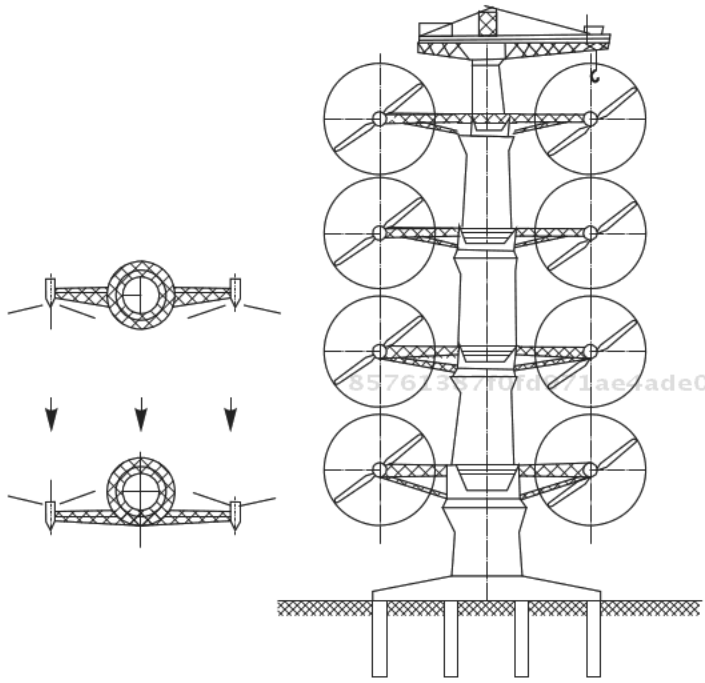

Figure 2.33 Multimodular WPP on the basic tower. Automatic orientation downwind.

946 W/sq.m. Accepting the wind power capacity factor as equal to 0,25, we find an average annual capacity of the wind units of the specified marks: 1,11; 1,85; 2,49; 2,94 MW. Thus, the number of hours of use of the rated capacity of each unit 7,3 MW at the height of 100, 200, 300 and 400 m makes 1335, 2230 and 3526 hours, respectively. The total output of the wind units is expected to average 147160 MW • hour/year, i.e. about 2520 hours of use of the common rated capacity. As we see, the power effectiveness of the considered WPP is sufficiently great even in Moscow.

The effect of self-orientation can be used in the floating wind turbine with an additional storm protected by a turn of wind-driven generators in the horizontal position [16].

The collinear wind units in combination with concentrators can be used in the most various configurations. Let us note only two schemes, allowing us to create large installations:

- tower type;
- ejector type.

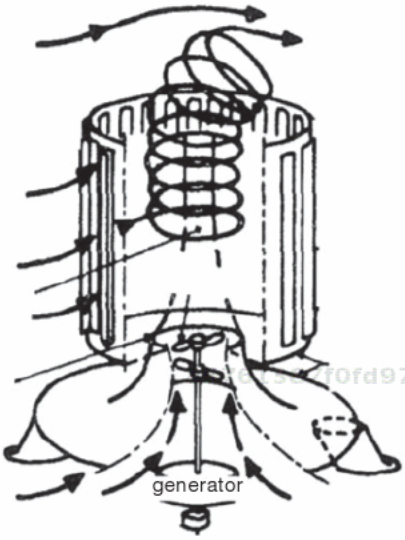

Figure 2.34 Tornado system for the transformation of the energy of currents. J.T Yen (1976). The power unit is located below (on the ground) in the airflow. The main advantage is the energy concentration and increase in the turbine rotation speed.

In the tower designs, like Tornado (Figure 2.34), the air stream is twisted by means of the directing shutters fixed in the vertical tower walls.

High vacuum is created over the impeller in the tower center. Air is delivered from the vertical axis to the impeller through the air receivers in the tower bottom. Numerous researches have defined the energetically optimum ratios between height H and diameter D of the tower: $\frac{H}{D} \approx 1,25$ Thus, the maximal capacity factor of the wind power counting on the transverse section of all construction makes 0,14 ÷ 0,20. The advantages of this scheme are simplicity of the power inventory, independence of the flow direction, and the possibility of obtaining larger simple capacities. Additional vacuum can be created behind the impeller by some other methods, for example, flowing off the dome in which top zone the unit is located (Figure 2.35). The effect can be strengthened by a roof over the dome.

The schemes of ejector type (Figure 2.36) allow us to use the effects of horizontal axis concentrators on the ejection line. The

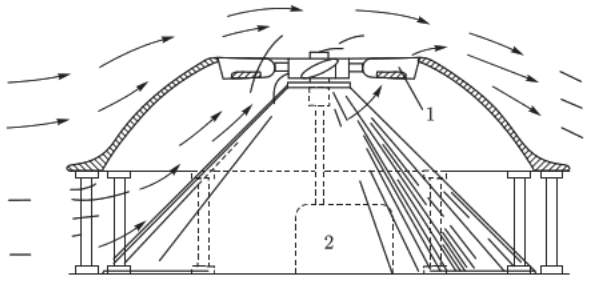

Figure 2.35 Dome WPP Unit 1 is placed in the vacuum zone, generator (2) – on the ground.

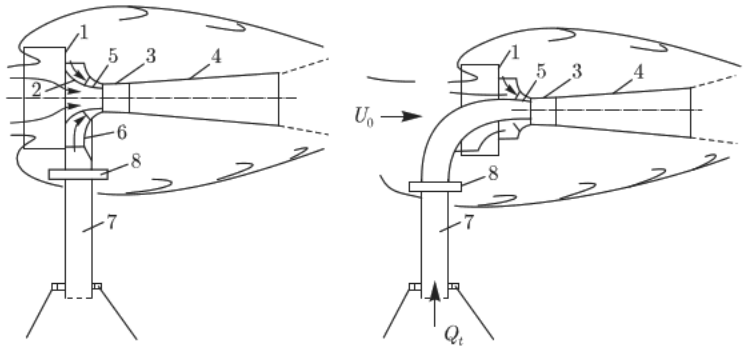

Figure 2.36 Ejector wind unit. 1 - accumulating reflector, 2 - concentrator (confuser), 3 - high vacuum mixing chamber, 4 - diffuser restoring pressure and focusing the system by the stream, 5,6 – directing the spiral channel of the turbine path, 7 - turbine air duct with high-speed turbines with electric generators in the bottom part, 8 - ejector rotary support. Left - ejection at a wall, right - ejection in the diffuser center.

effect of the density gradient is used on the vertical site of the route of the ejection stream, when heating the air ejection stream by passing through the thermal power plant or nuclear power plant graduation towers (in the long term, a direct cooling of the condensers of the thermal power plant, or the nuclear power plant, without the use of graduation towers is possible).

On one bearing tower, some ejectors increasing power effectiveness of the installation can be positioned. The ejection stream can be applied at the diffuser walls, via a spiral chamber as shown in Figure 2.36 (left), or as a solid jet in the diffuser center that can be even more efficient, since the pressure upon the diffuser axes is usually less than that at its walls.

The tower wind units and concentrators have a high material capacity; they have to be calculated on the maximal storm influences. A similar result of increase in effectiveness of a wind wheel can be reached by a more elegant design – by special flaps on the ends of the working blades. These flaps, being perpendicular to the rotation plane of the blades, form a rotating permeable confuser-diffuser (Figure 2.37).

The length of these flaps should not exceed 0,1D, and their power effect can be even larger. In particular, the recent researches confirmed a high performance of trailer flaps on blades of high-speed units. These flaps are positioned perpendicular to the blade axis, outlining a peculiar confuser-diffuser at blade rotation.

The idea of concentrators found development in the inventions of B.V. Voytsekhovsky and M.B. Voytsekhovsky (author certificates of the USSR ## 1280183 and 1229418) concerning the positioning of the working blades on a lateral area of an imaginary truncated cone or a pyramid. The axis of the cone (pyramid) is slightly inclined, so that its top and the foot directing the bases are located on the ground (or on the basic tower). The authors place a large number of blades on the cone surface, assuming the unit use will be in the mode of a low-speed machine completed with the pumping equipment.

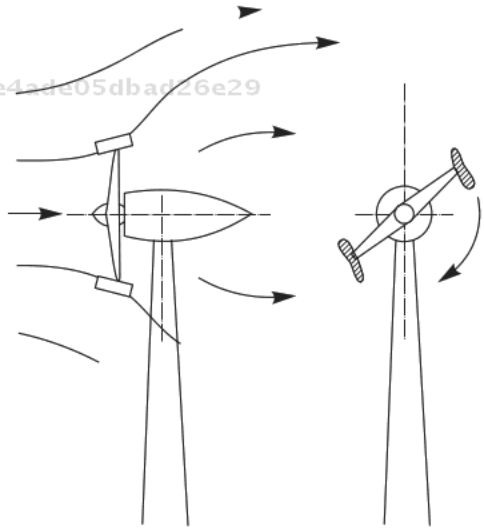

Figure 2.37 Diffuser formed by end transversal flaps.

References

1. The numbering of drawings, tables and formulas starts over in each section.
2. V. M. Lyatkher, Yu.B.Shpolyansky. Loadings on hydro-and wind units in the free stream and their power characteristics. Hydrotechnical Construction, No. 12, 1986, p. 16–22.
3. G.H. Sabinin. Theory and aerodynamic calculation of wind engines. – Tr. TSAGI, 1931, issue 104.
4. See part 3.
5. Hutter U. Moderne Windturbinen, 1979. Vachon W.A., Schiff D. Test performance of large wind turbines. – Int/ Wind Energy Symp., 5th Annual. Energy – Sources Technol. Conf. and Exhib.,N Orleans. March 1982, N. – Y., 1982, p. 137–157. Maekawa H. Application of the vortex theory to high speed horizontal – axis wind turbines. Bul. Of JSME. v. 27, N 229, 1984, p. 1460–1466.
6. T.Burton, D.Sharpe, N.Jenkins, E.Bossanyi, Wind Energy. Handbook, John Willey&Sons,Ltd, 2005, 617p.
7. Paul Gipe, Wind Power. Renewable Energy for Home, Farm, and Business, 2004, 496 p.
8. Fateyev E.M. Wind turbines and wind turbines, OGIZ, M. 1948.
9. Abbot J.H., Von Doenhoff A.E. Theory of wind sections including a summary of airfoil data, N.Y., 1959. Michos A., Borgeles G., Athanassiadis N. EaAerodynamic characteristics of NACA 0012 airfoil in relation to wind Generators, Wind Engineering, v. 7, N 4, 1983, p. 247–262. Ostowari C., Naik D. Post stall studies of twisted varying aspect ratio blades with NACA 4415 airfoil section. Part 1. Wind Engineering, v. 8, N 3, 1984, p. 176–194.
10. Maekawa H. Application of the vortex theory to high speed horizontal – axis wind turbines. Bul. Of JSME. v. 27, N 229, 1984, p. 1460–1466.
11. A.N. Militeev, Yu.B. Shpolyansky. Aerodynamic calculation of wind turbines with a horizontal axis of rotation – Proceedings of Hydroproject, 1988, issue 129, pp.139–145.
12. Lyatkher V. M. and Shpolyansky Yu.B. "Wind power installation", Author Certificate of the USSR, No. 1361371 of 22.08.87, Bul. No. 47, 23.12.87. Lyatkher V. M., Aleksandrov A.S. Shpolyansky Yu.B. Yuferov V. I. "Wind power installation", Author Certificate of the USSR No. 1357611 of 8.08.87, Bul. No. 45, 07.12.87.
13. Brian Kirke, Developments in ducted water current turbines, Sustainble Energy Centre, University of South Australia, Mawson Lakes, SA 5095, Australia.
14. Gourieres Le D. Wind Power Plants. Theory and Design, Pergamon Press, Oxford, N-Y,.., 1982.

15. The description of these and many other early proposals of experts of the USSR are available in the books: E.M.Fateev, Wind turbines and wind turbines, OGIZ, M.1948, Shefter Ya.I. Use of wind power, M; Energoatomizdat, 1983. Andrianov V. N., Bystritsky D. N., Vashkevich K.P. Sektokrov V. R. Vetroelektrichesky stations. M.-L. GEI, I960.
16. Milkovitsky S.I., Lyatkher V. M., Chumachenko V. G. Uvarov, L.A. Litavrin V.A. "The floating wind turbine", Author Certificate of the USSR No. 1221982, of 01.12.85.

3

Orthogonal Wind Units: Mathematical Models

The orthogonal power units with a working wing, a sail or a spin axis of all units being approximately perpendicular to the wind speed, are among mankind's most ancient mechanisms. According to the historical data, the simplest wind units with a vertical axis were used in Egypt, China, and Japan almost 2000 years ago. The most important advantage of the vertical axis orthogonal units is that they are independent of the wind direction. The orthogonal units can be divided into two types (Figure 3.1): One, where the working blades move more slowly than the wind, and two, where the blades move faster than the wind.

The units of the first type (items 1 - 5) usually have a low capacity factor of the wind power (below 0,3). Moreover, they are characterized by low velocity (the blade optimum velocity makes about 0.3–0.7 of the wind speed), that requires the use of heavy mechanical and electrical equipment to obtain the electric power.

In recent years, numerous improvements of the low-speed orthogonal units have been introduced in order to increase their power effectiveness. This goal is reached by introduction of control devices withdrawing the "sail" at the working element moving towards to the wind, and exposing the "sail" in the optimum

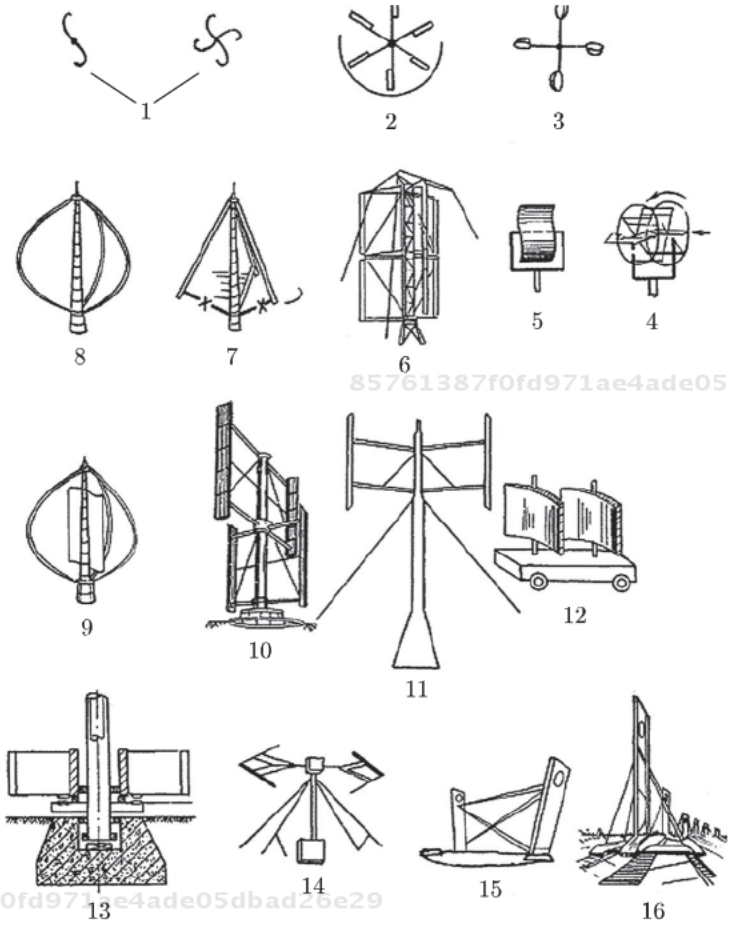

Figure 3.1 Packaging schemes of orthogonal power units.

situation at the working element moving downwind (in some inventions this is made automatically, for example, under the wind action) (Figure 3.2). Thus, due to the low speed of the unit, its specific materials consumption (per a power unit or an output) remains rather high.

The operation of the low-speed unit is principally defined by the velocity difference of the operation unit. (Figure 3.3).

The force D acting on the operation element is proportional to the square of the difference of the local flow velocity U and the longitudinal speed component V_x of the unit operation element:

$$D = C_D \rho (U - V_x)^2 s \, \text{sign}(U - V_x)/2 \qquad (3.1)$$

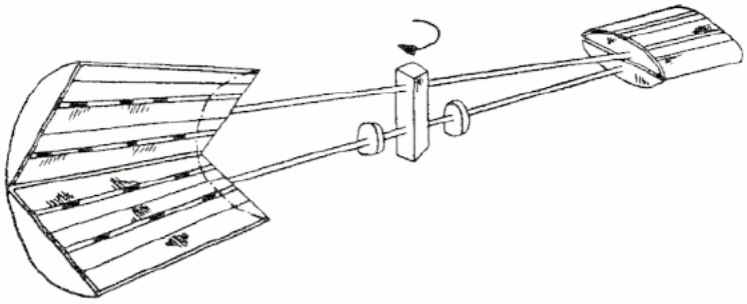

Figure 3.2 McMachon low-speed turbine (US Patent 4547125 of 15.10.1985).

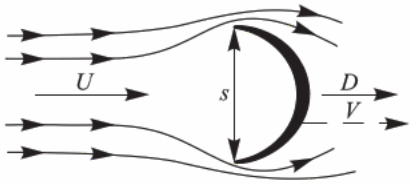

Figure 3.3 Scheme of flowing of the operation element of the low-speed power unit.

Here, s is the midsection area of the unit working element, and C_D – its resistance coefficient.

The flow velocity in the unit zone and its greatest possible effectiveness are found by calculation of an average power value per a turn by (3.1), by the technique of item 1. However, this effectiveness is never reached by low-speed machines, since a considerable proportion of the energy is spent for large-scale turbulence.

The unit local capacity developed by force (3.1) is defined by its multiplication at speed value V:

If V_x = V, local capacity (3.2) is maximum at:

$$\text{The power } P = DV \qquad (3.2).$$

If V_x = V, local capacity (2) is maximum at:

$$V = U/3 \qquad (3.3).$$

The unit effectiveness C_P in the formula $P = \rho\, C_P\, U_0^3 S/2$ cannot be exceeded:

$$C_P = C_D(U/U_0)^3\, 4/27 = 0.148\, C_D(U/U_0)^3 \qquad (3.4)$$

The condition (3.4) for low-speed machines provides a need to have the greatest possible resistance coefficient of C_D on the route site, where the working element moves along the flow. The resistance to the working element has to be the least on the oncoming movement site. This is reached by a special form of the rotor working elements (items 1, 3 in Figure 3.1), Figure 3.4, their turn in relation to the stream in motion (Figure 3.5), arrangement of the moving shutters (item 2 in Figure 3.1). The low-speed units have an important advantage of rather smaller power loss in the basic and running joints. This advantage can be demonstrated by the multi-blade shaftless wind units of big diameter and big power, considered below. The advantage of high-speed machines, like the axial orthogonal wind units, which working blades move 2 or 3-fold faster than the wind, is apparent.

The low-speed rotors can have a special design adapted for the reciprocal drive of piston pumps (Figure 3.6).

The high-speed orthogonal units (items 6 - 16 in Figure 3.1) usually transform the work made by the "pulling" force arising at flowing off the wing profile. If the traditional horizontal and low-speed

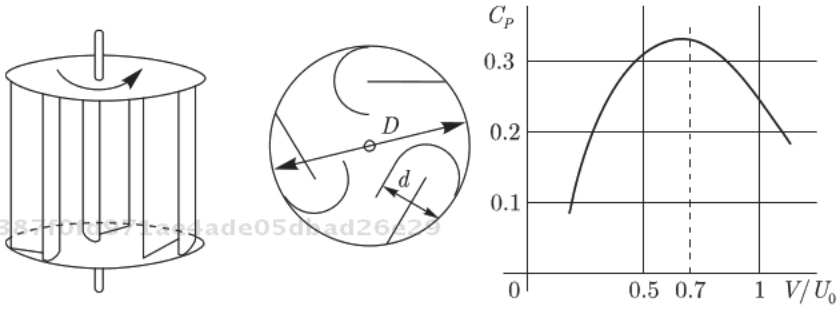

Figure 3.4 Low-speed power unit with directing fairings (Nguyen Vinh).

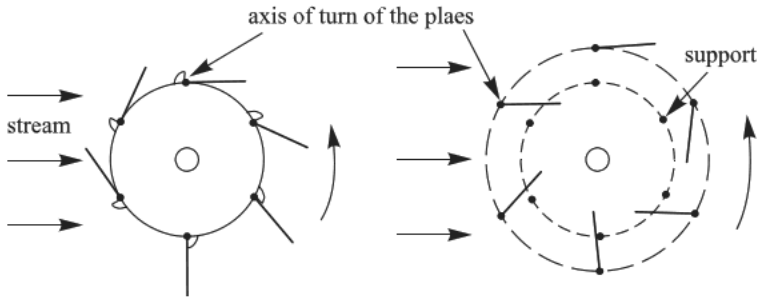

Figure 3.5 Rotors with rotary plates.

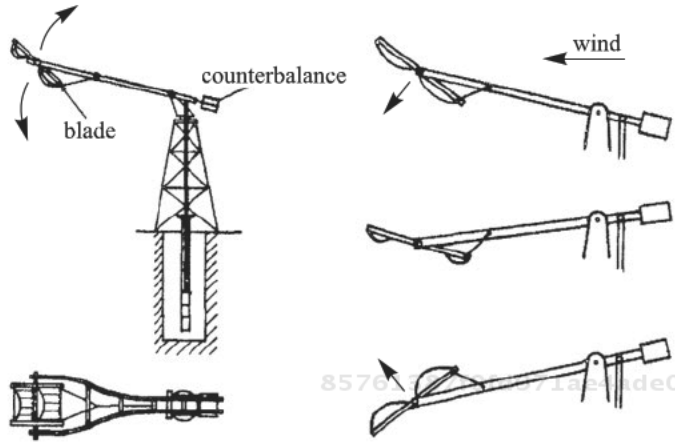

Figure 3.6 Wind-driven generator with a piston pump.

orthogonal wind units operate with any profile of blades, the high-speed orthogonal units operate only with aerodynamic profiles with a smooth shaped leading edge on which the "pulling" force is realized. An important advantage of the orthogonal machines with a vertical spin axis is their independence of the wind direction: the wind directions differ by height, only improving the unit operation.

The orthogonal wind units, being conceptually close to the modern ones, were actively built and tested at the 1920–1930 years. The invention of two character rotors belongs to this period, too:

- Sigurd Savonius low-speed rotor (1925, Finland) – Figure 3.7,
- Darrieus high-speed rotor (1925, France; 1931, the USA,) – items 6–11 in Figure 3.1.

The Savonius rotor uses both the action and the reaction of the stream, **rea**ction twice turning within to turn the rotor (Figure 3.7). The systematic research conducted by Savonius and repeated later, provided the optimum forms of rotors (Figure 3.8).

The system effectiveness reaches 30% at the thickness of the stream passing from one side of the rotor to another equal to 1/6 from the rotor working semicylinder diameter. The rotor effectiveness becomes improved at its greater relative height. Application of the height less than a rotor diameter is not recommended. The Savonius rotor, like many orthogonal machines, has so called dead zones – at some positions the rotor cannot be sinned independently

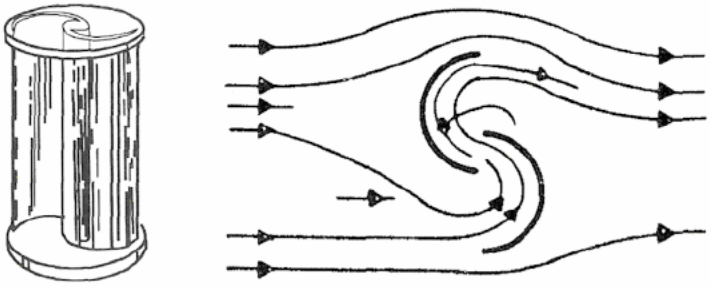

Figure 3.7 Savonius rotor – the design and the current scheme.

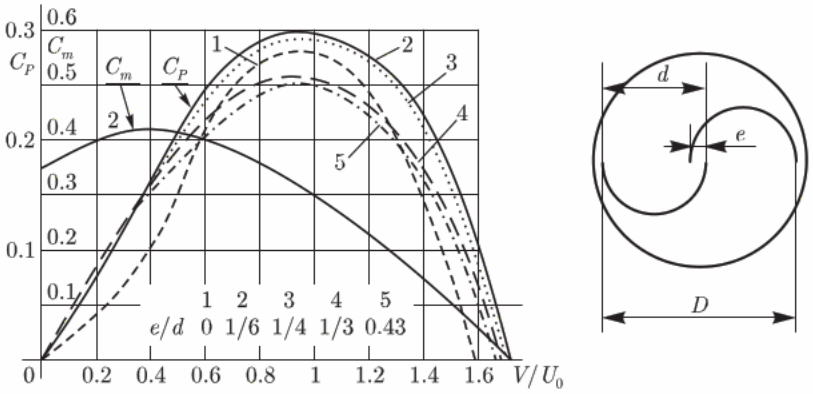

Figure 3.8 Torque C_m and effectiveness of C_p of Savonius rotors at different e/d.

(Figure 3.9), in spite of the fact that the average torque has a rather great value even at the smallest rotation speeds of the rotor (Figure 3.8 - line C_m). The orthogonal rotors are often made as many-tiered units (Figure 3.10).

When the rotor is positioned in the sector from 300° to 0°, the pressure coefficient is negative, and the rotor will not spin in the necessary direction.

Similar installations were invented by the brothers Voronins independently from Savonius (author certificate of the USSR No. 1654 of 30.09.1926). Later, it was proposed to equip the blades with internal flat sides and to make them displace under the influence of aerodynamic and centrifugal forces – in a storm the rotor becomes almost cylindrical, and at a light breeze the blades move apart. The same principle with many blades is realized in the Lafond turbine (Figure 3.11).

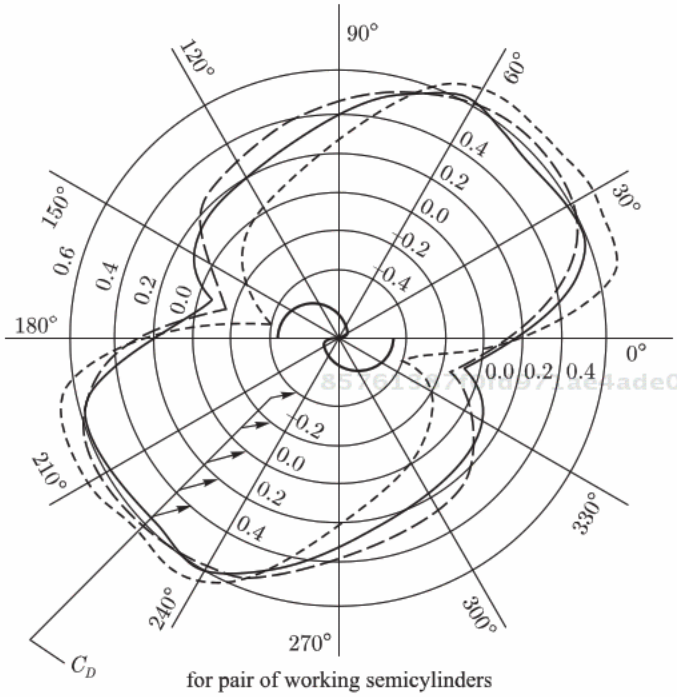

Figure 3.9 Chart of summarized pressure coefficient operating on a couple of working semicylinders of the Savonius rotor. Designations of lines correspond to Figure 3.8.

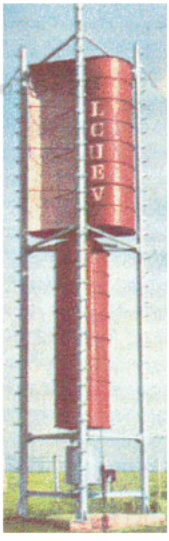

Figure 3.10 Two-tier Savonius rotor 4 kW at the wind 10 m/s. Diameter 3 m, height 14 m. In combination with the pump, it is capable of lifting water from a depth 7 m to a height 30 m. Expense to 7 m³/hour.

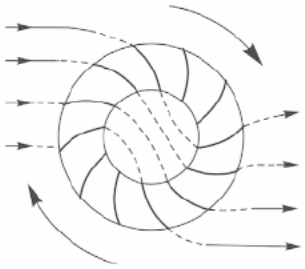

Figure 3.11 Lafond turbine.

The low-speed rotors – drum, revolving, with operated sails or wings - can be of the most various designs. Their main advantage is rather larger pulling efforts or torques. However, such units are not perfectly suitable for receiving the electric power, since their power effectiveness is low (the efficiency of a wind unit C_p is usually below 0,17 ÷ 0,20), and the mechanical and power equipment owing to low movement speeds of the working elements is relatively heavy. For example, the Savonius wind turbine with the blades span of 0,96 m and the height of 1,96 m had the rotor weight of 50 kg, and at the wind speed of 7 m/s developed the power of 50 W. If we assume the rotor effectiveness to be the same up to the wind speed of 14 m/s, the produced capacity could be about 400 W, and the specific material consumption of the rotor, 125 kg/kW; that is apparently significantly higher, than that of the high-speed units.

In the modern designs, the Savonius rotor is used as a starting one for the high-speed unit or as the main one for driving of pumps or mechanical equipment demanding a great moment at small rotation speeds of the rotor.

The high-speed Darrieus units (Figure 3.12) use the pulling force arising at the wing flow with moderated angles of attack (less than 15 ÷ 20°).

The product of this pulling force at the blade speed determines the rotor local capacity. If the traditional horizontal and low-speed orthogonal wind units operate with any profile of the blades, the high-speed orthogonal units produce energy only when using such aerodynamic profiles in which the "pulling" force is realized.

The fact of existence (realization) of pulling forces in the aerodynamic profiles remained a subject of discussion for many years. No wonder that the wind units using this force were met cautiously by the scientific community. Invented in 1927–1931, such units were not applied for a long time because of wrong

Figure 3.12 Commercial sample of the high-speed troposken wind turbine with a changeable ratio of height and diameter of the turbine (Flow Wind Corporation). Height 42–63 m, diameter 17–21 m, power 300–400 kW, wind during the operation from 4.5 to 27 m/s, calculated storm – 58.5 m/s. About 900 sets were installed in California in 1995.

representations about their allegedly small power effectiveness. In practice, the power effectiveness of these machines strongly depends on the experimental conditions, in particular on the Reynolds number, the form of the leading edge and the condition of the blade surface, and the intensity of the turbulence of incoming flow. The tests of small models in the wind tunnels provided, and still provide, low values of electrical power efficiency C_p in the ratio (4 in item 1) where Ω - area of the axis cross-section of the swept around figure. The field tests and more precise calculations executed in recent years in many countries disproved this delusion which used to be shared, in particular, by many aerodynamic engineers in the USSR. For a long time this error delayeddevelopment of wind engineering, and in many countries directed this development in the direction of perfecting the traditional wind units. According to the modern data, high-speed orthogonal units with optimum solidity and optimum profile of the blades according to power characteristics, are not inferior to the best collinear units. Figure 3.13 shows the largest experienced "troposken" power installation, with a diameter of 34 m (rated power 500 kW) created and studied in the Sandia laboratory. The form of a rotor

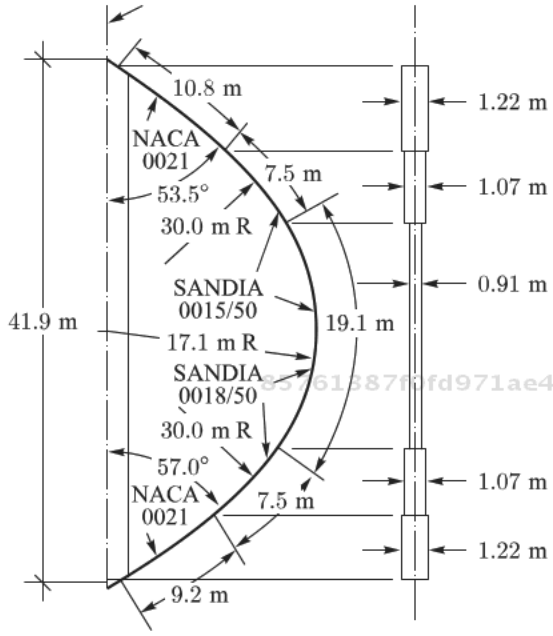

Figure 3.13 Two-blade Sandia-34 turbine.

of similar machines is replaced at a different rotation frequency and wind speed. The greatest efficiency of $C_p = 0.41$ was demonstrated by this machine at the rotation frequency of 28 rpm and tip-speed relation $z = V/U_0 = \omega R/U_0 = 6.34$ (Figure 3.14).

In large machines, in which capacity and output of the collinear units is reduced at non-complanarity of the wind, the advantage of orthogonal high-speed installations becomes especially noticeable. If the wind has different directions by height, that only improves the unit operation reducing non-uniformity of the torque. The largest high-speed orthogonal unit, 3,8 MW, height 108 m, was constructed in Canada; another unit, 1 MW, of a similar principle of operation but of another design, was constructed in England. The largest orthogonal and two-bladed (with turn of blades in the plan for 90 degrees) machines were designed (but not constructed) in Sweden – Figure 3.15.

Smaller orthogonal machines with the general capacity of 60 to 160 MW, that operated in the USA, England, Switzerland, Germany, Hungary, and Romania, are given in Figure 3.16.

These units have significantly smaller material capacity than the traditional ones. In the presence of a prevailing stream direction of

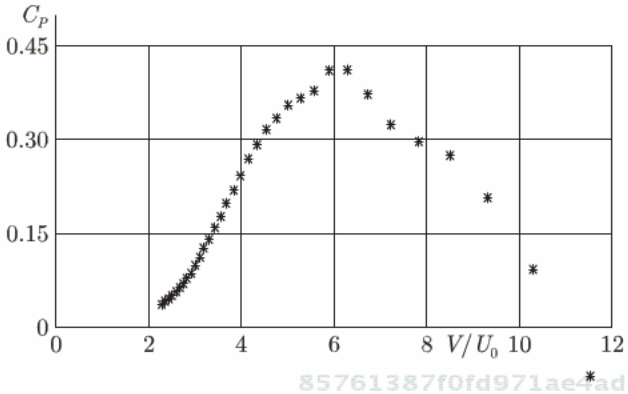

Figure 3.14 Efficiency of Sandia-34 turbine.

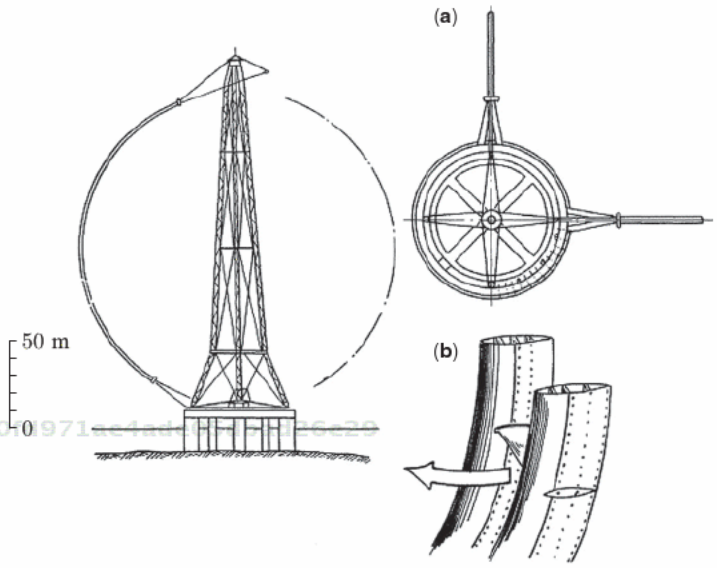

Figure 3.15 "L-180 Poseidon" according to Ljungstrom project. Canadian Patent 337.120, Oct.6, 1978, Danish 4146/79. Diameter of the turbine 180 m, power 20 MW, development 45 GWhour/year at average wind 9 - 9.5 m/s. 1980. Turn of working blades at 90° reduces pulsation of total loadings and torque.

air or water, the orthogonal unit axis can be horizontal or sloping (Figure 3.17).

The orthogonal units (both low-speed, and high-speed) in all variety of designs can be classified into two groups divided by an aero hydrodynamic attribute of a condition of the field of currents in the zone of the rotors:

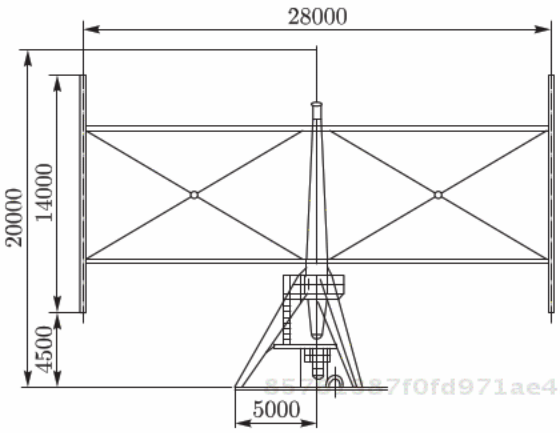

Figure 3.16 Operating 75 kW two-blade unit (at wind 11.4 m/s) – Germany, 1986.

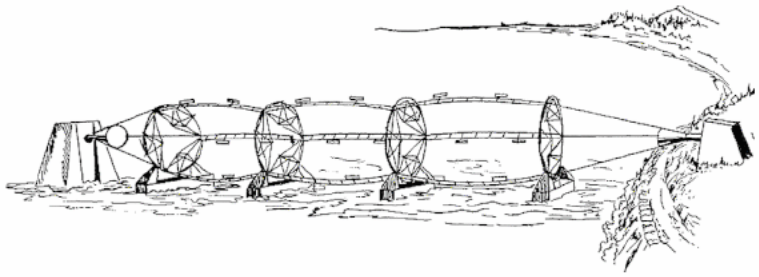

Figure 3.17 Orthogonal unit oriented across the prevailing wind direction.

- Common axial units, at which the diameter of the blade route is approximately equal to or less than the length of blades. At such machines, the upwind and downwind sides of the route of the blades are in various aerodynamic conditions owing to the stream braking;
- Units of a rather big diameter with the stream recovery in front the rear blade system, and the distinction stated above becomes insignificant.

In the first group units, the shadowing effects caused by distortion of the initial field of the wind speed in the motion zone of the blades are important:

$$U_{1,2} < U_0.$$

In the second group units, such distortion can be practically absent:

$$U_1 \approx U_2 \approx U_0. \tag{3.5}$$

Where U_1 - wind speed in the zone of the upwind site of the route of the blades; U_2 - the same for the downwind site of the route; U_0 - wind speed at a distance (on the way) from the wind unit. For providing a condition (3.5), spaced arrangement of the working blades is a necessary, but not a sufficient, condition. The distance between the blades "B" has to be such as to avoid overlapping of the zones E, where the relative disturbances of the initial speed field are greater than the preset small value (for example, 2 ÷ 5%).

Such zones were calculated depending on the attack angle at permissible variations of the module and the speed angle of the wind of 2% (Figure 3.18). The distance "B" between the blades along their route, providing lack of the relative shadowing with an accepted accuracy of 2% for the attack angles $\alpha > 7°$, makes:

$$B = (6 \div 7)b \tag{3.6}$$

The condition (3.6) provides a limiting of solidity: $\sigma \le \frac{\pi}{7 \div 8} = 0,39 \div 0,45$.

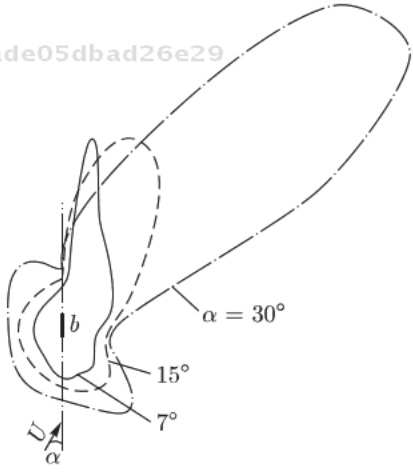

Figure 3.18 Zones of distortion 2% of the speed field at different attack angles of the stream to a plate.

The mutual interference of the blades is more noticeable at smaller angles of attack. It is necessary to consider that, irrespective of the assessment (3.6), the flow rate losses in the free wind unit zone surely occur because of taking of the stream mechanical energy. The insufficiency of the condition (3.6) is explained by this fact. Determination of speed in the wind unit zone is one of the central calculation problems of the wind turbines. For determination of this speed, the momentum conservation equation for the current tube covering the wind unit is usually considered, with a replacement in this consideration with some discontinuity surface (flat or cylindrical). From the works of Betz and Zhukovsky and onwards, some hypotheses concerning a hydrodynamic picture in the unit zone are entered to receive a loop system of algebraic equations.

A more efficient approach for definition of the field of currents in the wind unit zone is represented by a statement and solution of the complete hydrodynamic problem on flowing of a permeable surface which takes an impulse from the stream. Thus, the wind unit properties are reflected in tensor ratios connecting the local speed with the local dynamic reaction of the hypothetical surface replacing the unit.

If speed U in the wind unit zone is known, loads on the wind turbine blades and the rotor capacity can be found from the elementary wing theory.

At some point of the route of the blades set by the angle a^0_Λ, between the blade speed V and the wind speed on the way to wind unit U_0, the blade is circulated by an airflow with the relative speed of:

$$W = U - V \tag{3.7}$$

The vector **W** is directed to the peripheral speed of the blade motion at an angle:

$$\pi - \alpha = \arccos \frac{\left(V\left(U - V\right)\right)}{V\left|U - V\right|} \tag{3.8}$$

The blade is affected by the body force, perpendicular to W, -

$$F_y = C_y \frac{\rho W^2}{2} \Omega_\Lambda, \tag{3.9}$$

and the resisting strength, parallel to vector W, -

$$F_x = C_x \frac{\rho W^2}{2} \Omega_\Lambda, \tag{3.10}$$

where C_y - lift coefficient, C_x - resistance coefficient, ρ - air density, $\Omega_\Lambda = b \cdot L$, b - chord, L – blade length, Ω_Λ –blade area.

The sum of projections of these forces on the direction of the peripheral speed of the blade V gives the pulling strength:

$$F_\Gamma = F_y \sin\alpha - F_x \cos\alpha \equiv C_l \frac{\rho W^2}{2} \Omega_\Lambda, \tag{3.11}$$

and on the direction perpendicular to V - the normal force:

$$F_n = F_y \cos\alpha + F_x \sin\alpha \equiv C_n \frac{\rho W^2}{2} \Omega_\Lambda. \tag{3.12}$$

Where $C_l \equiv C_y \sin\alpha - C_x \cos\alpha$; $C_n \equiv C_y \cos\alpha + C_x \sin\alpha$.

The pulling (3.11) and the normal (3.12) forces depend only on the position and relative speed of the blade V/U (at a constant wind speed at approaching U_0):

$$\bar{F}_\Gamma = \frac{2F_\Gamma}{\rho U^2 \Omega_\Lambda} = C_l(\alpha) \frac{\sin^2 \alpha_\Lambda}{\sin^2 \alpha} \text{ or } \bar{F}_\Gamma^0 = \frac{2F_\Gamma}{\rho U_0^2 \Omega_\Lambda} = \bar{F}_\Gamma \left(\frac{U}{U_0}\right)^2, \tag{3.13}$$

$$\bar{F}_n = \frac{2F_n}{\rho U^2 \Omega_\Lambda} = C_n(\alpha) \frac{\sin^2 \alpha_\Lambda}{\sin^2 \alpha} \text{ or } \bar{F}_n^0 = \frac{2F_n}{\rho U_0^2 \Omega_\Lambda} = \bar{F}_n \left(\frac{U}{U_0}\right)^2, \tag{3.14}$$

$$\alpha = arctg \frac{\sin\alpha_A}{V/U - \cos\alpha_\Lambda} \tag{3.15}$$

where α_Λ - angle between the blade speed V and the wind speed U in the wind unit zone - differs little from the angle α_Λ^0.

$\bar{F}_\Gamma^0 \approx \bar{F}_\Gamma$ and $\bar{F}_n^0 \approx \bar{F}_n$ are usually supposed in practical calculations of the strength of the units, thereby considering a possibility of the wind speed pulsation in the wind unit zone up to the speed of the attacking flow. This phenomenon is also considered at the setting of the generator power. However, only the value of $\bar{F}_T$ is considered in calculations of the output.

The pulling force, defining the power characteristics, and the normal force depend on coefficients C_y and C_x, which are defined

experimentally for various profiles depending on the angle of attack:

$$\alpha_{\Sigma} = \alpha + \alpha_0, \tag{3.16}$$

where α_0 - turn angle of the blade chord in respect to the motion speed direction (positive, from the spin axis). An example of distribution of forces on the route of the unit of a rather big diameter is shown in Figure 3.19.

In the first group units, the wind speed U on frontal (U_1) side is greater than that on the shadow side (U_2) of the unit. Respectively, the aero (hydro) dynamic reaction operating on the blade on the front and rear sites of the route are different.

The mathematical models of the orthogonal wind units have different details. [1]

Here we will consider a general approach to the calculation of a picture of nonstationary currents in the zone of the wind unit or a group of units. The movement of air in the power unit zone is always turbulent. A turbulent flow description demands the introduction of some special hypotheses, many of which have a local character and are formulated differently for various conditions. One of fundamental suggestions in the field of description of turbulent flows is a representation of these currents by superposition of movements of different scale: non-isotropic low-frequency, large-scale movements and high-pitched locally isotropic pulsations. More specifically, the first version of such an approach can be found

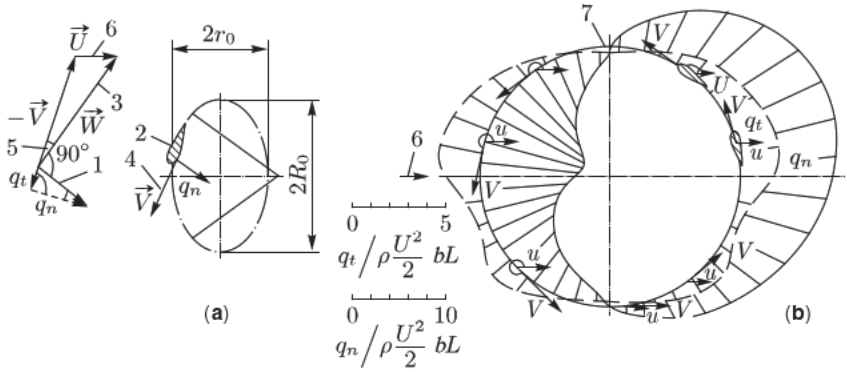

Figure 3.19 Scheme of flowing and loading on the blade of the orthogonal unit in different points of the route. Stream braking is not considered by the unit.

in the work of Reynolds (1891) where the average components of a hydrodynamic field were allocated, and the equations are now called by his name. The fundamental results in the description of a common structure of turbulent flows and, especially, their local isotropic components, were developed by A.N. Kolmogorov and his school [2]. As for the low-frequency, non-isotropic part of turbulence, especially important for engineering applications, its description for many years has been kept within the most prime models of "turbulent" (virtual) viscosity of Prandtl-Karman. In 1968, the author attempted an analysis of structural, non-isotropic components of turbulence on the basis of hydrodynamical equations linearized concerning these components [3].

Approximately during the same period, the irrotational (potential) turbulence model began to be widely applied to descriptions of the transformation of low-frequency turbulence in the streams. An essential defect of these approaches consisted of the impossibility of simulating a turbulent sliding friction, which in actual streams is formed by low-frequency, non-isotropic components of pulsations. The solution to this problem of creation of a loop system of the equations, including not only the first statistical moments of fields (average values), but also their senior moments (first of all – covariances – a turbulent sliding friction) suggested two ways.

The first way concerns a formal increase in the number of the equations for the senior moments of quasi-steady flows (idea of A.A. Fridman, 1923) with the introduction of heuristic connections between the senior moments through empirical "constants". This method resulted in a set of equations of Patankar-Spolding including 13 so-called empirical "constants" which actually varieds in different conditions. However, that little affected the results of calculations of the first two moments of currents. The modern computers usually realize three-dimensional nonstationary solutions of these equations (CFD software).

Another way considers a nonstationary solution of non-linear hydrodynamic equations, averaged by specifically selected space volumes (scales) [4].

Hence, the impulse conservation equation of a continuous medium is:

$$\frac{\partial}{\partial t}\int_W \rho\overline{U}dW - \int_W \rho\overline{F}dW + \int_W div\Pi dW = 0, \qquad (3.17)$$

where W – arbitrary volume, ρ – density, $\bar{U}$ – medium speed, Π – symmetric tensor of the second rank characterizing density of the impulse stream. The impulse stream through a surface unit perpendicular to the vector $\bar{n}$ is given by:

$$(\bar{P}_n \cdot \bar{n})\bar{n} + (\bar{U} \cdot \bar{n})\rho\bar{U}, \tag{3.18}$$

where $\bar{P}_n$ – vector of the surface force tension in non-viscous liquid.

$$\left(\overline{P_n} \cdot \bar{n}\right) = P, \tag{3.19}$$

where P – pressure (in the hydromechanics a spherical component of the stress tensor – the pressure – is accepted as a positive value at compression; contrary to all other models of the continuous medium).

Commonly in hydromechanics, the condition of arbitrary volume W is used together with an additional assumption of continuity of functions for rejection of the integral symbol in (3.17) and transition to differential equations. This is justified if the stream borders are outlined smoothly, and the current does not change much – slightly turbulent, deterministic, for example, laminar. At a turbulent flow, if $W \to 0$, the fluctuations of each item in the left part (3.17) grow, and the model with continuous functions and smooth borders becomes inconvenient. The essence of proposed model offers an assumption that continuity of the functions under integrals (3.17) is not used, and the volume of integration W is selected as small in comparison with the values of the current area, but great in relation to those scales of pulsations at which viscid dissipation of the turbulence energy takes place.

In practice, such a choice of volume is successful, if Reynolds numbers $\mathrm{Re} = \dfrac{UL}{\nu}$, made by the reference values of the stream L and the flow rate U averaged by L, are rather great, and in the range of pulsations there is a legible range of a local isotropic turbulence. Then, the linear dimensions of the volume W are selected a little smaller than $1/\chi_0$, where χ_0 – any wave number of the range of the wave numbers matching the local and isotropic disturbances. Usually, to save computing time, the grid size is increased by choosing χ_0 on the border between obviously nonisotropic disturbances and the range of local and isotropic pulsations.

The specified approach is effective for the calculation of average currents. If estimation of characteristics of the pulsation currents is necessary, one should consider dependence of the pulsation parameters on the value of the averaging platform – at larger values of the grid (in comparison with the integral scale of pulsations) the calculated amplitude of pulsations is much lower than the measured one. The proposed mathematical model is effective in the presence of singular points on the stream borders providing emergence of vorticity. The model can be applied in various modifications – from the calculation of two-dimensional nonstationary currents in the reservoirs with rough bottom (similar to Saint-Venant equations) to calculation of flow in two-dimensional (flat, axisymmetric problems) and, probably, in three-dimensional statements. In the most general view the equation of motion according to the proposed model is:

$$\frac{\partial \bar{\sigma}}{\partial t} + \sum_i \frac{\partial a_i}{\partial x_i} = \bar{g}. \tag{3.20}$$

The vector columns in the left part (3.20) mean:

$$\bar{\sigma} = \begin{vmatrix} \rho \\ \rho U_1 \\ \rho U_2 \\ \rho U_3 \\ e \end{vmatrix}, \quad \bar{a}_1 = \begin{vmatrix} \rho U_1 \\ p + \rho U_1^2 \\ \rho U_1 U_2 \\ \rho U_1 U_3 \\ (e+p)U_1 \end{vmatrix}, \quad \bar{a}_2 = \begin{vmatrix} \rho U_2 \\ \rho U_1 U_2 \\ p + \rho U_2^2 \\ \rho U_2 U_3 \\ (e+p)U_2 \end{vmatrix}, \quad \bar{a}_3 = \begin{vmatrix} \rho U_3 \\ \rho U_1 U_3 \\ \rho U_2 U_3 \\ p + \rho U_3^2 \\ (e+p)U_3 \end{vmatrix}. \tag{3.21}$$

Where $e = \rho\varepsilon + \rho \frac{1}{2} \sum_i U_i^2$ - total energy of the liquid volume, ε – its internal energy; $\bar{g}$ - column vector characterizing changes in the balance of weight, impulse and energy bound to the accepted method of space-time averaging of hydrodynamic fields and express properties of the currents – existence of internal sources or drains, removal or application of an impulse, depriving or introduction of energy.

In the cylindrical system of coordinates, the transition to which is set by the formulas:

$$x_1 = x,\ x_2 = r\cos\varphi,\ x_3 = r\sin\varphi. \tag{3.22}$$

the equations (3.20) become:

$$\frac{\partial \bar{\sigma}}{\partial t}+\frac{\partial \bar{a}_1 r}{\partial x}+\frac{\partial \bar{a}_2 r}{\partial r}+\frac{\partial \bar{a}_3}{\partial \varphi}=\bar{g}+\bar{f}, \tag{3.23}$$

where

$$\bar{f}=\begin{vmatrix} 0 \\ 0 \\ p+\rho U_{\varphi}^2 \\ -\rho U_r U_{\varphi} \\ 0 \end{vmatrix}, \tag{3.24}$$

U_r, U_{φ} – radial and angular speed components.

Integrating the equations by one of the coordinates, along which, in a piece with the length h, the curvature of current lines (or trajectories of particles) changes slightly, we obtain the two-dimensional equations (generalized Saint-Venant equations):

$$\begin{gathered}\frac{\partial q_i}{\partial t}+\sum_j \frac{\partial U_j q_i}{\partial x_j}-q_i h=-\frac{1}{2}\left(\lambda_{ij} U_j\right)U+\frac{\tau_i}{\rho}-\frac{\partial p}{\partial x_i}h; \\ \sum \frac{\partial q_i}{\partial x_i}=0; \quad q_i=U_i h.\end{gathered} \tag{3.25}$$

Where q_i – component of volume forces, τ_i – summarized tangential stresses of the external influence on the allocated layer borders with the thickness h, Λ_{ij} – hydraulic sliding friction coefficient operating on the allocated layer borders.

The equations (3.25) are well-known in the hydraulics, they are effective for calculation of the transfer processes with the minimum empirical information concluded in the friction coefficient Λ which may have a tensor structure. [5]

These equations are applied in the meteorology too, for example, at estimates of influence of the relief and creation of multiblades Wind Power Plants (WPP) on the current picture at a steady stratification fixing the thickness h of the ground layer.

Integrating the equations (3.20) by the space-time volume, within which the current is locally isotropic, and supposing changes of

the average values by one of the directions unessential, we obtain a set of equations approximately describing two-dimensional nonstationary currents, including non-isotropic turbulent disturbances of a vast scale:

$$\frac{\partial \rho U r^n}{\partial t}+\frac{\partial \rho U U r^n}{\partial x}+\frac{\partial \rho U V r^n}{\partial r}+\frac{\partial P\ r^n}{\partial x}=g_x r^n;$$
$$\frac{\partial \rho V r^n}{\partial t}+\frac{\partial \rho U V r^n}{\partial x}+\frac{\partial \rho V V r^n}{\partial r}+\frac{\partial P\ r^n}{\partial r}=Pn+g_r r^n; \quad (3.26)$$
$$\frac{\partial \rho r^n}{\partial t}+\frac{\partial \rho U r^n}{\partial x}+\frac{\partial \rho V r^n}{\partial r}=0.$$

Where U and V – speed components by the axes *ox* and *or*; n = 0, 1 – for cases of flat and axisymmetric currents; P – pressure including the component bound to the kinetic energy of isotropic pulsations.

As a matter of convenience of calculations, let us accept a ratio of pressure and density characteristic for weakly compressible gas at small Mach numbers:

$$P=B\rho^{\gamma},\ \gamma=2. \quad (3.27)$$

The ratio (3.27) is also convenient because the obtained solutions can be immediately transported to two-dimensional problems of heavy liquid movement with a free surface, and vice versa (gas-hydrodynamic analogy). At Mach numbers less than 0.4, the values γ do not, in practice, influence the results.

Taking into account (3.27), let us rewrite the set of equations (3.26):

$$\frac{\partial Q_1}{\partial t}+\frac{\partial Q_1 U}{\partial x}+\frac{\partial Q_1 V}{\partial r}+\frac{2B\tilde{\rho}}{r^n}\frac{\partial \tilde{\rho}}{\partial x}=g_x r^n;$$
$$\frac{\partial Q_2}{\partial t}+\frac{\partial Q_2 U}{\partial x}+\frac{\partial Q_2 V}{\partial r}+2Br^n\frac{\tilde{\rho}}{r^n}\frac{\frac{\tilde{\rho}}{r^n}}{\partial r}=g_r r^n; \quad (3.28)$$
$$\frac{\partial \tilde{\rho}}{\partial t}+\frac{\partial Q_1}{\partial x}+\frac{\partial Q_2}{\partial r}=0,$$

where $\tilde{\rho}=\rho r^n;\ Q_1=\tilde{\rho}U;\ Q_2=\tilde{\rho}V.$

This set of equations is solved by means of the implicit finite-difference scheme. The initial system (3.28) is approximated by a nonuniform rectangular grid defined as follows:

$$X_{1,i} = \sum_{m=0}^{i} \Delta_{1,m};\ \ X_{1,i-1/2} = \sum_{m=1} \Delta_{1,m} - \left(\frac{\Delta_1}{2}\right);$$
$$X_{2,j} = \sum_{m=0}^{j} \Delta_{2,m};\ \ X_{2,j-1/2} = \sum_{m=1} \Delta_{2,m} - \left(\frac{\Delta_2}{2}\right); \qquad (3.29)$$
$$i = \overline{O,K};\ \ j = \overline{O,N},$$

where K and N – number of joints by OX_1 and OX_2, and Z_i and $Z_{i\text{-}1/2}$ – coordinates of the grid clusters and the points located in the middle between the adjacent joints.

The difference approximation of partial derivatives is given by:
derivatives by time

$$\frac{\partial F}{\partial t} \sim \left\{\frac{F_{m,k} - F^0_{m,k}}{\tau}\Big|_n\right\}, \qquad (3.30)$$

convective members by their direction

$$\frac{\partial F_n a_n}{\partial x_n} \sim \left\{\frac{\delta a^1_m \left(F_{m+1} - F^1_{m-1}\right) + \delta F^1_m \left(a^1_{m+2} - a^1_{m-1}\right)}{\left(\Delta_m + \Delta_{m-1}\right)} + \right.$$
$$\left. + \frac{(1-\delta) a^0_m \left(F^1_{m+1} - F^1_{m-1}\right) + (1-\delta) F^1_m \left(a^0_{m+1} - a^0_{m-1}\right)}{\left(\Delta_m + \Delta_{m-1}\right)}\Big|_{k,n}\right\}; \qquad (3.31)$$

convective members by the normal direction

$$\frac{\partial F_1 a_n}{\partial x_l} \sim \left\{\frac{\left(a_{m+1} + a_m\right)^{\delta}_l F_{m+1,m} - \left(a_m + a_{m-1}\right)^{\delta}_l F^1_{m,n}}{\left(\Delta_m + \Delta_{m-1}\right)} - \right.$$
$$\left. - \frac{\left(a_{m+1} - a_m\right)^{\delta}_l |F|^1_{m+1,n} - \left(a_m - a_{m-1}\right)^{\delta}_l |F|^1_{m,n}}{\left(\Delta_m + \Delta_{m-1}\right)}\Big|_k\right\}; \qquad (3.32)$$

derivatives containing the pressure function

$$\frac{\partial P}{\partial x_n} \sim \left\{B\left(P_{m+1/2,k} + P_{m-1/2,k}\right)\frac{\left(P_{m+1/2,k} - P_{m-1/2,k}\right)}{\left(\Delta_m + \Delta_{m-1}\right)_n}\right\}, \qquad (3.33)$$

where $F = \{Q_1, Q_2\}$; $a = \{v_1, v_2\}$; $n = 1, 2$; $l = 2 - (n-1)^n$ – indexes characterizing the direction; $m = i(2 - n) + j(n - 1)$ and $K = (i + ½)(n - 1) + (j + ½)(2 - n)$ – indexes defining points of approximation; z_1 – means that the variable is taken from the top layer by time; z_0 – the variable is taken from the bottom by time; $\delta \in (0, 1)$– weight function allowing change of the degree of the scheme non-evidence; $\left(a_{m+1} + a_m\right)^{\delta}_{l,k} = \delta\left(a_{m+1} + a_m\right)^{1}_{l,k} + (1-\delta)\left(a_{m-1} + a_m\right)^{0}_{l,k}$.

The continuity equation in a difference representation is:

$$\frac{\rho^1_{i+1/2,j+1/2} - \rho^0_{i+1/2,j+1/2}}{\tau} + \frac{Q^1_{1i+1} - Q^1_{1i}}{\Delta_{1i}} j + ½ + \frac{Q^1_{2j+1} - Q^1_{2j}}{\Delta_{2j}} i + ½ = 0. \quad (3.34)$$

Let's write the difference scheme generally, having replaced the differential operators with the corresponding differences [6]:

$$\begin{aligned} &\frac{Q^1_1 - Q^0_1}{\tau} i, j + ½ + \lambda_{11}\left(Q_1 U\right) + \lambda_{12}\left(Q_1 V\right) + B\lambda_{13}\frac{\tilde{\rho}^2}{r^n} = 0; \\ &\frac{Q^1_2 - Q^0_2}{\tau} i + ½, j + \lambda_{21}\left(Q_2 V\right) + \lambda_{22}\left(Q_2 U\right) + Br^n\lambda_{23}\left(\frac{\tilde{\rho}}{r^n}\right)^2 = 0; \\ &\frac{\tilde{\rho}_1 - \tilde{\rho}_0}{\tau} i + ½, j + ½ + \lambda_{31}Q_1 + \lambda_{32}Q_2 = 0. \end{aligned} \quad (3.35)$$

The difference scheme is split by substitution of $\tilde{\rho}_1$ from the continuity equation into the motion equations, resulting in the system of two equations with two unknowns members, which is resolved by the Seydel iterative method, beginning the count from any direction. The obtained implicit difference scheme is divergent, steady at realization of the Courant criterion where the flow rate only appears as a normalized speed, and the number of exponent operations of the joints in the calculated area is economic.

The numerical solution of a difference analog of the equations (3.25, 3.28) at a choice of a grid step for the reasons described above, is well coordinated with the experimental data and allows for thereceipt of a complete nonstationary picture of large-scale currents. Figure 3.20 shows the plan of currents and some parameters in the scheme of a sudden expansion of a stream in the plan. In Figure 3.21 the relative length of a water swirl zone (L/b) is accepted as a stream characteristic. At continuous relative expansion of the stream and small Froude numbers $\left(\frac{U_0^2}{gh} << 1\right)$,

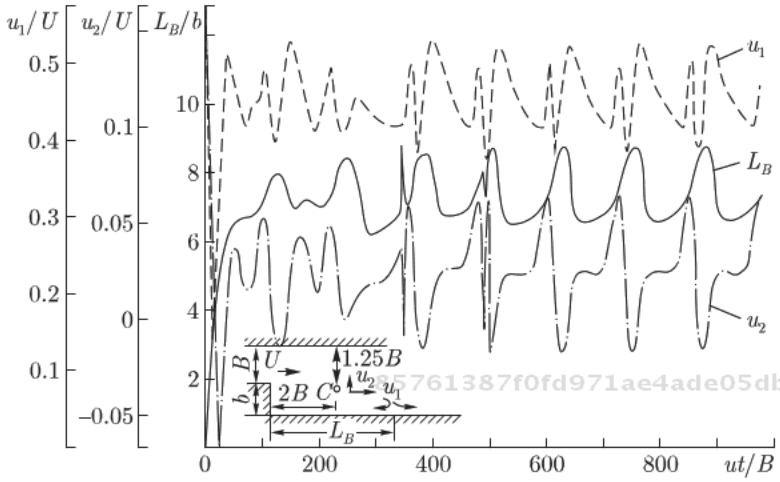

Figure 3.20 Example of calculation of the plan of currents on the site of a sudden stream expansion.

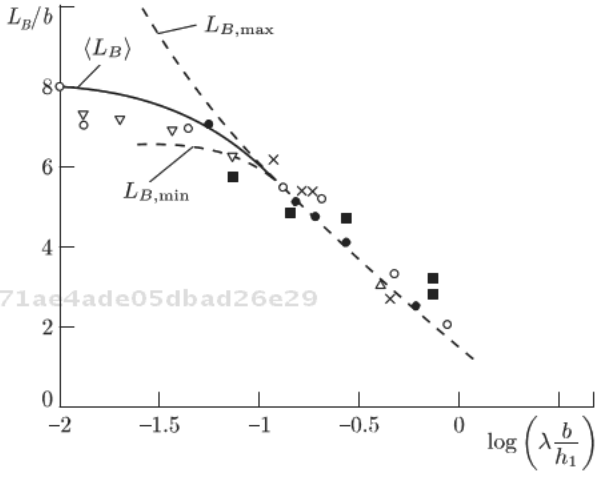

Figure 3.21 Relative whirlpool length at stream expansion in the plan behind the ledge of height b depending on the parameter $\lambda \frac{b}{h}$ according to the calculated and test data (dots).

the complex $\lambda \frac{b}{h}$ is usually considered to be a single parameter of the problem, where λ – coefficient of hydraulic friction (it is the first invariant at tensor structure of this coefficient).

Really, the experimental data obtained in similar conditions in different installations, are quite close and coordinated with the

results of these calculations (Figure 3.21). Actually, such matching is a consequence of a rather small distinction of the speed distribution, relative intensity level, and spectral distribution of the turbulence on the stream way to the studied site. The influence of these factors, which are usually not considered in the calculations and experiments, may be very great. There are calculated and test data about non-uniformity flow rate curves that are able to change the whirlpool length more than 3-fold.

The intensity of turbulent pulsations also makes a very noticeable influence; and according to trial and laboratory measurements, in the streams with actual pulsation ranges, this influence is much more than by calculations when imposing periodic speed disturbances, with some relative amplitude, to a stream in the inflow face.

The calculations of power units are carried out for the conditions of lack of volume of external forces and tangential stresses on the stream borders (in (3.25) $g_i = 0$, $\Lambda_{ij} = 0$ and $\tau_i = 0$). This situation is typical for a classical plane problem. It is important to emphasize, that even for lack of the external conditions generating vorticity and turbulence, the solution of a difference analog of the equations (3.25) for the areas with singular points at steady-state regional conditions does not come to a steady mode – the solution preserves the pulsation components (Figure 3.20).

The distribution of average speed and pressure values in quasistationary and nonstationary modes in the calculations and experiments under controlled conditions on the way to the calculated area is well coordinated (Figures 3.22, 3.23). In contrast, in distribution of the pulsation standards there is a systematic difference, on the one hand, bound to the mitigation effect on a big step of the difference grid, and on the other hand, that in calculations the isotropic part of turbulence is not reproduced. The question of direct numerical modeling of turbulent pulsations remains insufficiently clear, though some practical results in this direction are collected by different authors rather intensively.

When solving the problem of flowing of bodies by a free stream, the calculated area dimensions are selected to avoid the influence of external borders, where at a stream inflowing into the area the speed of an undisturbed current is set, and in the case of flowing out – "weak" boundary conditions appear. On the impenetrable surface of streamlined bodies the normal component of a flow rate is considered to be zero.

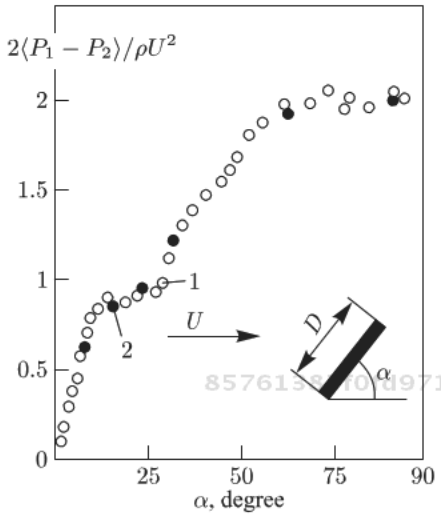

Figure 3.22 Average pressure difference upon a flat plate according to the experiments of TSAGI (1) and to calculations (2) without the use of empirical parameters.

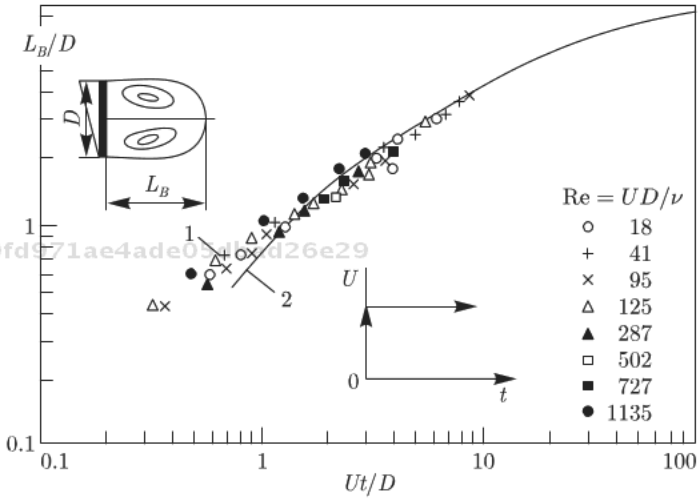

Figure 3.23 Whirlpool length behind a flat plate dispersed from the fixed condition. 1 – Taned experiments, 2 - calculation without the use of empirical parameters.

The equations (3.28), with the right member reflecting selection of an impulse in the wind unit zone, underlie a number of mathematical models of different complexity, allowing for a count of the necessary parameters of currents and influences. In particular, the

pressure drops on a flat infinite impenetrable plate which circulated at different angles of attack have been calculated. The calculation results appeared in a good agreement with the reliable test data (Figure 3.22).

The equations (3.28) can be written down in a polar or in a rotating coordinate system. In the rotating Cartesian coordinate system the equation (3.28) is:

$$\begin{aligned}
&\frac{\partial Q_1}{\partial t}+\frac{\partial Q_1 \upsilon_1}{\partial x_1}+\frac{\partial Q_2 \upsilon_1}{\partial x_2}+\frac{\partial p}{\partial x_1}=-2\omega Q_2-\omega^2 x_1 \rho; \\
&\frac{\partial Q_2}{\partial t}+\frac{\partial Q_1 \upsilon_2}{\partial x_1}+\frac{\partial Q_2 \upsilon_2}{\partial x_2}+\frac{\partial p}{\partial x_2}=2\omega Q_1-\omega^2 x_2 \rho; \qquad (3.36) \\
&\frac{\partial p}{\partial t}+\frac{\partial Q_1}{\partial x_1}+\frac{\partial Q_2}{\partial x_2}=0,
\end{aligned}$$

where υ_1 and υ_2 – speed vector components in the direction of horizontal orthogonal OX_1 and OX_2 axes, respectively, in the rotating coordinate system; ω – angular rotation velocity of coordinates; ρ – density; $Q_1=\rho\,\upsilon_1$; $Q_2=\rho\,\upsilon_2$; p – pressure bound to density by the ratio (3.27).

The approximation of derivatives in the left part (3.20) is carried out as in (3.28).

The approximation of the right member is carried out as follows:

$$\begin{aligned}
-2\omega Q_2-\omega^2 x_1 \rho=\Bigg\{&\left(\frac{1-\cos\omega t}{2}\right)\left(\frac{Q_1^1-Q_1^0}{\tau}\right) \\
&+\frac{\sin\omega\tau}{\tau}\left(\frac{Q_2^1+Q_2^0}{2}\right)+\omega\rho x_1\frac{\sin\omega\tau}{\tau}-\omega Q_2\Bigg\}_{i,j+\frac{1}{2}}; \\
2\omega Q_1-\omega^2 x_2 \rho=\Bigg\{&-\left(\frac{Q_1^0+Q_1^1}{2}\right)\frac{\sin\omega\tau}{\tau} \qquad (3.37) \\
&-\frac{1-\cos\omega\tau}{2}\cdot\frac{Q_2^1-Q_2^0}{\tau}+\omega\rho x_2\frac{\sin\omega\tau}{\tau}+\omega Q_1\Bigg\}_{i+\frac{1}{2},j}.
\end{aligned}$$

The different scheme in the polar coordinates has been applied to the calculation of currents in the zone of the permeable flat disk

with the concentrators and without them. Figure 3.24 shows an example of the calculation results of pressure changes on the disk and behind the disk in time.

The developed mathematical model is applied in practice in two versions.

In the first option, the unit is replaced with a permeable figure (a rectangular plate, a disk or a cylinder). The permeability is set by the flow rate value on the permeable figure mathematically replaced by a discontinuity surface on which there is a jump (difference) of pressure. The mathematical two-dimensional model is used for communication definition between these parameters – the flow speed U and the pressure drop Δp. The result, naturally, is various for two-dimensional

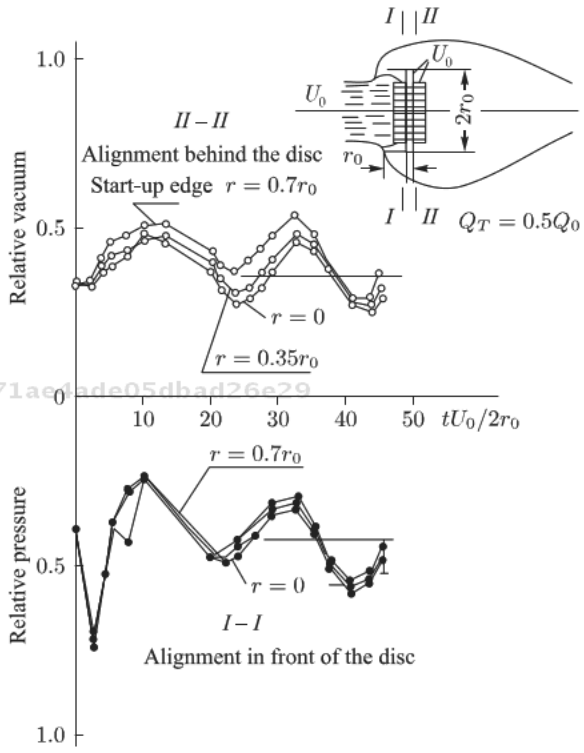

Figure 3.24 Calculation results of flowing off the permeable disk with concentrators (nozzles). The relative pressure on the pressure head side of the concentrator in the form of a cylindrical nozzle with the length equal to the disk radius (bottom plot). The relative vacuum behind the concentrator at application of half of the expense taken away from the pressure head side into the zone of the vacuum (top plot).

bodies of different forms. Moreover, it depends on the presence or absence of additional conditions, for example, a requirement of a trace symmetry behind a body or without such restriction (Figure 3.24). It is known that without a dividing wall behind the flat infinite plate, its resistance coefficient is equal to $C_D = 2$ (pressure reduction behind the plate -1.3), and with a dividing wall (condition of the trace symmetry) – the resistance coefficient $C_D = 1.5$, and the pressure reduction -0.8. All these data are consistent with our calculations.

In calculations of two-dimensional flowing off[?] the disk (the axisymmetric problem), a strong influence of the stream limitation was revealed – the impenetrable walls of the wind tunnel even at a small blockage (16%) is able to considerably overestimate an apparent effectiveness of the unit. The experimental value of the pressure drop on the round disk in a boundless stream $C_D = 1.2$ is very close to the results of calculations for the boundless environment [7].

1, 2 – flat plate (symmetric -2 and asymmetric -1 flowing), 3 – permeable cylinder, 4 – Betz-Zhukovsky theory.

The flow speed U is accepted as a calculated flow rate for determination of the local forces operating on the unit blades, calculated according to the partial theory of the wing, and summarized longitudinal force F_x, operating on the unit as a whole. This force is equated to the pressure force

$\Delta p\ \Omega$ on the permeable surface Ω, imitating the unit at the first stage of the calculation:

$$\Delta p\ \Omega = F_x(U) \tag{3.38}$$

From this condition we found the conditional calculated speed U in the unit zone, the load of blades and the unit power estimates:

- "theoretical" $P_t = \Delta p\ \Omega\ U$ and
- "practical" $P_p = M\ \omega$, where M – a torque on a unit axis from all forces operating on the blades and the design elements of the unit, ω – circular frequency of the unit rotation.

The main convention of this approach, which is usually called "the pulse theory", without consideration of non-uniformity and not-stationarity of the stream within the unit, supposes a need for use of the empirical characteristics of flowing of the blades obtained in conditions significantly different from the real conditions of the blades of power units. At all conventions of this calculation, its results when using line (1) of Figure 3.25, correspond to the direct measurements

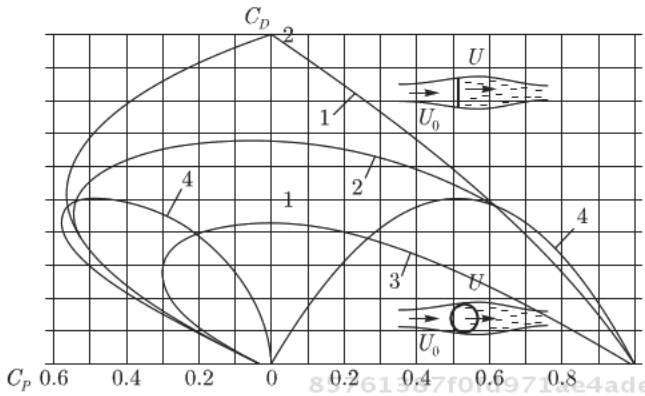

Figure 3.25 Relative pressure drop $C_D = 2\Delta p / \rho U_0^2$, relative speed on the permeable figure U/U_0, simulating the unit, and relative theoretical capacity of the unit $C_P = 2P\tau / \rho U_0^3 \Omega$.

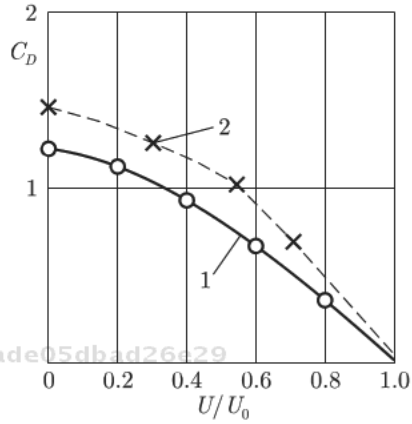

Figure 3.26 Dependence of the relative pressure drop on the round permeable disk from the relative flow rate through the disk. 1 - calculation ofthe two-dimensional Euler equation for an unlimited stream, 2 - the same with the permeable disk diameter equal to 0.4 from the pipe diameter in which it is established (16% of the area shadowing).

of the flow rate in the unit zone (Figure 3.27) and the data of measurements of the efforts operating on the unit as a whole (Figure 3.28).

The calculations of the unit effectiveness and loads of its elements when using the permeable plate model for the actual profiles yield close results on the other hand, the permeable cylinder model provides a strong underestimation of the results (Figure 3.29).

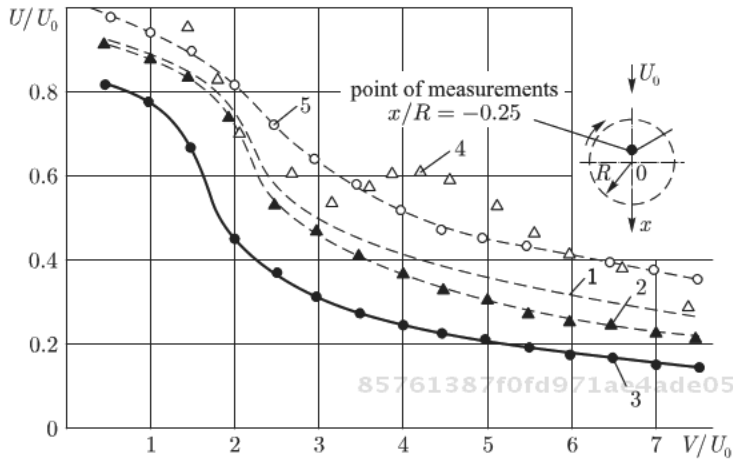

Figure 3.27 Relative speed of the environment in the power unit for different models of the "ideal" unit. 1, 2, 3 – by the respective lines in Figure 3.25 (right), 1–4 – σ=0.33, 5 - calculation by line 1 in Figure 3.25, σ = 0.20, 4 - experiments in the channel 1.5D wide.

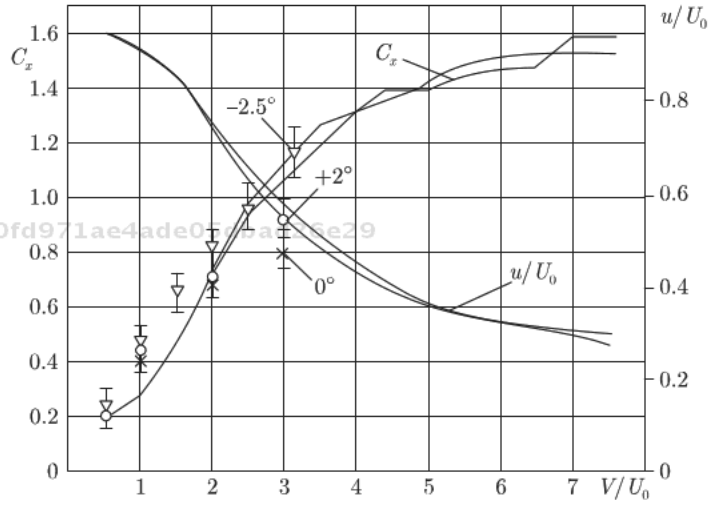

Figure 3.28 Speed in the unit zone of and the resistance coefficient C_D of the unit as a whole depending on the rotor rapidity. Solidity σ = 0.267. Lines – calculation at the blade turn with the NACA 23012 profile at 0° or at 2° from the tangent, dots – results of experiments of TSAGI on the model with diameter 3 m with Mi-2 helicopter blades (chord 0.4 m, length 2.55 m, flat side to the spin axis). The turn angle made - 2.5°, 0° and 2°.

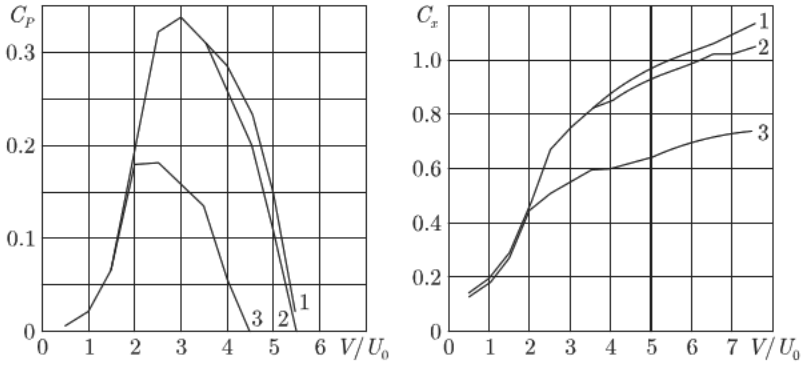

Figure 3.29 Efficiency (left) and pressure (resistance) coefficient (right) of the unit calculated by the pulse model for the unit with 2 blades with the NACA 0018 profile, solidity 0.2. 1 – asymmetrical flow plate, 2 – symmetrical flow plate, 3 – permeable cylinder

In practical calculations, it is recommended to consider the results relating to the permeable plate model with the asymmetrical flowing. The calculations for the pulse theory in this case, at the suitable consideration of additional losses in the design elements and the power path, and also at a suitable choice of the aerodynamic characteristic of the profile of blades, yield satisfactory results (Figure 3.30).

If the aerodynamic power losses on traverses and other design elements of the unit, and the mechanical losses in the supports, and the electric losses in the generators are not considered, then the calculation of power characteristics and loads of the system as a whole is self-contained, allowing comparison of the power characteristics of different options (Figure 3.31).

The accounting of resistance and characteristics of the generator in the pulse theory is very important.

Generally, the calculation procedure consists of the following: [8]

At fixed speeds of the blade leading edge V and the flow rate outside the unit:

U_0 for different values of the flow rate in the unit zone $U<U_0$, accepted as identical on all sites of the blade route, formulas of the partial theory of the wing calculate the value of the pulling F_t and normal F_n forces operating on the blade:

$$F_t = \rho W^2[C_y(\alpha - \alpha_0)\sin\alpha - C_x(\alpha - \alpha_0)\cos\alpha]bL/2 \quad (3.39)$$

$$F_n = \rho W^2[C_y(\alpha - \alpha_0)\cos\alpha + C_x(\alpha - \alpha_0)\sin\alpha]bL/2 \quad (3.40)$$

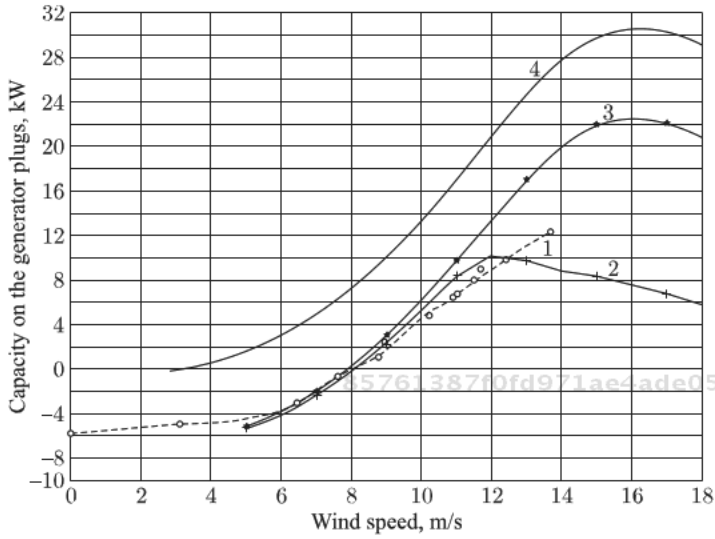

Figure 3.30 Test data (1) and calculations by the pulse model of a single-blade wind unit. Rotation frequency 82 rpm, 2, 3 – the losses are considered in the generator (by the no-load operation tests without a rotor – 0.45 kW) and by the frame elements resistance coefficient $\xi = 0.038$. 4 – calculation without losses. Lines 2 and 3 correspond to different characteristics of the profile of the blades. For line 2 the experimental data of a particular blade purge are taken at the Reynolds number corresponding to the traveling speed of the unit blades.

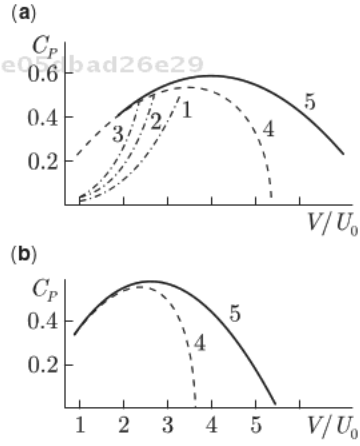

Figure 3.31 Efficiency of the "ideal" orthogonal unit at solidity $\sigma = 0.2$ (a) or 0.3 (b) and the blades of different profiles: 1 - NACA 0012, 2 - NACA 0015, 3 - NACA 0018. Lines 4 and 5 – different conditions of flowing of the modeling plate – symmetrical (4) and asymmetrical (5).

Where W – module of the relative speed of flowing of the blade, $W = |\mathbf{U} - \mathbf{V}| = U|\sin\psi/\sin\alpha|$

The angle α formed by vectors (-V) and W is defined by the expression:

$\alpha = \text{arctg}[\sin\psi/(V/U - \cos\psi)]$, where ψ – angle between U and V, α_0 – angle of turn of the blade chord concerning the blade speed vector V.

Projecting the forces operating on the blade on the current direction outside of the unit and carrying out averaging by the route of the blades, we find the average force operating on the unit in the lengthwise direction:

$$F_x = i\int(F_t\cos\psi + F_n\sin\psi)\, d\psi/2\pi \qquad (3.41)$$

Where i – number of blades.

Associating this force to the cross-section area of the swept around figure and the velocity head of the incoming flow, we find the unit resistance coefficient C_x as a function of the relative flow speed U/U_0 in the unit zone. By the value of this coefficient, according to Figure 3.25, we find the relative flow rate value in the unit zone and its effectiveness ratio C_p at the fixed speed of the blades. The capacity of the turbine calculated by this coefficient is greater than that of the turbine's local power obtained by direct averaging by the route of blades.

$$P = <(i\, F_t\, V)> \qquad (3.42)$$

However, this value has to be reduced by the losses caused by resistance of the design elements, resistance in the mechanical clusters, and losses in the generator. The influence of these losses is very great, and their calculation is rather difficult.

At trials of the complete units in a big wind tunnel of TSAGI (Zhukovsky), the characteristic of the generator and the multiplicator could be defined experimentally before the rotor installation. That made it possible to carry out calculations for the pulse technique and to compare the results with the experimental data (Figure 3.32).

The agreement of the calculations and experiments was good. At the exclusion of additional losses, an assessment of the power characteristics of the unit according to the pulse theory is well matched with the experiments in other cases, though the dispersion of results for the same design appears considerable (Figure 3.33).

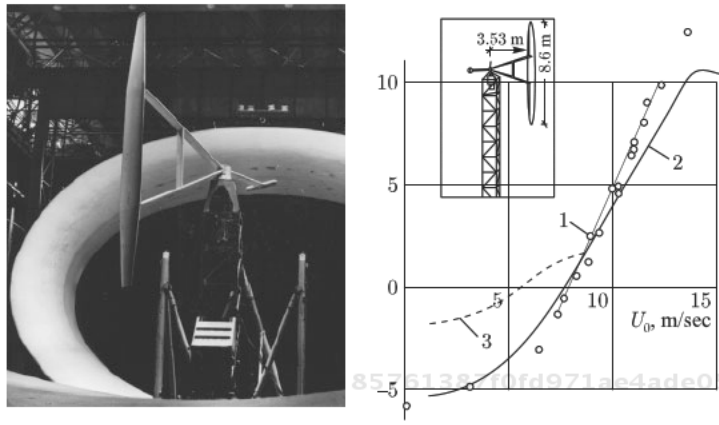

Figure 3.32 Single-blade orthogonal wind turbine tested in pipe 101 of TSAGI. Radius of the blade route 3.54 m, area of the blade 6.4m², average chord 0.74 m, length of the blade 8.6 m, GAW-1M profile. 1 – capacity on the standard motor reducer plugs at the generator rotation frequency 1500 rpm (speed of the blade 29.5 - 30.5 m/s), 2 - calculation by the pulse theory, 3 – capacity on plugs at 1000 rpm.

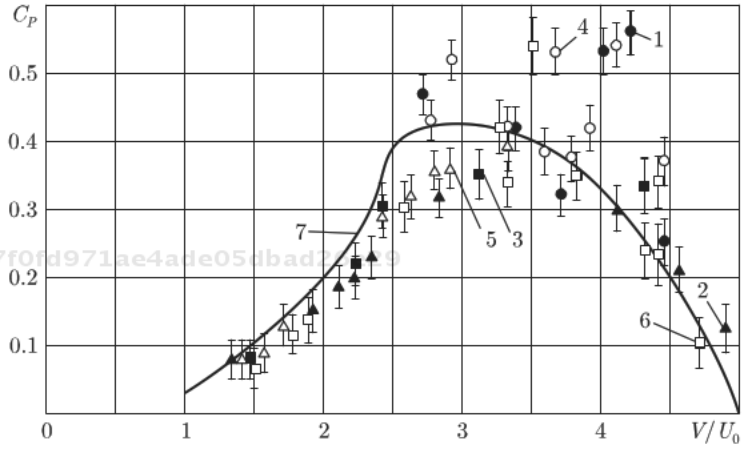

Figure 3.33 Efficiency of the wind units VL-2N depending on tip-speed relation. Losses are excluded. 1, 4 –VL-2 installation in the village of Nikulino, Moscow Region, 1983–84, 2, 5 – the same in Tallinn, 1985, 3, 6 – VL-2N installation, Tallinn, 1986, 1, 2, 3, - averaging less than 10 s, 3, 5, 6 – averaging more than 10 s, 7 – calculation by the pulse theory. [9].

The calculations for the pulse model are prime, allowing empirical adjustment at the expense of the change of coefficient of the aerodynamic resistance, accounting for actual aerodynamic qualities of the blades, transmission, and generator characteristics. All

these factors are realized in the program complex. Replacement of an actual wind-driven generator with a permeable figure taking an impulse (energy) from a stream, is productive at the calculation of the system of power units taking into account the local topography and the actual picture of currents outside the system.

The second approach to calculations of the power units being based on the same common mathematical model, consists of replacement of the actual blades with impenetrable rotating plates and calculation of the complete picture of currents, more reliable assessment of nonstationary normal loads of the blades, and receiving more reliable assessments of the local conditions at the leading edge of the blades for determination of the pulling forces and the actual capacity of the unit. As seen from Figure 3.34, standard atmospheric pressure on the aerodynamic profile and the flat plate differs at all angles of attack, except for a small range of the angles, where flowing of the profile is unstable.

The rotating system is used for calculations of the orthogonal wind units in an unlimited stream. The working blades in the mathematical model are replaced with impenetrable plates. Received results allow for confident estimates of the normal loadings operating on the blade (Figure 3.34). Consideration of the rotating plates is also useful for an assessment of the loads on the blades and the changes of the plan of currents in the wind unit zone. The normal loadings obtained by such calculations do not depend on the profile

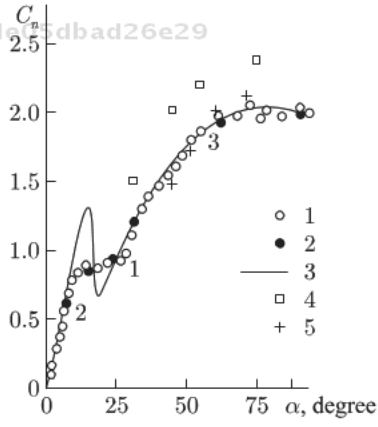

Figure 3.34 Normal load on the flat plate (1, 2, 4, 5) and the aerodynamic profile (3) depending on the angle of attack. 1 - experiments of TSAGI (Re = 0.8–1.1 10^6), plates with sharp edges [10] , 2 - calculation without empirical constants [11], 3 - experiments with the profile NACA 0012 (Re= 10^6) [12], calculation the free whirlwind method [13].

of the blades. In many cases, it can be considered accepted, since a normal load on the actual blade at small and larger angles of attack differs little from the load of a flat plate.

As the normal forces generally define rearrangement of a strongly unsteady flow, replacement of the actual blades with the plates probably reflects rather well the actual picture of the currents in the unit (Figure 3.35) and the actual normal loads on the blades (Figure 3.36).

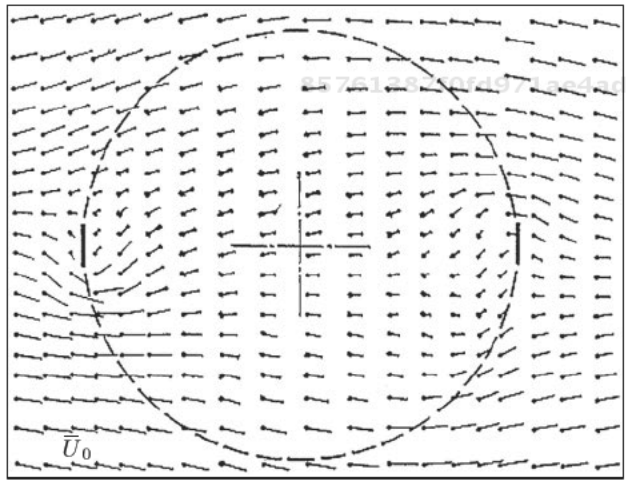

Figure 3.35 Instantaneous plan of currents in the transverse cross-section of the two-bladed unit at the blade position across the stream. $V/U_0=3$, $\sigma = 0.2$.

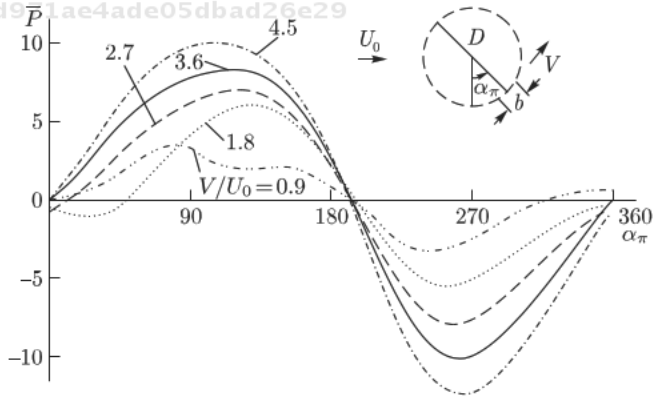

Figure 3.36 Normal loads on the blade of the two-bladed unit at different positions of the blade on the route and different relative traveling speeds of the blades V/U_0. Solidity 0.2. Loadings normalized by the velocity head of the free stream.

The calculation for this model allows estimation of the distinction of loadings on the rear and front sides of the route, to define loadings at different numbers of blades but identical solidity (Figure 3.37).

Additional and the most diverse assumptions are necessary for calculation of the pulling forces. However, a basis for these calculations is provided by the results of direct numerical model operation in the form of, for example, dependence of a flow rate from time in different points of the route of the blades (Figure 3.38).

For determination of the pulling forces and specification of normal forces at rather low speeds of the blade (i.e. at strong wind), it is possible to use a field of flow rates in the field of the rotor arrangement obtained by the solution of a problem of flowing of the system of rotating plates.

If we are to believe that the angle of attack of the blade on the route in the position α_π, is defined by the wind speed value in the same point of the route at the moment which is immediately preceding exaltation of the wind stream by the blade in some small vicinity of this point, then, according to the aerodynamic characteristics of the blade, it is possible to calculate the values of the pulling and normal forces, and the wind power capacity factor.

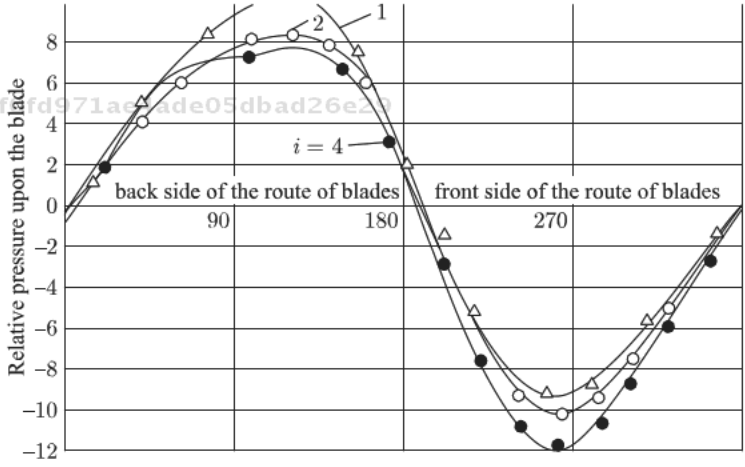

Figure 3.37 Normal load on the blade (positive from the rotation center) at different numbers of blades (i=1, 2, 4) but identical solidity $\sigma = 0.2$ and identical speed of blades V=3.6 U_0. Pressure – in units of velocity head on the way to the turbine.

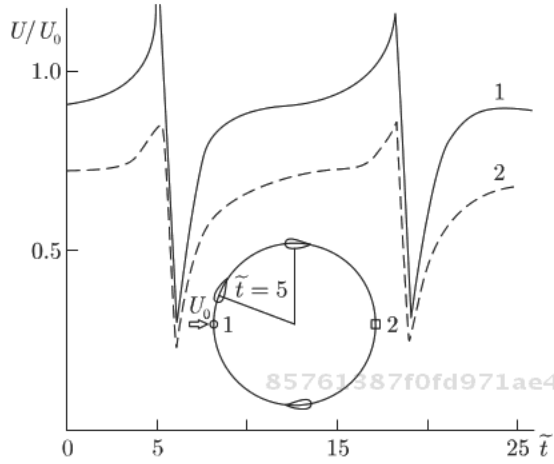

Figure 3.38 Change of the flow rate in time on the front (1) and rear (2) points of the route of two-bladed rotor with solidity 0.2. $V = 2.7U_0$, $t=t_\pi\pi/12\omega$.

The flow rate value in the considered point corresponding to the condition accepted above is given by:

$$\frac{\partial^2 U}{\partial t^2} = 0, \text{ here } t \in \left(\frac{t_1 + t_2}{2}, t_2 \right), \tag{3.43}$$

t_1 - an instant corresponding to the minimum flow rate in the considered point;

t_2 - an instant corresponding to the maximal flow rate in the considered point.

The changes of the flow rate in time at various points of the route for one turn of the rotor are qualitatively identical: after passing the plate, a period of sluggish restitution of the flow rate is observed, until the moment when again, a suitable plate starts influencing the flow rate at the considered point (Figure 3.38).

Having determined the speed at various points of the route, it is possible to calculate the pulling and normal forces operating on the blade with the given profile, assuming that the field of speeds in the field of rotation of these blades is close to the field of speeds induced by the rotating plates.

The normal forces calculated by the described scheme and operating on the plate appeared very close, further limiting consideration of the normal forces determined in the scheme with rotating plates.

At the fixed profile of the blades, the most important parameters defining values of the dimensionless loadings (coefficients of the pulling and normal forces) are the relative width of the blade $\frac{b}{D}$, the solidity $\sigma = \frac{ib}{D}$, and the relative peripheral speed of the blade (V/U_0). Depending on the design and dimensions of the wind unit and its operation modes, for ensuring the necessary durability of the rotor, the relative blade width may vary within some certain limits. A change of the solidity σ in the range from 0,1 ÷ 0,4 at $V/U_0 = 3,6$ in practice, does not affect the values of the aerodynamic loads of the unit blade $\bar{P}$, at the blade motion on the upwind (front) side of the rotation circle. On the shaded side at an increase in solidity, a decrease of aerodynamic forces operating on the blade is observed. The average (during the rotation period) load on the rotor axis for values σ = 0,1 ÷ 0,4 increases in proportion to the solidity.

$$F_x(\sigma_2) \approx F_x(\sigma_1) \cdot \frac{\sigma_2}{\sigma_1}. \tag{3.44}$$

The influence of the number of blades on the hydrodynamic loadings at the fixed solidity of the rotor and the constant relative speed of the blade, is demonstrated in the reduction of the maximum loads per a area unit of separate blades with the increase of the blades in number (Figure 3.39).

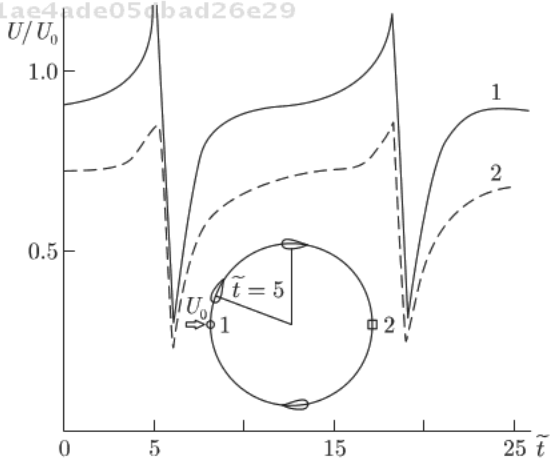

Figure 3.39 Load of the blade in the form of a plate ((1, 3) or in a cross-sectional profile with the characteristic by the experiments for stationary flowing (2, 4). Speed of blades $V = 1.8\ U_0$ (1, 2); $2.7\ U_0$ (3, 4).

For the rotors with the blades fastened by traverses to the central shaft, the influence of the central shaft on hydrodynamic loadings has been investigated. As proved by the calculations, the shaft influence with its relative diameter $\frac{d}{D} \le 0,075$ can be neglected.

Having calculated the field of speeds and using the empirical data on the flowing of profiles, it is possible to find the specified value of the normal forces and to determine the pulling forces. In practice, the normal forces do not differ from those defined for the rotating plates (Figure 3.39). The possibility of determination of the pulling forces, and the especially important determination of the resisting forces, from the design elements is an essential advantage of the method.

Without design resistance, the maximum efficiency of the orthogonal units determined by the pulse theory is approaching 0.6. The availability of the design joints and accounting of the objective parameters of profiles reduces this assessment 1.5 or 2-fold (Figure 3.40).

The calculations for the explained technique without engaging additional assumptions, are consistent with the known test data (Figure 3.41).

A special and very efficient option of the use of the same non-viscous liquid equations as in the previous model, but with the imposed vorticities for calculation of the orthogonal power units, is the method of discrete whirlwinds developed by Professor S.M. Belotserkovsky and his colleagues. He allowed the consideration of linear and non-linear, stationary and nonstationary problems of aerodynamics and hydrodynamics both for the elementary

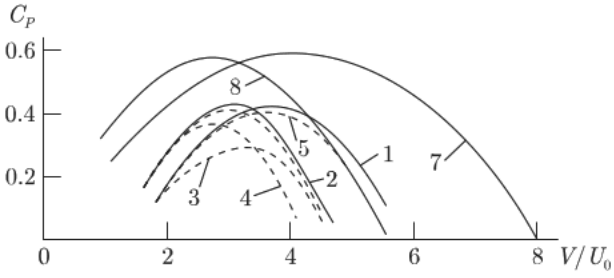

Figure 3.40 Power characteristics of "ideal" (7, 8) and "actual" units with the NACA 0015 profile, 2 blades, traverses and stays. R/H = 1, b/H = 0.2, $b_{stays}/b_{traverse}$=0.0011. 1, 3, 5, 7 – σ = 0.2; 2, 4, 6, 8 - σ = 0.3. 1, 2 – without design resistance, 3, 4 – considering losses from 2 traverses and 4 stays, 5, 6 – considering losses from 2 traverses only.

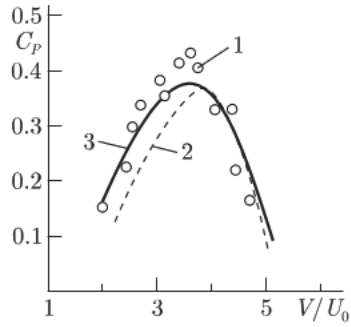

Figure 3.41 Efficiency of two-bladed orthogonal units by the experiments of H.M. Dress σ=0.22(1) [14] and P.J. Musgrove σ=0.17 (2) [15], calculations at σ=0.2 (3).

bodies, and for configurations as a whole from the uniform point of view.

In this method the body surface is replaced with a vortex layer, and then this layer and a trace behind it, are approximated by the system of discrete whirlwinds. The points, called calculation points, are selected on this body. In these points the impermeability condition is satisfied: i.e., in these points the sum of the speeds normal to a surface and those induced by whirlwinds, and the ongoing flow is equal to zero. The problem is reduced to the solution of the system of simple algebraic equations for the required circulation of discrete whirlwinds. The demanded class of solutions is allocated as follows. The discrete whirlwinds are positioned close to the wing edges where the solution approaches infinity, and the calculation points are positioned close to the wing edges where the solution has to be restricted. Also, the sums which replace the singular integrals in the carrying surface theory have to correspond to the principal values of integrals by Cauchy.

For this purpose, the internal calculation points have to be in the middle between the surface whirlwinds (or to approach such positions within a limit) at increase of whirlwinds in number. In such way, the method of discrete whirlwinds was first formulated in the doctoral dissertation of S.M. Belotserkovsky in 1955.

S.M. Belotserkovsky explains this method by an example of the flowing of a thin profile replaced with a vortex intensity layer $\gamma(x)$ (Figure 3.42) and the problem becomes reduced to a characteristic singular integral equation of the first row on a piece [0,1]. [16]

$$\int_0^1 \frac{\gamma(x)dx}{x_0 - x} = f(x_0), \quad x_0 \in (0,1). \tag{3.44}$$

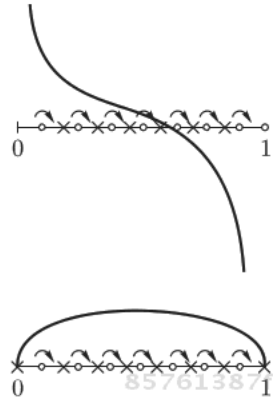

Figure 3.42 A thin profile replaced with the vortexes in the flow calculations.

Two grids of points for arrangement of discrete whirlwinds x_k and calculation points x_{0j} are taken:

$$x_k = \frac{1}{2n} + \frac{k-1}{n},\ k = 1,2,\ldots,n;\quad x_{0j} = \frac{j}{n},\quad j = 0,1,\ldots,n.$$

In the aerodynamics, three types of flowing of the profile are considered: circulating, irrotational and hammerless. The first one is based on the Chaplygin-Zhukovsky hypothesis of the extremity $\gamma(x)$ in the trailing edge, and serves for studying of bearing properties of the wings. In this case, on the leading edge of a thin profile the solution approaches infinity, and the integral equation is replaced with the following system of the algebraic equations:

$$\sum_{k=1}^{n} \frac{\gamma_n(x_k)h}{x_{0j} - x_k} = f\left(x_{0j}\right),\quad j = 1,\ldots,n. \tag{3.45}$$

The second type of flowing meets in the problems of profile fluctuations in the fixed liquid. Thus, both edges are in identical conditions, the value of summarized circulation is equal to zero, and the solution approaches infinity on the edges.

The following sets of equations are obtained:

$$\sum_{k=1}^{n} \frac{\gamma_n(x_k)h}{x_{0j} - x_k} = f\left(x_{0j}\right),\ j = 0,1,\ldots,n-1,$$
$$\sum_{k=1}^{n} \gamma_n(x_k)h = 0. \tag{3.46}$$

The last equation expresses a condition of irrotation, and the closest whirlwinds appear at both edges.

The third type of flowing is studied at the definition of not only the bearing properties of the wing, but also the wing deformation, at which, on the leading edge it is possible to avoid a flow separation obtained at $\gamma(x)$ approaching infinity. Instead of an integral equation, a set of the algebraic equations is obtained:

$$\gamma_{0n} + \sum_{k=1}^{n} \frac{\gamma_n(x_k)h}{x_{0j} - x_k} = f(x_{0j}), \quad j = 0,1,\ldots,n. \tag{3.47}$$

Where γ_{0n} - additional unknown bound to the deformation necessary for the vanishing of the leading edge intensity. Mathematically, this can be treated as a regulation factor, since the requirement to extremity $\gamma(0)$ and $\gamma(1)$ provides an excess calculation point.

Thus, the method of discrete whirlwinds possesses the following important features. It does not provide assumptions of character, of approaching infinity, of the solution on the ends of the piece, oron the breaks. The required class of solutions is allocated by a choice of the relative positioning of two sets (grids) - discrete whirlwinds and calculation points.

This method was applied to the creation of a set of programs for calculating the orthogonal power units. The calculation is carried out either for a two-dimensional stream (the main program) or for a three-dimensional representation - at research of multi-blade units of big diameter. Any option contains the process of formation of an aerodynamic trace behind the rotating wheel or wheels, from the start moment of the motion. The vortex trace is formed at the expense of evolution of the vortex descending from the rear blades, and at the separated flowing from the leading edges of the blades of the unit (Figure 3.43).

The calculation algorithm is based on the method of discrete whirlwinds. The sections of blades are simulated by thin carrying areas which are presented in the calculation scheme by the sets of discrete whirlwinds located on the profile centerline. The vortex trace behind the blades is also simulated by the discrete whirlwinds formed on the edges of the blades at each calculation instant. Thus, the instantaneous angle of attack on each blade is calculated, and if it exceeds some critical value, the flowing is considered separated with a descent of the vortex from the leading edge of the blade. The

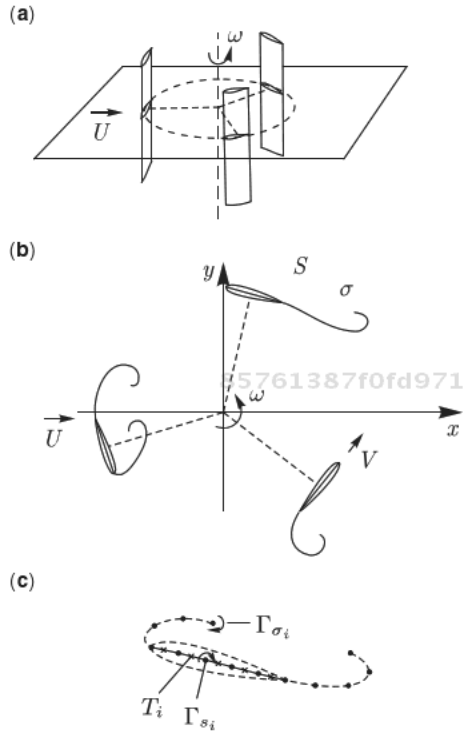

Figure 3.43 The scheme of the flowing of the rotor in a model with discrete whirlwinds.

circulations of the discrete whirlwinds Γ_{si} simulating the surfaces of blades, is defined from the impermeability condition of the blade in the reference points T_i (Figure 3.43 c). Free whirlwinds $\Gamma_{\sigma i}$ move at a local flow rate, keeping their circulation. In the course of the calculation the summarized and distributed loads on the blades, and also the torque and forces operating on the unit as a whole, are defined. The program uses semi-empirical dependences of the realization of pressure thrust and the profile friction drag. Calculation of non-stationary flowing proceeds until the quasi-stationary mode is reached (usually 3–5 turns of the wheel). After the calculation is completed, the average characteristics for the allocated calculation period (usually for the last turn) are defined. The program of two-dim ensional calculations allows consideration of the rotors with two groups of blades (Figure 3.44). At definition of the groups, the group with the maximal radius of the route is described first. The

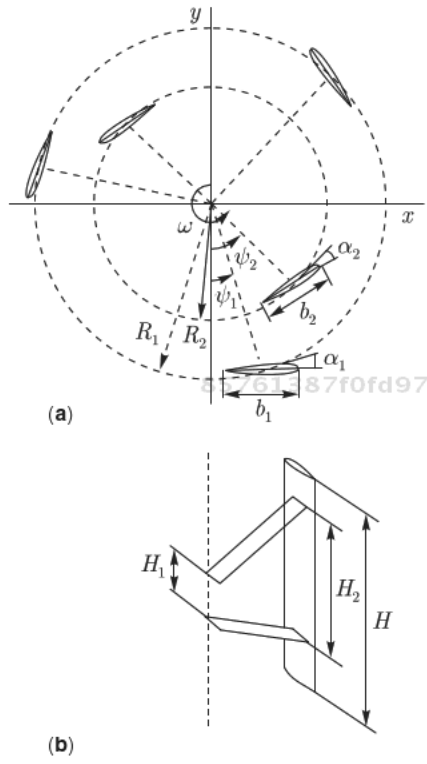

Figure 3.44 Rotor model with two groups of blades.

program can be applied to calculation of the rotation frequencies corresponding to the condition:

$$\omega R_{max}/U_0 > 0.1 \tag{3.48}$$

At $\omega R_{max}/U_0 < 0.5$–0.8 increased fluctuations of the results are observed, and a lag of calculations is possible.

The input data for the calculation includes the information on geometry of the power unit (Figure 3.44), kinematic characteristics of its motion and dynamic properties of the flowing environment. The blades of the unit are united into "groups of blades" located on one gyration radius, evenly distributed on a circle, having identical profiles and turn angles. The angular displacement of the groups of blades is one of the geometrical parameters.

An essential calculation element is the need for use of semi-empirical data to determine the pulling force operating on the blade.

The raising force operating on the blade can be presented by two components - normal to the chord, and the pulling force T which arises because of pressure reduction on the blade leading edge. The normal component is calculated without use of empirical data (like for a thin plate), and the pulling force is assumed proportional to the raising force with a constant of proportionality depending on the angle of attack and the cross-sectional profile. Actually, in the calculations the value of the pulling force coefficient obtained by generalization of the empirical data (Figure 3.45), and the restricted length of blades and curvature of the blade chord, according to the approximate formulas accepted in the aviation, are used.

Finally, the shape of the blades and the design elements of the machine (traverses, connection joints, etc.) are accounted for by the program, but with some conventions. The data necessary for the calculation and requested by the table at the program start are: [17]

Name of calculation
Number of groups of blades (no more than 3)
Number of blades
Radius of the route (m)
Chord of the blade (m)
Angle of attack (angle of the blade turn from a tangent, degrees)
Angular displacement of the group (degree)
Profile thickness (%)
Concavity (curvature) of the profile (%)
Position of the maximal concavity point (from the leading edge, %)
Number of traverses per a blade

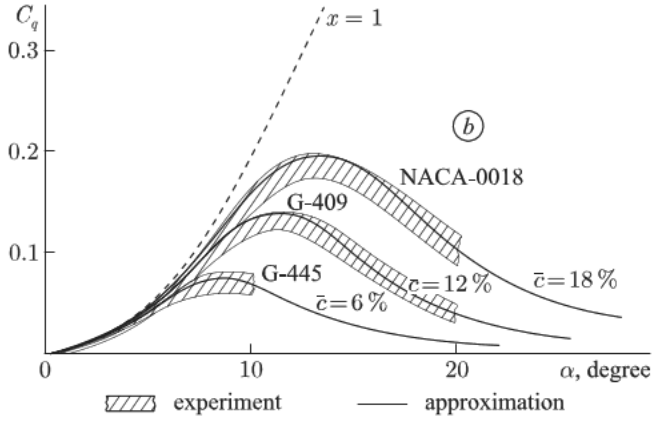

Figure 3.45 Generalization of the empirical data.

Distance between fastening points of the traverses (height) by the axis (m)

Distance between fastening points of the traverses (height) on the blade (m)

Chord of the traverses (m)

Profile thickness of the traverses (m)

Fastening type of the traverses (0 – open, 1 –elementary fairing, 2 - aerodynamically perfect fairing, climbed)

Wind speed (m/s)

Rotor rotation frequency (rpm)

Air density (kg/m^3)

Air kinematic viscosity (m/s^2)

Calculated period (number of turns)

Initial moment of averaging

End of averaging of forces, moments, fields of speeds

Remove impacts on the blades? (Y/N)

Output external files? (Y/N), Y – output data files for interaction with other program systems are generated

Output at each step (0 – only minimum, maximum, average, 1 – output at each 10°, 2 – output at each step, i.e., at each 2°)

The rotor height (m) determines the blade length for which the loadings are counted.

The rotor position (in time) and the torque value are displayed. The forces operating on the blade (H) – radial F_r, pulling F_t, components of the same force by the coordinate axis, aerodynamic moment concerning the blade leading edge M, and also the forces F_x, F_y, operating on the unit as a whole, torque concerning the spin axis (H_M), and capacity (kW) are represented. An example of delivery of the calculation results of currents and torque for the unit 1 or 10 MW with 6 blades at the speed of blades 3.06-fold greater than the wind speed of a, is shown in Figure 3.46.

The points in the upper part of the figure represent the whirlwinds formed at the end of the calculation which in this example included 3 turns of the rotor. Yellow pieces represent the unit blades; violet arrows show the value and direction of the flow rate. The speeds in the machine behind its front are still rather great; however on the way to the rear system of the blades and behind it, they decrease significantly. In this example, the flow is recovered at the expense of turbulent exchange. Such an account is carried out in other calculation programs of the space flowing of the units, based on the same ideas as the model of discrete whirlwinds.

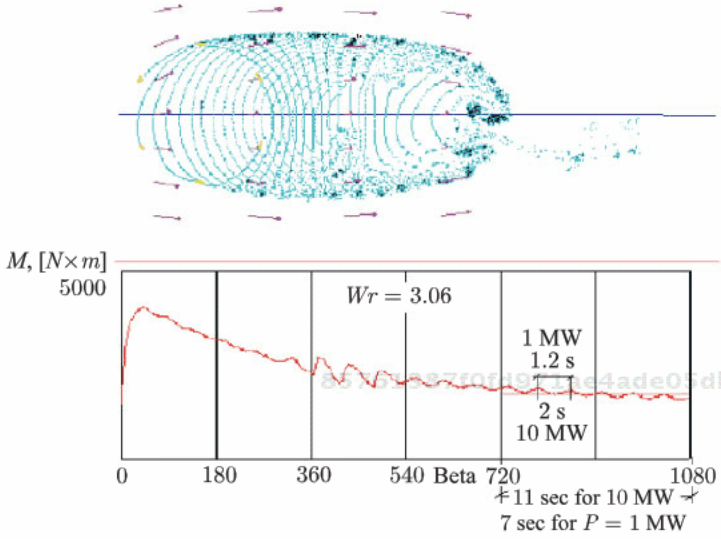

Figure 3.46 Picture of currents and plot of changes of the torque operating on the 6-blade orthogonal unit, calculated by the method of discrete whirlwinds.

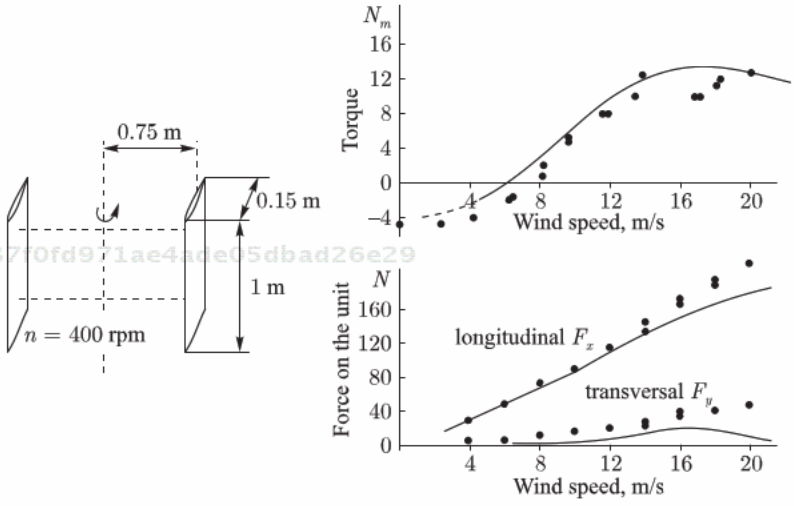

Figure 3.47 Data of experiments and calculations for the model with the blades of NACA 0018 profile. Dots – experiment, lines – calculation.

Serviceability of the program was confirmed by special experiments with a small model (Figure 3.47) and comparative calculations for the test conditions of models in a small pipe by TSAGI (Figures 3.48, 3.49), and the systematic tests of natural samples in a big wind tunnel of TSAGI in Zhukovsky (Figures 3.50–51).

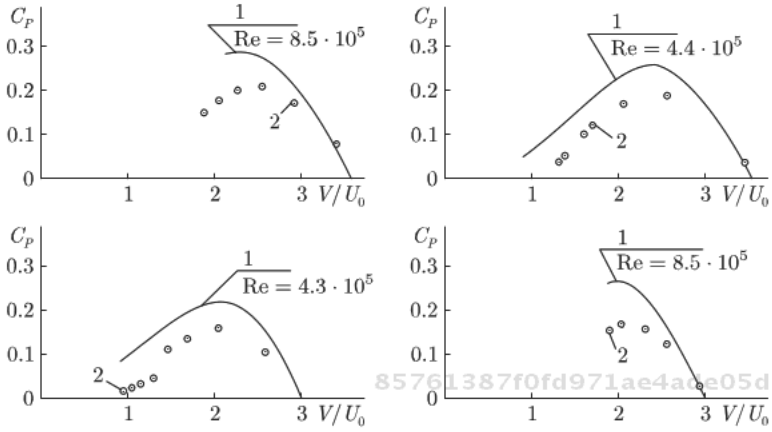

Figure 3.48 Efficiency of the orthogonal units by TSAGI experiments. Profiles of blades NACA 0015, chord 0.3 m. Top plots i=2, $\sigma = 0.205$, bottom plots i=3, $\sigma = 0.308$.

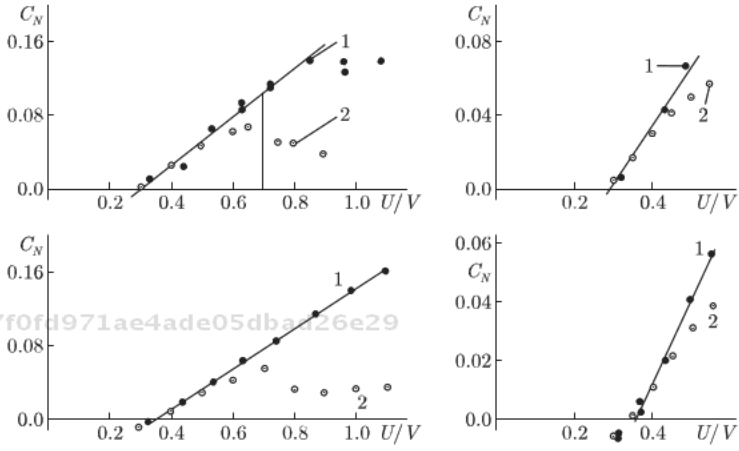

Figure 3.49 Power coefficients for two-blade (top) and three-blade units. 1 - test, 2 - calculation.

The comparison shown in Figure 3.47 is a rather convincing basis for use of the numerical model as the main operational means for design of the rotors of ordinary orthogonal units. This conclusion is also confirmed by other comparisons to the experimental data of TSAGI providing direct measurements of the torque on the rotor shaft of the orthogonal machine (Figures 3.48, 3.49).

According to all these data, the calculations underestimate the power effectiveness of the rotors that can be explained with the

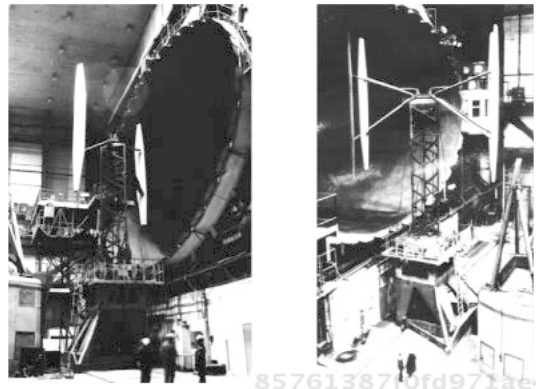

Figure 3.50 Two and four blades orthogonal units tested in 101 pipes of TSAGI.

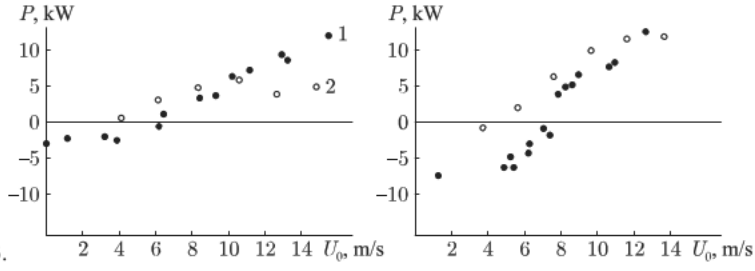

3.

Figure 3.51 Capacity on the generator plugs of 2-blade (black dots) and the rotor capacity calculated by the method of discrete whirlwinds (empty dots) depending on the wind speed. The rotor diameter 9 m, profile of blades GAW-1M, chord of the main (root) parts of the blade 0.9 m, length of this part 3.76 m, average chord of the blade tails 0.65 m, their total length 4.64 m. Traverse chord 0.465 m, traverse thickness 0.088 m. The rotor rotation frequency 38.8 rpm. (left) or 51.6 rpm. (right).

influence of the shadowing brought by the models in a pipe of limited dimensions (pipe diameter 6 m, routine diameter of models 1.8 m, height 2.4 m). As for comparisons of the natural power measurements to the calculated data, we should consider the influence of losses in the mechanical joint of transmission, and reducer and electromagnetic losses in the generator. Such tests and calculations were carried out in a big wind tunnel of TSAGI (Zhukovsky) for two and four blade wind units prepared for serial production (Figure 3.50).

The comparison of the results of the experiments and calculations is shown in Figures 3.51 and 3.52.

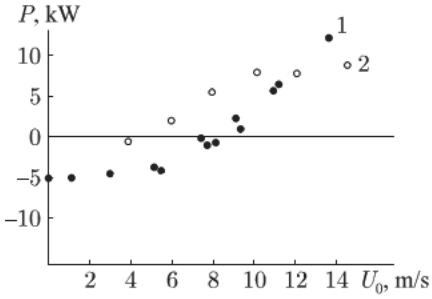

Figure 3.52 Capacity on the generator plugs of 4-blade VEU (black dots) and the rotor capacity calculated on a method of discrete whirlwinds (empty points) depending on the wind speed. The rotor diameter 9 m, profile of blades GAW-IM, chord of the mid-range of the blade 0.9; length of this part 3.76 m, average chord of the blade tails 0.65 m, their total length 4.64 m. Traverse chord 0.465 m, traverse thickness 0.088 m. The rotor rotation frequency 38.8 rpm. One pair of blades is shifted concerning another at 45°.

Considering possible inaccuracies in manufacture of large rotors, it is possible to recognize the demonstrated agreement of calculations and experiments as satisfactory.

The described approaches appear the most perspective. However, at such model operation the influence of the Reynolds criterion reflecting the action of viscosity forces is not shown in an explicit form. Actually, an implicit influence of this criterion is considered at a choice of conditions of applicability of the methods, and at record of the boundary conditions. However, in the problems where the influence of the Reynolds number can be great (problems of boundary layer with sticking), a direct consideration of this factor is desirable.

There is another way of describing the turbulence bound to the development of semi-empirical multiple parameter models expanding a set of Reynolds equations due to the heuristic equations for turbulence, energy, and speed of its dissipation. So-called model "k-ε" and its polynomial modifications are especially popular in the modern literature. The use of these models would probably allow better understanding of the great influence of the Reynolds number on the aerodynamic properties of the wing profiles. It is important to note, that dependence of the aerodynamic characteristics of wings on the Reynolds number weakens at an increase in the intensity of the turbulence of the ongoing flow. Despite the apparent clarity of the problem, the variety of results of purges of similar

profiles in different wind tunnels is surprising. The distinctions in pre-thrust and post-thrust zones are especially great at larger angles of attack. If in calculations of normal forces (C_n) this affect is small, then in values of coefficients of pulling forces (C_l) the observed distinctions are very great.

The tests of particular models of the wind units confirm an insufficient determinacy of the power estimates obtained in the models, even those of a rather vast scale. Figure 3.53 presents the results of three testing series of a model of a single-blade wind unit with a GAW-1 profile in the wind tunnel of TSAGI.

The series differed by the rotation frequency of the model, and therefore, by the values of the Reynolds number, made by the speed of the blades. As we see, the greater the Reynolds number is, the better are the power characteristics. It is possible to try to understand these strong changes, having presented the results in the function of the Reynolds number made by the radius of curvature

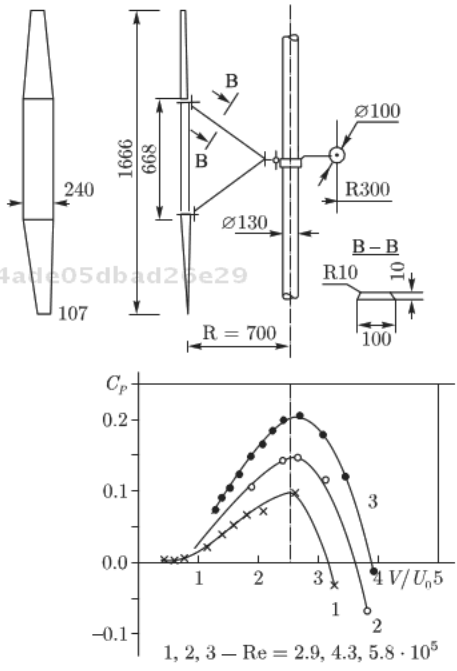

Figure 3.53 Power efficiency C_p of as tip-speed relation (V/U). Tests of single-blade model with the trapezoidal blade, profile GAW-1, chord in the mid-range 240 mm, on the ends – 107 mm, model radius R=700 mm. The last line in the table – Reynolds numbers (Re). Automodeling comes at Re > 5.8 10^5.

of the blade's leading edge, because the pulling force is defined by the processes exactly near the blade's leading edge. Nevertheless, it appears that the influence of changes of the speed of the blades is too great and can hardly be explained with a change of Reynolds number only. Probably, the model deformation caused by different centrifugal forces matters also. At the tests of another model, which deformation of blades was limited by the traverses fixing the ends of blades, the influence of the Reynolds number was less noticeable (Figure 3.54).

The distinctions of the test data of models of the same wind units (in different scales, but at close values of the Reynolds number) executed in a low-turbulent wind tunnel and in a high-turbulent hydraulic tray in TsAGI are very remarkable. Practically in all cases, the relative power characteristics were much higher in the high-turbulent flow (Figure 3.55).

Trials of the same rotor of the model wind unit in the wind tunnel of TSAGI and in natural conditions in the Institute of the Atmosphere Physics (IFA) of the Academy of Sciences of the USSR, were organized in Tsimlyansk in order to check this observation. The model wind unit of the author's design (type VL-2N) had an upright located spin axis. Pieces of helicopter blades with chord 0,4 m and profile NACA 23012 (flat part outside) were used as working blades. The length (height) of the blades was 2,55 m. In the middle part, the blades were connected by a horizontal traverse fixed on a vertical shaft equipped with a pulley in the bottom part for the belt drive and a brake.

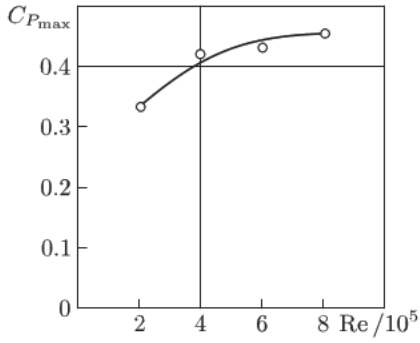

Figure 3.54 Influence of the Reynolds number at low turbulence. Tests of a wind rotor of frame type.

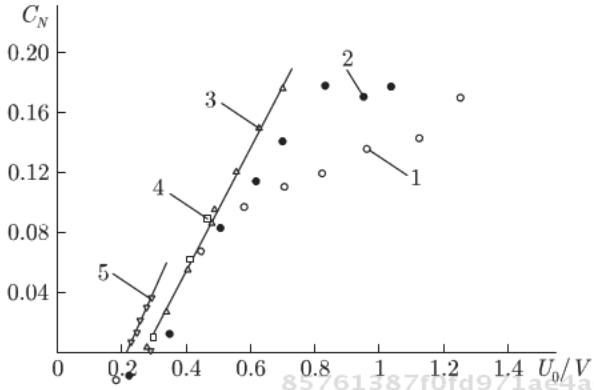

Figure 3.55 Test data of models of two-bladed turbines in the wind tunnel of TSAGI (1–4) and in the hydraulic tray (5). 1–4 – wind unit with diameter 1950 mm, length of console blades 1200 mm, NACA 0015 blade, chord 300 mm, solidity 0.308, constant rotation frequency 150, 200, 300, 400 rpm (Re_V = 3.3, 4.4, 6.6, 8.8×10^5), 5 - water-wheel with diameter 200 mm, chord 30 mm, length of blades 250 mm, solidity 0.3, flow rate 1–1.2 m/s (Re_U = 1.13–1.44×10^5)

The belt drive connected the rotor shaft with an asynchronous motor-generator3,5 kW. Changing a pulley on the motor-generator axes, it was possible to establish the rotation frequency 112, 151, 173 rpm. The measurement data obtained in the polygon (see below) are received at the rotation frequency 112 ± 3 rpm. The traverse height over the ground was 4,1 m; the distance of the blades from the center (radius of gyration) - 1,5 m. The same rotor was tested in the wind tunnel of TSAGI with the diameter 6 m, before the trials. In the laboratory and in the polygon, the tests were carried out at various angles of the turn of the blades. [18]

The fullest data have been obtained at a turn of the blades at 2° outside from the spin axis.

For measurements of characteristics of the wind speed field, two acoustic anemometers, allowing the measurement of pulsations of various wind speed components, and two sets of sensors of average wind speed $\bar{U}(z)$ (seven speed sensors in each set), allowing the measurement of a high-rise course $\bar{U}(z)$ in range of heights from 1,3 m to 9,6 m, were established near wind unit (WU) at different distances from it, and at the height of 4,1 m. One set of sensors $\bar{U}(z)$ and the acoustic anemometer were established from the upwind side of WU and provided the characteristics of a non-disturbed stream, and the second anemometer and the set of sensors $\bar{U}(z)$ - the wind

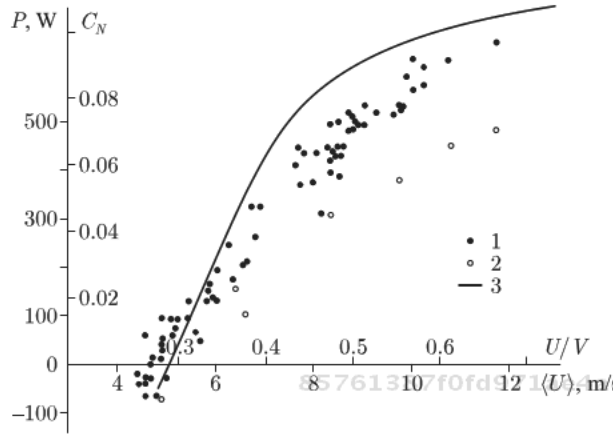

Figure 3.56 Dependence of the rotor power on the speed of the ongoing air flow. 1 – measurements in the polygon, 2 – tests in the wind tunnel, 3 – calculation by the pulse model at $\xi_{\Sigma} = 0.03$.

shadow area of WU at various distances from it. The installation sites of sensors changed in different experiment series, depending on the wind speed.

The results of simultaneous measurements of the rotor power I and the wind speed $\bar{U}$, averaged by identical ten-minute intervals, are presented in Figure 3.56.

The rotor capacity was determined by the value of the active energy delivery for a fixed time (10 minutes) with addition of losses on the generator engine, in the transmissions and the basic and running clusters. These losses, defined at the removed rotor, made 500 W in autumn tests; and 550 W in summer (wind speed up to 6,5 m/s).

The numerical model used, includes a solution of a different analog of the two-dimensional equations (3.28). The impulse selection by the wind unit was simulated by a representation of function g_i, by the corresponding expression accepting nonzero values on the contour of blades and including the aerodynamic characteristics of the blades, their relative positioning on the route, and orientation concerning the traveling speed.

The boundary conditions were set as follows: a constant expense by time at the input, and the condition of the impulse free transfer at the output. The top and bottom borders of the area were

positioned rather far from the unit, at 8D to each side, and considered impenetrable.

The calculated scheme provided a planned picture of the currents in the horizontal plane, and the rotor power value at various relative wind speeds (Figure 3.56). The design values (line 3) are close to the data of natural measurements, although they exceed the data observed in the pipe considerably.

As stated above, in the wind tunnels the routine purges of profiles even at identical Reynolds numbers yield considerably varied results, depending on the intensity and range of the speed pulsations of the environment. At low-intensity turbulence, the influence of the Reynolds number is great, and even at its values exceeding 10^5 (in the considered experiments $Re_v = Vb/\nu \sim 5\ 10^5$).

Taking this into consideration, this attempts to connect a dispersion of natural points observed in Figure 3.56 and their difference from the laboratory data with the influence of turbulence or variability of the vertical profile of wind speed $\langle U \rangle(z)$.

A relative turbulence intensity during the measurements varied from 0.14 to 0.24, the mean value being $\frac{\sigma_u}{\langle U \rangle} = 0,18$. The observed data related to high turbu lence intensity are much higher than the mean values (Figure 3.57).

$$1 - \frac{\sigma_u}{\langle U \rangle} : < 0.17 \quad 2 - 0.17 < \frac{\sigma_u}{\langle U \rangle} < 0.20 \quad 3 - \frac{\sigma_u}{\langle U \rangle} > 0.20 \quad 4 - \frac{\sigma_u}{\langle U \rangle} < 0.02$$

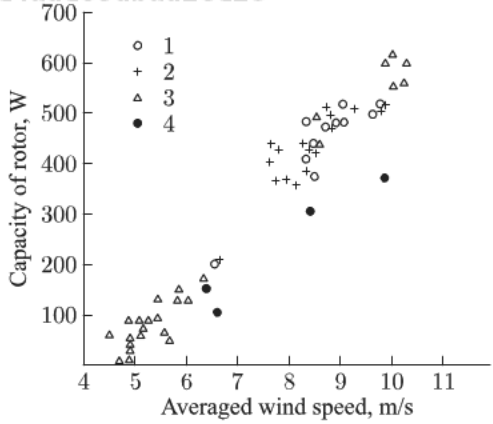

Figure 3.57 Capacity of wind turbine's rotor at different turbulence intensity.

As seen from Figure 3.57, the data obtained in the natural conditions in a turbulent stream are found much higher(at 30–40% around the maximal C_p values), than those obtained in the wind tunnel with small levels of turbulence, where $\frac{\sigma_u}{\langle U \rangle} \approx 0,02$ (points 4). The calculation results better match the natural data, than the laboratory measurements. Figures 3.56, 3.57 show a wide spacing of the natural supervision data exceeding a possible error of measurements. Still, the larger data variability was recorded in other series of the natural supervision on larger experimental wind turbines tested in the settlement of Dubki (Dagestan), near Moscow and near Tallinn. Probably the data variability is bound to a distinction of the spectral characteristics of the wind turbulence spatial structure. The atmosphere turbulence influence on the conditions of flowing of the blades and power of the wind units should be studied carefully. The first steps in this direction were taken by the author in 1987 at the trials of the wind-driven generator in Tsimlyansk.

There are data from foreign colleagues confirming a wide spacing of the results of natural measurements, significantly exceeding possible errors of the equipment (Figure 3.58). Remarkably, the trials of the same machine in a wind tunnel actually did not yield dispersion results (Figure 3.59). Probably, the influence of turbulent structures of the streams can be essential in many cases.

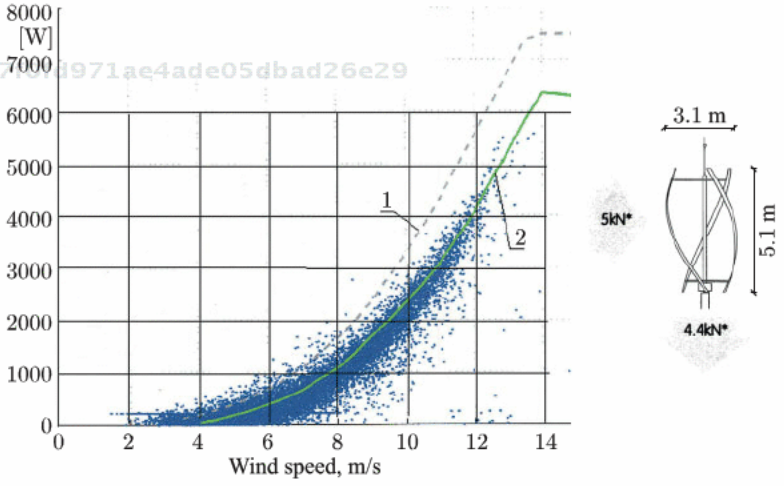

Figure 3.58 Capacity of the English orthogonal wind unit according to the field tests [19].

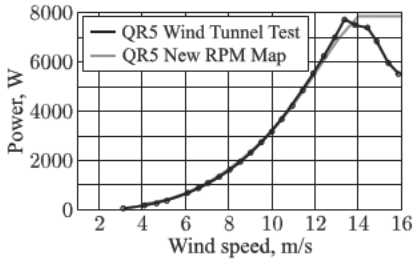

Figure 3.59 Test data in the wind tunnel. The maximal capacity is recorded at the wind 13.5 m/s that corresponds the rotor effectiveness about 34%. The maximum $C_p = 0.42$ is stated on the site.

References

1. Ion Paraschivoiu, Wind Turbine Design: With Emphasis on Darrieus Concept, 2002, 438 p. Brian Kirke, Vertical Axis Wind Turbines: With particular Emphasis on Self-acting Variable Pitch Darrieus Type Turbines, 2012.
2. A.N.Kolmogorov. Local structure of turbulence in incompressible liquid at very large Reynolds numbers, ,1941, vol. 30 DAN of USSR, No. 4. The review of works of this school – see A.S.Monin, A.M.Yagl's books, the Statistical hydromechanics, 1965, M, "Science", vol. 1, 2.
3. V. M. Lyatkher, Turbulent pulsations in the viscous sublayer, DAN of USSR, 1968, vol. 180, No. 2, V. M. Lyatkher, Turbulence in hydroconstructions, 1968, M, "Energy", 408 p.
4. V. M. Lyatkher, A.N.Militeev. Hydraulic researches by numerical methods, Water Resources, 1981, No. 3, p. 60–79.
5. V.M.Lyatkher, A.N.Militeev, S.Ya.Shkolnikov, Numerical model operation of turbulent open flows, Water Resources, 1987, No. 1, p. 35–41. V. M. Lyatkher, S.Ya.Shkolnikov, Tensor structure of coefficient of a hydraulic friction. Water Resources, 1981, No. 5, p. 58–62.
6. Numerical model and appropriate programs for computers developed by A.N.Militeev.
7. Test data from the book by P. Zheng "Separated flows, vol.3, "World", M, 1973, p. 15. Technique and results of calculations – V.M.Lyatkher, D.N.Militeev. Energy characteristics of the orthogonal units transforming energy of currents, News of Academy of Sciences of the USSR, Power engineering specialist and transport, 1988, No. 3, p. 93–99. V.M.Lyatkher, Yu.B.Shpolyansky. Loadings on hydro- and wind units in the free stream and their power characteristics. Hydrotechnical construction, 1986, No. 12, p. 16–22.

8. V.M. Lyatkher, N.G.Gvazava, Yu.B.Shpolyansky. Mathematical model of orthogonal power units, AN Messages Freight. Soviet Socialist Republic, 1988, vol.130, No. 3, p. 601–604.
9. V.M.Lyatkher. Wind power use. J. Power construction, 1986, No. 5, p. 55–60.
10. E.G.Petrov, V. G. Tabachnikov, Tr. TsAGI, 1974, issue 1621, p. 102–109.
11. V. M. Lyatkher, A.N.Militeev, D.N.Militeev, Aerodynamic loads of the wind unit elements with vertical spin axis, News of Academy of Sciences of the USSR, the Power engineering specialist and transport, 1986, No. 4, p. 138–146.
12. F.W. Riegeles, Aerodynamische profile, 1958, Munchen, R.Oldenbourg, 264 p.
13. S.M. Belotserkovsky, M.I.Nisht, Separated and continuous flow of thin wings true liquid, 1978, M, Science, 397 p.
14. H.M. Dress. II Int. Symp. of Wind Energy Systems, Oct.1978, Amsterdam, v. E4, p.81–88.
15. P.J. Musgrove, J.D. Mays, II Int. Symp. of Wind Energy Systems, Oct.1978, Amsterdam, v. E4, p.39–60.
16. S.M. Belotserkovsky. Main ideas of methods of discrete whirlwinds and discrete features, Cybernetics questions. Numerical experiment in an applied aerohydrodynamics, 1986, M. pp. 3–23.
17. Method and calculation program of two dimensional statement was developed in 1994 by S.A. Teselkin under the leadership of S.M.Belotserkovsky according to the Requirement specification of the author. In 2004 the program was upgraded by S. D. Shipilov, and in 2008– A.V.Lyatkher in relation to the modern computing tools. In 2008 A.S. Belotserkovsky and S.V.Alekseev developed the version of the program for calculation of space flow of power units in new author's options.
18. N.G.Gvazava, S.L.Zubkovsky, V.M.Lyatkher, et al. Impact of air turbulent flow on the wind power installation, Academy of Sciences of the USSR, Power engineering and transport, 1990, No. 2, p. 116–124.
19. http://www.quietrevolution.co.uk/.

4

Ordinary Orthogonal Windmills (Vertical-Axis Wind Turbines –VAWTs)

Orthogonal units (both low-speed, and high-speed) at all variety of designs, are possible to divide on an aerodynamic sign of a current's field in a zone of rotors into two groups:

- Ordinary axial units, diameter of the route of blades at which it is approximately equal or less than the length of blades. At such units, windward and lee side of the route of blades, owing to braking of a stream, are in various aerodynamic conditions;
- Units of a rather big diameter in which, before a back system of blades there is a restoration of a stream and the distinction stated above, is insignificant.

In units of the first group, the effects of a solidity connected with the distortion of an initial field of the speed of the wind in a zone of movement of the blades are important:

$$U_{1,2} < U_0.$$

In units of the second group, such distortion can be practically absent:

$$U_1 \approx U_2 \approx U_0. \tag{4.1}$$

Here U_1 - wind speed in a zone of the upstream site of the route of the blades; U_2 - the same for a leeward site of the route of the blades; U_0 (or U further, for simplification) - wind speed at a distance (on the way) before a windmill.

Change of the loads of the blades and, on the unit as a whole, on the route of blades is, therefore, in time the source of vibration of high-speed orthogonal units. For reduction of imbalance of the loadings, some blades in one circle are installed (usually no more than 3–4, Figure 4.1), some are applied curvilinear blades (figure 4.2), and some circles of blades (Figures 4.3, 4.4) are arranged.

Figure 4.1 At the left windmill NIIES (10 kW), in the center the two-level unit of JSC New Energetic (50 kW), on the right - units of the Chinese firm JOC and JSC Vertical (10 kW).

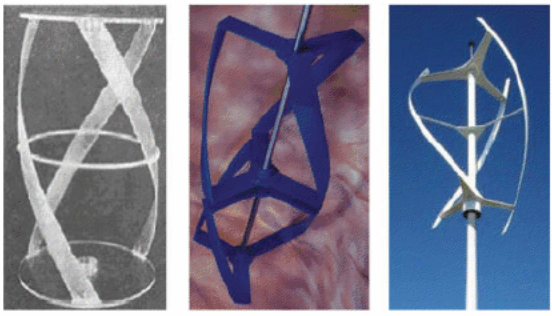

Figure 4.2 Orthogonal turbines with the counterbalanced total loading. At the left – the model tested by the author in the USSR in 1981, in the center – "A.M.Gorlov's helical turbine" (USA, 1995), on the right the modern serial unit of low power (USA, England) [1].

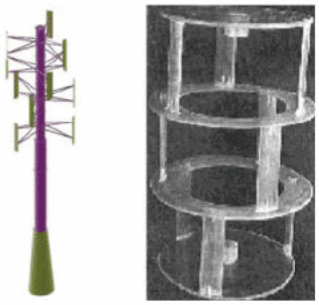

Figure 4.3 The low-vibration four-level unit with 3 direct blades in each circle (at the left). On the right – hydraulic model of the three-level turbine [2].

Figure 4.4 Modern balanced windmill (VAWT) 3 kW [3].

Turbines with curved blades were tested in the USSR in 1981–82 (Figure 4.2) and protected by the copyright certificate (N 1150395) with a priority of January17.1983.

The similar idea of ensuring constancy of a torque and the total force operating on the unit, at the expense of a screw form of axis of the blade, was used by prof. A.M.Gorlov in the US Patent 5451137 of September19.1995 (helical turbines).

In modern serial units reduction of vibrations is reached at the expense of the use of two circles with three counterbalanced blades in each circle and an arrangement of basic and power knots between circles (Figure 4.4).

Turbine P capacity depending on the speed of a running stream of U and linear speed of blades $V = \pi Dn/60$ can be presented in two forms:

$$P = C_P \rho U^3 S/2 \qquad (4.2)$$

$$P = C_N \rho V^3 S\sigma/2, \Gamma \text{ Here } \sigma = ib/D \qquad (4.3)$$

Here S = D H- swept area - area of axial section of a figure, contoured by blades, (S σ) – the area of a median surface of the blades, σ - solidity, i-number of blades, b - length of a chord of the blade, D – diameter of the route of blades, ρ –density of air, U-stream speed outside influence of the unit, V – the linear speed of blades. The coefficients of C_P and C_N depending on the outlines of the turbine, the ratio of the speeds of V/U, the quality of blades, and the Reynolds's number are connected by identities

$$C_N = C_P (U/V)^3/\sigma \quad (4.4)$$

$$C_P = C_N (V/U)^3\sigma \quad (4.5)$$

The power performance of the turbine $C_p(V/U)$ significantly depends on the design of the turbine and those conditions in which it will be used. In the same boundary conditions, the influence of the form of the turbine, such as the quantity and a form of section of blades, and the traverse, speeds and turbulence of a stream is great. According to calculations and experiences, C_N power factor with the fixed blades in the working range of the turbines, is approximately described by the linear function:

$$C_N = B\,(U/V - B_0), \text{ if } \quad B_0 < U/V < B_{lim} \quad (4.6)$$

Actually, record (4.6) means that at a constant speed of the blades (V =const), the capacity of the turbine is directly proportional to the first (instead of the third!) stream speeds. It is revealed in tests of orthogonal turbines of a miscellaneous like (Figures 4.5, 4.6)

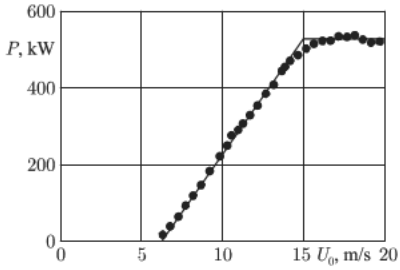

Figure 4.5 Capacity two-bladed orthogonal windmill of Darieus depending on the wind speed on the rotor equator (Sandia, D=34.2m, N=41.9m, σmin=0.053, the frequency of rotation is 34 rpm. Natural measurements with the cleared blades, January-April, 1989) [4].

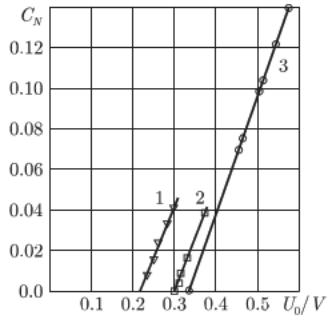

Figure 4.6 Power factor of C_N of orthogonal turbines depending on stream speed. Results of tests: The 1-two-level optimized turbine with direct blades in a wind tunnel, $\sigma = 0.3$ [5], 2 – the turbine with curved blades on Figure 4.2 in a hydraulic canal at a speed of stream of 1 m/s, $\sigma = 0.45$ [6]; 3 – the optimized "helical" turbine on Figure 4.2 in the pool at a speed of broach of 0.6–2.4 m/s, $\sigma = 0.45$ [7].

Thus, the power characteristic of the turbine can be approximately set by only three parameters. Parameter $1/B_0$ is the maximum relative speed of the blades reached by the turbine without braking, or, conversely, the B_0 parameter is the minimum relative speed of a wind at which the turbine starts working. Parameters B and B_0 define the efficiency of the turbine:

$$C_P = B\,(U/V - B_0)\,(V/U)^3\sigma,\ U/V > B_0 \qquad (4.7)$$

Maximum efficiency is equal respectively

$$(C_P)_{max} = 4B\sigma/27\,B_0^2 \text{ for } V_{opt} = 2\,U/3B_0 \qquad (4.8)$$

Orthogonal units are very sensitive to the form of the rotor and the blade, the zateneniye degree (solidity $\sigma = ib/D$),the Reynolds's number, and the condition of the surface of blades. At $Re=Vb/\nu$ Reynolds's insufficiently large numbers the model of the orthogonal unit can show such low efficiency that it simply won't consider. This actually also happened to the invention to Darrieus – the patent of 1920 of nearly 50 years wasn't demanded as all small models which were tested in pipes, showed low efficiency of turbines. Failures can be caused by the influence, it would seem, of minor factors – energy losses in basic knots, an unsuccessful design of the elements of fastening the blades, etc. So, the single-blade axial wind turbine tested full-scale, owing to the influence of losses on

constructive elements and a small zateneniye, showed low power efficiency: $C_p$max=0.174 (figure 4.7).

On the contrary, hydraulic tests of a model of the single-blade turbine with a practical exception of the losses on the constructive elements and an optimum solidity, showed the most achievable efficiency to $C_p$max=0.56 (Figure 4.8)

It is necessary to notice, however, that these (and all other) tests in a hydraulic canal were carried out at a rather small width of the

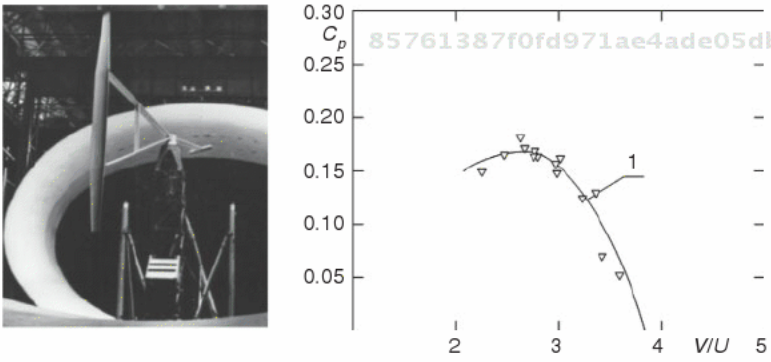

Figure 4.7 The single-blade orthogonal wind turbine on tests in 101 wind tunnels of TsAGI. Diameter of a rotor is 7.1 m. Frequency of rotation is 82 rpm (V=30.6 m/s), power is 11 kW. The area of the blade is 6.4 sq.m. Maximum chord of 0.9 m, GAW-1M profile. $\sigma = 0.11$. Results of tests in a pipe (right): Re=1.9 10^6.B =0.64, $B_0 = 0.245$. $C_p$max=0.174.

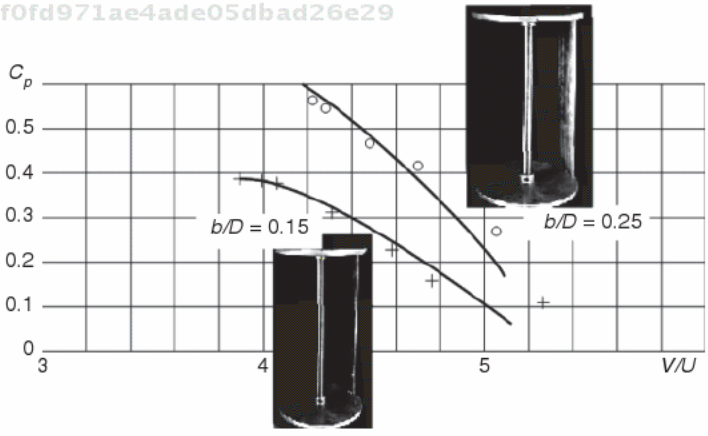

Figure 4.8 One blade on a disks with the balance weight. Chord of the blade of 50 mm. (top line) and 30 mm (the bottom line), NACA0015 profile. D=200mm, L=300mm. Tests in a hydraulic canal section 1 × 1m² at a speed of water of 1 m/s.

canal in relation to the diameter of the turbine. Because of this, efficiency could be overestimated by approximately 15 %.

Systematic tests of models of axial windmills were made in a wind tunnel of T-2 of the Central Aero-Hydrodynamic Institute (TsAGI) in Moscow – at the action of a stream of air with a different speed (up to 20 m/s). A small wind tunnel of TsAGI (T2) in a zone of placement of models, has a cross section in the form of the correct hexagon with the entered circle with a diameter of 6 m (Figure 4.9).

In experiments, models of turbines with vertical blades of the aerodynamic profile which have been rigidly fixed in average part on two horizontal cores (traverses), which through flanges were rigidly fixed vertically to a shaft, were used. The shaft with the model and the electric drive providing a constant set frequency of rotation was fixed on the aerodynamic scales, allowing measurement of all components of forces and a torque, operating on a system at a different speed of a stream. Model spin to a certain (specified) frequency of rotation, which has remained approximately constant. Changed (steps) wind speed in the pipe from zero to the maximum value. When fixed speed wind and given speed were measured torque and force components in the model (longitudinal and transverse).

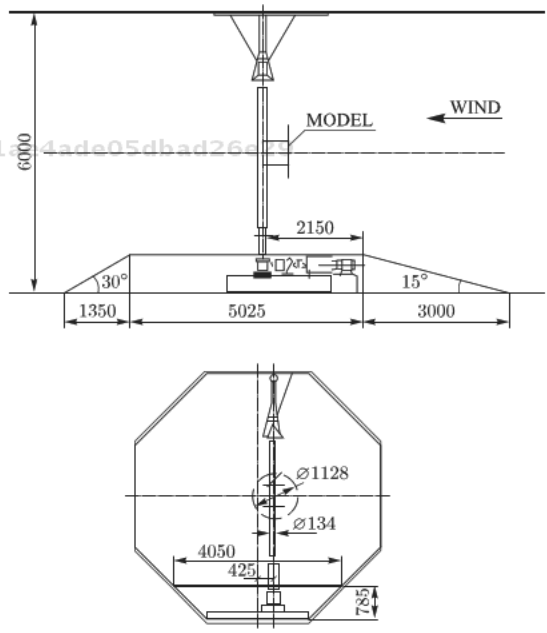

Figure 4.9 Small wind tunnel of TsAGI for testing orthogonal units.

Tip-speed relation V/U (relative speed of the blade) — varied at the expense of the change of speed of a stream of U in a pipe. Such a technique of carrying out tests provided to get at[?] the aerodynamic characteristics at Reynold's constant number Re_V, determined by the district speed of the blade V and its chord of b. Change of the number of Re_V from experiment to experiment resulted from the change of frequency of the rotation of the model. In other experiments in a big wind tunnel of TsAGI (Zhukovsky town) with complete models (actually with natural samples of the unit), including real basic knots and the generator, the technique of tests was other – the model was fixed on a rigid support, promotion of the model was carried out by its asynchronous generator in a mode of the engine passing under the influence of a wind to a mode of the generator.

Forces operating on the system weren't measured, and the torque was determined by the electric power output, or at tests for lack of a wind - by a curve "free moving" model, i.e. by changing the frequency of rotation of the model in time. [8]

Systematic experiments with models in a small wind tunnel were shown by the following results. [9] The increase in solidity, increases a torque by unit axes, but reduces the optimum speed of its rotation so that the maximum power efficiency is observed at a solidity from 0.20 till 0.30 (Figure 4.10).

The increase in the number of blades in the axial car at preservation of an optimum zateneniye leads to a steady decrease in the efficiency of the unit. The thickness of the blades shouldn't be less than 15% (Figure 4.11).

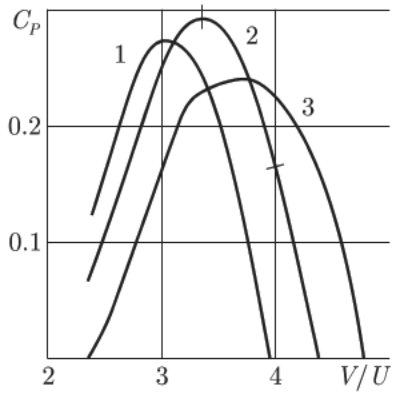

Figure 4.10 Efficiency of the Power Unit at σ = 0.2 (i=4), 0.15 (i=3), 0.1 (i=2) – the line 1, 2, 3 respectively.

Influence of the relative thickness of a profile of blades at small (Figure 4.11 – $Re = 2 \times 10^5$) and average (Figure 4.12 – $Re = 3.5 \times 10^5$) Reynolds's numbers. Lines 1, 2, 3, 4 correspond to the relative thickness of the blades 0.24, 0.18, 0.15, 0.12. The tests are in a wind tunnel, diameter 6m, with the model's diameter 1.14m

The design and the arrangement scheme of a traverse is very important. At an arrangement where the traverse on the ends of the blades is reached, the reduction of vortex losses on the blades and the efficiency of a rotor is maximum (Figure 4.13) [10].

The form of a profile of blades and chord turn concerning a vector of speed of the aerodynamic center of the profile matters. At a symmetric profile an optimum angle of a turn about 4–5° with carrying out of a sock of the blade outside (Figure 4.14). The corner of the installation of the blade not only changes optimum rapidity, but also significantly influences the size of maximum efficiency.

In Figure 4.15 it is clear that the more solidity and thicker the blade, the more optimum the angle of a turn of the blade (the pitch of the blades)

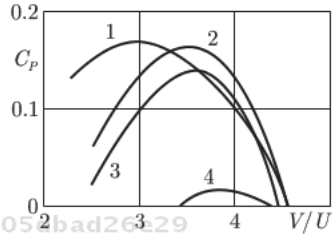

Figure 4.11 Influence of relative thickness of a profile of blades at small Reynolds's number ($Re_V = 2 \times 10^5$). Lines 1, 2, 3, 4 correspond to relative thickness of blades 0.24, 0.18, 0.15, 0.12. Tests in a wind tunnel diameter 6M with models diameter 1.14m.

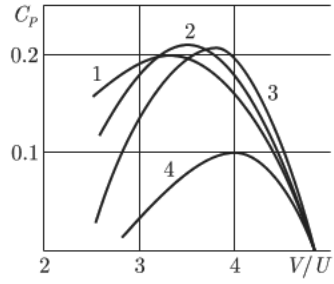

Figure 4.12 Influence of relative thickness of a profile of blades at averages Reynolds's number ($R_{eV} = 3.5 \times 10^5$). Name of lines as in fig .4.11.

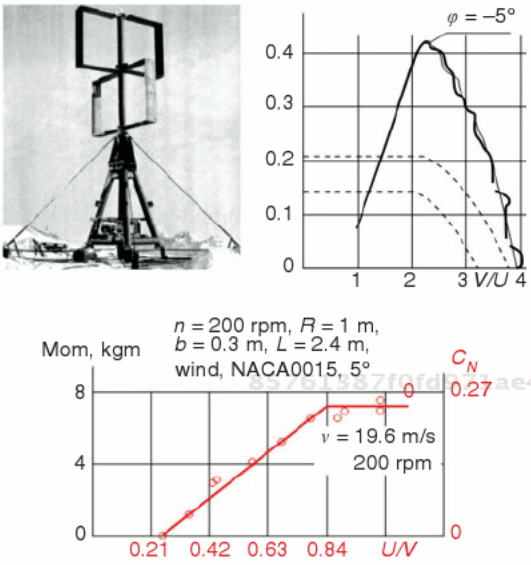

Figure 4.13 Two-level windmill high power efficiency on tests in nature (area Oaklets (Dubki), Ru, 1986[10]). Solidity 0.3, optimum speed of blades V = 2.25U (efficiency of 45%), maximum speed of blades V_{max} = 4U. Power of the unit is 16 kW. According to the same scheme the project of the unit with a power of 1000 kW was executed. On the right – results of tests of a model in a wind tunnel.

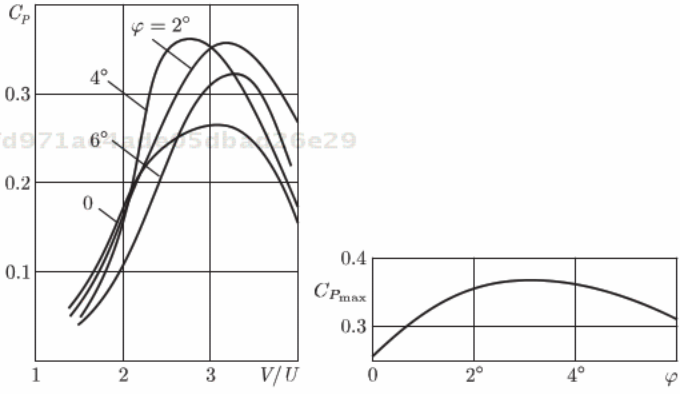

Figure 4.14 Characteristics of a model of the unit with direct blades with parameters: σ = 0,2; λ = 5; i = 2; with NACA0018, L/D = 0.5 received at constant number $Re_v = 2 \times 10^5$.

The influence of a corner of a turn of the blades was checked on models with a different solidity and the optimized profile of the blade. For these purposes, a series of the small models (Figure 4.16), differing was created and tested by that blades were rigidly fixed

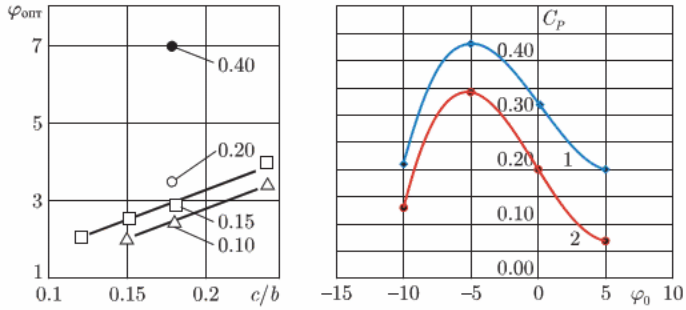

Figure 4.15 Optimum angle of a turn of symmetric blades with the NACA profiles in units of a various solidity (at the left).Influence of a corner of a turn of blades of a rotor of a frame design (on the right) *Re*: 1: 4,0·10⁵, 2: 2,0·10⁵.

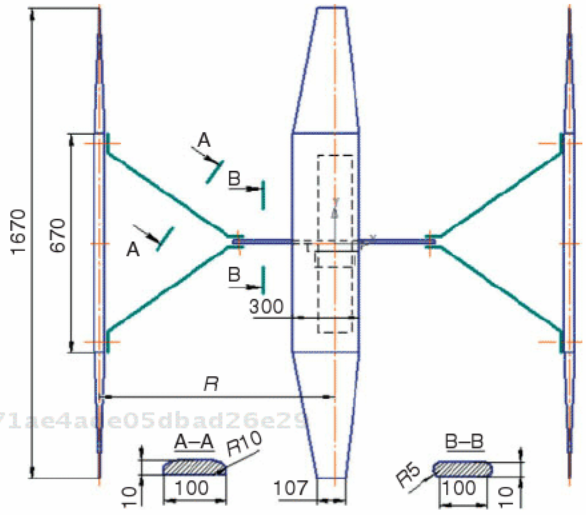

Figure 4.16 Cross section of model with the blades having the GAW-1 profile.

on traverses of quite certain size. It excluded changing the position of the blade concerning the rotation center during[?] tests.

The blade which had a trapezoidal form with a cross section of GAW-1, was made of a dry tree, carefully polished and varnished. For the purpose of control of its aerodynamic qualities, purges of the motionless isolated blade with different angles of attack were made at a speed of a stream of air 20, 30 and 40 of m/s (Reynolds's number 2.8, 4.2 and 5.6 × 10^5). The technique of the tests corresponded to the usual "purges" of wings of planes and helicopters.

Aerodynamic qualities of the blade appeared high (Figure 4.17), though they didn't reach those values which were taken into consideration for squared long blades.

At the same number of blades equal to 4 (Figure 4.16) and the same angle of a turn of blades (5°), change of the radius of the route allowed definition of the influence of the degree of solidity of a rotor (Figure 4.18), that the most effective of those tested is the rotor with the greatest diameter of 2.4 m with the minimum

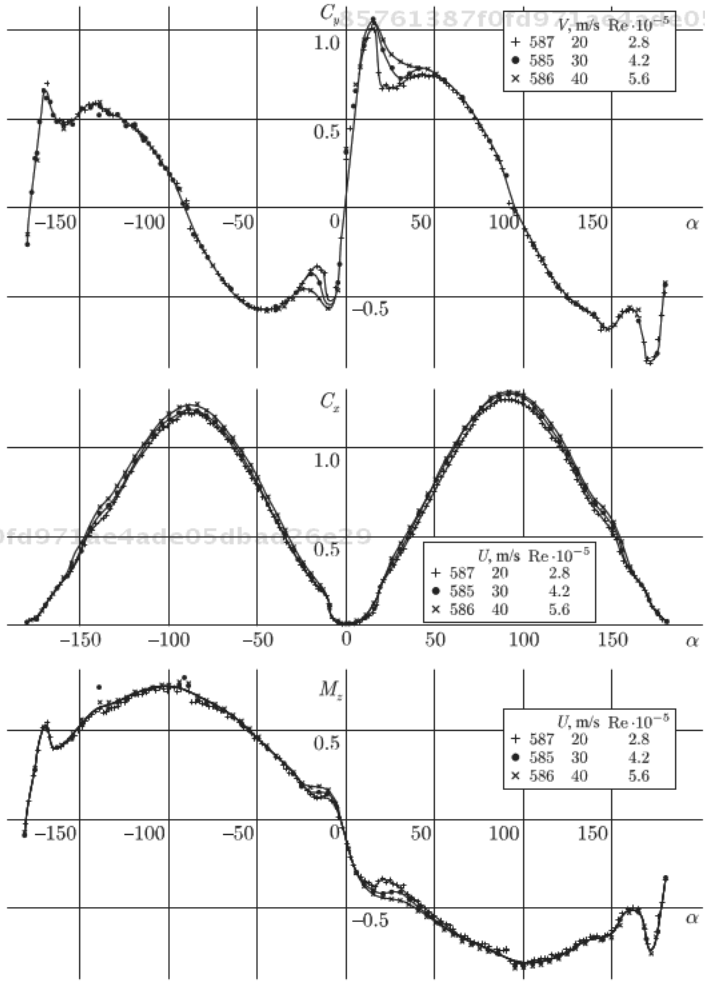

Figure 4.17 Aerodynamic characteristics of the blade of a trapezoidal form with the GAW-1 profile.

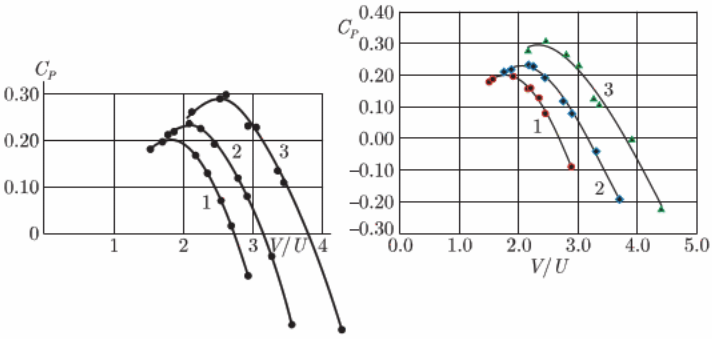

Figure 4.18 Influence of the diameter of the unit on characteristics of the four-blade rotor, i=4, $\varphi = -5°$,
1 – R=0.8 m. $\sigma = 0.5$, $\lambda = 1.05$, Re = 4.5 10^5,
2 - R=1.0 m. $\sigma = 0.4$, $\lambda = 0.835$, Re = 4.7 10^5
3 - R=1.2 m. $\sigma = 0.334$, $\lambda = 0.7$, Re = 4.9 10^5

solidity $\sigma = ib/D = 0.33$. Here i – number of blades, b – an average chord of the blade, D – a diameter of the route of blades. The maximum value of efficiency in this option made $C_p = 0.302$ at $V/U = 2.5$. The effectiveness ratio of the C_p unit connecting the capacity on a turbine P shaft with the capacity of the stream running on the turbine:

$$P = C_p \rho U^3 D H/2$$

Here ρ – density of the environment, D - diameter of the turbine, H - its height (length of blades)

As the length of blades L in these experiences didn't change, the relative height of a rotor of $L/D = \lambda$ didn't remain a constant. However, this factor in this case ($\lambda > 0.7$) shouldn't have a noticeable impact. It is expected that its influence will start showing up at $\lambda < 0.5–0.3$

With a diameter of the route of the blades of 2.4 m and the 4 blades influence on a corner of a turn of the blades (Figure 4.19) was checked. It is established that an optimum angle of a turn is the corner ranging from 2° up to 5° with carrying out of a sock of the blade outside from a tangent to the route of the aerodynamic center of the blade. The Reynolds's numbers in all instances was approximately identical (4.9 10^5) and sufficient for achievement of self-similarity.

The received results were specified at unit tests with the traverses fixed on the ends of blades that provided the effect of maximizing

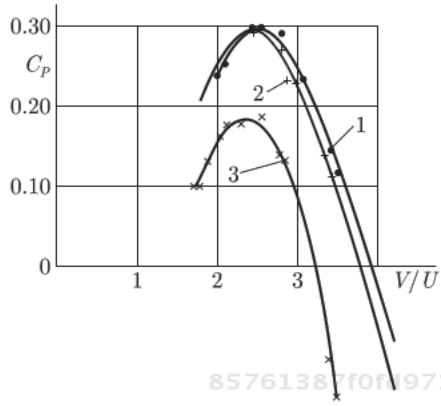

Figure 4.19 Influence of a corner of a turn of blades in the 4-blades unit. Re = 4.9 105 σ = 0.334, λ = 0.7
1 - φ = -2°, 2 - φ = - 5°, 3 - φ = -10°

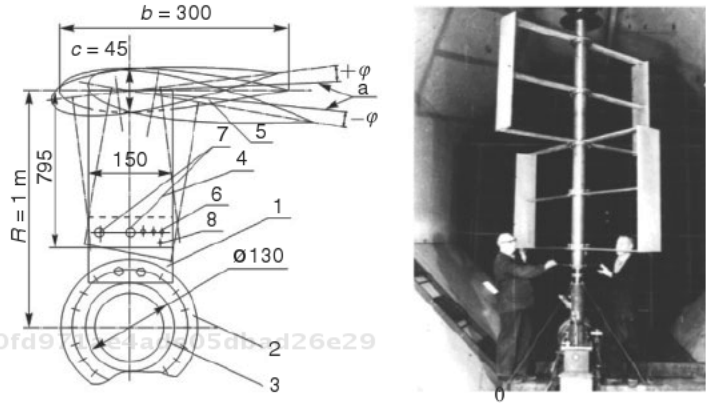

Figure 4.20 Diameter of the model (on a blade sock) 1820 mm (at angle –5°), length of the blade is 1200 mm, height of the model is 2400 mm, (two level model with turn of circles on 90°) the NACA 0015 Profile. R-the radius of the route of blades, with – profile thickness, φ – a angle of a turn of blades. 1-trailer traverses, 2 - flange, 3- shaft, 4 – a rigidity traverse, 5 – the blade, 6,7 – elements of fastenings.

the length of the blades. The scheme of fastening and the size of a traverse are shown in Figure 4.20. In these instances the rectangular blade with the NACA 0015 profile and a 300mm chord was used that made it possible to estimate the effect of fastening a traverse by the ends of the blades and to specify the limits of self-similarity on the Reynolds's number.

Tests of this model confirmed high efficiency of the found decision (Figure 4.21). The two-bladed model made it possible to receive more accurate results on the influence of a corner of a turn and a form of fixing of the blades – bilateral fastening and a rectangular shape of blades is better than console fixing of blades of a trapezoidal form.

Systematic experiences[see comment 8] in hydraulic trays 1 wide and 2m with a filling depth near 1m and the speed of the current at 1–1.5 m/s, carried out in the Research Sector of the institute of Gidroproyekt made it possible to draw the following conclusions of rather axial orthogonal units [11].

1. Not optimized orthogonal cars can have low efficiency (less than 20%). Reduction of the diameter of a shaft with 0,15 to 0,1 D improves rotor characteristics (C_p max = 0,21) a little. The fairing device on a shaft doesn't give a positive power effect. Installation of trailer washers on the free ends of blades considerably increases the capacity of the driving wheel (C_p max =0,26); for 10% rapidity increases in a characteristic optimum.
2. The assumption of the essential influence of losses on console blades is confirmed. The accounting of this result led to the refusal of trailer sites with a creation of a frame design of the driving wheel. The efficiency of the power of a stream for such rotordoubled; level of

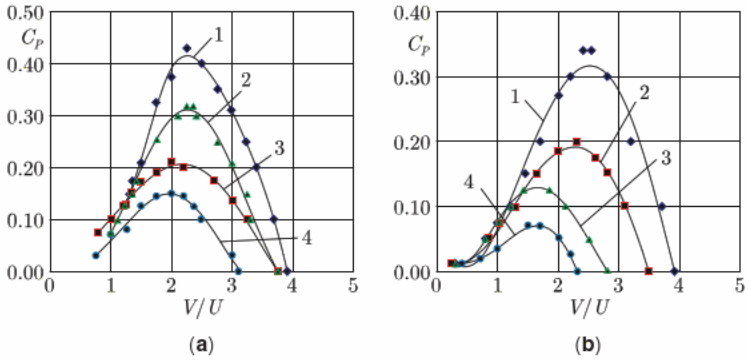

Figure 4.21 Maximum efficiency of a frame two-bladed rotor with a solidity 0.3 reaches C_p =0.43 at V/U = 2.2
a) Re = 4,0·10^5 , b) Re = 2,0·10^5. 1: φ = -5° ; 2: φ = 0; 3: φ = -10°; 4 : φ = +3°.

power qualities of a frame rotor was much higher than at existing windmills ofother types, having exceeded in some cases [see comment 8]a known border of Betz-Zhukovsky for a free stream that is probably connected with the limited width of the development channel.

3. The design of the fastenings of blade's system has a great impact. The best results are received when fastening blades on streamline spokes (Figure 4.22).
4. Influence of the height of a rotor. The difficulties of the constructive plan arising at calculations of driving wheels with high rotors, resulted in the need for more careful assessment of the influence of a rotor's height. Two and three-blade driving wheels with the rotor height of H=0,4; 0,6; 0,8; 1,0 D at b=var were investigated. In Figure 4.23, dependences of maximum efficiency (1) on rotor height in a single-tier two-bladed rotor (b=30 mm) are shown.

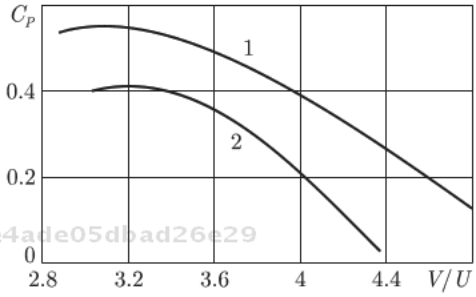

Figure 4.22 Power efficiency of two-bladed rotors on disks (2) and frame type (1).

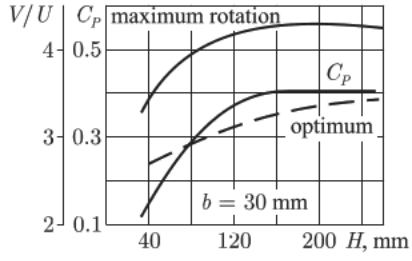

Figure 4.23 Influence of a rotor's height. 1 – max C_p 2 – optimal V/U, 3- max V/U.

From the schedule it can be seen that, for providing effective designs of axial rotors, the height of a rotor has to be accepted not less than 0,6 by D.

5. Influence of relative lengthening of the blade. In Figure 4.24 is shown the generalized schedule of dependence of the power qualities of a rotor from the relative lengthening of the blade (L/b). It is visibly clear that the minimum admissible relative length of the blade for lack of washers (the console scheme) has to be not less than five of its chords (L≥5b). The narrow blades are more sensitive to relative height, i.e. for blades b = it is necessary to appoint 0,125 D relative lengthening within L≥7b.

A power of the blade and, therefore, its "pulling" component, and with another — leads to the solidity growth, and also to the increase in the frontal resistance of a wheel. In schemes of a 6. Influence of the length of a chord of a profile. The length of a chord of a profile (b) doubly influences the power qualities of a rotor: on the one hand, the increase in a chord conducts to increase the carrying two-blades rotor with blade's chord b = 20, 25, 30, 44, 50 mm are tested. Thus, the solidity changed in wide limits (from 0,2 to 0,5). From Figure 4.25 it is visible that narrow blades (b≤0.1D) don't provide sufficient pulling force.

The efficiency of power is lower than 20%. Maximum efficiency of a rotor is observed at a chord of the blade of 25–30 mm (0,125 D) and (σ = 0,25). The further increase in a chord and, respectively, solidity degree, judging by data of this series, doesn't lead to improvement of power qualities. Sharp reduction of efficiency at σ < 0,25

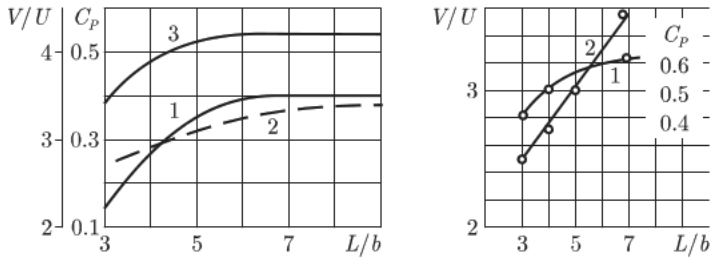

Figure 4.24 Influence of the lengthening of blades. 1- C_p max, 2 – V/U optimum, 3-V/U max.

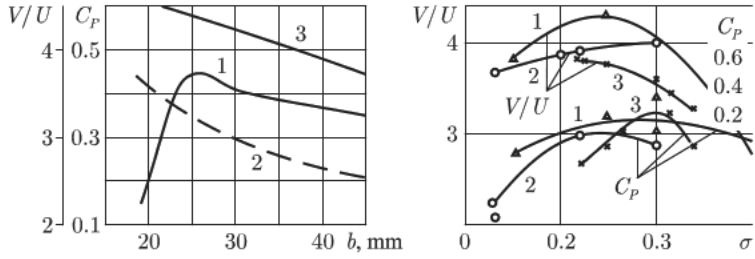

Figure 4.25 Influence of length of a chord of the blade (left). 1- $C_p$max, 2 – V/U optimum, 3-V/U max. Influence of solidity (right). 1 – single-tier with disks, 2 – single-tier console, 3 – two level frame.

can be partly connected with that with a length of a chord of the blade, smaller 25 mm, and blade speed of about 3 m/s Reynolds's number turns out only 75000. As efficiency twice smaller understating was established by experiments in a wind tunnel takes place even at Reynolds's numbers 300000. The increased turbulence of a stream in a hydraulic flume has to reduce the influence of the criterion of Reynolds, however, most likely it took place after all. For a check of this effect, tests of rotors with a diameter of 400 mm in another flume 2 m wide and up to 1.5 m in depth, were organized at a stream speed of up to 1.6 m/s.

Tests confirmed the qualitative conclusions given above, but quantitative estimates of the efficiency of all units appeared higher. For example, the maximum efficiency of two-bladed two level rotors on traverses with a solidity 0.315 and $b_t/b = 44/63$ reached $C_p = 0.6$ at V/U =3.7 However, even on this large model, introduction of horizontal extensions with a diameter of only 0.3 mm on the middle of each circle reduced the efficiency of a rotor by two (Figure 4.26).

According to tests in this flume, the maximum efficiency of the two-bladed unit at solidity 0.315, 0.265 and 0.220 made 0.6, 0.5 and 0.35, respectively. Optimum speed of the blades – from 3.5 to 3.7 speeds of a stream. In this case the optimized design of two level rotors showed close results and in a small flume (Figure 4.27).

6. Influence of the thickness of a profile of the blade. The admissibility of increase in thickness of the blade was considered. Rotors with NACA 0015, 0018, 0024 blades were tested. Comparison of power characteristics showed that at Re numbers = $1 \bullet 10^5$ "thick"

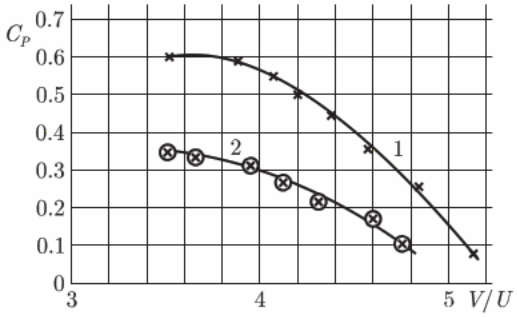

Figure 4.26 Two level, two lopastny rotor in a big tray (2×1.5×20 m) D = 400 mm, b = 63 mm, b_t = 44 mm, H=800mm, L = 4 00 mm. 1-without extensions, 2-s extensions with a diameter of 0.3 mm. U = 1 m/s.

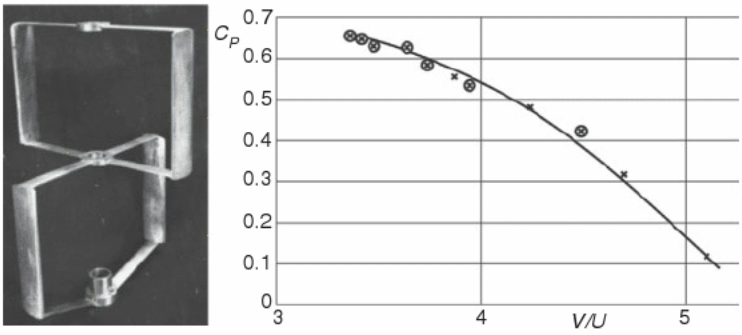

Figure 4.27 The optimum model tested in a canal 1 m wide of D = 200 mm, b = 30mm, L/b = 4.16, b_t/b = 0.5, the ends of blades are rounded on an outline a traverse. C_p = 0.661, V/U = 3.35.

blades (24%) provide the same level of power qualities of rotors.

7. Influence of the number of blades. The influence of the number of blades in a rotor on its power characteristics is considered at two preconditions: at constancy of a solidity (σ =const; b=var) and at constancy of length of a chord of the blade (σ = var; ib = const) - Figure 4.28. The maximum efficiency and rapidity are fixed at single-blade rotors. It was noticed that with the growth of the number of blades at lower of their chord operability of a rotor sharply falls despite constancy of a solidity (σ = 0,25=const). It isn't necessary to use in blade projects b≤0.1 D width.

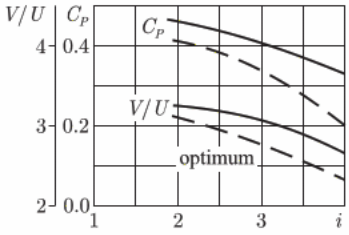

Figure 4.28 Influence of the number of blades at a constant solidity 0.3.

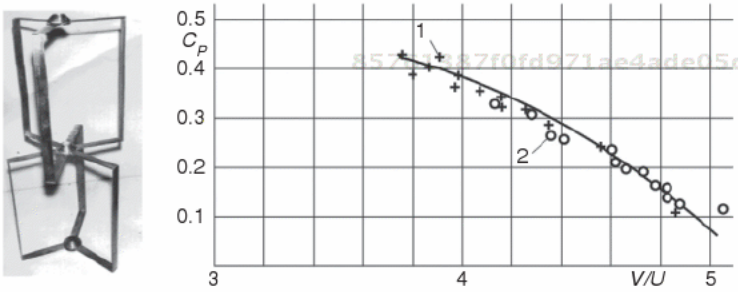

Figure 4.29 Three-blade a rotor in a big tray. D=400 mm, b=30mm, b_t=30mm H=800mm, L=400 mm.
1-U=0.84 of m/s, 2-U=0.68 m/s/.

Control tests of the three-blade turbine with a diameter of 400 mm with a solidity 0.225, carried out at speeds of stream of 0.68 and 0.84 m/s, yielded identical results on efficiency, but a little great values of optimum rapidity in comparison with the results received in a small flume (Figure 4. 29). Increase in a chord to 44 mm, i.e. solidity by 1.5 times didn't change an efficiency maximum, but reduced the optimum speed of the blades to V=3.25U.

Lifting the efficiency of orthogonal units can be attempted at the expense of the improvement of aerodynamic qualities of lopastny system, for example, by the use of trellised blades (Figure 4.30) or the biplane scheme (Figure 4.31). Finally, in connection with the practically limitlessness of wind power resources, the power efficiency of the unit, how many its technical and economic indicators – the cost of the established kilowatt matters not so much at a fixed settlement speed of a wind and the cost of the received kWh of energy.

The cardinal increase of development of the orthogonal power unit was expected by the introduction of management by an interface and the aerodynamic characteristic of the blade. The elementary

Figure 4.30 The 30 kW windmill in the suburb of Riga.

Figure 4.31 Windmill of the big power with blades according to the scheme of a biplane (project).

decision consisted of giving the chance to turn the blades to an angle of attack, near-critical that corresponds to the maximum pulling force of a wing (Figure 4.32).

Another decision provides the kinematic management of the blade or its flap for the purpose of providing the best conditions of a flow, taking into account the direction of a wind and the position of the blade on the route (Figure 4.33).

Tsikloturbina in principle Figure 4.33 or the known similar scheme of a rotor of Fokht-Schneider [13] were carried out in practice, (Figure 4.34) are studied theoretically and experimentally.

Certainly, the maximum efficiency of turbines remains in the limits determined by the known theorem of Betz-Zhukovsky, but

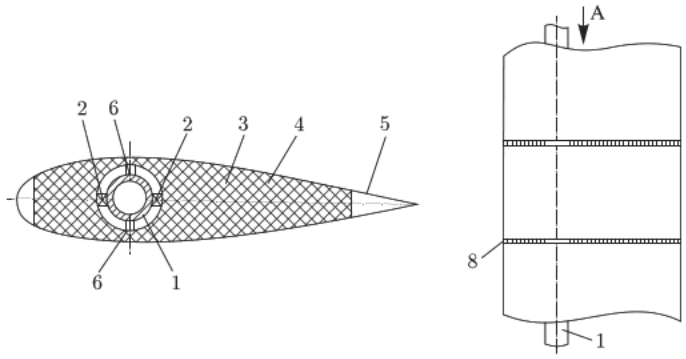

Figure 4.32 The wing consists of sections (on the right), each of which independently chooses the optimum situation answering to a critical angle of attack when equally effective aerodynamic forces pass from a point located before a support, to a point located behind a support. The blade slightly "ransacks", being constantly in a zone of a maximum of the pulling force [12].

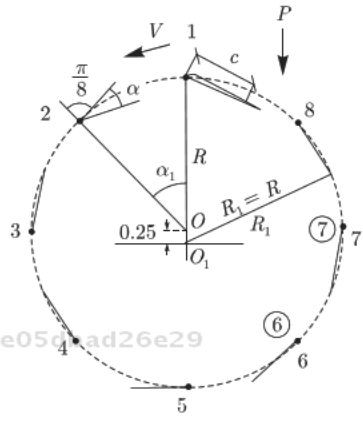

Figure 4.33 Mechanical control blade or flap turn. About - the center of the route of a sock of the blade, O1 – the center of the route of a tail of the blade, 1 – 8 – provisions of the blade on the route. The provision of a point of O1 changes under the influence of a weather vane – this point in an aerodynamic shadow of an axis of a rotor.

the general characteristic of the turbine changes so that energy development in areas with a variable wind for lack of another system of regulation can appear higher.

The difference found, however, wasn't considerable and hardly justifies complication of the unit and reduction of its reliability at the expense of additional mobile connections.

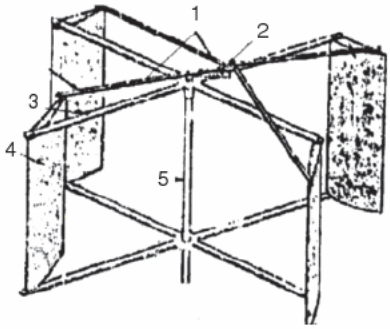

Figure 4.34 Management of the turn of the blades in the Iwanata unit (1978). 1 – operating drafts, 2 – an axis of the hinge of management, 3 – rotor traverses, 4 – working blades, 5 – a unit shaft.

The same effect, can be reached more reliably, using a system of operating streams, podavavemy blades in an interface in the necessary points of the route (Figure 4.35)

Systematic research of orthogonal wind-driven generators with jet management of circulation on the blades according to the original scheme (Patents US 0014792,0045329, 0003090) are conducted at the University of Western Virginia (USA). According to data from experiments at a solidity 0.1, a turbine with direct blades had a maximum of efficiency of 35% at V/U = 5, and at jet management, the maximum of efficiency up to 42% at V/U = 4–4.5[15].

The general increase of development of axial cars can be reached by a change of the geometry of a rotor depending on the speed of a wind (Figure 4.36).

For small and average cars, imbalance of loadings is eliminated by the device of screw blades with the counter direction of screw axes of blades in circles of the unit different in height. It can be realized in each circle of the many-tier unit. The spatial farm formed by working blades levels loadings and can perceive them without a high central shaft. The smoothed (constant) torque is transferred or to a short central shaft (Figure 4.37A) or perceived by the linear (arc) generator located on a circle, outlined by working blades (Figure 4.37B).

Lack of such decision is too high solidity brought by a lattice of blades, and as a result rather low efficiency of wind power and, therefore, rather high material capacity. [17] Elimination of the specified shortcomings is reached by each turbine being supplied

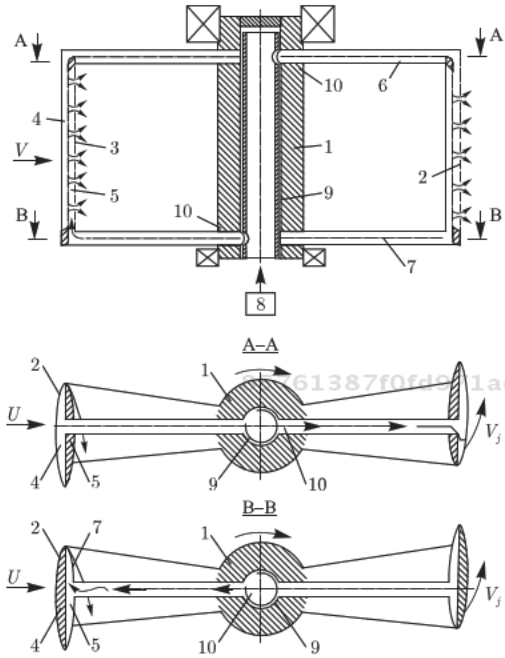

Figure 4.35 Jet management of circulation on blades of the working unit. On hollow to a shaft (1) hollow traverses (6 and 7) and hollow blades (2) with slot-hole nozzles (3) are fixed. [14] Cavities in the blades are executed in the form of the isolated chambers (4) and (5).To one, other of cameras through traverses is reported with a shaft cavity. Stream giving on this or that part of the blade happens from the supercharger (8) via the distributor (9) and openings (10). Turning a shaft (9) we change the moment of release of streams on the route of blades. Streams increase the lifting and pulling forces of profiles.

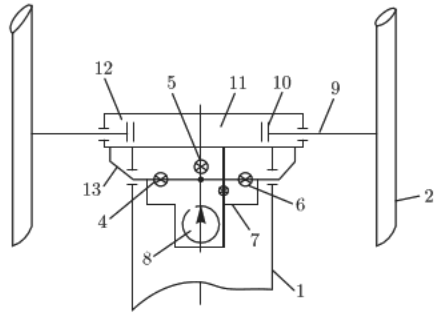

Figure 4.36 Hydraulic actuator and the valve allow the change of the diameter of a rotor and the balance of wings. [16]

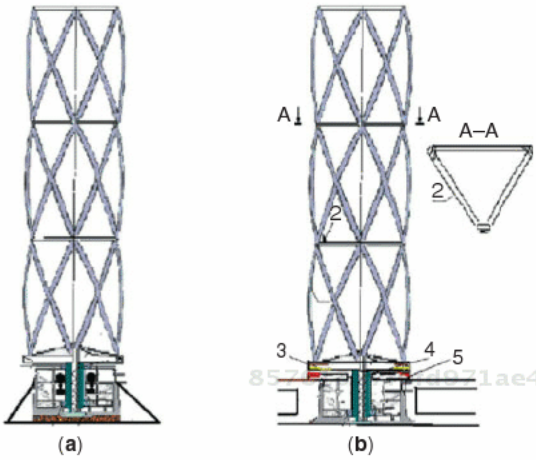

Figure 4.37 Vibration-free windmills with a self-bearing aerodynamic design. A) With torque transfer on the central shaft. C) With the linear (arc) generator under the blades.

with the blades of an arrow-shaped form bent on screw lines, going in opposite directions from the turbine middle. Some options for realization of this idea are developed. In the option shown in Figure 4.38, the generator has one short-circuited rotor being the general element for both circles of turbines, moving in one direction.

Basic rollers (7) at external rings of the turbine can be replaced with single bearings on the central pole, perceiving radial loadings from blades through the thin previously tense strings. The balanced turbines of other designs with arrow-shaped screw blades can be applied in units with bilateral linear (arc) generators with the magnetic field running diversely on the different parts[?] of the inductors. Such a scheme (Figure 4.39), completely exempts support from a torque and pulsations of basic reactions. In option on Figure 4.30, the linear (arc) electric unit installed between turbines is used. In its structure there is an inductor executed in the form of a flat magnetic conductor with a yoke and gear zones, placed on both sides of a yoke. In the grooves of the inductor, the three-phase winding executed from ring coils which cover a yoke, and the jet tires placed on both sides of the active surfaces of the inductor and remote from them by working gaps, is mounted. The magnetic conductor of the inductor becomes isolated motionless plates.

The lateral active faces of coils of two phases of a winding are shifted parallel to a longitudinal axis of the inductor, one

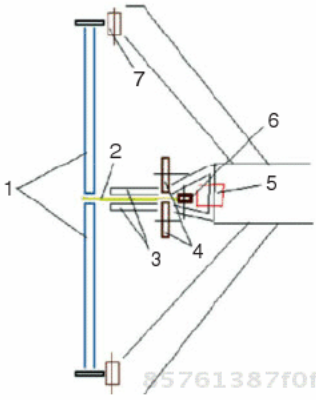

Figure 4.38 Scheme of a suspension bracket of a rotor and output capacities. 1 – the working blades bent on the screw line, 2-short-circuited rotor, 3 – a magnetic conductor, 4 – the rollers fixing the provision of a rotor in a magnetic field, 5 – a winding forming the running field, 6, 7 – the rollers perceiving lateral reactions.

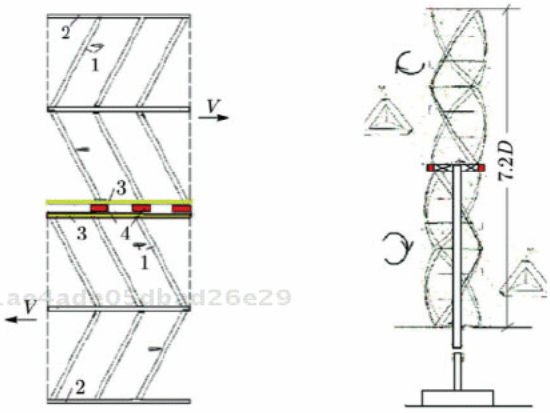

Figure 4.39 Development of a surface of the power unit. 1- the blades of an aerodynamic profile focused exactly opposite in the top and bottom turbines, 2 – the rings uniting the external ends of blades, 3 – the short-circuited ring rotors uniting the ends of blades, turned to motionless inductors of the generator (4). V – speed of movement of the blades of turbines.

concerning another, and pofazno - in the counter direction; coils of these phases are placed on both sides from coils of the third phase the same as it was carried out on hydro-units. More effective design of the generator with the unified inductors located on both sides of a shortly closed rotor is also possible. It allows for the reduction twice of a settlement gap in the generator.

Blades of the turbines located on the different parts of inductors are focused exactly opposite, providing for the rotation of the turbines in opposite directions according to the movement of running magnetic fields of inductors. Such silent, vibration-free windmills can settle down, for example, on a vessel or on a roof of a high building, decorating the landscape and providing the consumer with electric power, fresh water, heat or cold. A roof and building will change the performance of windmill. [18]

Certainly, the blade outlined on the screw line, can be approximated by pieces of direct blades. In this case, the simple and easy design convenient in production and reliable (Figure 4.40) turns out.

An important feature of our cars is the scheme of management of the units. In this scheme, use of modern converters of the frequency, allowing for change of the frequency of rotation of the unit with search of a maximum of the given-out power and restriction of this power within generator rated capacity, is provided. Such a scheme provides the maximum development of the unit and doesn't demand information on the speed of a running stream. In units of less power (for example, in Figure 4.40) a simpler scheme is applied – the unit is started from the sensor of the wind speed at a low speed of rotation, and at achievement of a certain power with a certain duration, switches over to a high speed of rotation and back. At excess of face value or emergence of a dangerous vibration, the unit slows down and is disconnected from a network.

The design on Figure 4.40 is the "module" offered the consumer. Such a module can horizontally settle down if a wind has the primary direction, for example, along a valley or the mountain gorge. One, two or three such modules can settle down vertically on a

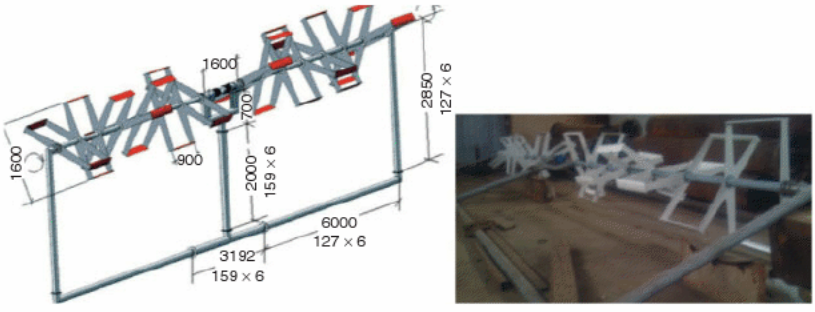

Figure 4.40 Balanced windmill 11 kW with counter rotation of rotors and standard two high-speed electric equipment for work in an electric network.

uniform support, forming the balanced 11, 22, 33 or 44 kW unit. If necessary the support can be supplied with delays (Figure 4.41).

For individual consumers in zones with low winds there can be an interesting block of windmills, constructed according to the same scheme, as in Figure 4.40, but in smaller dimensions (Figure 4.42).

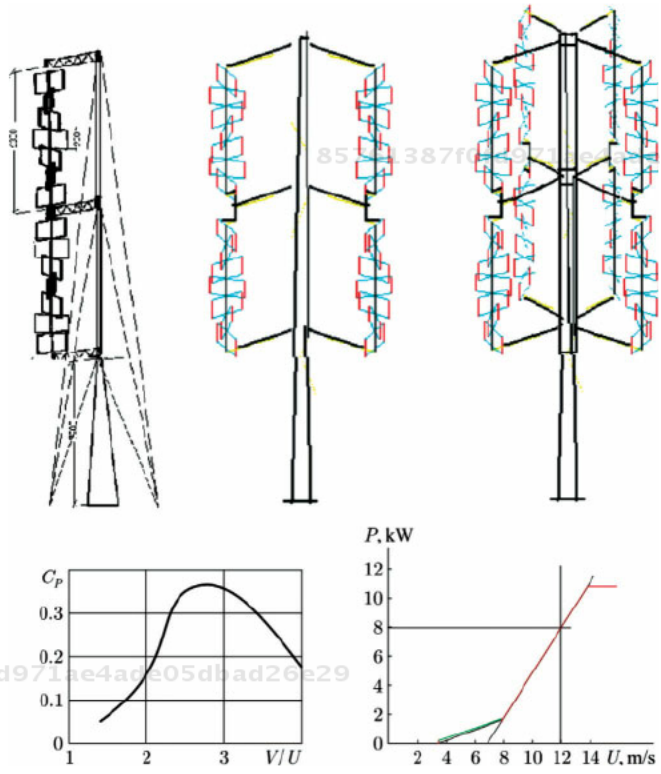

Figure 4.41 Orthogonal balanced windmills with the 11 kW module. From blocks the 11, 22, 33, 44 kW installation can be gathered. Power: $P = \rho C_p U^3 D L/2 = 1.25 C_p U^3 *1.6* 0.9*14/2 = 12.6*C_p U^3$, W from one unit.

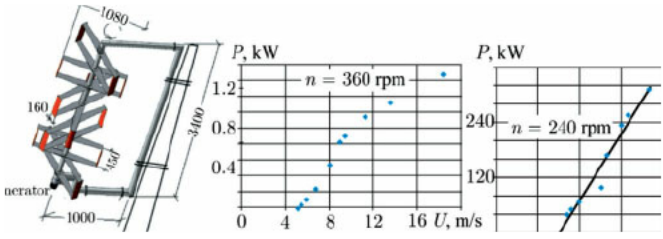

Figure 4.42 The block of windmills, 1000 watts, with a shaft in the form of an aluminum pipe with a diameter of 50 mm and weighing 0.6 kg/m.

The block of windmills can have a bearing designed from plastic pipes or from aluminum pipes of the same diameter, as a rotation axis (50 mm), and is equipped with the standard electric equipment applied in modern cars with an exit at the stabilized constant tension. Inertial forces, which are better compensated at the placement of two blades in one circle, become the main loading here. From similar blocks the wind power station with a rated power, for example, in 3÷5kW can be collected at a wind of 10 m/s according to the Figure 4.41 scheme. It is clear that the guaranteed capacity of the system will be defined by the capacity of accumulators, the capacity of applied inverters, and the set duration of its use. For example, with the settlement duration of the maximum mode, the guaranteed capacity can be 2÷3 times more than the face value.

For difficult climatic and topographical conditions, the design of a wind power tower and the technology of its construction is considerably simplified in the patent [19]. In this decision, working blades are in pairs united in triangles, and their bases and tops form the rigid triangles creating in the plan a Magen David look (Figure 4.43).

This wind power unit consists of several (three or more) isosceles triangles, whose lateral sides form the inclined blade, each horizontal section of which has the hollow aerodynamic profile, oriented with the small deviation angle outside from the tangent to the circle, described by the center of this profile during the work of the unit. The bases of the triangles are located horizontally at a

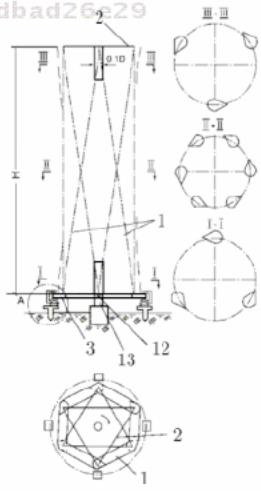

Figure 4.43 Construction of the wind power unit, which consists of three triangles (6 working blades).

small height from the ground and are connected with each other. The planes of the triangles are located with a small deviation from the vertical line outside, and the vertexes of the triangles are connected by the traverses, which form a horizontal regular polygon with the diagonals forming rigid triangular elements.

The pyramid, formed by the inclined blades and the horizontal traverses, can be fixed in the lower part at a plate steel ring with an electro-conductive cover plate, which fulfills the functions of the rotor of the linear (arch) generator, whose inductors together with electromagnets of vertical off-loading and vertical supports, are elastically fixed at several posts around the edges of steel ring.

The inductors are supplied with blowers, guiding the warm air towards the steel ring at which, besides the blades, a light housing with mobile shutters is fixed, which receives the warm air from the blowers and guides it into the internal cavities of the blades. The ends of the blades in the upper part are supplied with deflectors, which create the aerodynamic draught, which facilitates the movement of warm air along the internal passages of the blades from below upwards. The vertexes of the lower polygon are connected according to the scheme of bicycle spokes with the central bearing set on the short supporting shaft, which receives the horizontal force. The wind power unit is installed without the use of a high crane through uniform tightening of the vertexes of the forming triangles, which are turning from the horizontal position relative to the flapping hinges, located at the bases of the triangle's sides by pairs in the plane of each triangle. Figure 4.43 shows the version of the wind power unit, which consists of three triangles (6 working blades). Figure 4.44 shows the construction of the vertical support, which carries the inductor of the linear generator and the electromagnets of vertical off-loading.

A wind power unit consists of three or more vertical elements in the form of isosceles triangles (1), whose lateral sides form the inclined blade, each horizontal section of which has the hollow aerodynamic profile, oriented along the tangent to the circle, described by the center of this profile. The bases of the triangles (1) are located horizontally at a small height from the ground and are connected with each other. The planes of the triangles (1) are located so that their vertexes are connected with each other by the traverses (2), which form a horizontal regular polygon (in Figure 4.43 – the triangle). The pyramid formed by the inclined blades of the triangles (1) and the horizontal traverses is fixed in the lower part at the rotor (3)

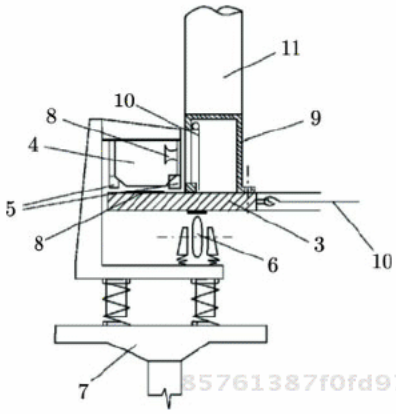

Figure 4.44 The version of supporting assembly.

of the linear (arch) generator in the form of the plate steel ring with an electro-conductive cover plate, whose inductors (4) (Figure 4.44) together with the electromagnets of vertical off-loading (5) and the vertical supports (6) are elastically fixed at several posts (7) around the edges of the steel ring (3). The inductors (4) are supplied with blowers (8), guiding the air flow towards the steel ring (3), at which is additionally fixed a light housing 9 with mobile shutters (10) receiving the warm air from the blowers 8 and guiding it into the internal cavities of the blades (11) of triangles (3). The ends of the blades in the upper part are supplied with deflectors (not shown in the figures), which create the aerodynamic draught, which facilitates the movement of warm air along the internal passages of the blades (11) from below upwards. The vertexes of the lower polygon are connected according to the scheme of bicycle spokes with the central bearing (12) (Figure 4.44) set on the short supporting shaft (13), which receives the horizontal force.

Installation works as follows. At low wind speed the electromagnets (5) of off-loading of supports (6) are turned on, and the parking brake is turned off. The power unit begins to revolve under the action of the wind, and upon the reaching of a specific value of rotational speed, the inductors (4) of the linear generator are switched to the power network. The heat released by the inductors is directed by the blowers (8) through the shutters (10) and the duct (9) to the blades (11), freeing them from frozen snow and ice. The improved aerodynamic efficiency of the blades (11) ensures further driving of the blades up to speed, and increase in the power generated by the inductors (4) into the power network.

For all orthogonal windmills, the braking problem is actual at the dispersal and shutdown of a network and the protection against a hurricane when the wind-driven generator doesn't work anymore, or from a strong wind when the unit works, but it is desirable to reduce an ometayemy surface. In the first domestic units this problem was solved by mechanical braking under the influence of falling freight and a system of blocks (Figure 4.45) [20].

In the English version of the VAWT (Figure 4.46) the blades are folded in a vertical plane passing through the axis of rotation of the unit.

Another possible option when the blades turn around traverses (Figure 4.47) [21]:

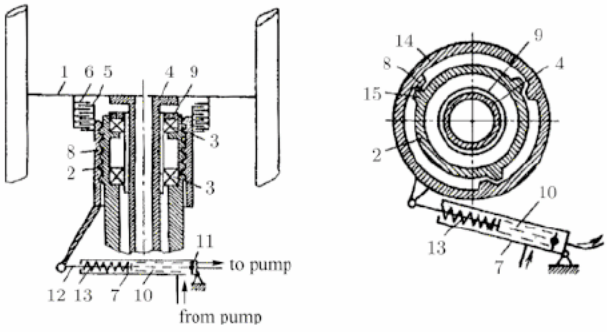

Figure 4.45 System of braking of the rotor (1) connected with the block of basic disks (6) and shaft (4), located in the bearing hub (3) placed in the motionless case. On this case through a multiple-pass carving (2) the feedwell is located (8), bearing brake rings (5) and connected with giroprivody (7), containing a hydraulic cylinder (10), the valve of dumping of pressure (11) and the brake spring (13), which action can be replaced with the force of weight of the lifted freight. Under emergencies, pressure in the cylinder (10)is dumped, a spring (13) or freight turn the feedwell (8) and squeeze brake a kolets (6) and (5).

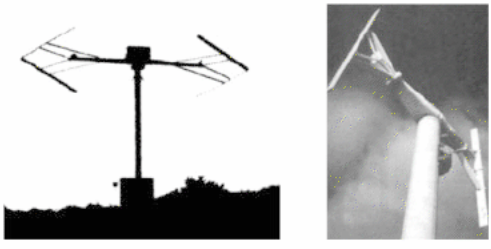

Figure 4.46 Wind turbines with a diameter of 6 m (at the left) and 25 m (on the right) with changeable geometry of a rotor of a design of P.J. Musgrove. England, 1982. Capacity of the large unit – 100 kW. England.

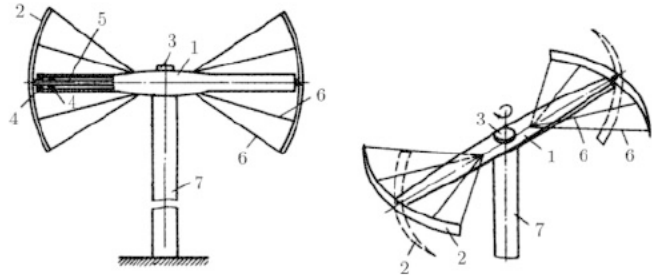

Figure 4.47 Rotor with the blades (2) fixed on a traverse (1) through a shaft (5), located inside traverses in support (4) and connected with the mechanism of turn (3) on a support (7).

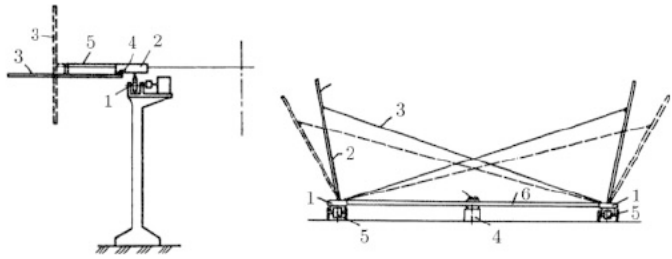

Figure 4.48 Rotor with the taken-out support (1) on which the ring (2) bearing traverses (5) and vertical blades (3) which at a rotor stop under the influence of the weight come to horizontal situation moves and are fixed by the lock (4) [23]. Right – a rotor of great power with support (5) and generators under the blades (2) having hinges (1), allowing blades to change a tilt angle that protects generators from overloads, and a rotor from destruction at a strong wind.

Protection against a hurricane of the stopped axial car, with the generator under blades, can be reached by a blade turn in a horizontal or inclined situation (Figure 4.48) [22].

A number of constructive measures are offered for unloading of a knot of fastening of the working blade to a traverse (Figure 4.49, 4.50) [24].

In JSC Vertikal and JSC NIIES designs protection against dispersal is carried out by turn a traverse (Figure 4.51).

Serious danger to a unit of this kind is connected with vibration of a rotor and blades. The offered measures (Figure 4.52) reduce, but don't eliminate this danger [26]. The finding offers the use of curved blades, and many-tiered and multi-blade rotors.

The increase in efficiency and reliability of the axial car can be reached by the introduction of several circles of blades with a different diameter of the route (Figure 4.53) [27].

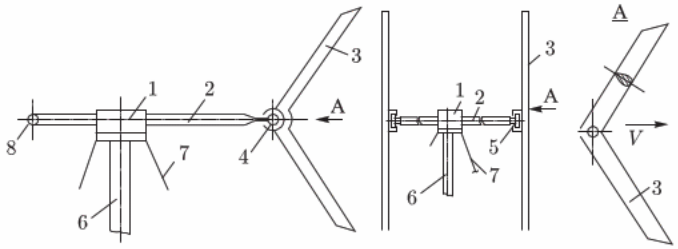

Figure 4.49 Elimination of the torque usually transferred to the central basic hub (1) through a traverse (2), is reached by the device spherical (4) or the cylindrical (5) hinges allowing free turn of the arrow-shaped wings (3). The return sweep of the wings provides stability of the system. The unit is located on a rack (6), strengthened by delays (7) and counterbalanced by a counterbalance (8) or symmetrically located wings.

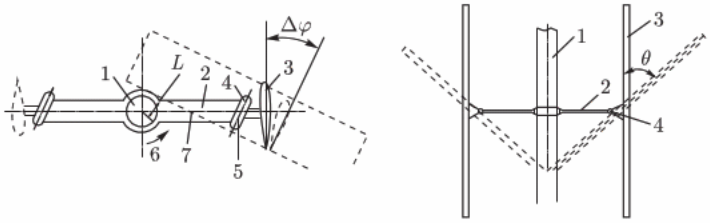

Figure 4.50 The axis of the hinge (4) can be inclined to an axis traverses. During the work, the rotor has the constant capacity, and the greatest efficiency – at the vertical position of the blades (3). When strengthening a wind of the blade under the influence of the centrifugal force (the top part is slightly longer than the lower part of blades), turn on a corner θ. Such a turn changes a corner of the installation of the blades on Δφ, reduces the efficiency of a rotor, keeping its frequency of rotation and capacity [25].

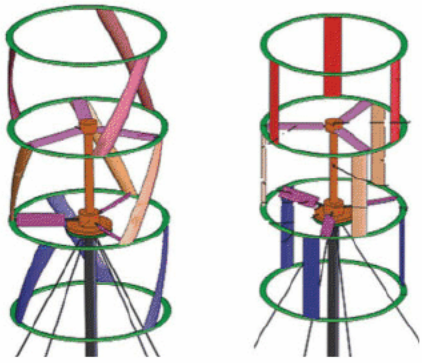

Figure 4.51 Wind-driven generator with rotary traverses (E.V.Solomin) bent (at the left) or direct blades.

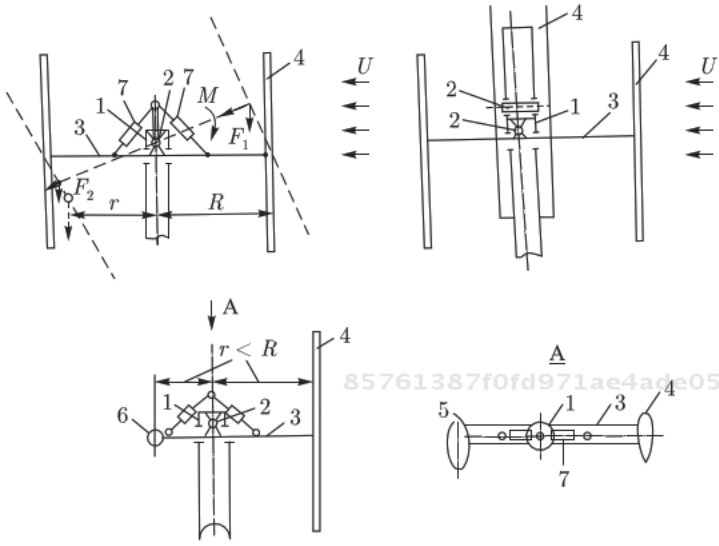

Figure 4.52 Traverses of a rotor (3) are supplied with dampers of fluctuations (7), and the centers of gravity of the blades are located at one level, the traverse is lower and hinge (2) axes are lower.

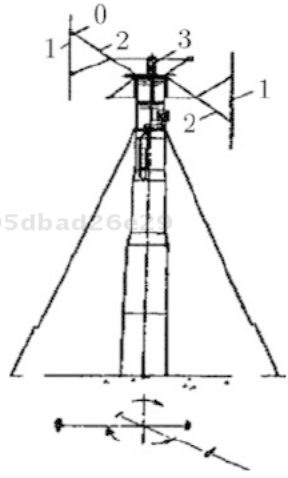

Figure 4.53 The part of a rotor that has a high zateneniye provides self-start, and the part of a rotor that has a low zateneniye provides higher efficiency and capacity at light breezes.

The many-tiered scheme allows for the increase in efficiency of the electric generators of installations at the expense of the use of counter rotation of circles (Figure 4.46) reducing the danger of a pretsessiya [28].

The many-tier units working for one shaft or on different shaft with counter rotation can be grouped in high powerful systems (Figure 4.55) [29].

In axial, blades can directly be fixed on a unit shaft (the "jump rope" scheme - troposken) or on traverses. The increase in the single power of such units, at the expense of length a traverse and blades is limited to durability and a material capacity a traverse, need of a keeping of a certain speed of movement of blades. As a result, with an increase in the diameter of a rotor frequency, its rotation

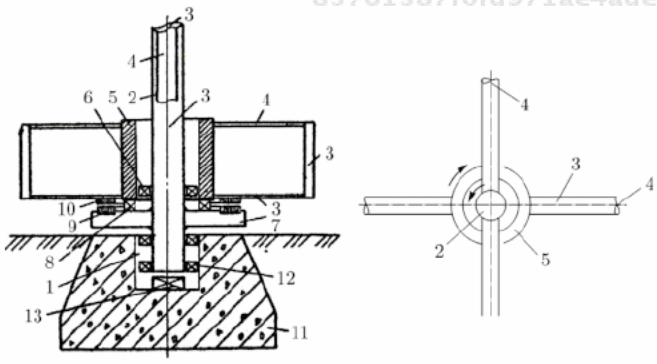

Figure 4.54 Blades on different circles are focused in opposite directions that provides counter rotation of a stator of the generator (9) placed on a disk (7) and a rotor of the generator (10), the bottom circle placed on traverses. Efficiency of the unit at a solidity 0.3 according to data of tests can reach 45%.

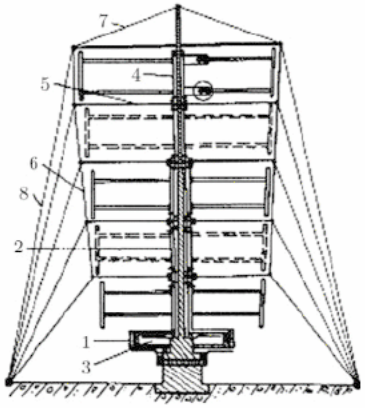

Figure 4.55 Many-tiered windmill with pairs of counter rotation of rotors.

decreases, and the material capacity of brakes, a reducer, and the electrotechnical equipment increases.

Full-scale tests of a serial of orthogonal, with one, two and four identical blades (Figure 4.56), were carried out in the largest subsonic aerodinamic pipe TsAGI (Zhukovsky town, the Moscow region) [30].

At the design of the units, special attention was given to a choice of a form of the blade and manufacturing techniques. The accepted blade was a trapezoidal form (Figure 4.57)

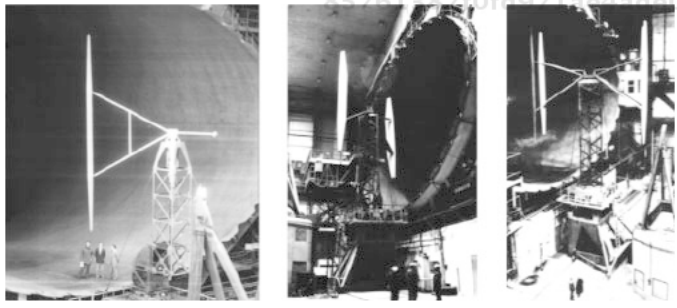

Figure 4.56 Full-scale tests serial orthogonal turbines with one, two and four identical blades.

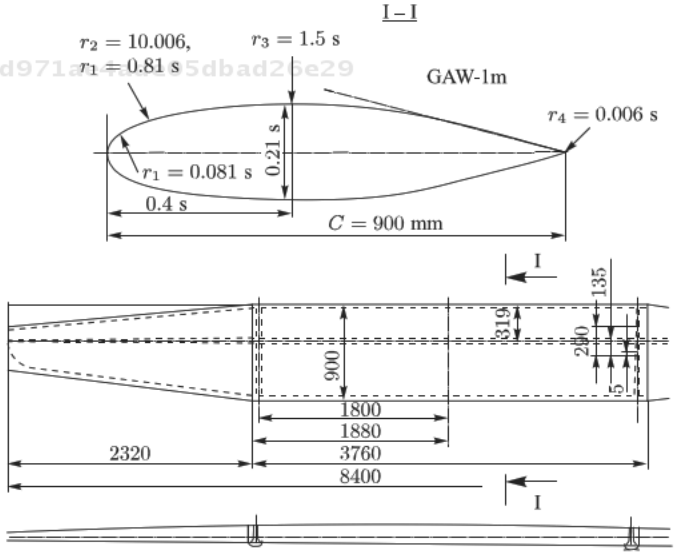

Figure 4.57 The form of blades (GAW-1 m) in the tested units.

The length of the central part is 3760 mm, the width is 900 mm, the distance between the axes of support of is 3600 mm, the full length of the blade taking into account trailer rounding is 8600 mm, without rounding, it is 8400 mm. The real square covered is 6.4 m^2, the average length of a chord of a profile is 0.76 m. The profile of the blade was considered in two options – the asymmetrical (GAW-1) having the best aerodynamic qualities, and the symmetric, offered by the author and called the GAW-1M. At this profile, the bottom surface repeats outlines of the top surface of the GAW-1 profile. The outline of a sock of the blade with the GAW-1 profile in the top (thick) part is close to a NACA 0021 profile outline, and an outline of a sock of the lower (thin) part of a profile is close to the NACA 0015 profile. The coefficient of the pulling force, for the GAW-1 profile, almost in all range of angles of attack, is more than at the NACA 0015 or NACA 0020 profiles. The maximum coefficient of carrying power of cy for the GAW-1 profile at Rec Reynolds's numbers = Vc/ν = (6–8) 10^6 reaches 2.0–2.1, that is 25–30% higher than at the best profiles of other known series. At decrease in numbers of Re, quality of a profile sharply decreases. It was shown at a purge of the model of a wing of a trapezoidal form with the GAW-1 and GAW-1M profiles, for which Re_c at numbers = (0.28–0.56) $10^{6,}$ coefficients of c_y didn't exceed 1.1 and 0.8 for asymmetrical and symmetric profiles, respectively. The small model of the single-blade turbine with a wing of 0.25 m^2 which had the GAW-1 profile, didn't show as being expected, high power qualities at those numbers of Re_c = (0.14–0.58) 10^6 which managed to be reached in a small wind tunnel of TsAGI. Taking this negative result into account, full-size blades were made with a symmetric profile GAW-1M (fig. 57). Blades were made of the plastic reinforced by fiber glass, the calculation in special forms with the subsequent heat treatment. The surface of the blades turned out to be very smooth. The mass of the blade is –78 kg. Blades after production at the plant were subjected to the static loadings imitating aerodynamic loadings at a detachable and continuous flow, and also the action of centrifugal forces. At set settlement, the total load of the blade of 2800 kg,plastic (residual) deformations weren't noted at loadings in 1.5 and twice exceeding the settlement. In some cases, local loadings reached 3338 kg/m^2 at an average calculated value of 438

kg/m^2. The single-blade wind turbine (Figure 4.56) had a rotor diameter 7.05m, balanced by means of a cylindrical counterbalance of a streamlined shape at a distance of 1.8m from a rotation axis. The rotor through basic and brake knot was connected about the MP2–315-15–80 motor reducer (the manufacturer – TAMBOVPOLIMERMASh plant) to the 11 kW asynchronous generator 4AM132M4-U3 built in it, nominal sliding of 0.0267, critical sliding of 0.175, a nominal torque of 72 Nm, a critical torque of 307 Nm. On the basis of preliminary tests of a system without a rotor, mechanical and electric losses in the system of the generator reducer were defined:

Capacity on a shaft, kW	0.4	4.58	7.44	10.8	14.1	18.6	24.5
Electric Capacity on plugs of the generator, kW	0	3.55	6.40	9.43	12.6	16.0	20.1
Losses of power, kW	0.4	1.03	1.04	1.37	1.5	2.6	4.4

Results of tests of the wind turbine in a big wind tunnel of TsAGI T-101, the smallest of which section size almost twice exceeded the blade length, are shown in the table. Rather low efficiency of a single-blade rotor can be connected to a low solidity of the rotor ($\sigma = 0.11$), and also to a big aerodynamic resistance to the traverses, made of duralumin with a vertical strut, and a counterbalance.

Results of tests single-blade windmill in a big wind tunnel of TsAGI.

Wind speed U_0, m/s
0 3,1 6,44 7,58 8,76 8,94 10,2 11,0 11,7 11,0 10,2 9,3 8,3 7,3 10,1 10,9 11,5 12,4 13,7

Blade speed V, m/s
29 29 29,4 29,6 29,9 29,9 30,1 30,3 30,5 30,3 30,2 30,0 29,8 29,7 30,2 30,3 30,5 30,6 30,6

Capacity on plugs, kW
-5,85–4,92–3,06–0,58 1,06 2,39 4,79 6,65 8,91 6,92 4,52 2,66 0,53 -1,33 4,8 6,4 8 9,8 12,3

Capacity on rotor P, kW
-4,82–3,89–2,06 0 1,66 3,29 5,89 7,75 10,3 8,07 5,62 3,56 1,03 -0,63 5,9 7,5 9,2 11,2 13,8

V/U_0
3,9 3,41 3,34 2,95 2,75 2,61 2,75 2,96 3,22 3,59 4,07 2,99 2,78 2,65 2,47 2,23

Efficiency, C_P
0 ,068 ,127 ,153 ,160 ,177 ,167 ,146 ,122 ,05- ,158 ,160 ,168 ,162 ,148

Power coefficient, C_N
0 ,016 ,031 ,055 ,071 ,092 ,075 ,052 ,034 ,010- ,055 ,069 ,083 ,10 ,123

Apparently, from the information in the Table, the loss on a rotor for lack of a wind reached nearly 5 kW. If these losses were successfully eliminated, the efficiency of the turbine would exceed 40%. The possibility of an increase in the efficiency of the turbine at the expense of an increase in a solidity, follows from this finding that the power factor of C_N characterizing relative size of power, removed from unit of area of working blades, reaches high value 0.123 at a relative speed of a stream of $U_0/V = 0.45$.

With the same blades it was designed, made and tested in the same wind tunnel windmill, allowing application of two and four-blade rotors with a diameter 9m and more. Traverses at this rotor were made of steel, without an intermediate rack with an external section of 465×88mm^2 with a rounding off of a forward edge and a smooth narrowing of a local edge (the power part of a traverse had a section of 234×88mm^2 at the area of a section of metal 37 of cm^2 and the moments of inertia 284 and 2389 cm^4. Traverses at an axis of rotation fastened on a crosspiece put through a support of a rotor on an axis of the animator of MP2–500-13–80-00, with the transfer number 18.6. As the generator, the asynchronous U3 engine 4AM250 8/6 with a rated power of 40 and 50 kW was used with frequencies of rotation of 750 and 1000 rpm. Nominal slidings 0.0133 and 0.015, critical slidings 0.0449 and 0.0515. Critical torques in the generator 1017Nm and 966Nm mode. The mass of the generator is 510 kg, the total mass of the power knot together with brake system of 1684 kg. The crosspiece of a rotor was arranged so that it was possible to fix one more set from two blades shifted in the plan at 45 degrees from the previous couple. The 2-speed generator made it possible to carry out tests at two speeds of rotation of a rotor – 38.8 +/-0.1 and 51.6 +/-0.1 rpm. (speed of blades 18.2–18.3 and 25.3–25.4 of m/s). Previously, it was established that losses from idling of the motor-generator at a small speed of rotation make up from 1.2 to 1.7 kW, and at a great speed of rotations, from 1.4 to 1.9 kW. Power consumption during the operation of the motor with a reducer made up respectively 1.79 and 2.52 kW. These values of losses of power increased to the power measured on the plugs of the generator at the calculation of the power of a rotor. Results of measurements of active power on the generator plugs, carried out by different methods – registration of instant values of a vector of current and on the counter of the energy, yielded similar results, showing that with a lowl frequency of rotation, the two-bladed car comes to a mode of delivery of power at lower speeds of a stream,

than four-blades with a rotor of the same diameter with the same frequency of rotation (Figure 4.58).

In this regard, the two-bladed car appeared more effective. However, at a wind speed greater than11 m/s, capacity at a four-blade windmill is significantly more. The increase in frequency of rotation, sharply increases losses in power knot; therefore, even at the two-bladed car, delivery of power begins only at a wind speed greater than 8 m/s (Figure 4.59).

Power delivery at all tested orthogonal cars pulses with a frequency twice exceeding the rotation frequency. The number of blades affects only a form of the curves of current – at the four-blade car the change of current is much smoother and is much closer to a sinusoid (from some constant component!) than, for example, at the two-bladed car (Figure 4.60).

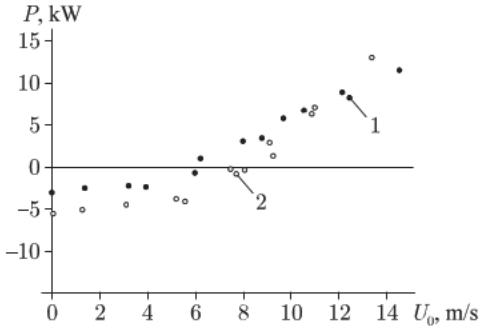

Figure 4.58 Capacity on plugs of the generator, 1 - two blades, 2 - four blades. Frequency of rotation is 38.7–38.9 rpm (V = 18.2–18.3 m/s).

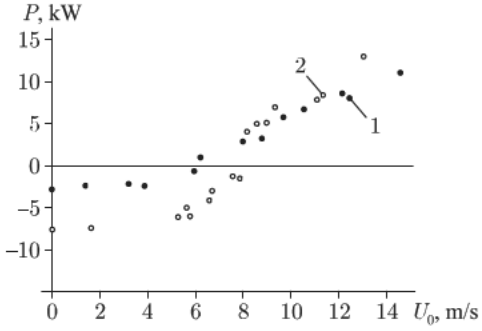

Figure 4.59 Capacity on plugs of the generator of two-blades windmill with a frequency of rotation of 38.8 (1) or 51.6 (2) rpm.

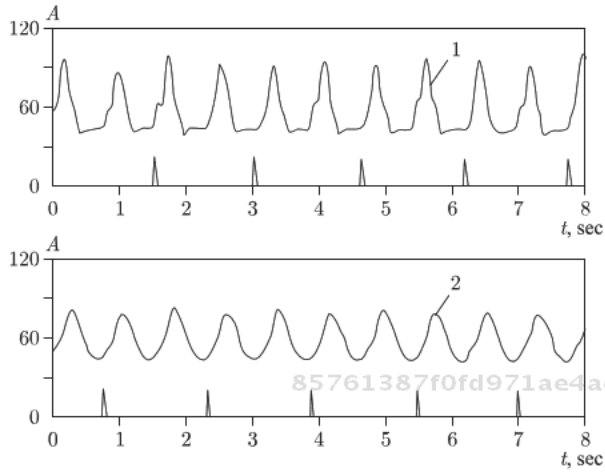

Figure 4.60 Current is one of the phases of the generator, two-bladed (1) and four-bladed (2) windmill with a frequency of rotation of 38.8–39 rpm.

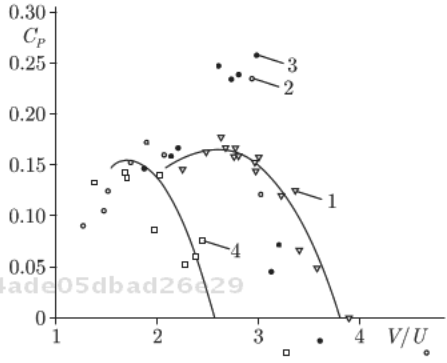

Figure 4.61 Efficiency of the windmills. 1 – one-bladed rotor, σ=0.11, Re=1.6 10^6; 2 and 3 – two-bladed rotors for low (38.8 rpm (2)) and high (51.6 rpm (3)) frequency of rotation, Re= 1 and 1.3 10^6; 4 – four-bladed rotor (38.8–39 rpm).

As the solidity of the two-bladed unit σ = 0.164 is more near optimal, the efficiency of its rotor of C_p appeared above, than at the single-blade unit (Figure 4.61).

Values of the power factor of C_N at one and two-bladed units are approximately the same (Figure 4.62).

It means that at solidity change from 0.11 to 0.164, the relative picture of the currents about blades doesn't change. At the four-bladed unit having a solidity 0.33, the power factors and efficiency

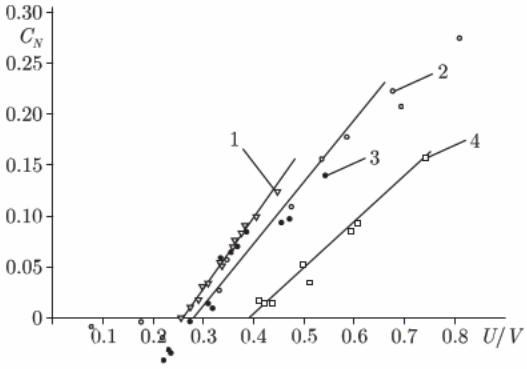

Figure 4.62 Power factor of the windmills. The numbers are the same as in Fig. 61.

Figure 4.63 Two levels windmill of 50 kW.

are lower. In the practical relation, obviously, to do the unit four-bladed in one circle is inexpedient. For an increase in power at low wind speeds, the rotor was redesigned and made two-leveled (Figure 4.63); that provides an increase in the swept area and preservation of the high power factor characteristic of windmills with a small solidity.

All units tested in a pipe showed lack of additional aerodynamic noise, however, in all cases the swing of installations with a frequency approximately equal to the doubled frequency of rotation was observed. Results of the measurements will be coordinated

with settlement data, but visually, the scope of fluctuations represented was menacing. It forced the entering of additional guy extensions and mainly, the return to designing the vibration-free counterbalanced units according to the schemes described above.

When developing large axial orthogonal cars there arose an idea to use the wings of the planes which have fulfilled a flight resource. This idea leaned on that fact that settlement loads of wings (for example, the Yak-40 plane) were much higher than loads of these blades in a wind-driven generator design. In realization of this idea, the 130 and 1000 kW experimental installations (Figure 4.64) were constructed, and detailed laboratory researches (Figure 4.65, 4.66) are conducted.

Judging by data of the projects, this idea could justify itself economically, but its realization was stopped after the disintegration of the USSR. Certainly, these projects could return to practice only with the modification, loadings providing aerodynamic balance and elimination of vibrations.

Comparison of technical and economic indicators of the units with a power of 130 and 1000 kW, carried out without taking note of the cost of the removed earth, showed that the increase in single power in this case leads to deterioration of specific indicators of efficiency [21]. So, on the 130 kW unit, the mass of a metalwork per 1 kW of rated capacity made about 16 kg/kW, and for units with a capacity of 1000kW – from 78 to 96 kg/kW. Thus, the number of hours of use of rated capacity by smaller cars is 1.7 – 4 times

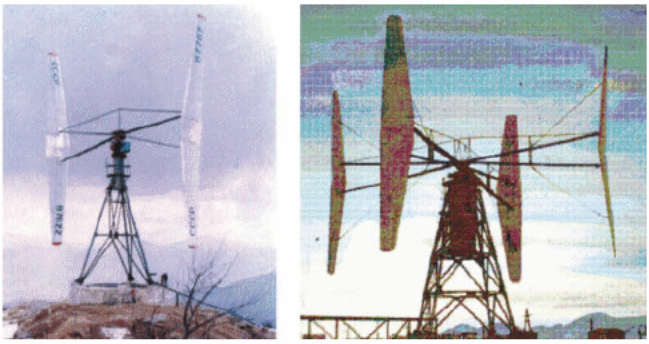

Figure 4.64 Orthogonal windmill 130 kW with wings from the YAK-40 plane on the pass Chormozak in Tadzhikistan. Diameter of a rotor of 21 m, the area of one blade Ω_b= 70 m^2, 1988 (at the left), windmill 1000/500 kW in the settlement Beringovsky (The Magadan Region), 1991 (on the right).

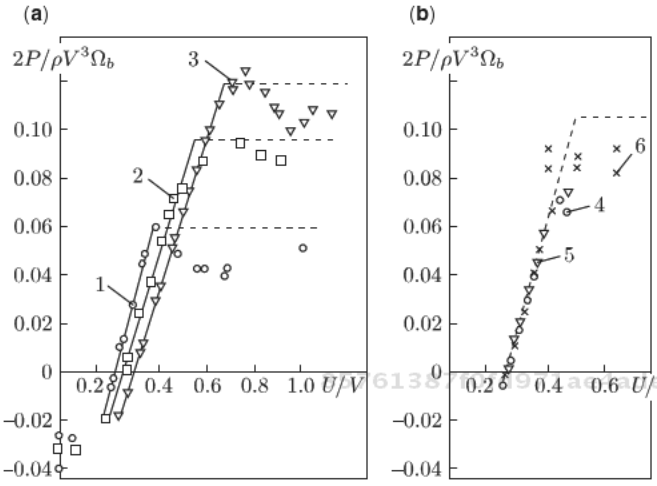

Figure 4.65 Effect of the relative curvature of the blade path on the relative power of the type Figure 4.64 unit with 2 wings from the YaK-40 airplane for a Reynolds number $2.5{\cdot}3.0{\cdot}10^5$ (a) and $4.8{\cdot}5{\cdot}10^5$ (b); At (1), (2), and (3) the wings are turned 3.5° outward from the tangent to the path, $D = 30$, 21, and 18 m, experiments of TsAGI at a scale of 1:15; At (4), (5), and (6) the wings are turned 4–4.5°, $D = 23.4$ and 28.2 m, experiments of TsAGI; At (6) $D = 21$ m, calculations on a digital computer according to the two-dimensional scheme.

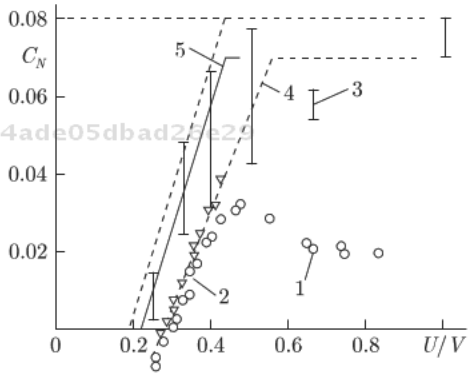

Figure 4.66 Relative power of the rotor of Figure 4.64 with 4 blades as a function of the relative wind speed according to the data of experiments of TsAGI (1 and 2) and calculations (3); (4) calculations on the basis of the model of the "ideal" unit and empiral wing drag polar; (5) averaging of the results of calculations by the two-dimensional model reproducing the low-frequency turbulence of the wake behind the rotor. The vertical lines show the boundaries of fluctuations of the numerical results as a function of the vortex shedding phase and state of turbulence of the atmosphere in front of the rotor; $\sigma = 0.32$; $\mathrm{Re} = 3.4{\cdot}10^5$ (point 1) to $5.2{\cdot}10^5$ (point 2).

more than on the large. It is clear that, to aspire to increase in single power of units in such a configuration, it is inexpedient. Windmills designed according to the Figure 4.48 scheme (on the right) yielded other results [32]. It appeared that on a specific material capacity, units with a diameter of the route of blades of 200–250 m, and blades about 100 m long can be optimum. Specific consumption of metal on the unit as a whole on the 20–25 MWt such units in the optimized options – to 70–80 kg/kW, including an expense of aviation materials on blades – to 12 kg/kW. Problems in these units are mechanical and aerodynamic losses in basic knots and constructive elements.

The small or middle orthogonal windmills do not have the same problems.

For provision of energy of the isolated power grid(for example, light source) it is able to use the balanced highly effective high-speed orthogonal small wind turbine of low power (Figu.67).

The power element of this small unit may be the simplest of all included elements, that may be purchased in U.S. markets (Figure 4.68)

Optimization of configuration of the orthogonal unit is carried out on the basis of a series of experiments with the orthogonal units having the form of a frame. Research showed that such form is successful, for it provides the effect of the trailer washer eliminating

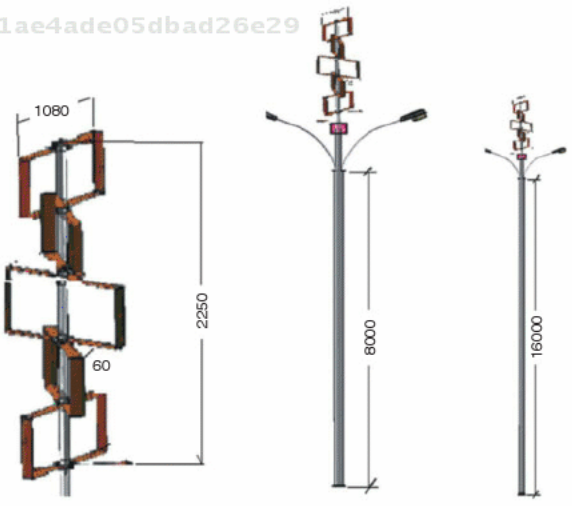

Figure 4.67 The balanced two-blades variant of a small power windmill (lanky).

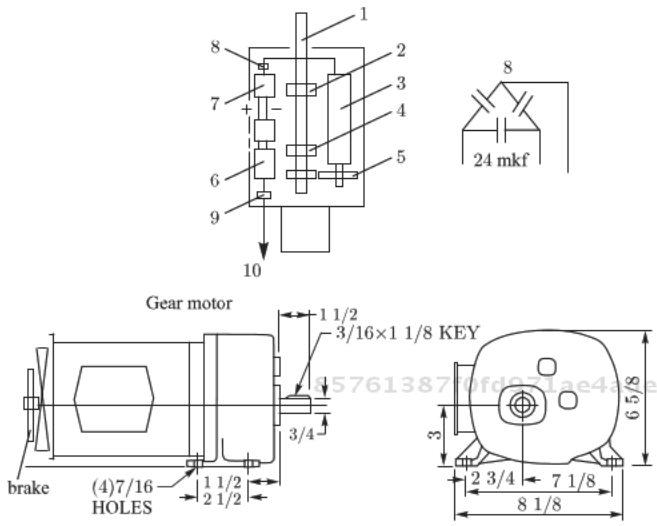

Figure 4.68 At 250 rpm, 250 -360 W, From the generator an exit via condensers on the controller and the battery with ballast loading. It is recommended to accept for a demonstration sample 250 rpm, circular frequency 26.4 1/with, acceleration of 38.3 g. Centrifugal loading of 29 kg. The asynchronous generator itself holds a rotor from dispersal at a strong wind. At an emergency shutdown of loading dispersal of the unit is prevented by a centrifugal brake 1-Shaft of windmill, 2″x 1/8″, steel, 2 – mounted ball bearing NTN 5 RYR3, 2″, 3 – 3 phase parallel shaft gear-motor, 155 rpm, 1/3 HP, 11:1, NTN 4Z388, + brake (www.suco-tech.com). *In Russia -5.8 kg (Electrostal), 1760 R and transfer 1:4 are completed with the ACORUS engine generator 63B6,1000 of rpm.*, 4 - – mounted ball bearing NTN 5RYR3, 1 15/16″, , 5 - changeable gear, 6 - battery 24 V (2 units of 12V, 100 Ah, 7-controller ADN20–24-3PM-C, , 8-capacitors, 9 – light control, 10- lamps.

trailer whirlwinds on a face-to-face site of the route where the vacuum on a sock of the blade is especially important. It was noticed that solidity $\sigma = ib/D = 0.3$ (i-number of blades, b-a chord of the blade, D – diameter of the route of blades), at two blades in one circle gives close to maximum efficiency, and not too much optimum rapidity. It was necessary to specify an arrangement traverses and a corner of a turn of the blade. The optimum angle of a turn is defined rather accurately and doesn't depend on the Reynolds's number. The tested model can be considered as a head sample of a fragment effective windmill. For such a sample it is instructive to provide the dimensional characteristics of an averaged torque moment received at different frequencies of rotation (Figure 4.69).

At frequencies of rotation of a rotor 100, 200, 300 and 400 rpm, which in each series were supported by almost constant, linear

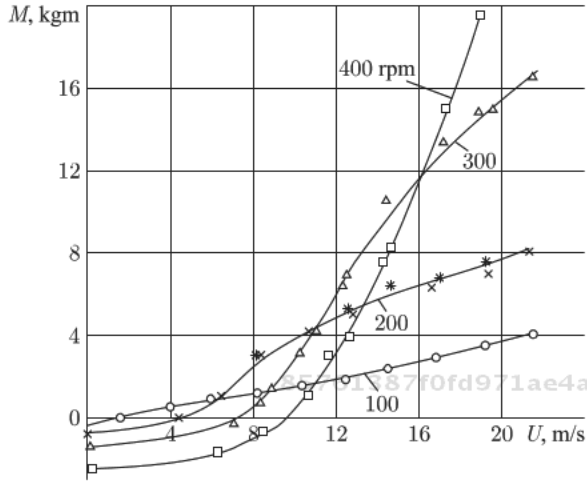

Figure 4.69 An averaged twisting moment on a shaft two-story two blades VAWT by height H = 2.4 m, diameter D = 2R = 1.82 m, with blades in length L = 1.2 m, profile NACA 0015, a chord b = 0.3 m (solidity 0.3), it is developed outside on $\varphi = 5°$. At a wind of 12 m/s the maximum capacity of 2 kW at 300 rpm.

speeds of blades made 10.5, 21, 31,5 and 42 m/s accordingly. At low air stream speeds, the turbine at first overcomes the moment of forces of resistance (a mechanical and aerodynamic friction) and only at great enough wind speed develops a positive twisting moment and is capable of giving out energy.

The efficiency of the turbine estimated on size of the power factor C_p in the formula, the turbine connecting capacity with the speed of a stream and the area of cross-section section of the turbine, has appeared depending on speed of blades. It can be interpreted as the influence of viscosity of the environment (influence of number of Reynolds Re=V b/ν, made on speed and a blade chord). With an increase in the speed of the blades, the role of losses decreases, and also, the efficiency of the turbine grows. The reduction of a steepness of curves observed on fig.4.69 at growth of speed of a stream is rather important. It is especially appreciable at speed of rotation of 200 rpm. In a zone of wind speed of 20 m/s (relative speed of blades nearby 1) the increase in the speed of a wind at a constant frequency of rotation doesn't cause an increase in a torque moment and capacity of the turbine. This circumstance is considered when choosing the established capacity of the generator of orthogonal turbines and defines the advantages of the asynchronous generators included in a powerful network. Such generators having a little changing frequency

of rotation, are kept by a network, and don't allow the turbine to increase capacity and to be dispersed at an increase in the speed of a stream above settlement values. Results of experiments are counted for the parameters of the turbine offered by us for the accepted nominal frequency of rotation of the turbine of 250 rpm (fig. 4.70).

This important experimental fact, of restriction of capacity at an increase in wind speed, but with a constant frequency of rotation, proves to be true also according to the calculations executed on the program of a method of discrete whirlwinds. In fig. 4.71 the capacity of windmill (VAWT), carried to the area of the cross-section of turbines with an identical solidity 0.3 is presented as the wind speed, at a constant speed of blades, V=13.08 m/s. Points 1, 2, and 3 correspond to the number of blades of the turbine with an identical chord of the blade 0.6m. It is accurately visible that, at a stream

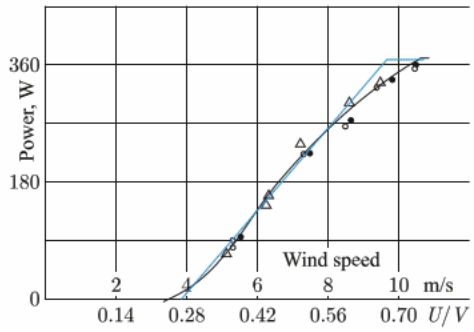

Figure 4.70 Capacity (power) of the windmill as a function of wind speed with a constant frequency rotation of 250rpm.

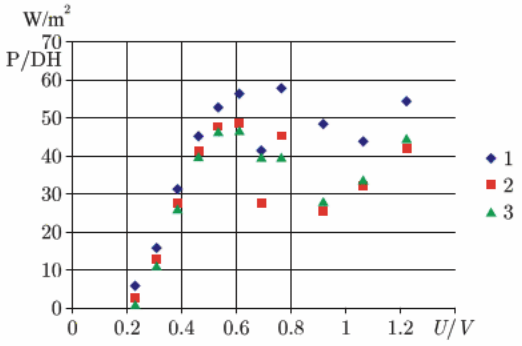

Figure 4.71 Capacity of VAWT with an identical solidity 0.3 and constant speed of blades V=13.08 m/s. Points 1, 2, 3 are correspond to number of blades of the turbine with an identical chord of the blade 0.6m.

speed of U, bigger 0.7–0.8 from the speed of blades V, the turbine P capacity with increase in the speed of a stream doesn't increase. A similar conclusion is reached, if the capacity of the turbine carries to the area of a surface of its blades (Figure 4.72)

Additional increase of efficiency of the offered turbine is reached by the use of easy blades with profile GAW-1 (fig. 4.73), having higher aero qualities than tested earlier and usually applied profiles NACA.

Traverses (arms) have a well streamlined profile (Figure 4.74).

The loadings operating on a rotor of the turbine, are presented on Figure 4.75.

The proposed solution will allow each individual economy to be provided with a reliable, inexpensive power source which hasn't been connected to an external supply of fuel. It will allow improved (mechanized) processing and provide for long storage of products.

The technical solution differs in novelty (Patent US 8007235 B1 for low powers and individuals-Figure 4.76, Patent US 7741729 B2 for average capacities and collectives- Figure 4.77), providing high power efficiency at a low material capacity, and high reliability.

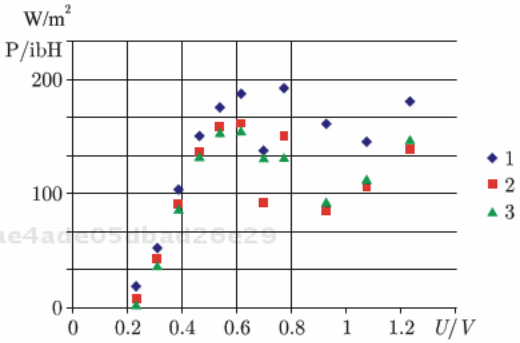

Figure 4.72 Capacity of VAWT, carried to the area of blades of turbines with an identical solidity 0.3. Speed of blades V=13.08 m/s. Points 1, 2, 3 are correspond to number of blades of the turbine with an identical chord of the blade 0.6m.

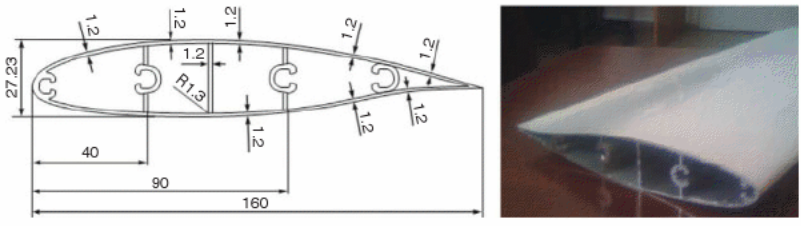

Figure 4.73 A profile and a general view of the blade of the turbine
The admissible bending moment 76 kgm. Mass of the blade of 0.45 m – 0.75 kg,

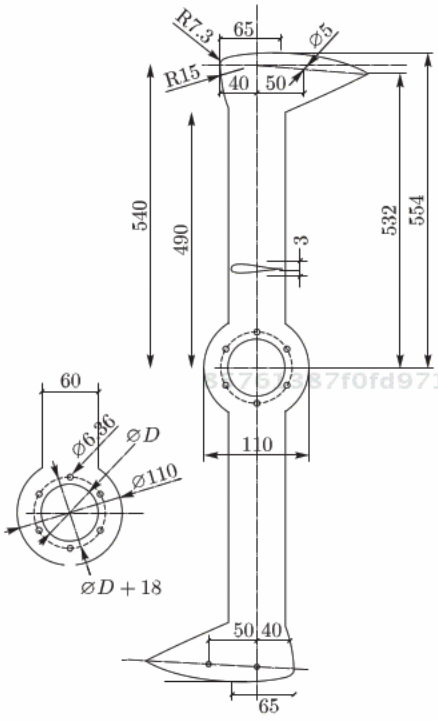

Figure 4.74 Arm of turbine.

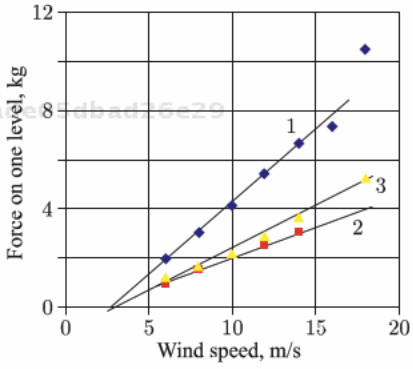

Figure 4.75 The forces operating on the turbine at a rotation frequency of 250 rpm, (1)–the maximum force transferred to an axis of rotation from one circle, (2) – the average longitudinal force transferred to an axis of rotation from one circle, (3) – the maximum force operating from a wind on one blade from an axis of rotation.

High power efficiency and reliability is reached by use of the balanced vibration-free unit with the vertical axis, the work of which doesn't depend on the wind direction, the perfect rotor construction, and power equipment.

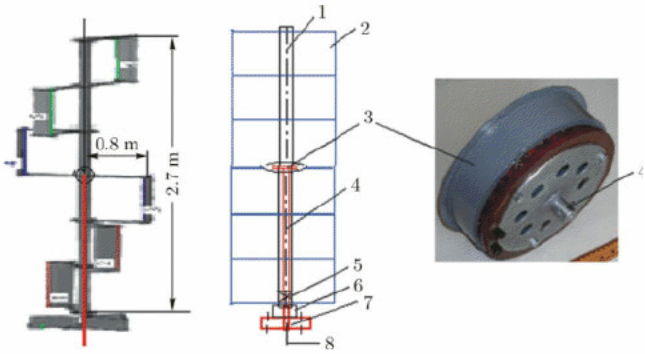

Figure 4.76 (1) – the top half shaft of the turbine, (2) – the top circle of the turbine, (3) - the generator with a flange for connection of half shafts of the turbine, (4) - a motionless hollow bearing axis of the generator with a cable conclusion, (5) – the radial-stop bearing, (6) – a centrifugal brake, (7) – a turbine support, (8) – a cable conclusion. 0.75 kW for wind 11 m/s, 600rpm.

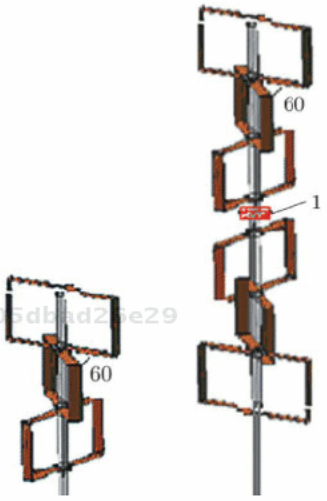

Figure 4.77 Options of configuration of a rotor with a rated power of 1.5 kW (on the left) or 3 kW (on the right) at a wind of 11 m/s. The generator (1) is in the midle part of a rotor.
Diameter of the rotor is 1.8 m, the circle height (blade length) is 0.9m, a chord of the blade of 0.16 m, a GAW-1 blade profile, a chord turn on 2° rather aerodynamic centers, traverses of a streamline shape with a section of 40×2 mm² (a point 2) or 80×5 mm² (points 1). At a wind of 11 m/s – the optimum frequency of rotation of 390 rpm (V/U=3.3), capacity for option at the left - isn't lower than 1.2 kW, efficiency isn't lower than 30% in the range of speed of a wind from 3 to 12 m/s at change of frequency of rotation in proportion to wind speed. At a wind more than 12 m/s the frequency of rotation is constant is limited – no more than 450 rpm.

The blades of the unit have the optimized profile and are made by the extrusion method, providing high quality at low cost. The minimum number of blades (one or two in each circle) with optimal solidity allows the reception of a rather high speed of rotation at a light breeze, and high efficiency of the electric generator without the gearbox.

The many-tiered design of a rotor with the generator in average part provides the unit with self-start at a light breeze, and a low pulsation of torque and aerodynamic forces.

The modern electronic controller in combination with a centrifugal brake, provides the optimum (limited) rotation speed of a rotor at any wind with the maximum delivery of energy on the battery of accumulators, with simultaneous protection of accumulators against a recharge.

At the request of the customer, installation can be understaffed with the inverter providing delivery of the demanded power over time, corresponding to battery capacity.

The performance of the unit with one blade in store is shown in Figures 4.78, 4.79

b=160mm,u=11m/s,	D1.6m	1bl	bt=0.04	d=0.002	20	GAW1

The regime points of a single-blade, 6-level rotor with a diameter of 1.6 m and the general height of 2.7m with the generator of 900 Watts of the GudCraft Co. are shown in Figure 4.80 . For a wind of 11 m/s the frequency of rotation is 610 rpm, the torque of 11.5 Nm, the power is 730 Watts. At a wind of 5.5 m/s the frequency of rotation is 380 rpm, the torque of 1.6 Nm, and the power is 11 Watts. Use of other generators with more cool moment characteristics

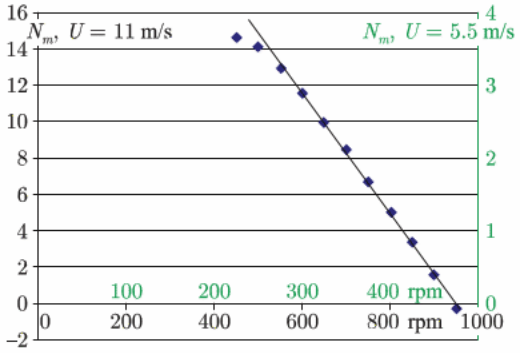

Figure 4.78 Torque Mom (total) Nm vs rpm

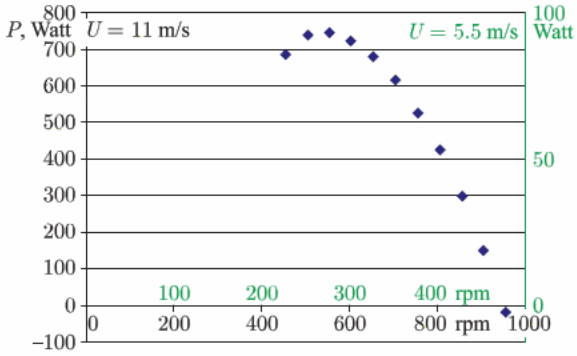

Figure 4.79 The total capacity for wind speed 11 and 5.5 m/s.

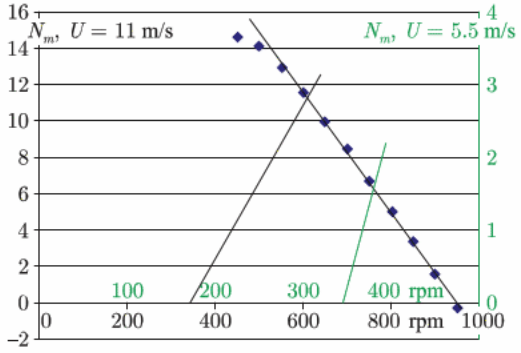

Figure 4.80 Regime points of a single-blade, 6-level rotor with a diameter of 1.6 m and the general height 2.7m with the generator of 900 Watts of the GudCraft Company. At a wind of 11 m/s the frequency of rotation is 610 rpm, the torque of 11.5 Nm, the power is 730 Watts. At a wind of 5.5 m/s the frequency of rotation is 380 rpm, the torque of 1.6 Nm, and power is 11 Watts.

and a smaller initial frequency of rotation (for example, the JSC Vertikal generator) would allow reception at a wind of 11 m/s, the power of 750 Watts, and at a wind of 5.5 m/s – about 90 Watts. Influence of the generator is essential, especially in a zone of light breezes.

The capacity of the three-level turbine (fig.77) with a diameter of 1.8 m and with a general height of 2.7 m with two blades in each circle, developed on 2° at optimum regulation, is given by a formula $P = 1.13(U/11)^3$, kW $n = 390(U/11)$, rpm $U < 12$ m/s

At a wind speed of $U > 12$ m/s, by means of a mechanical brake, the rotation frequency is kept constant at n=450 rpm, and the capacity changes not monotonously ranging from 1.5 to 3 kW

(Figure 4.81). Circles of the turbine are developed from each other on 600. Loads of circles of the turbine are presented in Figure 4.81–4.83. At a wind bigger than 26 m/s, the turbine stops.

At a wind of 26 m/s, the unit stops on a mechanical brake. In on right option (Figure 4.77) the system is completely balanced and only the constant pererezyvayushchy force, the unit and pulsation weight caused by wind turbulence is transferred to a support. At a wind of 12 m/s and frequency of rotation of 425 rpm, the pererezyvayushchy force and a torque in the basis of a rotor are almost constant, the bending moment periodically changes with a frequency of 850 rpm (Figure 4.84).

Storms in these conditions aren't dangerous to a wind-driven generator. Practically without development loss, the diameter of a rotor can be reduced to 1.6 m with an increase of the nominal

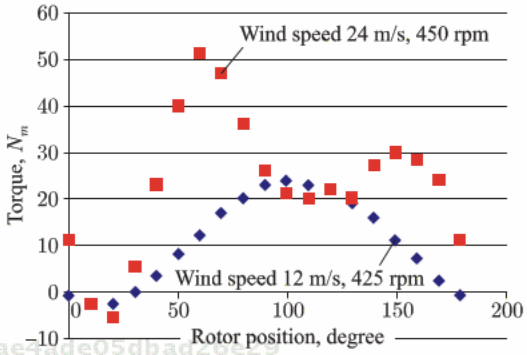

Figure 4.81 Torque on an axis of one circle of a two-bladed rotor.

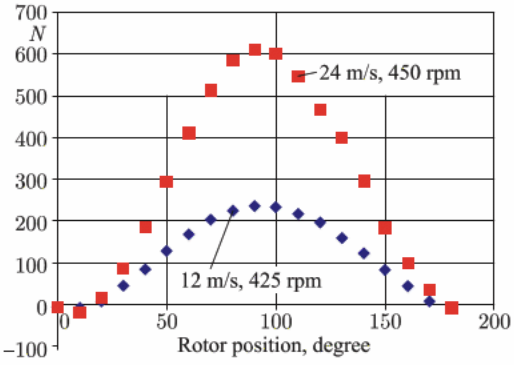

Figure 4.82 Longitudinal force is at one circle.

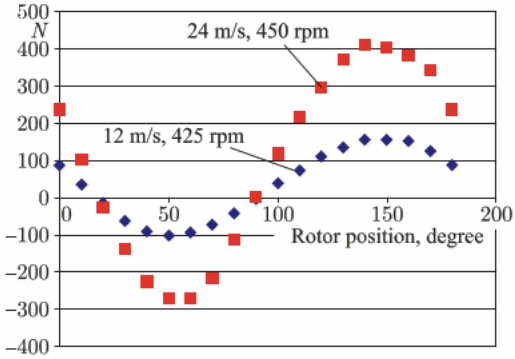

Figure 4.83 Cross force is at one circle of a two-bladed rotor.

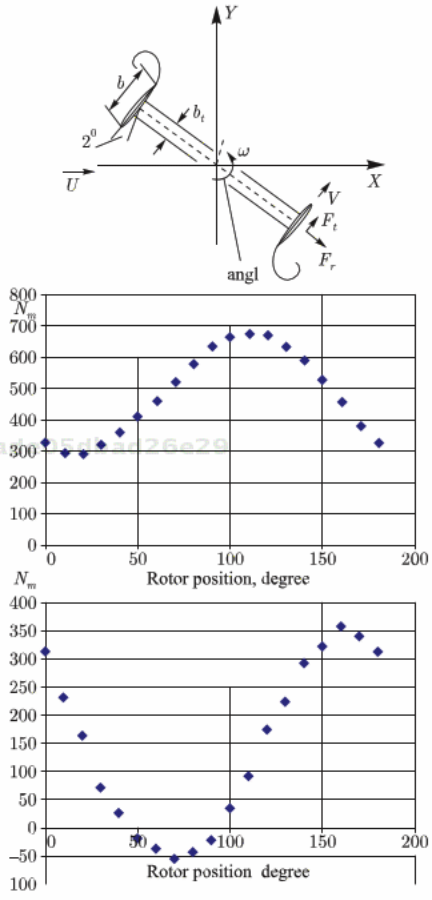

Figure 4.84 The bending moment (Nm) in the rotor basis from longitudinal (at the left) and cross forces.U=12m/s, 425rpm.

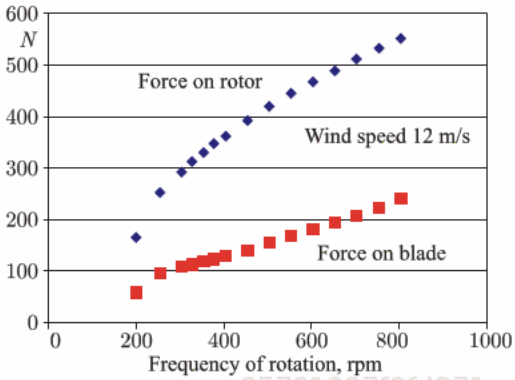

Figure 4.85 Force on a rotor (average for a turn) and on the blade (maximum). 2 blades, Wind of 12 m/s.

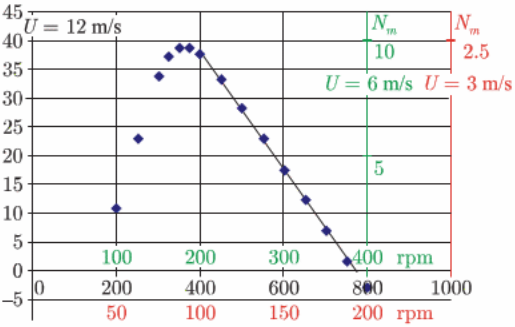

Figure 4.86 Total torque moment (Nm).

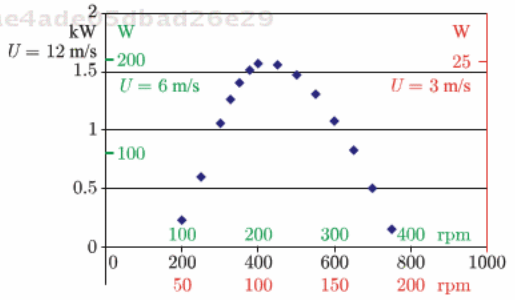

Figure 4.87 Capacity of a two-bladed three-level rotor.

frequency of rotation to 425 rpm at a wind of 11 m/s. The maximum capacity of a rotor in such a configuration at optimum regulation, is given by a formula

$$P = 1.1\,(U/11)^3\,,\ n = 425\,(U/11),\ U < 12\ \text{m/s},\ n < 475\ \text{rpm}$$

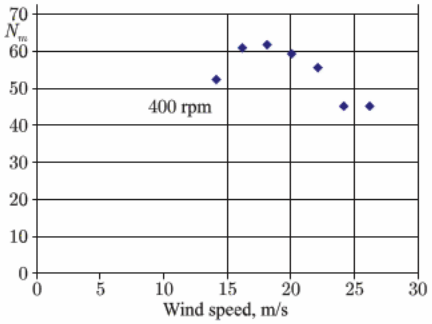

Figure 4.88 The torque operating on a rotor. 400 rpm.

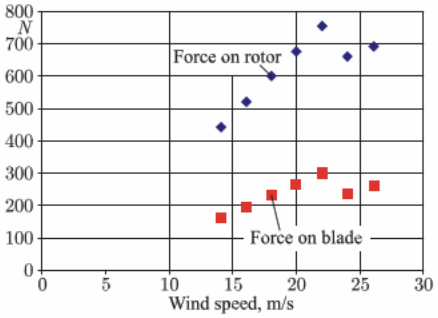

Figure 4.89 Load of a rotor of 1 (N), max. load of the blade of 2 (N) of L=0.9m, 2 bl, 400 rpm, D1.8, b=0.16, 2 grad.

The conditions of regulation and the maximum loadings at hurricanes are almost the same as with a rotor diameter of 1.8m. The advantage of the reduced diameter is in a more effective (more high-speed) generator and a more reliable (more high-speed) centrifugal brake.

If using the generator with the 900 Watts constant magnets, offered by the GudCraft company (www.gudcraftonline.com), at a wind of 12 m/s our car will give out about 900 watts with a frequency of rotation of 650 rpm, and at a wind of 6 m/s – about 40 Watts with a frequency of rotation of 370 rpm (Figure 4.80). The moment characteristic of this generator looks like

M= 0.04324(n-345) , n>345rpm. M=0, n<345rpm

On the contrary, at the bending-around moment characteristic of the generator of JSC Vertikal (Russian Federation) the maximum possible capacity of a rotor on a formula

M=0.889(n-75) , n>75rpm. M=0, n<75rpm

can be received at any wind by the corresponding selection of electric loading. Overview of designs of modern ordinary vertical-axis wind turbines (VAWT), traditional methods of their calculation and the results of the tests are reflected in the well-known books and articles by Ion Paraschivoiu (Canada).

References

1. Details - on a site http://www.quietrevolution.co.uk.
2. V.M.Lyatkher. Windmills of new generation. Energy. Economy. Equipment. Ecology. M.2009, No. 8, p. 30–33, No. 9, p. 7–14.
3. E.Solomin, Metodologiya of development and creations of vertically axial wind power installations: monographs Chelyabinsk: Publishing house UralGU. – ISBN:978-5-696-04199-5. – 2011 . – 256p. Basis of creation of wind power installations: – Saarbrucken (Germany): LAP LAMBERT Academic Publishing GmbH & Co publishing house. – ISBN: 978-3-8473-3504-7. – 2012. – 268p.
4. T.D.Ashwill, Measured Data for the Sandia 34-m Vertical Axis Wind Turbine, SAND91–2228, 119p.
5. P.G.Baklushin, K.P.Vashkevich and V.V.Samsonov. Works of Hydroproject, issue 129, M, 1988, p. 98–105.
6. Lyatkher V. M., Ivanov I.I. Skosareva S. M. Hydrotechnical Construction, 1986, No. 11, page 33–38.
7. A.Gorlov, Turbines with a Twist, in book Macro-Engineering and the Earth, World Projects for the Year 2000 and Beyond, pp.1–36.
8. V.M.Lyatkher, Tests of head samples orthogonal windmills. Hydrotechnical Construction, 2002, No. 3, p. 31–39.
9. Tests were carried out by P.G.Baklushin, K.P.Vashkevich and V.V.Samsonov. Results are published on Saturday. Works Gidroproyekta, issue 129, M, 1988, p. 98–105. Industrial aerodynamics, issue 3 (35), M.Mashinostroyeniye, 1988, p. 159–170 and 171–182. Journal of Wind Engineering and Industrial Aerodynamics. Vol.39, N°1–3, May 1992.
10. I.I.Ivanov, N.A.Malyshev, etc. Copyright Certificate USSR No. 1242637, 1986.
11. Ivanov I.I. Ivanov G. A. Perfilov O. L. Model researches of rotor driving wheels of wind power stations, Works of Hydroproject, issue 129, M.1988, p. 106–113.
12. V.Lyatkher, Copyright Certificate (CC) USSR 1325186, March 05.1985.
13. L.Prandtl, Hydroaeromechanics, IIL, M, 1951, p. 319.
14. V.M.Lyatkher and V.L.Smirnov, CC. USSR 1765495, October 03.1989.
15. G.M.Angle II, F.A.Pertl, Mary Ann Clarke, J.E.Smith, Lift Augmentation for Vertical Axis Wind Turbines, International Journal of Engineering,

vol.4, Issue5, pp.430–442, D.McGrain, G.M.Angle II ,J.P.Wilhelm, Circulation Control Applied to Wind Turbines, ASME 2009, 3rd International Conference on Energy Sustainability, Volume 2, Paper no. ES2009–90076 pp. 905–910.

16. V.M.Lyatkher, M.Sh.Misrikhanov, V.S.Fadeev, CC. USSR 1657721, June16.1989.
17. V.Lyatkher. Non-Vibrating Units for Conversion of Fluid Stream Energy, Patent US 7741729 B2, Jun.22, 2010.
18. S. Mertens, Gijs van Kuik, Gerard van Bussel .Performance of an H-Darrieus in the Skewed Flow on a Roof. Journal of Solar Energy Engineering ASME, NOVEMBER 2003, Vol. 125 , 433–440 p.
19. V.M.Lyatkher. Wind power installation with a vertical axis of rotation, Patent RF 2240443, May 05.2003.
20. V.M.Lyatkher, S.A.Sirotin, V.L.Smirnov, CC USSR 1682620, June 12. 1989.
21. B.L.Istorik, V.M.Lyatkher . CC USSR 1164457, November 16.1983.
22. V.M.Lyatkher, O.P.Bortsov, D.N.Militeev CC USSR 1201549, June 25. 1984.
23. V.M.Lyatkher, CC USSR1694979, July 13.1989.
24. V.M.Lyatkher CC. USSR 1437566, August 07.1986.
25. V.M.Lyatkher, CC. USSR 1645602, May 26.1989.
26. V.M.Lyatkher and V.L.Smirnov, CC USSR 1645600, May 26.1989.
27. V.M.Lyatkher, Patent RF 2079702, May 04.1995.
28. V.M.Lyatkher, CC USSR 1281737, March 28.1985.
29. P. Hlopenkov, CC USSR 1307081, 1986.
30. V.M.Lyatkher, Tests of head samples orthogonal windmills, Hydrotechnical Construction, 2002, No. 3, p. 31–39.
31. V.M.Lyatkher, Environmentally friendly transformation of energy of atmospheric, river and oceanic currents, Hydrotechnical Construction, 1989, No. 8, p. 10–18.
32. V.M.Lyatkher, Technical and economic bases of the accelerated development of windpower, M, 1990, 67 pages.

5

The Largest Open Wind Turbines on the Ground or Sea

The idea of offered wind turbines of big power consists in using the effect of turbulent vertical hashing of the streams providing restoration of energy of a stream on the way to a back system of blades (Figure 5.1) [1]. Certainly, and in this case strict equality of the speeds of a stream on all route of blades and outside the unit in the presence of a selection of wind power is impossible. However, considering that the local potential capacity of a stream is proportional to the third degree of its speed, even small increase in local speed of a current at the expense of turbulent transfer of energy from the layers of a stream which aren't passing through cross section of the turbine, can give noticeable effect.

Then working blades of an aerodynamic profile in these installations settle down vertically (or obliquely) and move on the ring route of big diameter. The first option of such a car was carried out with the use of helicopter blades and asynchronous generators located on the axes of the wheels on which sits the ring bearing the blades (Figure 5.2).

For compensation of torque and cross forces of the turbine they can be placed one over another with the counter direction of movement (Figure 5.3).

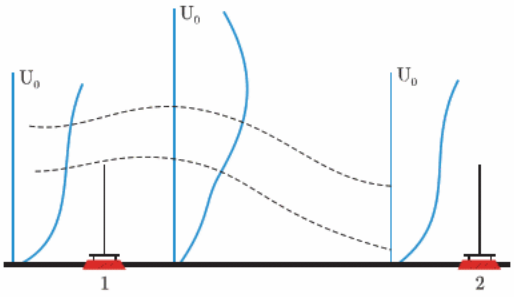

Figure 5.1 The vertical turbulence mixing go up the power of wind before the rear order of blades.

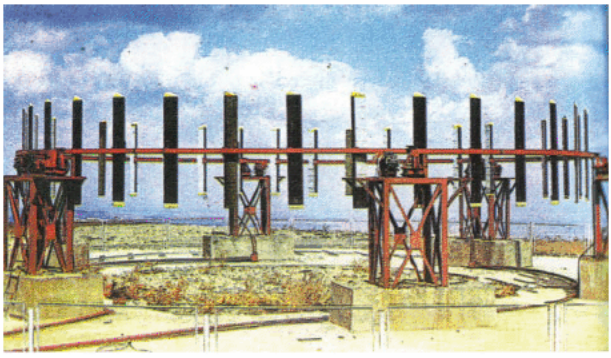

Figure 5.2 The first operating life-size model of a multi-blade wind turbine of 20 m diameter with an output of 150 kW with wheel gearboxes and the usual generators (without special suspending and linear generator). 1987.

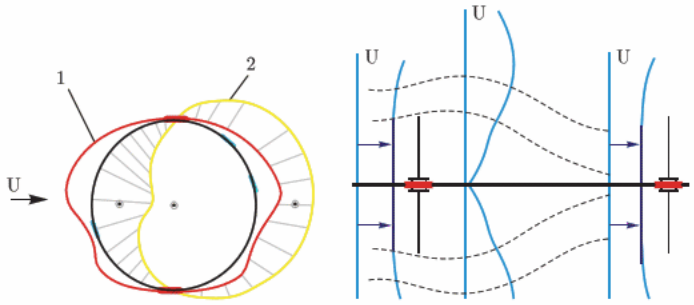

Figure 5.3 Distribution of loadings on the route of the blades and the scheme of restoration of a stream in front of a back system of blades at the expense of a vertical turbulent exchange. 1 – the pulling force, 2 – normal pressure. V = 3U.

In this case, the presence of a smooth surface of earth (Figure 5.4) or a water surface (Figure 5.5) can carry out the positive function of concentrating a wind.

The quantitative effect of restoring energy behind a frontal system of blades for real conditions of a three-dimensional non-stationary task, was estimated on the example of a numerical model of the turbine reproducing the main features of the two-level, multi-blade unit with oncoming traffic of circles of the turbine (Figure 5.6)

For calculations the simple model developing known ideas of "discrete whirlwinds" (professor S.M.Belotserkovsky) was used. This model doesn't contain empirical coefficients and approved on a big material of classical experiments. Calculations are carried out for the same speed of a wind of 10 m/s and the speed of blades of 20 m/s. Loading (radial force), operating on one of 6 blades decided on a chord of 160 mm. The turbine (top) rotates counterclockwise, the bottom – clockwise. In Figure 5.7 – 9, the results of the calculations of the unit with a diameter of 2.4 m for three options of the length of blades – 0.3 m, 0.6 m and 0.9 m are presented. The beginning of coordinates answers the moment when the blade moves towards a wind. Apparently, while the blade is at the front loading negative (force is directed to the center) and the maximum effort to the short blade (0.3 m) is 3 times less than on the longest blade (0.9 m) and points of maxima don't coincide. The maximum loads of blades of 0.6 m and 0.9 m are observed almost in one place and

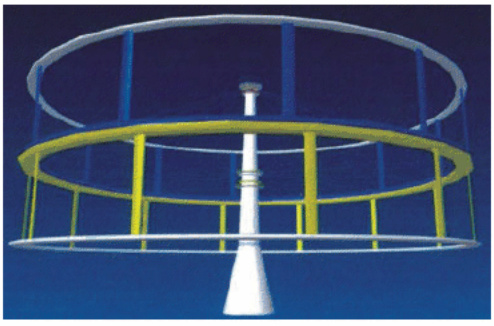

Figure 5.4 The idea of the unit consists in using of the effect of mutual compensation of torques and transverse forces acting on the blades, which move in opposite directions; the effect of the increase of efficiency of the electric generator at a doubling of the speed of crossing the magnetic fields of the inductor and armature of the induction generator.

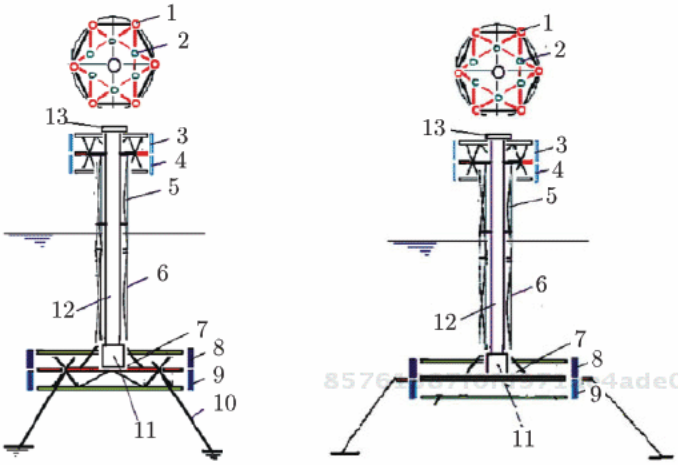

Figure 5.5 High power multiblade wind power unit with a counter rotor linear (arc) generator between the rings (top) . Large multiblade wind turbine on the large hydro unit (down)") Tidal and wind power Complex. Options of a design of the hydrounit with the superfluous buoyancy, being the basis for a counterbalanced orthogonal wind turbine. (1)-Knots of an arrangement of inductors of the generator and basic and running systems of the wind turbine, (2) – knots of fastening of a basic tower to a motionless rigid board of the wind turbine, (3 and 4) – blades of the top and bottom circles of the wind turbine, moving in opposite directions, (5) – the tubular support (farm) bearing of wind turbine, (6) – the through farm calculated on the action of waves and ice, (7) – the rigid board of the hydrounit having superfluous buoyancy, (8 and 9) - blades of the top and bottom circles of the hydrounit moving in opposite directions, (10) – trosses of fastening of the system to a bottom or anchors, (11) – the viewing chamber with transparent walls, (12) – lift mine, (13) – an observation deck with a platform for reception of helicopters.

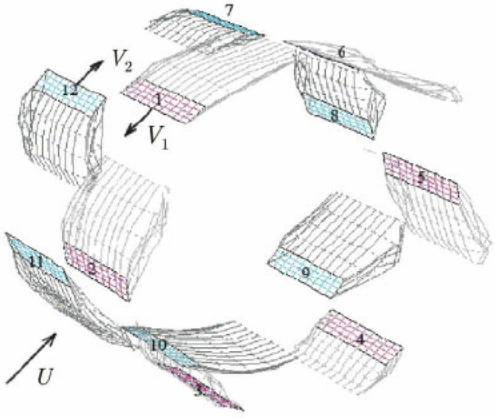

Figure 5.6 Scheme of spatial calculation of turbines of counter rotation.

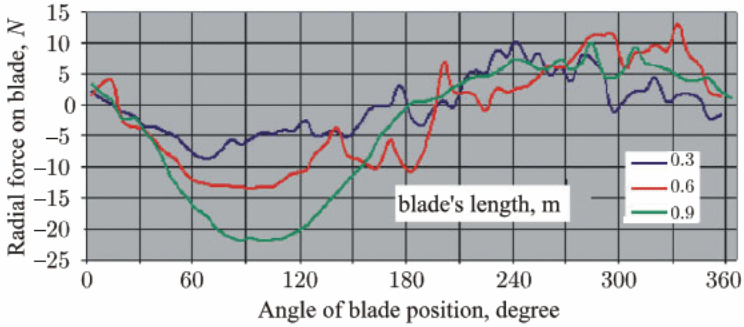

Figure 5.7 Load of one blade of the 6-lopastny two-story car at a speed of 10 m/s and the speed of blades of 20 m/s. Diameter of the route is 2.4 m, a chord of 0.16 m.

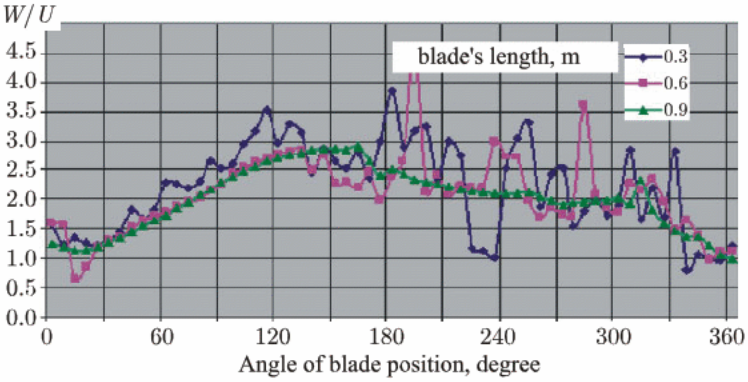

Figure 5.8 The module of speed of a stream in points of the route of blades at a distance of one chord before a blade sock. Speed is measured in shares of speed of a stream in front of the turbine.

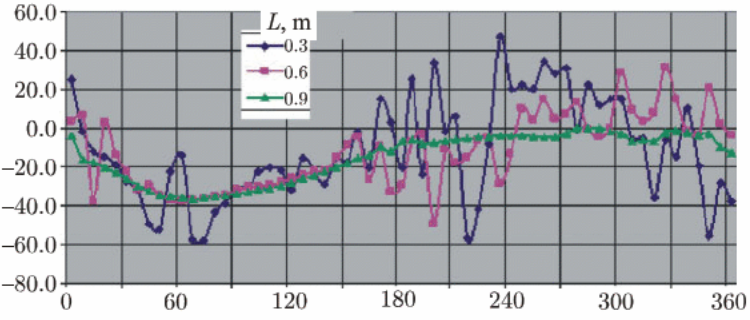

Figure 5.9 Local angle of attack in front of the blade at a distance of one chord

differ approximately at 1.6–1.7 times, that approximately corresponds to a ratio of the lengths of blades.

An interesting occurance is observed on a back site of the course of the blade. Loading on the back part of the route, naturally, is

directed from the rotation center (positive), it pulses (the whirlwinds running from the blades at the front) affect, but, the most important, - in a zone of the first maximum (240–2750) load of the short blade almost same, as well as on long. Stream speeds on the back part of the route of blades at short blades are much higher, than at long blades [?](Figure 5.8). The maximum load of the blade towards a rotation axis in this case doesn't exceed 23H, and from an axis of rotation 13H. The total longitudinal loading operating on one turbine with 6 blades 900 mm high and a chord 160m, doesn't exceed 120H. It is obvious that energy restoration before a back system of blades happens rather actively and offered multi-blade units of big diameter will have the highest power rates!

The proposed wind power unit includes two ring rotors one above another in the form of regular polygons, on which the blades of the aerodynamic profile are vertically fixed, oriented in opposite directions. There are the preliminary projects of the units for the low and high wind areas with 1,000 (Figure 5.10) and 10,000 kW per unit. The diameters of the rotors are 80 and 160 m, the lengths of the blades are 16 and 25m, the numerals of the blades in one ring are 12 or 6 in accordance with the blade's chord 2 (3) or 4 (6) m. The design wind speeds are 12 and 16 m/s.

The ends of the blades are sealed into a light durable rim with the well-streamlined shape of the cross section. The upper ring rotor, which carries the inductors of the linear generator, is connected

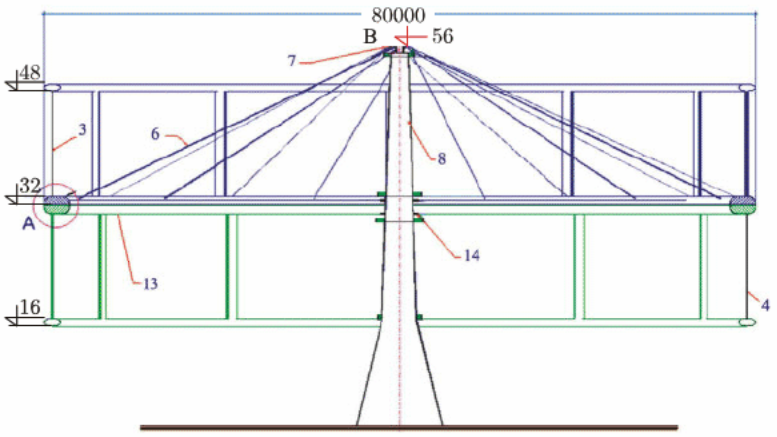

Figure 5.10 Cross section of wind turbine for the area with small or middle wind. U_d= 13m/s, P = 1000 kW.

by the stretchings with radial thrust bearing, located at the top of central pylon.

The lower ring rotor, carrying a strip from electrically conducting materials and a steel core, is suspended from the upper ring rotor by the wheels with the aid of the electromagnets of the vertical action, which ensure the fixed clearance between the inductors of the linear (arc) generator and the strip, fulfilling the functions of the short-circuited rotor. This clearance is controlled by special sensors and limiting wheels (fig.11). Similar systems are working in the Trans Rapid or Maglev railways in many countries.

The lower ring rotor is stressed under the action of horizontal stretchings, connecting it with the radial bearing, fixed on the central pylon. The upper ring rotor is also stressed by subhorizontal ropes, which go to the radial thrust bearing, located a little bit higher than radial bearing. Inclined ropes go from each angle of the upper rotor polygon, horizontal and subhorizontal ropes go only from those corners, in which the blades are fixed.

Concrete design studies are made for wind power units with a capacity of 1,000/2000 and 10,000 kW, although principally similar type units can have a larger capacity.

Power units with the capacity, for example, of 10,000 kW work as follows. At the wind speed of approximately 5 m/s, the signal of the wind speed sensor initiates the turning on of the electromagnets

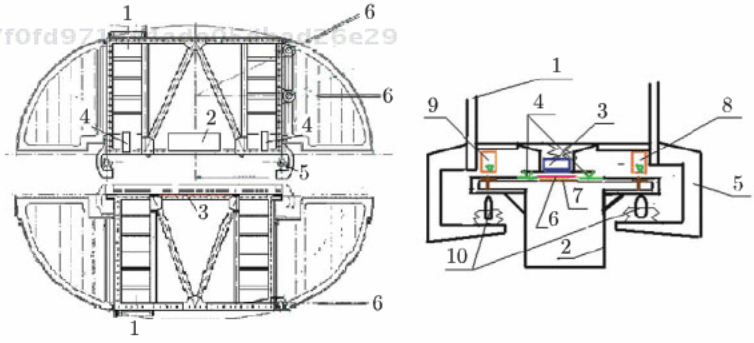

Figure 5.11 Cross section of the rings (left).(1)- vertical blades, (2)- inductor of linear generator, (3) – core of linear generator, forming a part of the construction of the lower ring rotor; (4) - electromagnets of vertical action, (5) – polyamide wheel, which fixes the clearance between the inductor and the armature (current-conducting plate), (6) - cable stretchings connecting the ring rotor with thrust bearing located at the central pylon.
Details of support (right).

of the system of suspension, and disconnection of the parking brake. Under the action of the wind the blades of the upper and lower tiers of the wind power unit begin to move in opposite directions and are brought up to the speed of approximately 14 m/s. At the signal of the sensor of revolutions, the first six symmetrically located inductors of the first group of inductors are turned on. With an increase of power over 700 kW at the signal of the sensor of power. the remaining 6 inductors, which work at the voltage of 0.8 kV in the network through the step-up transformer 0.8/10 kV with capacity of 1.5 kVA, are turned on. With an increase of power over 1,400 kW at the signal of the sensor of power, the inductors with a voltage of 0.8 kV are turned off, and the group of the inductors with high voltage and with the total nominal capacity of 4000 kW are connected directly to the local network with high voltage. With an increase of power over 4,000 kW at the signal of the sensor of power, the following group of inductors is connected and so further to the total power of 12,000 kW. With the reduction of power, the turning off of the groups of the inductors is produced in the reverse order. At a power greater than 12,000 kW, corresponding to the speed of the rotor's motion of 4854 m/s (relative speed of the inductors and the short-circuited rotor of the generator is 96 m/s), at the signal of the sensor of the blade's speed some inductors are transferred into the state of electrodynamic braking, and in the case of the breakdown of the electrical network are included the shields of aerodynamic braking and, if necessary, the emergency brake with the drive from the standby battery. The necessary reactive compensators are installed near the inductors, inside the upper ring. Storage batteries together with the switches and the transformer are located in the base of the pylon. The torque developed by the blades on the upper and lower rings of the wind power unit must be identical. Practically, this is achieved by the fact that the absolute speed of the upper ring increases and of the lower ring decreases (maintaining the relative speed of the rings) with the corresponding decrease of torque on the upper ring and an increase of the torque on the lower ring until their alignment. This property always takes place at the steady portion of the torque characteristic of the wind power unit. The power unit continues to work with the nominal capacity up to the wind speed of 30 m/s. It stops with the stronger winds. The calculated storm wind is 70 m/s. In spite of its significant overall dimensions, the wind power unit is simple in the installation and does not require special hoisting equipment. The

rings include 24 straight elements (Figures 5.12, 5.13), connected with the pilon by the bearings (Figure 5.14). The upper rotor is supplied with L-shaped cantilevers (Figure 5.15), carrying brake linings, on which the brake shelf of the lower rotor lies down when the electromagnets of the suspension are turned off. The upper and lower rotors and also the sections of stretchings adjacent to them are protected by the fairings of the aerodynamic profile, the upper fairing having the vertical descent in the nose section, which overlaps the horizontal slot between the fairings.

The upper ring of the rotor is supplied with aerodynamic brakes flaps (they are not shown in the figure), which are opened when the speed of the rotor's motion exceeds the design values or at the

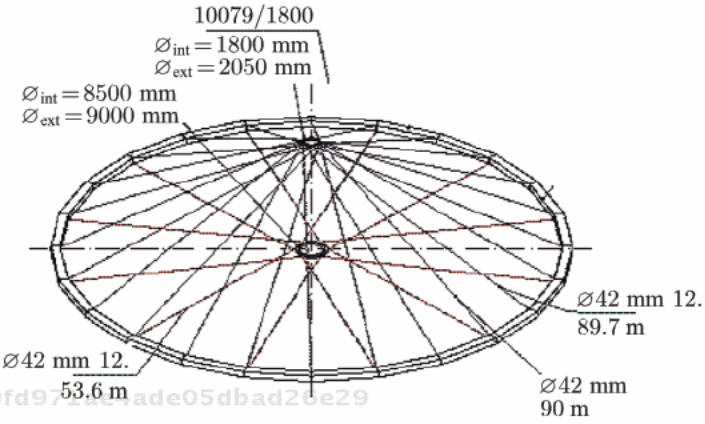

Figure 5.12 Upper ring.

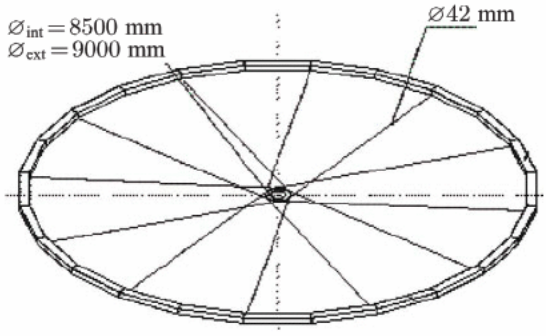

Figure 5.13 Lower ring.

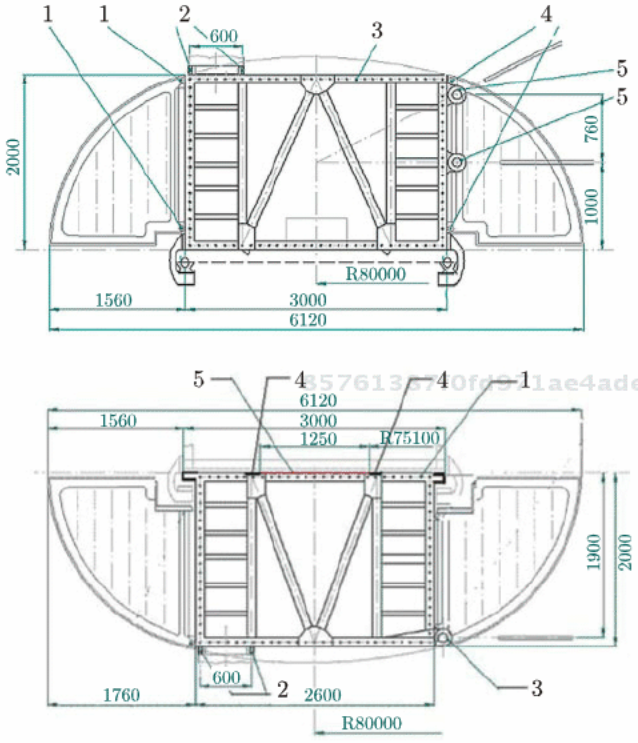

Figure 5.14 Cross section of rings.

signal of the control system, which controls the wind power unit's functioning. The mechanical parking brake, which fixes the position of the rotors of the idle wind power unit and also fulfills the functions of emergency braking, is located at the central pylon in the zone of radial thrust bearing.

The counter rotation of the rotors releases the central pylon from the torque developed by the blades, and ensures the mutual compensation of transverse forces, acting on the rotors; that reduces the summary load on the central pylon, decreases the specific consumption of materials and increases the reliability of the wind power unit. Many blades in the rotors decrease the total torque moment and force pulsations. With 6 blades in the ring, the power pulsation amplitude in the nominal regime is about 10%. With 12 blades in the ring, power pulsation is negligible.

The frames of the units were designed to determine the deformation, vibration, and stability (Figure 5.16).

The power production of such units can be noticeably increased due to the jet control of the boundary layer on the blades. The

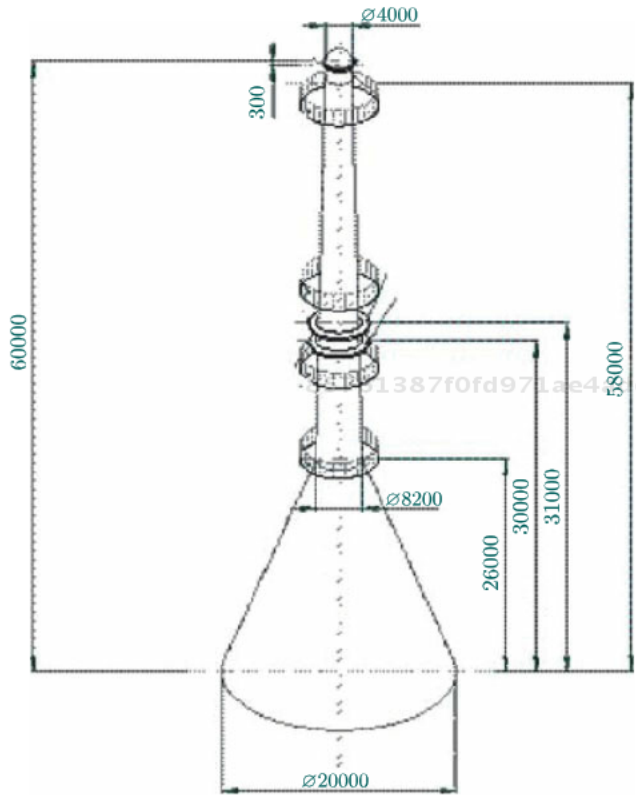

Figure 5.15 Pilon.

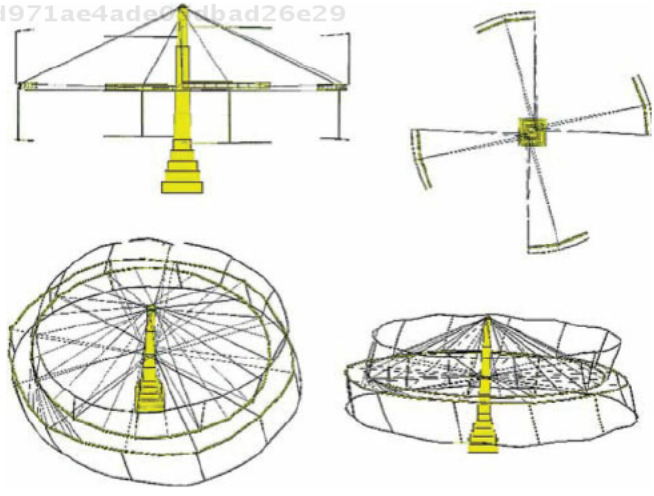

Figure 5.16 Design results of a wind turbine of 10 MW. Maximum displacements of rings – radial 180 mm, vertical 252mm, the sags of rings 1.9–7.3 mm, of pilon 270 mm.

central supporting pylon of such wind power units can be fixed on the underwater pontoon, having excess buoyancy (Figure 5.17).

With the aid of the ropes and the system of piles, this pontoon is fixed in the space, and the entire system is capable of withstanding hurricane winds and gale waves.

Similar power units can be used for converting the energy of sea currents, in particular, tidal streams. The construction of hydro power units is even somewhat simpler and the effectiveness is higher due to the possibility of using the buoyancy of separate assemblies and the smaller difference in the calculated and the "storm" speeds of flows.

The aerodynamic characteristic of a wind power unit rotor is obtained as a result of calculations and model tests of one half of the unit (upper or lower) in the hydraulic head channel with a cross-section of 6×2.5 m^2 at a flow water speed of up to 2.2 m/s. The diameter of the blades route of the model was 2.7, 3.34 and 3.98 m; the length of the blades was 0.72 m or 0.485 m at the chord of 0.12 m and GAW-1 profile. The quantity of blades varied from 3 to 12. The inductors of the linear generator were reproduced on the model. The diameter of the ring with the short-circuited rotor was accepted as 2333 mm, the diameter of the blades route was larger due to the traverses rigidly fixed on the rotor ring. The blades were located cantilevered[or cantilevering?] (Figure 5.18). In the proposed optimized construction, the blade tips are united by a ring

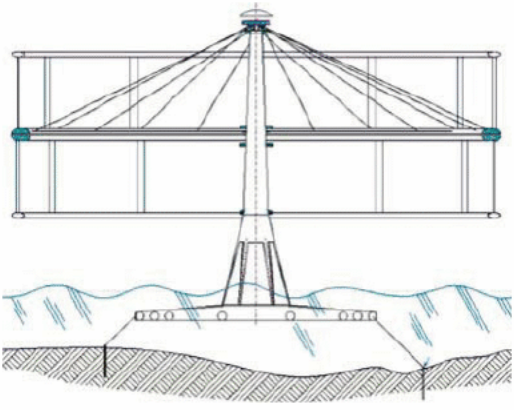

Figure 5.17 Wind power unit on the water. The wind turbines are completed in the dry dock and floated to the power plant area.

Figure 5.18 Model of a multiblade rotor in a hydraulic channel.

that must decrease tip eddy losses and increase the effectiveness of wind power unit.

The experiments measured the velocity distribution along the walls of the channel and in the axial cross sections, before and behind the model. The velocity along the walls changed not more 2%. The water flowing around the turbine in the model with a diameter of 2.7 m and in the prototype are considerably accelerated; the same and test results were not invalid. The good efficiency of the turbine explained by the transverse turbulent power, transitions to the back row of blades.

The efficiency of the turbine in the prototype will change for different conditions of atmospheric turbulence and stratified degree. This problem must be researched in the future.

For accepted overall sizes, the power of the wind power unit rotor depending on the wind speed of U_0 before the wind turbine, is determined from the formula

$$P = C_p \rho U_0^3 D H/2 \qquad (5.1)$$

The power factor (efficiency) C_P depending on the wind speed and the blades speed varies within a wide range – from a maximum of 0.55 to zero (fig.19). Efficiency of the best modern traditional wind turbines (HAWT) is not more 0.38 only. Therefore, the formula (1) can be conveniently used only for evaluation of maximum values of power, which can be taken off from the proposed

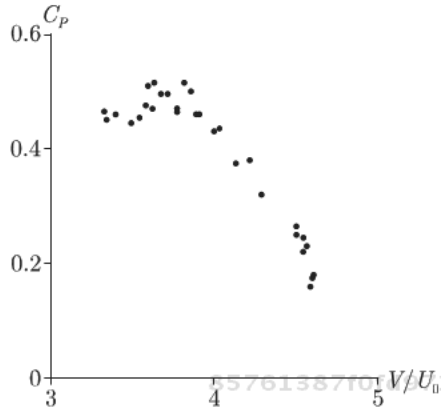

Figure 5.19 Efficiency of a multiblade wind power unit rotor according to the data of tests in a water tunnel. The diameter of rotor is 3.34 m in the channel with a width of 6 m. The blades height is 0.72 m, the chord is 0.12 m, and solidity is 0.22.

wind power unit at the optimum speed of the blade's motion V, which changes depending on the wind speed.

The experiments showed that even in the tested, not optimized scheme with 6 blades (solidity is 0.22–0.26) the efficiency of the rotor can exceed $C_p = 0.4 \div 0.5$ at blades speed exceeding wind speed by a factor of 2.9÷3.2 (Figure 5.19).

For the practical calculations, it is more convenient to represent the power of the rotor in another form

$$P = C_N \rho V^3 \text{ i } bH/2 \qquad (5.2)$$

Within the wide range of influencing variables, the coefficient C_N for orthogonal turbines is the linear function of the relative flow speed (fig.20) and two parameters:

$$C_N = B\,(U_0/V - B_0) \quad \text{when } B_0 < U_0 / V < 1 \qquad (5.3)$$

At the graph of Figure 5.19, the parameter B_0 is the coordinate of the intersection of experimental straight lines with the X-axis; the parameter B is the slope ratio of these straight lines.

At the fixed wind speed, the parameter U_0/B_0 characterizes the maximum speed of the blades rotation, up to which the rotor can speed up without the external braking moment

$$V_{max} = U_0/B_0 \qquad (5.4)$$

$$V_{opt} = 2/3\, V_{max} \qquad (5.5)$$

The value of power efficiency C_P can be represented in the following form

$$C_P = C_N \sigma (V/U_0)^3 = B \sigma (V/U_0)^3 (U_0/V - B_0) \qquad (5.6)$$

And maximum efficiency will be

$$C_{P\,max} = 4 B \sigma / 27 B_0^2 \qquad (5.7)$$

The value of the speed of the turbine blades V_{opt}, which correspond to its maximum power, amounts to 2/3 of the accelerating blade's speed (4)

		1	2	3
$U_0 = 2.1$- 2.3 m/s				
	B	0.58	0.61	0.88
	B_0	0.228	0.208	0.201
	C_{Pmax}	**0.43**	**0.46**	**0.58**
	V/U_{optim}	**2.9**	3.2	3.3
$U_0 = 1.8$–1.9 m/s				
	B	0.53	0.62	0.58
	B_0	0.245	0.24	0.211
	C_{Pmax}	0.34	0.35	0.35
	V/U_{optim}	**2.7**	2.8	3.2

The wind-power unit is supplied with the system of automatic control and monitoring, which includes the transducers of wind speed, rotor rotation speed, relative position of rotors, phase power, generation, vibration, the system of data analysis, the system of control instructions issue, and the mechanisms of command implementation.

The upper ring rotor, which carries the inductors of the linear generator, is connected by the stretching with the radial thrust bearing, located at the top of the central pylon. The mark of the bearing at the top of the pylon is 60–100 m. The diameter of the rings is 80 or 160m. The size of the blades is 16×4 for 1MW unit, 25×3 or 25×6 m^2 for 10 MW unit. The main parameters of the units are shown in the table.

Nominal power, kW	1000/2000	10000
Cut-in wind speed, m/s	3	5
Nominal wind speed, m/s	12.5/16.5	16.5
Stop wind speed, m/s	25	30
Number of blades in one ring	6	6 or 12

The linear generator is an important element of our unit.

The inductors of the linear (arched) generator are located at the upper ring, and its short-circuited rotor is located at the lower ring. This arrangement is justified by the fact that in some regimes, the significant attracting force between the inductor and the rotor appears and discharges the electromagnets of suspension. The inductors of the generator, made in the form of separate units (Figure 5.21), were tested under the actual conditions in the Kiev design office of linear electric motors at a special section of the railroad about one kilometer in length. The inductor was placed at the roadway (on the sleepers between the rails) and was connected to the network of alternating current. The short-circuited rotor, in the

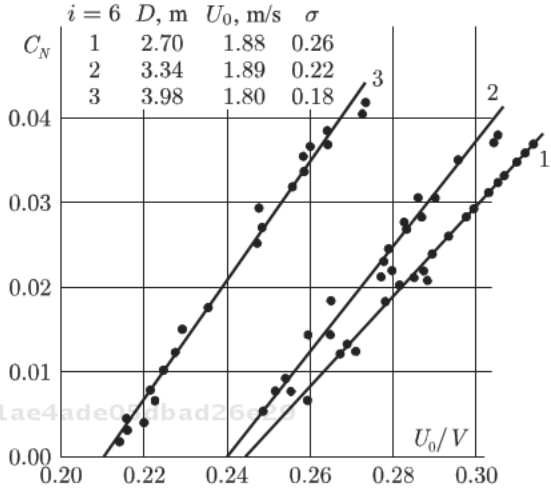

Figure 5.20 Power factor C_N according to the data of laboratory tests.

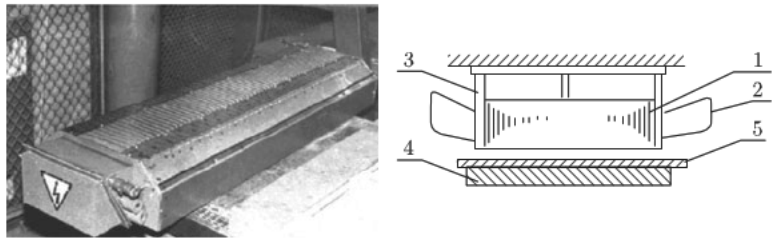

Figure 5.21 Generator inductor unit with a capacity of 84 kW ,50 Hz, 660 V, mass 830 kg (left). 2800×660×250 mm. Cross section of the linear generator (right).1, 2 – wires, 3 – frame, 4 – iron, 5 – aluminum (or cuprum).

form of a ferromagnetic strip with a thickness of 12 mm and the width of 600 mm, and the conducting aluminum strip with a thickness of 4 mm of the same width, was suspended under the bay with the length of 20 m, which "was dragged" above the inductor with a different speed, with a clearance of 3±0.5 mm. The results of voltage and current measurements on the terminals of the generator were compared with the results of calculations by the procedure, which was widely used in the design office LED (Kiev) during the creation of linear electric motors of different designations. It turned out that the working procedure of calculating linear engines, allows us to forecast with confidence the energy characteristics of linear generators (Figure 5.22).

The units of generator inductors in the wind power unit are joined by electrical power cables, which are brought out along the guys to the central pylon, where the coil-rings ensuring the generation of electrical power into the network, are located. The counter rotation of rotors, each of which bears the blades oriented in opposite directions, ensures high relative speeds between the inductors of the linear generator and the current-conducting plate; that reduces the mass of inductors and increases the efficiency of the wind power unit.. The generator efficiency under the nominal conditions according to the data of the tests of the first models was not lower than 0,80. Contemporary products ought to be more effective. The

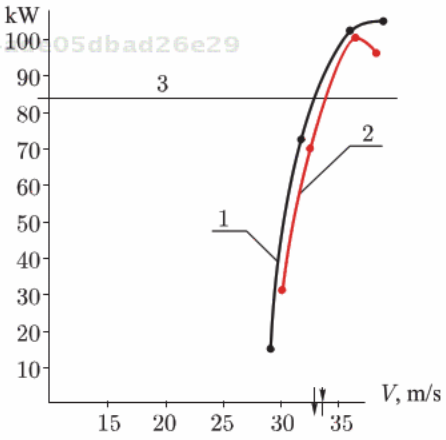

Figure 5.22 Power of the generator inductor unit LAG-1 depending on the rotor speed at a frequency of 50 Hz and a voltage of 660v. (1) – experiment, (2) –- calculations, (3) - nominal. The rating is reached at the relative speed of the inductor and rotor of approximately 33 m/s

overall sizes of one type of tested inductor were 1430×420×175 mm, the mass was 220 kg, the capacity at the nominal relative speed of the armature and inductor, which was equal to 22.5 m/s, amounted 22 kW at voltage of 380 volts (10 kg/kW only!). With the aid of two capacitors of КЭК2–0.8–80 type, the power factor of each module increased to the value of 0,988. The second type of the tested inductors had overall sizes of 2800×660×250 mm and the mass of 830 kg. At the relative speed of the armature and the inductor of 38 m/s each of these inductors generates the power of 84 kW at the voltage of 660 V (9.9 kg/kW).

With an increase in the relative speed of electromagnetic fields in the generator up to 50÷100 m/s, the material consumption of the generator decreases. The combining of the inductors into the units with different nominal armature speeds allows us to begin to use the wind energy from the relatively small values of wind speed.

A model with one ring and linear generator was tested in the large aerodynamical tube (Figure 5.23).

For units of this kind, it is very important to optimize a design of the basic knots and the generator. Under normal conditions, it is preferable for the inductor to be two-sided, static, and fixed between the squirrel-cage rotors (Figure 5.24).

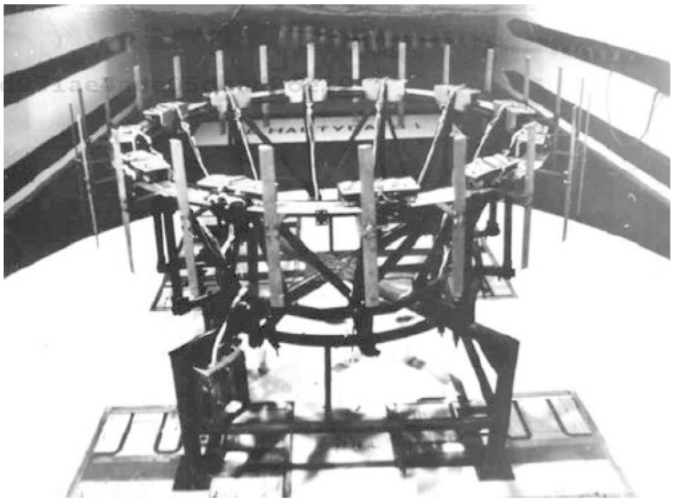

Figure 5.23 The model of a one ring multiblade power unit with a linear generator in the large aerodynamic tube. The rotor diameter is 2330 mm, the flow speed in the test is up to 50 m/sec.

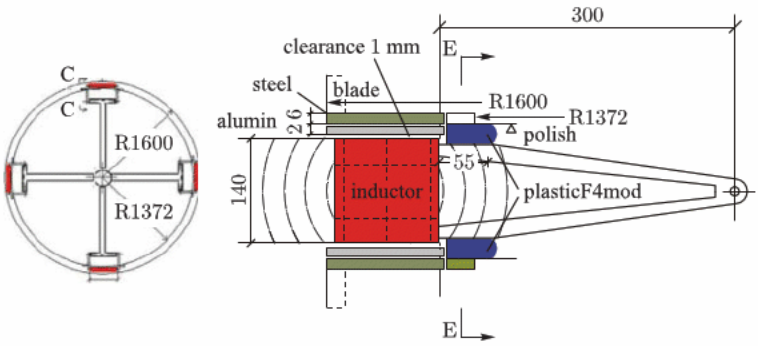

Figure 5.24 Solution with 4 inductors for asynchronous generator for the model in Figure 5.27.

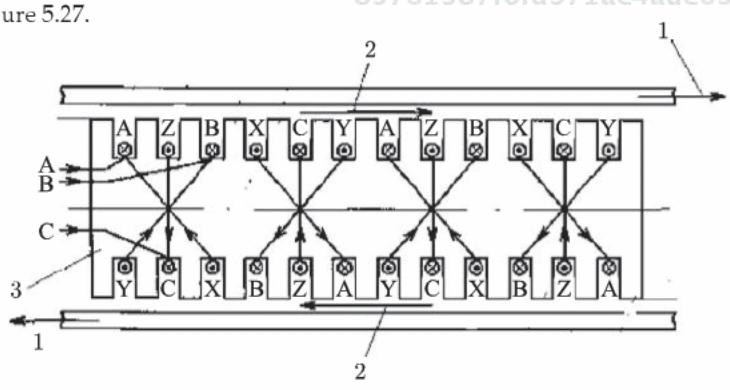

Figure 5.25 The arrangement of magnetic field forming coils that travel in opposite directions on either side of the inductor. A, B, C - Inductor front side phase winding inputs, X, Y, Z - Inductor back side phase winding inputs (1) – The cage rotors rotation direction, (2) - The magnetic field direction, (3) – The inductor body.

The movement of a magnetic field on either side of the inductor in opposite directions is provided by the cross winding arrangement (Figure 5.25, 5.26).

The compression magnetic forces that act on the inductors and on the turbine frame are controlled by the sliding bearings with metal PTFE (Polytetrafluoroethylene - teflon) liners that are fixed on the inductor ends. The inductor current frequency is automatically configured by the control system in order to attain the maximum power while maintaining the standard parameters of the electric current given to the grid or to individual loads.

The hydraulic model of the unit with the linear generator on Figure 5.24–5.26 was made (Figure 5.27) and tested in air and in water flow.

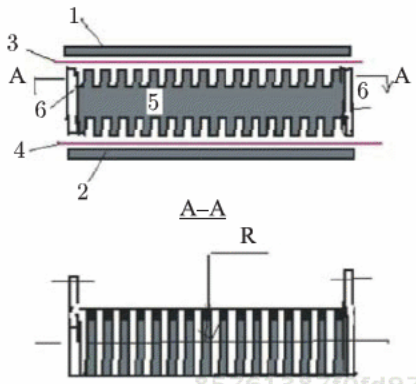

Figure 5.26 The winding ready inductor base design
1, 2 – Magnetic field conducting stationary plates, enclosing the magnetic field
3, 4 – Counter moving aluminum plates (flat rings),
5 – The inductor body made from magnetic field conducting sheets with winding slots.

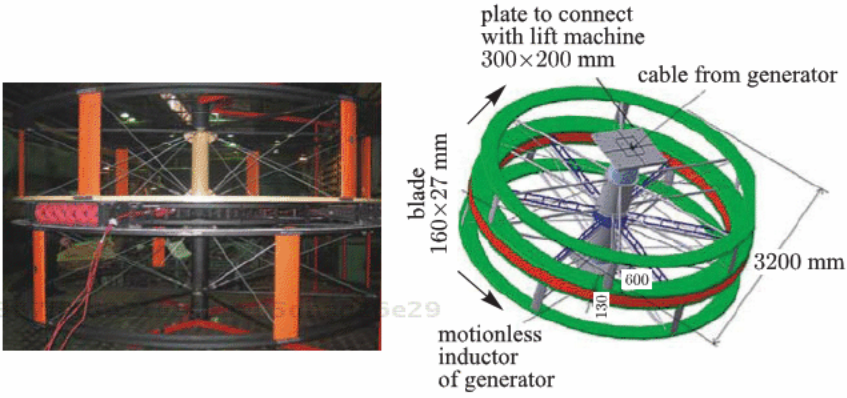

Figure 5.27 Model of the multi-blade unit for the use of the energy of currents. Option for tests in water.

Tests of the model (Figure 5.27) in water showed operability of the design, but revealed a big negative role of friction in the generator support, increasing at the expense of the action of forces of an attraction in the generator, and big losses of energy in constructive elements of a rotor. Work to improve basic knots proceeds in each new project. The new model of a wind turbine had the facilitated design of a rotor (without cross communications).

Tests of a full model with real blades, rims, and the generator are begun in the laboratory without creation of an air stream. Test objective: to check and optimize the basic knots and generator. As a

result of the first cycle of tests, the coefficient of friction of the basic systems (Figure 5.28 is defined - 31), the operation of inductors of the generator (Figure 5.32) is debugged. The design of the model allows for changing the number of blades in each circle.

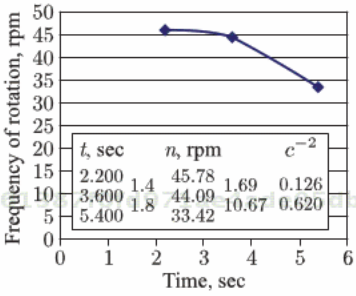

Figure 5.28 The turbine without blades. The short-circuited rotor disperses the inductor, which is then disconnected.
The change of frequency of rotation in time is registered. The mass of the moving system is 15 kg (a rotor – 10.1, a ring of 4.9 kg), the moment of inertia of 21.6 kg of sq.m. The change of the circular frequency of rotation for the last cycle $\Delta\omega = 1.117$ with-1, and derivative of circular frequency $\Delta\omega/\Delta t = 0.620$ s^{-2}
Brake moment $0.620 \times 21.6 = 13.4$ Nm. Friction force $13.4/1.2 = 11.17$ N,Coefficient of friction $f = 0.076$.

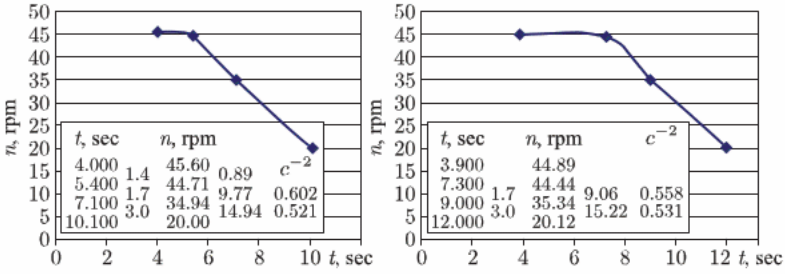

Figure 5.29 The turbine with 6 shortest blades (300 mm, the mass of the blade is 490 g). The top ring uniting the ends of blades, no. The mass of moving system of 18 kg, the moment of inertia of 25.9 kg sq.m. The rotations derivative of circular frequency shown in the last columns of tables on both schedules, on the average make $(0.602 + 0.521 + 0.558 + 0.531)/4 = 0.553$ sec^{-2}. Brake moment $25.9 \times 0.553 = 14.32$ Nm. Friction force 11.94 N. Factor of friction $f = 0.0677$.

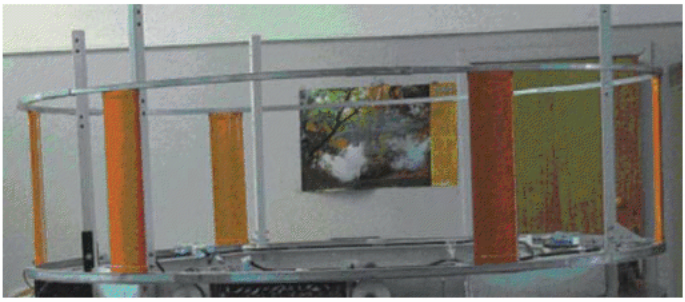

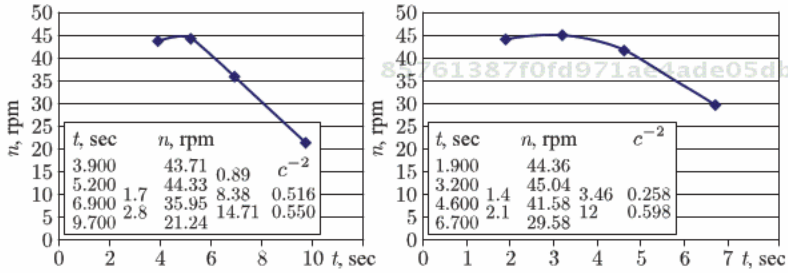

Figure 5.30 The turbine with 6 blades of average length (600 mm, the mass of one blade 988 g). The mass of the top ring - 3.56 kg, the bottom ring-4.92 of kg, the mass of a rotor of-10.1 kg, mass of blades of-5.93 kg, the general rotating weight of-24.51 kg. The inertia moment – 35.3 kg of sq.m Average value derivative of the circular frequency of rotation (0.516+0.550+0.598)/3 = 0.555 about the Brake moment 35.3 × 0.555 = 19.58 Nm, Force of braking is 16.32 N.Koeffitsiyent of friction of f = 0.068.

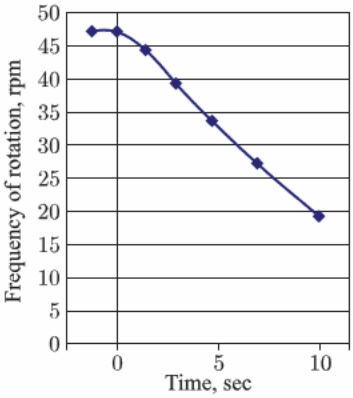

Figure 5.31 Turbines with blades of the maximum length (900 mm, weight is 1.164 kg). Between turbines motionless bilateral inductors, exciting are located movement of rotors in opposite directions. In an operating mode (at water flow or air action) inductors brake the turbine, giving out electric energy in a network. The mass of rotating parts of one turbine of 25.56 kg, the moment of inertia of 36.81 kg of sq.m. Example of record of change of frequency of rotation of the bottom turbine with the 6 longest blades after the shutdown of inductors (run off turbines). Average coefficient of friction of f = 0.0392.

Figure 5.32 The bilateral inductor before installation on model.

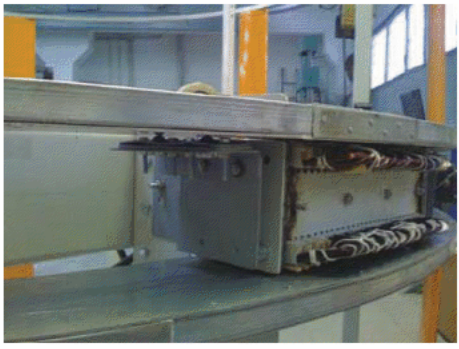

Figure 5.33 The spherical support fixing a gap between the top rotor and the inductor.

As the coefficient of friction was too big, replacement of the roller support of the model by a spherical (Figure 5.33) was made.

Such a replacement is essential at tests in a wind tunnel.

Tests of the generator showed its working capacity, but rather low efficiency. In this regard, for the main models the scheme of the generator was changed (Figure 5.34), allowing expectations of a significant increase in its efficiency.

Drawings of support on an airbag were developed. However, they appeared expensive. Spherical supports were put into place. These supports reduced the friction a little and caused wear of the plates of a short-circuited rotor. Taking this into account, the basic knots of the model were once again changed. Spherical supports were cleaned, and put in their places in the latest large model in diameter of 2.4 m conic support on internal ball quality bearings

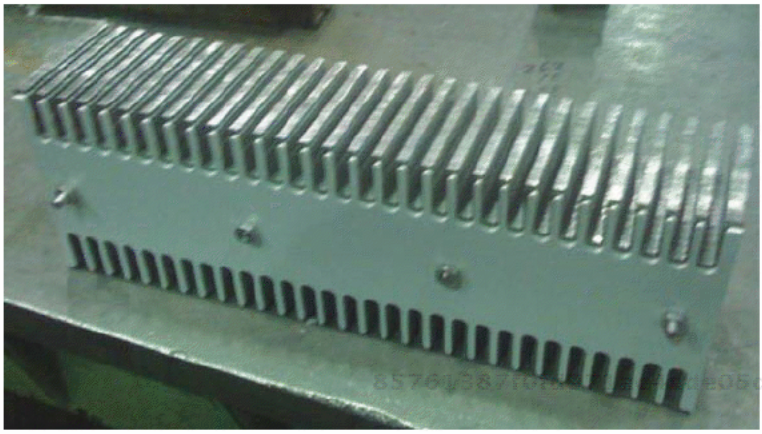

Figure 5.34 Two-side inductor high efficiency.

with low friction. The konical of a basic contour was expected to avoid sliding in contact between a rotating ring and a support. This change yielded positive results – noise and model vibration decreased, and power consumption of inductors of the motor-generator decreased.

Inductors were connected according to the "star" scheme and electricity was supplied by an alternating three-phase current of 380 volts voltage. Thus, model rotors rotated in different directions with identical frequencies of 70–72 rpm that corresponds to blade speeds of about 9 m/s. The consumed current on each phase was 3,2 amperes.

To improve the supply of a stream to workers, the blade constructive knots between the turbines rotating in opposite directions, were closed by a streamline casing with a toroidal appearance (Figure 5.35).

The capacity, capable of exiting the unit, will be defined by the dimensions of the blades, the speed of a wind, and a control system regulating the frequency of the current in the generator. The model is made with 3 sets of blades – lengths 0.3, 0.6 and 0.9 m. At the blade length of 0.9 m, the expected characteristics of the unit is shown on Figure 5.36.

For example, if the wind is10 m/s, and the blade speed is25 m/s (the generator is calculated on speed of blades of 30 m/s), the capacity which is given out by a rotor (without losses on a friction in support), is expected to be approximately

$$P = 1.25 \times 0.3 \times 103 \times 0.9 \times 2.4 \times 2/2 = 810 \text{ watt}$$

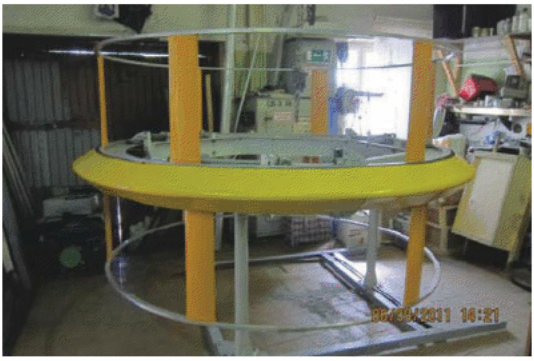

Figure 5.35 A general view of the model prepared for testing in a wind tunnel.

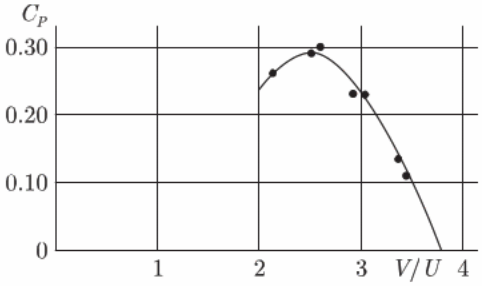

Figure 5.36 Efficiency of a rotor of the turbine as relative speed of blades.

At smaller blade lengths, the efficiency of the turbine should be higher (at the expense of a wind power transfer down), but the area of the cross-section section of the turbines is less, so expect big capacity difficultly.

For real units of big power, the other scheme of the linear generator can be more effective, in which considerable clamping efforts aren't raised in a short-circuited rotor less electric losses at the expense of decreasing a settlement (nonmagnetic gap between a rotor and inductors (Figure 5.37).

Actually, in this option two generators are used, each of which consists of several couples of motionless inductors located one over another with a gap in which the short-circuited rotors connected with turbine blades (Figure 5.38) take place.

All inductors are connected consistently, but according to such scheme that magnetic fields in the generators of the top and bottom circles move in opposite directions.

By changing the winding pitch of the stator it is possible to change the design speed of relative motion of the rotor and the

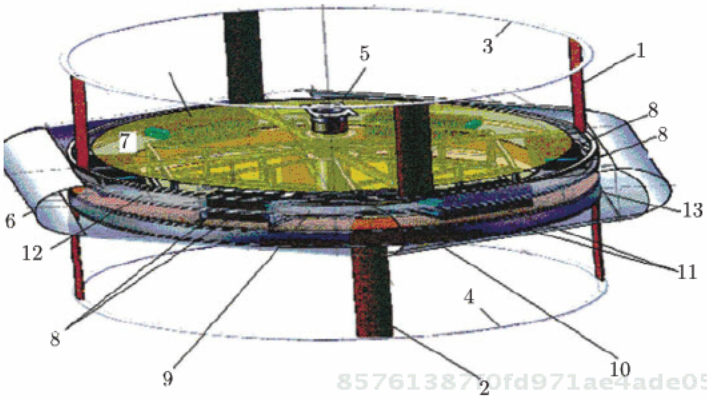

Figure 5.37 The General view of the hydrounit 2.5.(1 and 2) – blades with profile GAW-1, focused in opposite directions, (3 and 4) – the streamline rings distributing loadings between blades and creating spatial rigidity of turbines, (5) – the central basic knot (CBK), perceiving horizontal loadings on turbines from outside a stream, (6) – toroidal flow director, the forming smooth approach of a stream to blades of turbines,(7) – a cover of a casing of the turbine, closing the motionless bridge and the rotating traverses of the turbine transferring radial loadings on CBK,(8) – motionless inductors of the top turbine, (9) – a short-circuited rotor of the top turbine - the flat copper ring connected with the top number of blades, (10) – a short-circuited rotor of the bottom turbine, (11) motionless inductors of the bottom turbine, (1)2 – a bearing ring of the top turbine, (1)3 - a bearing ring of the bottom turbine.

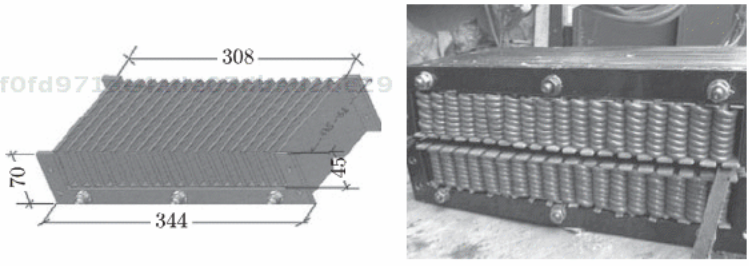

Figure 5.38 The General view of the inductor before packing of windings (at the left) and steams inductors with windings in working order (from outside a stream).

stator within wide limits, attaining the greatest generation of wind power units at the specified wind regime. The performance of the wind turbine of 1000 kW power is shown on Figure 5.39.

Dependence of the relative time t of usage of the installed capacity depending on the average annual wind speed at the height

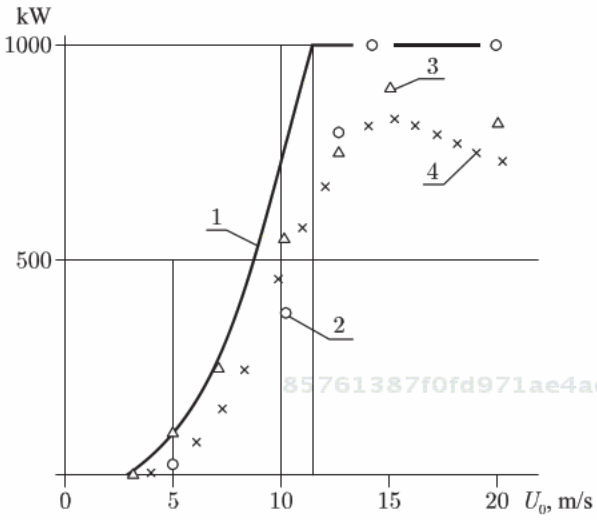

Figure 5.39 Power of optimized rotor of proposed wind power unit (1) and specifications of wind power units with traditional assembling (2–4): (2) – "Raduga - 1", (3) – "NEG Micon", (4) – "Fuhrlander".

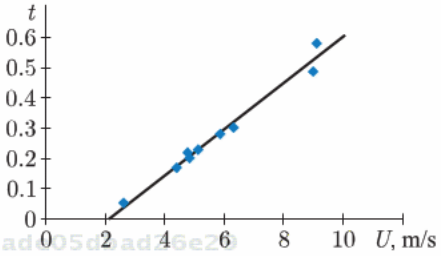

Figure 5.40 Relative time of usage of the installed capacity of the wind power unit depending on the average annual wind speed at the height of the generator.

of the rotor at the wind power unit site is graphed at fig.40. The parameter t is well described by the linear function

$$t = 0.075\,(U - 2),\ U > 2\ \text{m/s} \tag{5.8}$$

With known t, the annual power generation E (MWh) of the described installation with the capacity of 10000 kW is determined from the formula

$$E = 87600\ t \tag{5.9}$$

Using formulas (8, 9), it is possible to calculate the net cost of energy obtained from the proposed wind power unit, taking into account the fact that the expenditures on its operation in the automatic operating mode on powerful electrical networks are negligible. It is not difficult to see that the effectiveness of the wind power unit is sufficiently high.

To estimate the real efficiency of the proposed wind turbines many drafts were made. The best were the largest units with power 2 MW (one ring system – Figure 5.41) or 10 MW (two – ring system – Figure 5.42). The largest wind turbine is the most efficient.

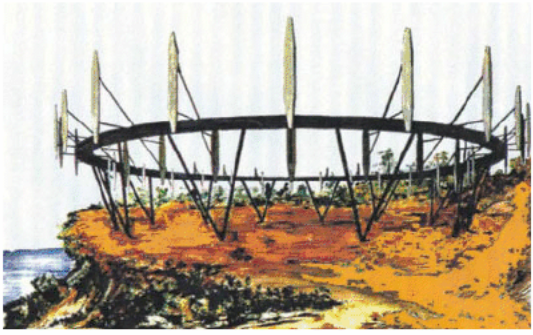

Figure 5.41 Wind turbine 2 MW for Vung Tao (Viet Nam) and Nakhodka (Russia). $D_{max} = 72m$.

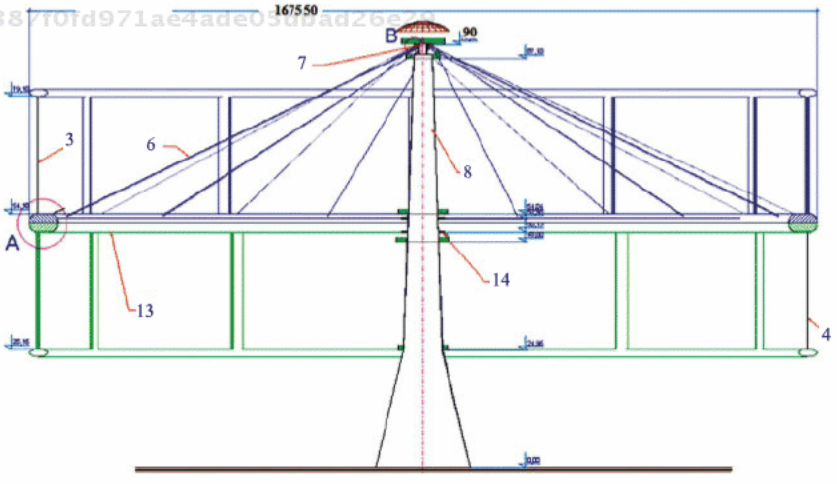

Figure 5.42 Wind turbine 10 MW on the ground or on the Sea.

The wind power unit with the nominal capacity of 10 MW (at wind speed 15–16 m/s) must have mass above the foundation of approximately 871tons (87kg/kW) two times smaller than at the best traditional units Vestas 1800 (see Table to compare).

	VESTAS 1800	MLP 10000
Blades, ton	34	22.8
Kg/kW	18.9	2.28
Generator +, ton	61	90
Kg/kW	33.9	9
Tower +, ton	200	758
Kg/kW	110	75.8
Total under foundament,		
Ton	315	871
Kg/kW	175	87.1

Averaged capacity of our unit 10 MW is from 19 to 43% of rating at the average annual wind speed from 5.5 to 8.5 m/s. The power production of such units can be noticeably increased due to the jet control of the boundary layer on the blades. The central supporting pylon of such a wind power unit can be fixed on the underwater pontoon, located at the depth of 5–10 m or more, and having excess buoyancy. With the aid of the ropes and the system of piles this pontoon is fixed in the space, and entire system is capable of withstanding hurricane winds and gale waves.

The corresponding calculations, executed for the depth of water up to 20 m (conditions of a wind park in New York), show that the total costs of the installation in the case of its serial production at the Russian Engineering Plant will not exceed 800–900 dollars per kW, and in regions where the average wind speed exceeds 8.5 m/s, the installed capacity will be used for about 4000 hours per year.

With the big diameters of installations characteristic of these units, the central support would not be - the wind turbine turns into the train curtailed into a ring (Figure 5.43, 5.44).

For similar multi-blade cars with long routes crucial importance has friction resistance in support- running knots and aero (hydro) - the dynamic resistance of constructive elements. The role of these resistance is so great that in separate designs large wind power

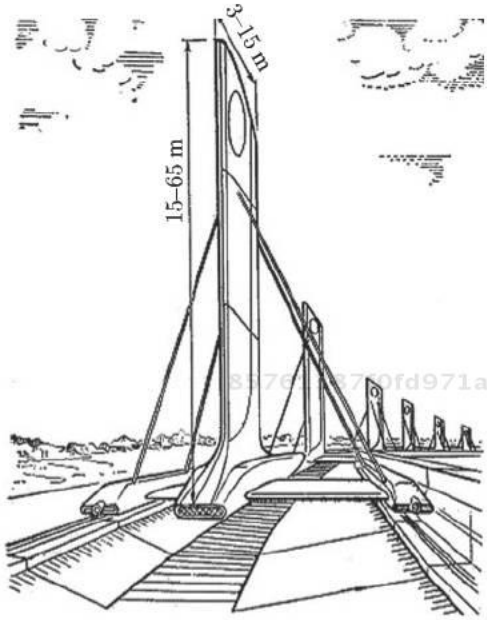

Figure 5.43 Carts with blades move on the ring route.

Figure 5.44 Fragment of the patent of the USA, 4302684, November 24, 1981 (Laird B. Gogins).

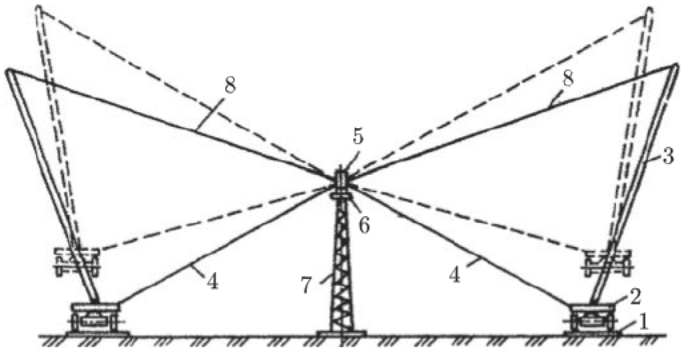

Figure 5.45 Radical decrease in friction in support. The hub (5) is mounted on a rack (7) at a height exceeding the heights of an arrangement at the center of gravity of the blades and carts.

turbine's provide the option of almost full refusal of mechanical losses at the expense of use of centrifugal forces (Figure 5.45) were considered.*)

Under the influence of the speed power unit in a circle outlined by blades appear less than on the way to the unit, however, owing to turbulent vertical hashing of speed in a circle considerably increase. It is important to choose the correct distance between the blades which is recommended -by the technical and economic analysis, considering that the mutual influence of the blades starts showing up if the distance between blades "B" (in light) is less than 6b. Thus, the maximum expedient number of blades equally

$$i_{\min} = \frac{\pi D}{7b} = 0,45\frac{D}{b}. \qquad (10)$$

Multi-blade units can be realized with the blades installed on separate carts, connected in a ring moving on a platform (the train curtailed into a ring – Figure 5.46, 5.47) [2], or, alternatively, with the blades which have been rigidly closed up in a uniform ring, moving on a motionless support (Figure 5.48).

For the purpose of increase in rigidity of the system and power of the unit, two horizontal rings, connected by working blades in one horizontal plane (Figure 5.49) or in two planes carried high(Figure 5.50) can be used. In both options, construction of the choice that breaks out of a basic ring platform on one central pole

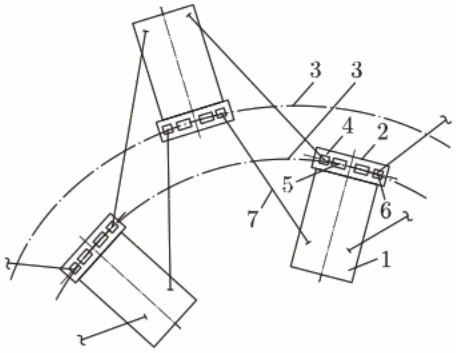

Figure 5.46 The separate carts which have been flexibly connected between one and other.

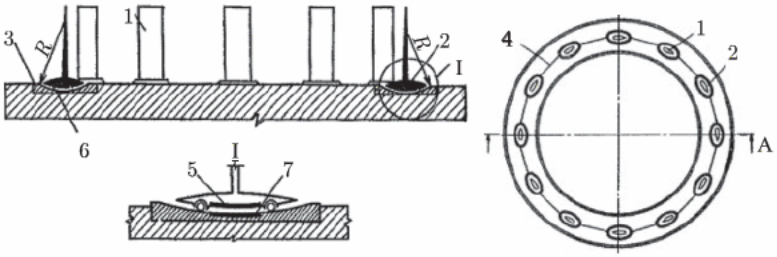

Figure 5.47 Each cart is connected with neighbors, but independently chooses a position of balance in a route trench.

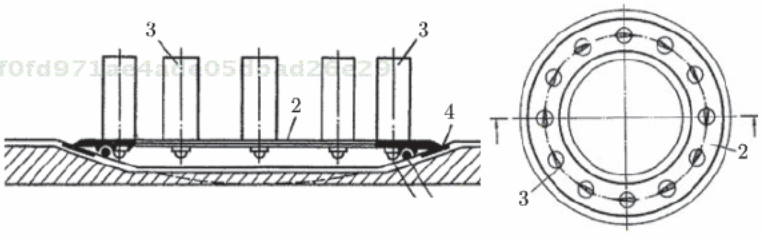

Figure 5.48 Blades on a rigid ring, but the ring itself chooses a position of dynamic balance. [3]

(Figure 5.51) can give perspective. The pole in this case, isn't mobile and holds an internal torovy surface on which the external cover with the blades, slides. It is possible, of course, to add [or choose or build] an option with a rotating pole.

The opiraniye of the driving wheel with the blades on skating rinks with the direct drive of standard generators (Figure 5.52) was

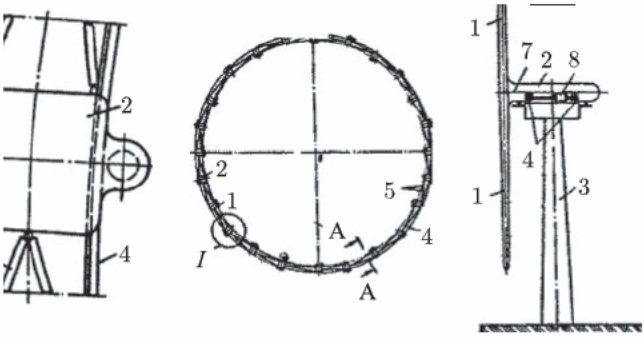

Figure 5.49 Rigid communication between carts exclude their independent movement on the route. [4]

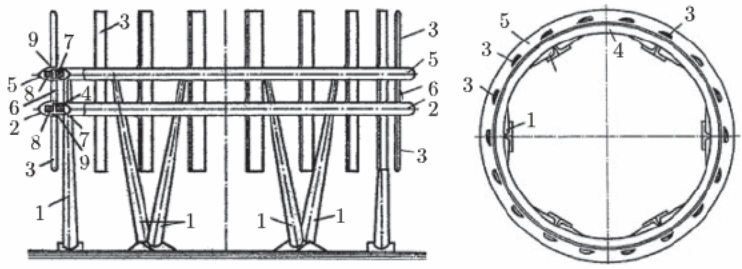

Figure 5.50 Two horizontal rings give spatial rigidity to a system of large diameter.

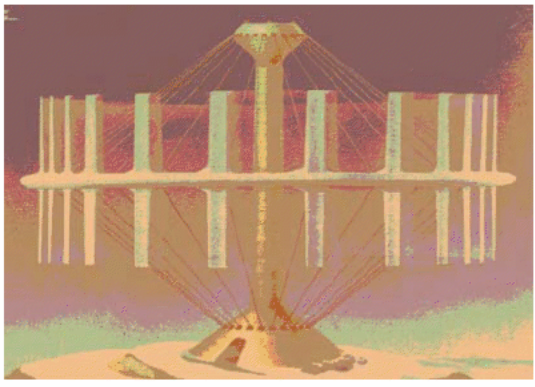

Figure 5.51 The internal motionless basic ring is fixed on a pole. Creation of the modern car with two rings rotating in opposite directions was the following step. [5]

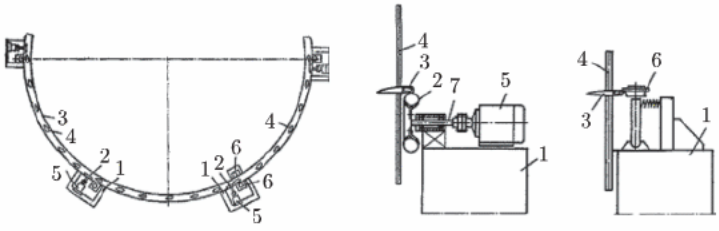

Figure 5.52 Opiraniyes of a ring with blades on skating rinks demands big rigidity of a ring. Otherwise, losses on friction are excessive. [6]

the simplest scheme of the multi-blade car. This plan was carried out; however, losses onthe skating rinks (in the form of automobile wheels) were too big.

These configurations are connected with the creation of new wear-proof basic knots with little friction and linear generators. Both of these problems have the technical solutions applied in adjacent areas. It is established that in an appropriate design, for example, electromagnetic support, losses on friction can be reduced to 100 W on 1 kN of loading. It qualitatively changes the prospects for the use of multi-blade units of large diameter. Detailed design studies are executed for the multi-blade unit in which the external mobile ring bearing blades, slides on an internal motionless rotor (Figure 5.53). The model of such a unit was tested in a wind tunnel (Figure 5.24).

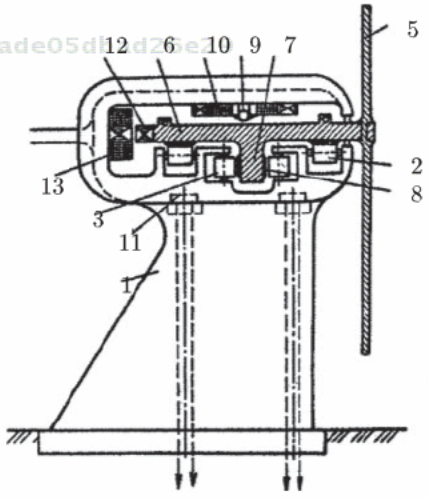

Figure 5.53 The rigid ring bearing blades, on the wheel support unloaded by electromagnets in a complex with the linear (arc) generator. [7]

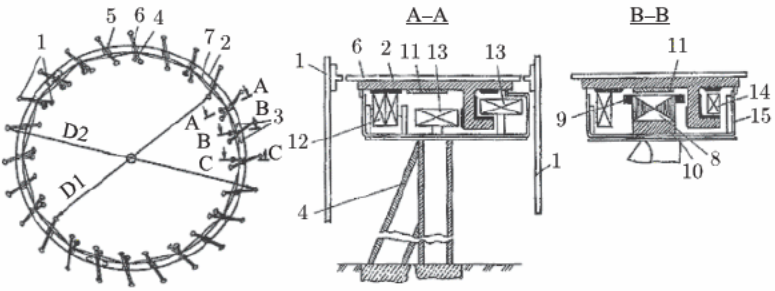

Figure 5.54 Rigid ring on electromagnetic subweight with two rows of blades on the different parties of basic not subother farm and the linear generator.

The project of this unit with D= 40 m and P= 2 MWt already considered the difficulties revealed at the tests of the first multi-blade car. It was modified by the expense of introducing two rows of blades – from the external and internal parts of a basic motionless ring (Figure 5.54) and finished according to the engineering design related to the conditions in Vungtau's (Vietnam) regions and Nakhodka (Figure 5.41).

In this project, the practical experience of the creation of trains on magnetic subweight of the Transrapid company (Germany) and the Russian enterprise"TEMP" [8] was considered. Economic consequences of the disintegration of the USSR took away the chance to carry out these projects.

References

1. V. Lyatkher, Power Unit, Patent US 7586209 B1, Sep. 8, 2009, Patent US 8007235 B1, Aug. 30, 2011. Patents RU 2245456, May 22, 2002; 2242634, May 05, 2003.
2. V.M.Lyatkher, C.C. USSR 1209919, April 04.1984. M.S.Bruk, O.P.Bortsov, V.M.Lyatkher ,C.C, USSR 1182196, February 15.1984.
3. V.M.Lyatkher, M.S.Bruk, O.P.Bortsov C.C. USSR 1188364,February 15.1984.
4. V.M.Lyatkher, O.P.Bortsov, D.N.Militeev, A.G.Sverchkov C.C. USSR 1273640, July 23.1985.
5. V.M.Lyatkher, A.Yu.Koyransky, L.A.Pronina C.C. USSR 1381274,July 31.1986.
6. V.M.Lyatkher, D.N.Militeev, R.L.Yafarov C.C. USSR 1373859, July 24. 1986.

7. V.M.Lyatkher, V.P.Molomin, C.C. USSR 1694978, June 27.1989, C.C.USSR1758280, Dec.28. 1989.
8. V.F.Molkov,Yu.D.Sokolov,A.T.Gorelov,E.V.Kozachenko,V.M.Lyatkher, Patent RF 2000468 , Nov. 30. 1990.

6

The Unit Without External Rotation

Wind farms like "Tornado", offered J.T.Yen in 1976–72 [1], differ in that concentration of energy is carried out by a motionless system of air-directing designs (a permeable tower of the unit), providing deep fall pressure in the system center. In the numerous known projects realizing the idea of J.T.Yen, in a zone of lowered pressure, the traditional wind-driven generator, but with a vertical axis of rotation in which special air ducts move the air outside the tower (Figure 6.1) is established. A specific feature of these "Tornado"-type wind power stations proposed in 1972–76 by J.T. Yen is that energy concentration is achieved by a stationary system of air-guiding structures (penetrable tower) providing a big pressure decrease in the system center. The known numerous decisions realizing the idea of J.T. Yen have a traditional wind generator in the decreased pressure zone equipped with a vertical rotation zone and supplied with air taken outside the tower by special air ducts (Figure 6.1).

This scheme has some disadvantages. The main disadvantages are a sharp bend and flow expansion coming through the working element that decreases the system efficiency. System efficiency in our project is increased by the usage of pressure air ducts

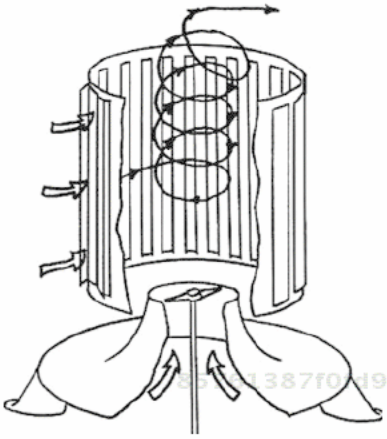

Figure 6.1 The "Tornado" scheme in initial option.

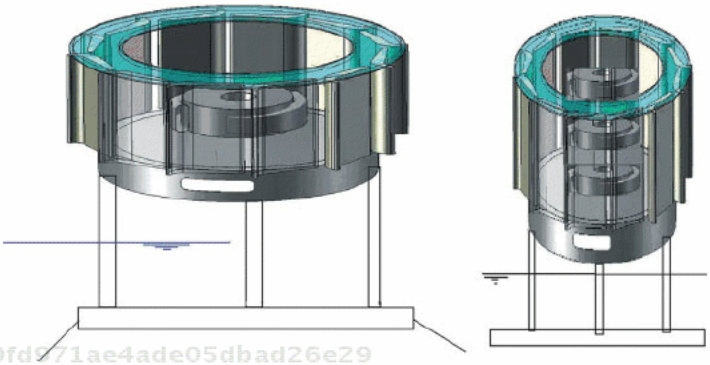

Figure 6.2 General view of a wind-power plant "TORMOD". On the left – a one-stage plant; on the right – a three-stage plant.

discharging air into the central zone of decreased pressure in the tangential direction to the main vortex acting inside the tower (Figure 6.2). This system is called Tornado – Modified (TORMOD). [2] The power plant scheme is shown in Figure 6.2.

The power plant's structure is similar, environmentally friendly, isn't equipped with external moving elements, and has an aesthetic appearance. Applied manufactured elements of power-generating equipment (power generators) are effective, reliable, and endurable. The plant is located over the water surface on an immersed floating platform. The design of the power plant includes a structural directional tower construction made of composite materials and

forming a vortex inside the tower, pressure air ducts and innovative air orthogonal turbines (Figure 6.3).

To make the additional pressure decrease in the vortex center, the tower can be equipped with a roof in a form of an ellipsoid providing the ejecting action of high-speed flow at upper levels of the tower and protecting the tower's internal parts from precipitation (Figure 6.4).

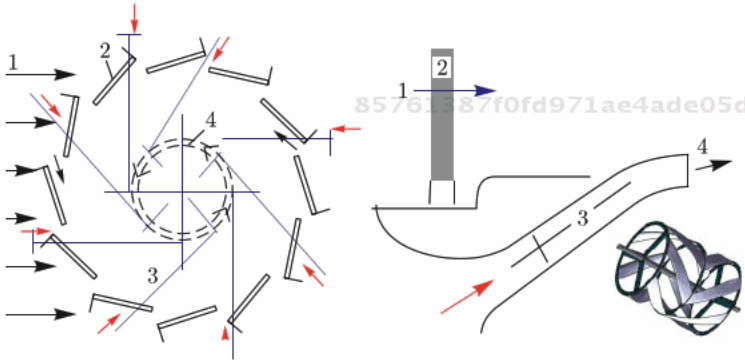

Figure 6.3 Plan (on the left) and section of one of the air ducts with a turbine (separate view). Orthogonal balanced turbines in the "TORMOD" system of modified "Tornado" units. Tower plan (on the left) and section of the water duct (air duct) route with a turbine. (1) - original flow direction, (2) – plates forming a swirl of flow in a definite direction (optimal swing of the plates is chosen during the adjustment procedure. It's possible to use a structure with an individual swing drive of each plate selected via computer program), (3) - axes of pressure pipelines supplying the operating medium in the rotation direction of the main vortex at a tangent to a body of rotation (4) in the tower foundation.

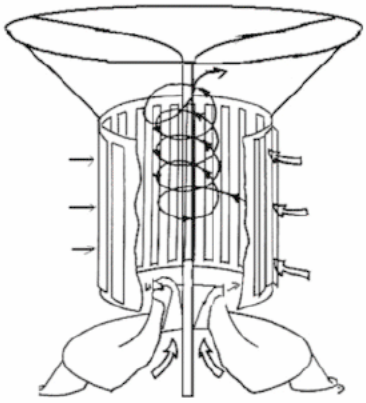

Figure 6.4 Modified scheme of "Tornado" wind-power plant with an ellipsoid ejecting roof and orthogonal turbines in the air ducts ("TORMOD" system).

Pressure air ducts have rectangular cross-sections. High-speed orthogonal turbines are located in them. Such a turbine at any time has equal overall aerodynamic flow resistance. This eliminates the main weak point of orthogonal turbines with straight vanes in pressure flow, i.e. high vortex formation (instability) and big energy losses connected with it. Aerodynamic balancing of the turbine is achieved by the usage of arrow-shaped vanes that provide not only the consistency of total resistance and torque but also the consistency of supporting resistance forces (Figure 6.5) [3].

Curved vanes can be approximated by sections of straight vanes (Figure 6.6).

Turbine edges look like flat rings combining the vanes and connected with shafts by 3 aerodynamically clean spokes (traverses). Vanes opposed to each other are also connected in the middle part of the turbine via a flat ring. It's possible to make the turbine edges at individual spokes without a combining ring (Figure 6.7). The quantity of turbines, number of vanes, and their dimensions are determined on the basis of optimization calculations.

Systematic experiments with one-stage orthogonal turbines with straight vanes were executed on the hydraulic bench of the JSC "Research Institute of Power Structures"

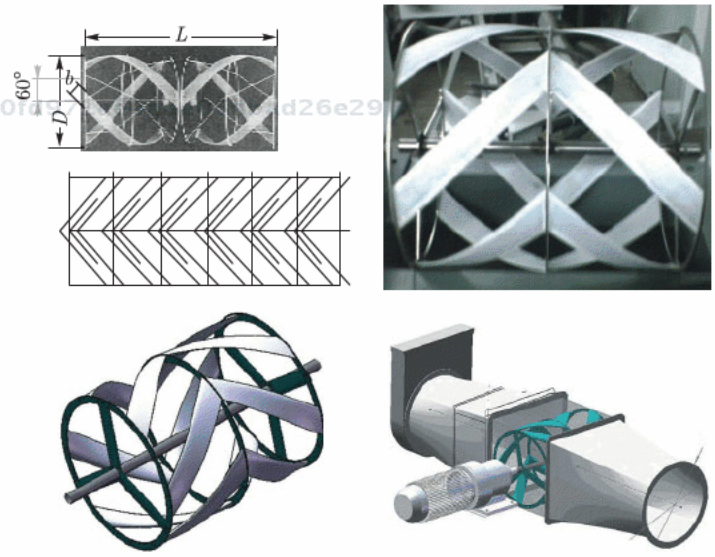

Figure 6.5 Balanced turbine with 6 arrow-shaped vanes. At the top: photo of a model with three curved vanes and presentation of a turbine with 6 vanes.

Figure 6.6 Curved vanes' approximation by sections of straight vanes.

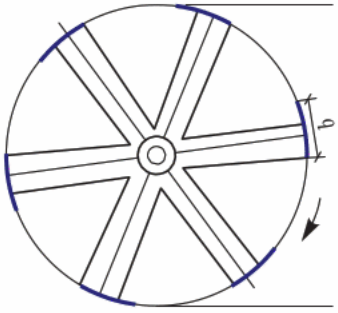

Figure 6.7 Variant of turbine edge.

(Moscow) using a turbine with a diameter of 250mm, vanes with a length of 200 mm, and a chord of 50 mm (Figure 6.8) [4].

The vanes profile was similar with the symmetric profile NACA 0024, which chord was bent over the circle corresponding to the vane's route. Traverses of the same profile had a chord two times less than the vanes chord.

In view of the results of these experiments, the universal characteristics were determined which connect the relative specific capacity of the turbine $Y = P/\rho\,(\Delta p/\rho)^{3/2}$ and the relative speed of its vanes $X = V/(\Delta p/\rho)^{1/2}$.

Herewith, P (kW/m^2) is the turbine capacity related to the area unit of the turbine cross section, V is a linear speed of the turbine vanes, ρ is a medium density, Δp is a pressure difference of the turbine (pressure on the turbine). The change of specific output

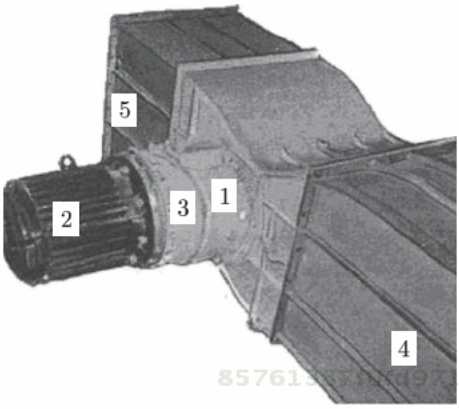

Figure 6.8 Orthogonal turbines in pressure flow. (1) - turbine in shell, (2) - generator, (3) - multiplier, (4) – intake water duct, (5) – branch.

versus specific speed of the turbine vanes at different solidity $\sigma = ib/D$ is shown in Figure 6.9. Here, i – the number of the vanes at one stage, b – vane chord, D – turbine diameter.

The equations of the lines shown in Figure 6.9 that correlate the turbine specific output $Y = P/\rho(\Delta p/\rho)^{3/2}$ and the specific speed of its vanes $X = V/(\Delta p/\rho)^{1/2}$ are as follows:

At solidity of 1.2 $Y = 0.526 - 0.192X$
At solidity of 0.6 $Y = 0.709 - 0.195X$
At solidity of 0.4 $Y = 0.835 - 0.195X$

Obviously, it would be reasonable to reduce solidity and to increase the turbine speed.

The experiments currently performed with standard «Tornado» systems showed that pressure reduction in the center of the tower (at air ducts outlet) could achieve the value 9 times higher than the wind pressure at the entrance to the tower (Figure 6.10).

When the wind velocity at the entrance to the power plant is 12 m/s the $\Delta p/\rho$ value in the air ducts of each turbine (3) (see Figure 6.2) will be about $9 \times 72 = 648$ $(m/s)^2$, and the turbine maximum specific output with solidity 0.4 will be about $0.5 \times 1.25 \times (648)^{3/2} = 10.4 kW/m^2$ at vanes speed of $1.8 \times (648)^{1/2} = 45.8 m/s$. The turbine speed $n = 60V/\pi D = 930.4/D$. At turbine diameter of 1m it is possible to select the motor-generator speed of 1000 rpm and the output of about 25 kW (received from one machine with a diameter of 1 m and length of 2,4, for example). The centrifugal acceleration applied to the turbine vanes will be 428g. It is possible

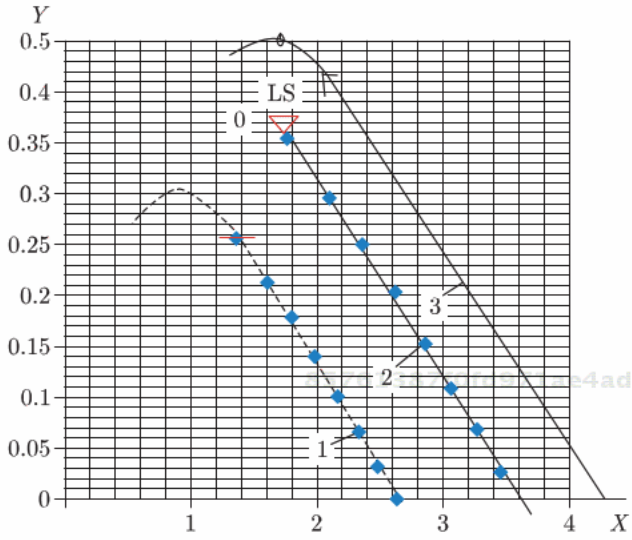

Figure 6.9 Turbine performance diagram. Solidity 1.2, 0.6 and 0.4 - lines 1, 2, 3.

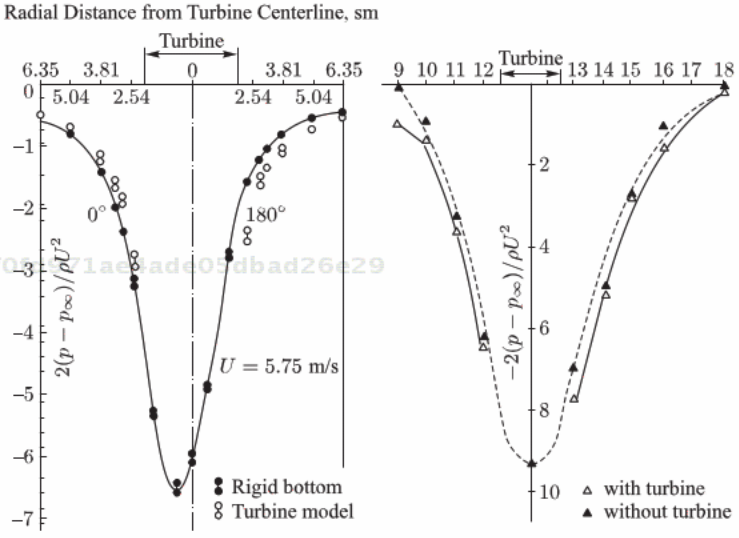

Figure 6.10 Relative pressure distribution along the tower diameter. Experiments performed by different scientists [5].

to replace the curved vanes with straight sections (see Fig.A-3-6) with 0.6 m of vane span between supports and to use standard aluminum vanes produced by our company (vane chord is 160 mm, weight per unit of length is 1.65 kg/m and the allowable

bending moment is 780 Nm). When the turbine is operating with its maximum efficiency, the flow velocity near the vanes does not exceed 0.4 of the vane speed. Thus, the relative air velocity is 1.08 of the vane speed and the aerodynamic load per unit of vane length will not exceed $0.16 \times 2 \times 1.25 \times (1.08 \times 45.8)^2/2 = 489$ N/m. At a centrifugal load of 6928 N/m the maximum bending moment of span will be $(6928+489) \times 0.6^2/8 = 334$ Nm. It is obvious that a turbine with our vanes can be used.

Usually, the wind energy efficiency relative to the tower cross section does not exceed 0.15. **To get the output of 50 kW at a wind speed of 12 m/s and a power factor of 0.15 (relative to the tower cross section) the tower diameter should be 13 m, and the height of the tower should be the same.** Based on the results of numerical modeling we can see that if we reduce the turbine height, the system efficiency increases (Figure 6.11).

The system efficiency increase relative to the tower height decrease is known [6]. However, the mentioned efficiency increase is possible only in combination with our proposal to increase the vortex stability inside the tower through the action of operating fluid streams.

The research is aimed to increase the system efficiency and to reduce the tower height 2–3 times. This will be achieved by the construction of several air discharge stages, that will assure the increase of the flow swirl and additional decrease of pressure in the center of the tower.

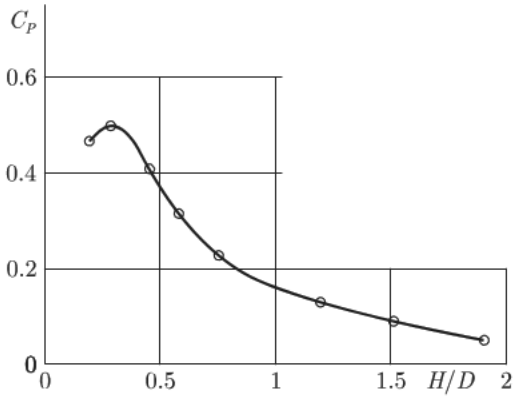

Figure 6.11 Height and diameter ratio effect on the wind power plant efficiency.

The simplest variant consists in installation of 2 air ducts with turbines and generators with a capacity of 25 kW each at one stage along the tower perimeter. In this case the channels cross section should be 2.4 m^2. With the turbine diameter of 1m the generator speed can be about **1000 rpm** at rated wind speed and **750 or 500** rpm at low wind speed. These standard generators are available. For example, the engine 5A225M12/6CH with fields speeds of 1000/500 rpm, capacity of 25/15 kW and weight of 335 kg meets these requirements. For the wind power plants with lower capacity it will be possible to use cheaper generators with more rpm.

The advantage of our construction over the traditional one is that the operating fluid (air or water) flow maintains circulation. It holds out hope of a positive result. The main distinctive feature of the present proposal is the possibility to construct vibration-free and silent high-power wind turbines without multipliers with standard electrical equipment that makes the system a low-cost one.

At estimated wind velocity of 12 m/s and the system efficiency ratio of 0.5 the cross-section area of the tower for the plant with the output of P(kW) is determined by the formula Ω (m^2) = 1.85 P (kW). For a three-stage machine the tower height H can be taken equal to its diameter D. In this case H= D= $1.36\sqrt{P}$

The higher the plant output is, the bigger its economic effectiveness. The effectiveness increases due to the fact that the wind velocity grows as the height increases and due to the reduction of power-generating units cost. For the output values of **50, 2000 and 160000 kW** we get the following values of the tower diameter: 15, 100 and 1000 m - **H = 0.3D**,

P = $0.625\ C_p \times 0.3D^2\ U^3\ W = 0.625 \times 0.5 \times 0.3D^2\ U^3 = 0.0938\ D^2\ U^3$, W

Wind unit power P = **$9.4\ D^2\ U^3 10^{-5}$, kW**

The example of calculation results are follow

U, m/s		6			8			10			12	
D, m	10	20	50	10	20	50	10	20	50	10	20	50
H=0.3D												
P, kW	2	8	50	4.7	19	118	9.2	37	231	16	64	400

The cost of one kW of power will be between $2,000–1,200 for the first units and at two times smaller in serial. We propose to construct the new, largest power wind station on the surface of Eria Lake near Cleveland (Figure 6.12).

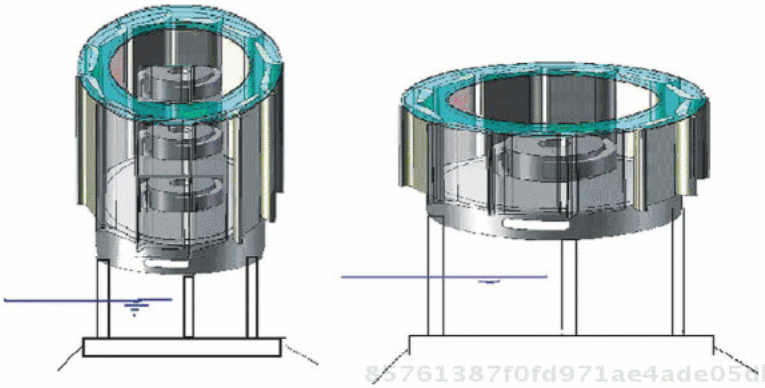

Figure 6.12 Wind power plants on the water surface. **D=1000 m, H=300m, U =12 m/s, P=160 MW**.

The main advantages of the proposed solution are the following:

1. There are no external rotating elements. All turbines are located in channels the entrance of which is closed by lattices. It ensures the full safety of birds.
2. The power equipment is in a construction; therefore, additional acoustic radiation will be minimal.
3. The directing system (tower) can be constructed from an easy, cheap material and have an attractive architectural appearance. If necessary this construction can have additional functions – for example, inhabited apartments, piers, restaurants, and museums.
4. Speeds of movement of air in, channels much more wind speed before a tower. It allows the use of rather cheap and easy power equipment (turbines and generators).

References

1. J.T.Yen, Tornado-Type Wind Energy System:Basic Consideration, 1976, BHRA ,Cambridge, E4-47 – E4-64.
2. V.M.Lyatkher. Power Generating System, Patent US 8461712 B1, June 4, 2012.
3. V. Lyatkher, Patent US 7741729 B2, June 22, 2010.

4. B.L.Istoric etc., Journal "Hydrotechnical Construction", 1998, N12, pages 35–44.
5. DARPA Conference Call, Dr. Deborah Furey, Barbara K. McQuiston & Ray Ellis, January 7, 2010 3 PM Eastern Time (2 PM Central Time), The TWECS Project's New Approach to the Tornado Wind Energy System (TWECS).
6. S.S.Ayad, Numerical Study of the Performance of Tornado –Type Wind Energy Systems, J. Energy, vol.7, N2, 1983, pp.134–140.

7

High Jet Power Station

Our purpose is a proposal to create an operating demonstration of a wind power unit (model) repeating basic elements of future trial wind power plants b with the capacity of 50–100 MW, having high economic efficiency, and full ecological safety [1]. Our proposal refers to wind-power engineering, namely to wind power plants that use the energy of altitude jet streams. Technical results consist in efficiency coefficient increase, material-output ratio decrease, plant safety improvement, provision of secure communication with the land. Altitude wind power plant includes aerodynamic components in a form of a framework, the units of which are located on the elliptical surface; the framework is connected with ground support by cables and on the framework along its span there are located orthogonal well-balanced bladed rotors arranged at an obtuse angle in relation to each other. The cables are performed in a form of sectional hoses, the sections of which are filled with helium and are connected by gates. Rotors are located between framework units, their blades are equipped with jet devices of circulation control.

There is known an altitude aerostatic plant that holds aircraft performed in a form of cargo-carrying kite, the load-bearing

surface of which has an annular wing consisting of aerodynamic components with differences in curvation and chord by span. Around the periphery of the ring there arranged are wind-engines behind the rear edge of the aerodynamic components and wind-engines in a horizontal plane before aerodynamic elements; note that the engines have different rotation directions. Each wind-engine has a compressor of centrifugal type, speed-increasing gear and blade propeller mechanically connected with each other. Flow parts are interconnected by connection of the outlet of the following part with the inlet of the previous one. Note that the outlet of the last compressor is connected with the input of a power machine located on land by pressure hose (Patent of the Russian Federation No. 2064085). The disadvantage of this decision is the need to use an aerostatic structure as well as insufficient security of the system in case of land fixture rupture.

There is known a wind plant for high altitudes (Patent of the USA No. 4659940). It consists of a load-carrying surface along the span of which there is located a sectional wind-catching device with generators, attached with the help of attaching elements on the support. The wind plant has a fixed balloon in a form of load-carrying surface with an empennage. Along the span of the load-carrying surface there is a sectional wind-catching device formed by several multi-blade rotors with horizontal rotation axis located close to each other. Rotor annular rim is installed with the possibility of rotation at roller supports attached in cantilever fashion on a load-carrying surface, where there is installed a two-shaft generator. The disadvantage of this decision is the need to use an aerostatic structure, rotors with horizontal rotation axis, and lack of secure connection with the land.

There is known "the best invention of 2008y" SWP technology (www.skywindpower.com) using 4 HAWT located vertically in the angles of the frame, connected with the ground by the cable-tross. The disadvantage of this decision is the low efficiency of the wind power system in cross wind flow.

The technical results of our proposed unit are: efficiency coefficient increase, material-output ratio decrease, plant safety improvement, and provision of secure communication with the land.

The technical results are achieved by the fact that in an altitude wind power plant consisting of a load-carrying aerodynamic component connected with ground support by means of

cables and orthogonal well-balanced bladed rotors arranged at an obtuse angle in relation to each other along its span the aerodynamic component is performed in a form of a framework, the units of which are located at an elliptical surface, cables are in a form of sectional hoses, the sections of which are filled with helium and are connected by gates;; rotors are located between framework units with their blades equipped with jet devices of circulation control.

Furthermore, in wind power plants rotor blades are made with channels for air supply control through the holes on the blades surface into jets that control the circulation around the blades. This makes it possible to control the value and direction of the total average lifting force that is applied to rotors and plants in general.

Orthogonal rotors rotate in opposite directions, providing the balancing of torques and lateral forces.

Jet devices in rotor blades designed for local circulation, control increase in plant power generation and, if necessary, in conditions of no wind at a plant, lifting and lowering create lifting force, direction and value that can be changed allowing for control of the plant as an aircraft. Rotor axes form obtuse angles that provide for the system turning down the wind and its stable balance. In case of cable rupture or destruction of one of rotors, the plant overturns and smoothly lands on the ground maintaining automatic control by radio beacon station. The sections of the cable, performed in a form of hoses, and some elements of the frame are filled with helium under excessive pressure and create a lifting force of cable allowing optimization of wind plant position by height.

The main constructive ideas of the balanced turbines are protected by patents of Russia 1150395, 2240444 and 2327059 (Lyatkher V. M.), patents of the USA 7741729 (Lyatkher V. M.) and 5451137 (Gorlov A.M.). These windmills were discussed in p.4 of this book.

New innovative technologies and materials can improve the yield and power of wind turbines and can improve the ratio energy yield of investment costs. Currently, parallel developments are the R&D activities in the field of high altitude wind turbines. The power and maximal energy will increase for these turbines, because of the higher average wind speed at higher altitudes. This will increase the economic feasibility of wind energy. Figure 7.1 shows the distribution of streams of wind power over Moscow at different times is shown years.

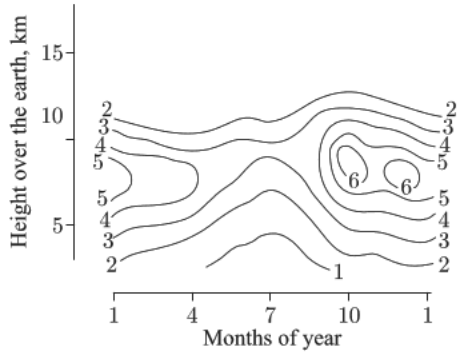

Figure 7.1 Isolines of mean annual streams of wind power (kW/sq.m) over Moscow.

In Figure 7.2 [2] distribution of height of the density of a stream of wind power over the different cities of the world is shown. In fig.3 [2] the height of zones of a maximum of a stream of energy of jet currents where it would be desirable to place high-rise wind power stations is visible.

The wind power plant operation principle is the following. Each power plant consists of three structures, connecting in one space building. Each of structures consists of three or more assemblies of orthogonal rotors united by one building unit (Figure 7.4 shows the structure model with three rotors, which is the minimal plant model), the components of which are located at an imaginary elliptical plane (Figure 7.5). The orthogonal rotors create circulation which assures the necessary lifting capacity in normal conditions.

The power extracted P(W) of a orthogonal turbine or complex turbines may be defined by the following relation

$$P = C_N \rho V^3 \Omega_b / 2, \text{ where } \Omega_b = A\sigma, \sigma = ib/D \qquad (7.1)$$

Here V (mps) = πDn/60-blades speed, Ω_b (m^2)- area of blades, A = D H– swept area,σ -solidity, i- numeral of blades, b – chord of blade, D – blade's way diameter, ρ (kg/m^3)– density of air. Power factor $C_N$is function of the turbine shape, advance speed ratio V/U, roufness of the blades surface, etc. U (m/s) – steady free-stream wind velocity.

Power factor C_N is approximated by linear function

$$C_N = B\,(U_0/V - B_0) \quad \text{if } 0 < V < U/B_0 \qquad (7.2)$$

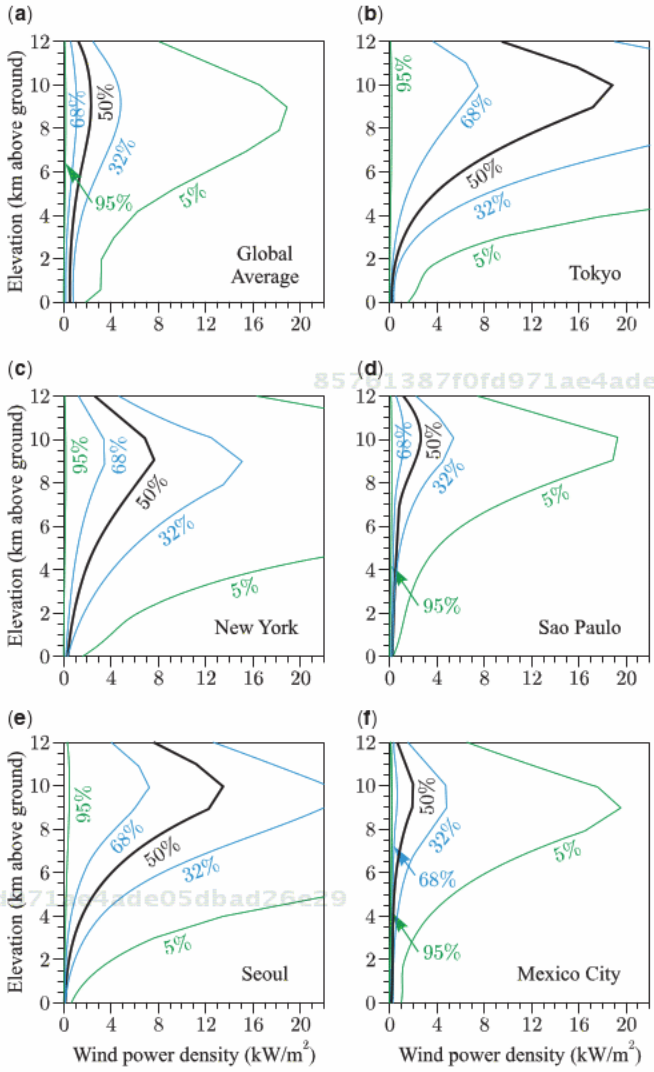

Figure 7.2 Wind power density (kW/m²) that was exceeded 5%, 32%, 50%, 68%, and 95% of the time during 1979–2006 as a function of altitude from the NCEP/DOE reanalyses by Cristina L. Archer, and Ken Caldeira. The profiles of the five largest cities in the world are shown in (b-f). The global average profile (a) is the area weighted mean of values like those represented in panels (b) through (f) at all grid points.

Parameter $1/B_0$ is the maximum of blade speed without a brake torquet moment and constant wind speed.

$$n_{max} = 60U/\pi DB_0 \,(\text{rpm}) \qquad (7.3)$$

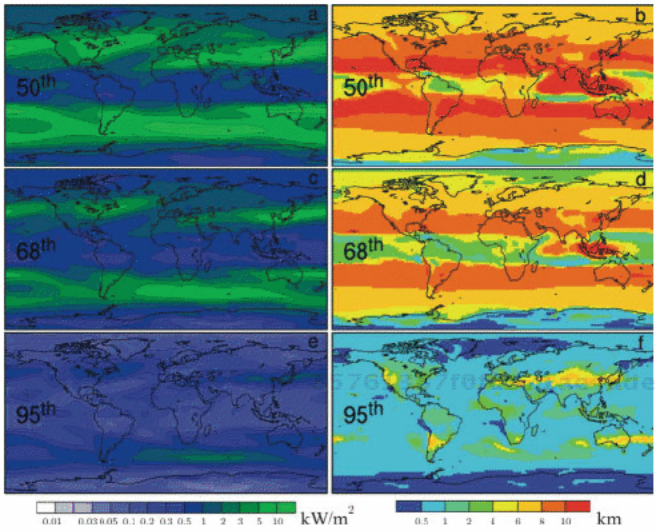

Figure 7.3 Optimal wind power density (kW/m^2, left panels) and optimal height (km, right panels) that was exceeded 50%, 68%, and 95% of the times during years in 1979–2006 from the NCEP/DOE reanalyses by Cristina L. Archer, and Ken Caldeira.

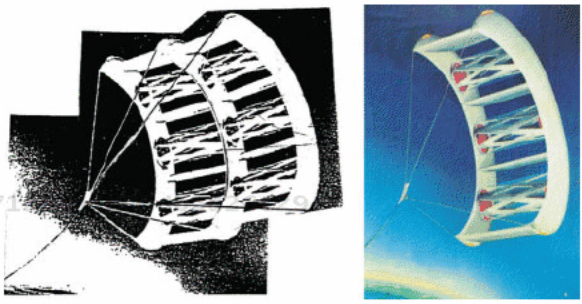

Figure 7.4 The blocks of High-Altitude Wind Power Plant.

Turbine capacity as a function of frequency of rotation and wind speed is

$$P = B\rho\pi^2 D^3 H\sigma n^2 (U_0 - B_0 \pi D n/60)/2\ 60^2 \qquad (7.4).$$

Maximum of turbine capacity P_{max} will be with frequency of rotation n_{opt}

$$n_{opt} = 2/3\ n_{max} = 40U/\pi D B_0 \qquad (7.5),$$

$$P_{max} = C_{Pmax}\ \rho\ U^3\ A/2\ , C_{Pmax} = 4B\sigma/27\ B_0^{\ 2} \qquad (7.6).$$

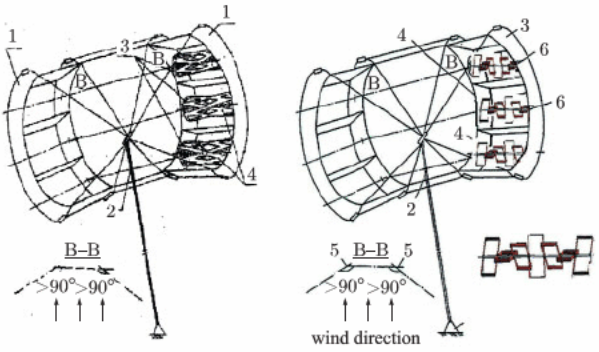

Figure 7.5 High-Altitude Wind Power Plant (HAWPP) with 3 blocks included Orthogonal Turbines for Conversion of Jet Streams in Atmosphere.(1) – Building consists of 3 (or more) rotors. (2) – The power block is tethered by a hollow divided cable filled by helium or hydrogen and transmitted power to the ground, (3) – rotor and generator, (4) – blades in variant with high solidity.

For the 3-blades turbine ($\sigma = 0.45$), optimized by prof. A.Gorlov was fined: $B_0 = 0.336$, $B = 0.60$. Turbines with 3 and 6 curved blades ($\sigma = 0.45$ and 0.90), proposed and tested by author in 1981y were shown: $B_0 = 0.28$ and 0.34, $B = 0.44$ and 0.14 for $\sigma = 0.45$ and 0.90. These results may be used to estimate the sizes of turbines, blocks and plant. Many other results are published in the book of V.M.Lyatkher "Renewable Power. Effective design" (Russia, 2011) and in p.4 this book.

If designing wind speed according to the nominal capacity 50 MW will get 35 m/s, power efficiency blades, the speed has to be about 50 m/s. The total surface of the blades must be 6,410 m^2, solidity $\sigma = 0.45$ and the sizes of the plant will be 120×120 m^2, one block – 40×120 m^2.

Besides, the rotor blades are equipped with jet local circulation control devices. These devices are to boost the energy generation by the plant, and when it is necessary (there is no wind, or the plant is being lifted or lowered), they can create the lifting capacity, the direction and value of which can be modified, which permits the plant to be guided like an aircraft. The axes of the rotors form an obtuse angle, which makes the plant turn downwind automatically and keep its stable equilibrium. In case of emergency (cable breakdown or destruction of one of the rotors) the plant turns over and goes smoothly down to the ground or to the lake. It can still be automatically controlled through radio beacons.

The operation of the circulation control system is based on the idea that letting out an air stream to the blades at the right moment can change considerably the lifting capacity of the blade in the wind flow, change its direction, and even create the lifting capacity on the rotor revolving in the still air.

Jet devices in the rotor blades designed for local circulation control, increase plant power generation and, if necessary, in conditions of no wind at plant lifting and lowering, create lifting force, direction and value that can be changed allowing plant control as an aircraft. Rotor axes form an obtuse angle that provides for turning the system turning down wind and its stable balance. In case of a cable rupture or if one of rotors is destroyed the plant overturns and smoothly lands on the ground maintaining automatic control by the radio beacon station. The sections of the cable, put together in the form of hoses, are filled with helium under excessive pressure and create the lifting force of the cable allowing optimization of wind plant position by height.

Rotor blades are equipped with jet devices of local circulation control. These devices should increase power generation and, if necessary, in conditions of no wind at plant lifting and lowering create lifting force, direction and value that can be changed allowing plant control as an aircraft. Rotor axes (in plan) form an obtuse angle that provides system automatic turning down the wind and its stable balance. In case of accident (for example, cable rupture or one of rotors destruction) the plant overturns and smoothly lands to the ground maintaining automatic control by radio beacon station.

The idea of circulation control systems on the blades consists in the fact that at the right moment of jet supply on the blade it is possible to significantly change blade lifting force in the wind stream, to change its direction and even to create lifting force at the rotor that is rotated in stationary air. In real altitude, the wind station jet control scheme should be more complicated. To the simple elements there are added elements that in case of an emergency cable rupture allow the system not only to descend smoothly, but to move in a specified direction so that the landing is completed in a specified place, for example, on the surface of the specified water body. Such a complicated movement is performed due to the use of independent circulation control systems at each rotor (Figures 7.6, 7.7). This allows the provision of the necessary lifting force vector and moment that deliver the station to a specified landing point during falling (or lifting).

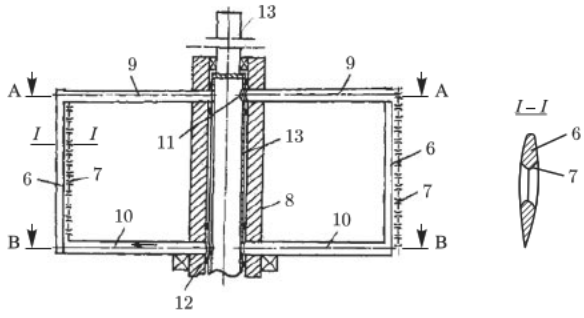

Figure 7.6 Longitudinal section of plant blades (one layer).

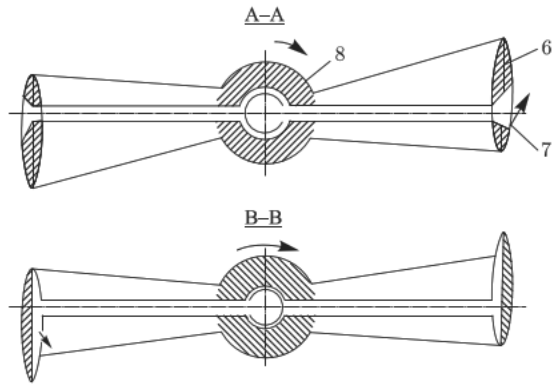

Figure 7.7 Sections of channels supplying air to blade surface for circulation control.

The altitude wind power plant consists of carrying aerodynamic element (3) connected with ground support (1) with the help of hollow cable (2) with orthogonal blade rotors (4) arranged along the element at an obtuse angle in relation to each other, carrying inductors and rotors of line (curved) electric generators. Aerodynamic element (3) is performed in a form of framework, the units (5) of which are located at the elliptical surface, the cable (2) is performed in a form of sectional hoses, the sections of which are filled with gas and connected between themselves by gates. Rotors (4) are located between framework (3) units (5), their blades (6) are equipped with jet devices (7) of circulation control. Rotor (4) blades are supported at the shaft (8) by cross bars (9), (10). Holes (11) and (12) position adjustment for controlling the maximum lifting force point is performed by the distributing shaft (13) or special system of automatically controlled valves.

The plant is operated as follows.

The original lifting force is provided by coactions of the lifting force of gas-filled hoses (2) and the lifting force created by the work of generators of the rotors (4) in engine mode at adequate action of jet devices (7) of circulation control at rotor (4) blades (6). With the help of jet devices, for example, changing the position of holes (11) and (12) of distribution shaft (13) in relation to the land, it is possible to change the "support" direction and, thus, control the position of the wind plant in relation to the ground.

Torque moment developed by rotors (4) at wind stream approach is transmitted to the generators, and from the generators the generated power is supplied to the ground through current-conducting elements located in rod (2).

The arrangement of each pair of rotors (4) axes at an obtuse angle in relation to each other, provides automatic turning of the whole system down wind and provides it stable balance. In case of an accident (cable 2 rupture) the plant turns and smoothly lands maintaining automatic control by radio beacon stations from the land. Rotor (4) rotation and the plant's smooth descent is performed due to power batteries arranged at the plant and the generators operation in engine mode.

Each blade (1) has two separate volumes, connected with the shaft of the turbine (2) by traverses (3) and (4). The tube located in the traverse (3) is connected with the outside volume of the blades. The tube in the traverse (4) is connected with the inside volume of the blades. The distribution shaft (8) gets inside the shaft of turbine (2). The distribution shaft has two opposite holes (6) and (7). The distribution shaft is connected with a high pressure volume or pump by line (5). When the high pressure air is going through the hole (6) at the right traverse (3) and through hole (7) at the left traverse (4) the lift force acts at the right. In the opposite situation the lift force will act at the left. Figure 7.8 shows the lift coefficient as a function of the impulse of the control jet going through the holes in the blade. Similar results have been obtained while testing the blades on a circular track. The schemes demonstrate that the lift coefficient C_L at the zero attack angle reaches $C_L = (C_L)_{max} = 1.2$, which is close to the practically attainable maximum for the ordinary aircraft profile. As is known for the wing with flaps deviated on 8–10 degrees coefficient $(C_L)_{max}$ reaches 2.4 and more. The control jet operation is in general, similar to the ordinary high-lift device operation (Figure 7.8).

Jet management of circulation on the blades of the orthogonal turbine is an essential element of the offered project of the highly

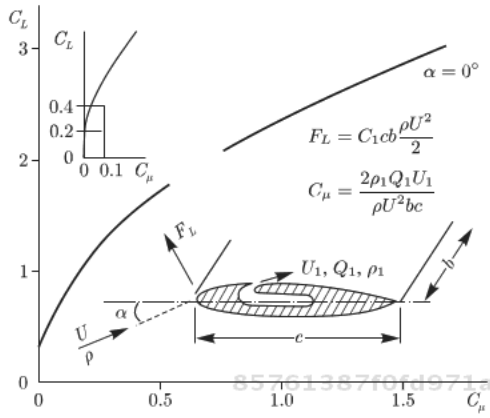

Figure 7.8 Coefficient of lifting force as an impulse of a jet control.

effective wind power station transforming energy of high-rise jet currents. In this project, management of circulation on the blades is used for formation of the carrying power providing maneuvering (lifting, lowering) the block of the power plant, irrespective of a mode of the wind. Stationary modes of a flow of profiles with jet control circulation are studied quite in detail [3].

The influence of jet management in non-stationary conditions, characteristic for modes of a flow of blades in orthogonal turbines, was studied on the instructions of the author on an oscillatory installation in a flat hydrodynamic pipe at the Institute of Mechanics of the Moscow State University of Lomonosov in 1989–1991 [5]. Tests are carried out in the conditions of a flat task with a considerable excessive of water pressure (2.5 bar), excluding aeration and cavitation on the blade, with the careful accounting of possible mistakes. Non-stationary and stationary characteristics were received for the NACA-0010, 0015, 0017.5, 0020 profiles with a chord of b=0.2m at a stream speed to m U=10.2 m/s. Change of an angle of attack was carried out or with sign preservation – under the law

$$\alpha = 15°\text{Sin}\,(2\pi ft) + 15° \qquad (7.7),$$

or according to the scheme closer to the real operating conditions of turbines, – with sign change:

$$\alpha = 14°\text{Sin}\,(2\pi ft) - 1° \qquad (7.8).$$

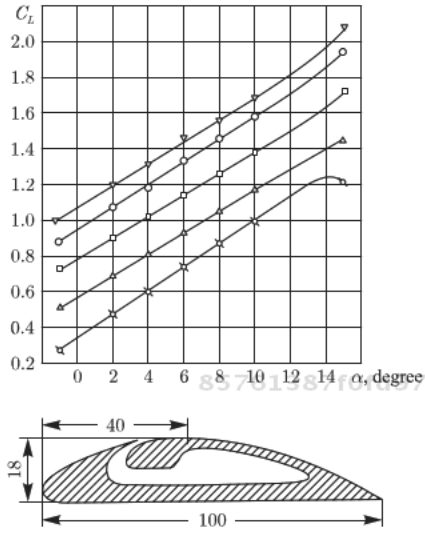

Figure 7.9 Coefficient of a lifting force of a wing on tests in water as an angle of attack at impulses of a jet 0, 0.05, 0.10, 0.15 and 0.20 [4].

Nonstationarity is characterized by a number of Strukhal

$$Sh = bf/U \tag{7.9}$$

In the same hydrodynamic pipe with considerable excessive water pressure (2.5 bar), on the same oscillatory system on which were tested a profile without jet emission, characteristics of two options of blades of the NACA 0021 profile with a chord of b=200 mm with release of a flat jet by thickness of a=0.83mm in tail part of a profile (at distance 0.65b from a profile sock) – option 1 in Figure 7.10 and in head part of a profile at distance 0.30b from a profile sock – option 2 were studied. The influence of a jet is characterized by the relative size of an impulse

$$C_s = (U_1/U)^2 (a/b), \tag{7.10}$$

U_1 – expiration speed of the jet, U –speed of a running stream.

Change of the angle of attack was set by a blade turn concerning an axis located in the middle of the blade (0.50b from a sock):

$$\alpha = 14.5^\circ \mathrm{Sin}\,(2\pi ft) \tag{7.11}$$

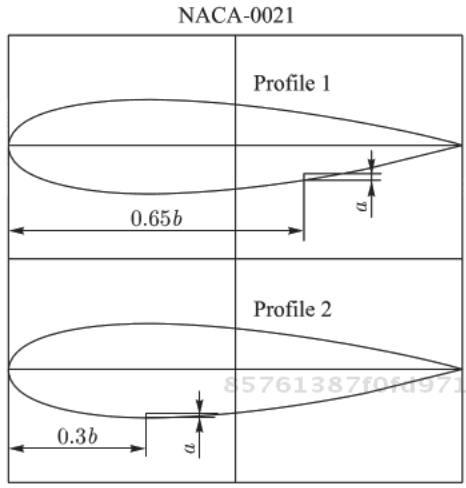

Figure 7.10 Options of an arrangement of a crack for giving of a jet, b = 200 mm, a = 0.83 mm.

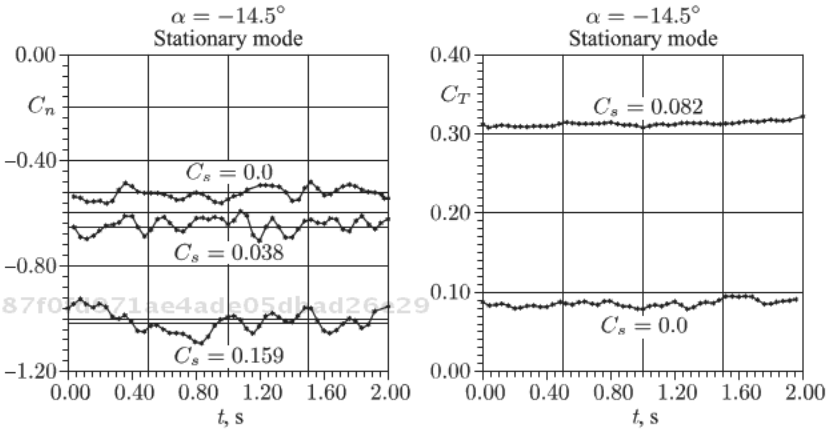

Figure 7.11 Option 1. Jet on shady side at the end of a wing.

The general conclusion of the completed tests is that, at both options of jet arrangement, its action on a shady side very effectively increases the lifting and pulling forces in stationary and in non-stationary modes (Figures 7.11 – 7.15).

In the studied range of change of number Strukhal 0<Sh<0.113 and a relative impulse of a jet

$0<C_s<0.155$ influence of a jet is considerably shown only when it is on shady side of a profile. In this case in both constructive options

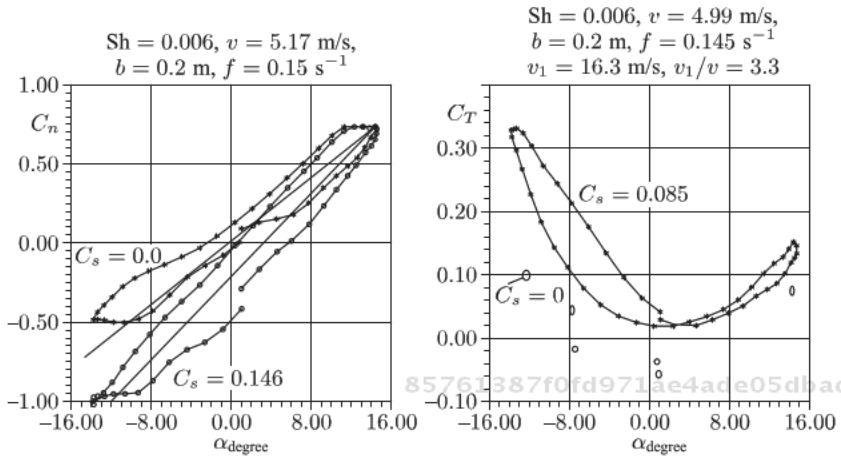

Figure 7.12 At negative corners a jet on the shaded party. Jet influence at small numbers Strukhal.

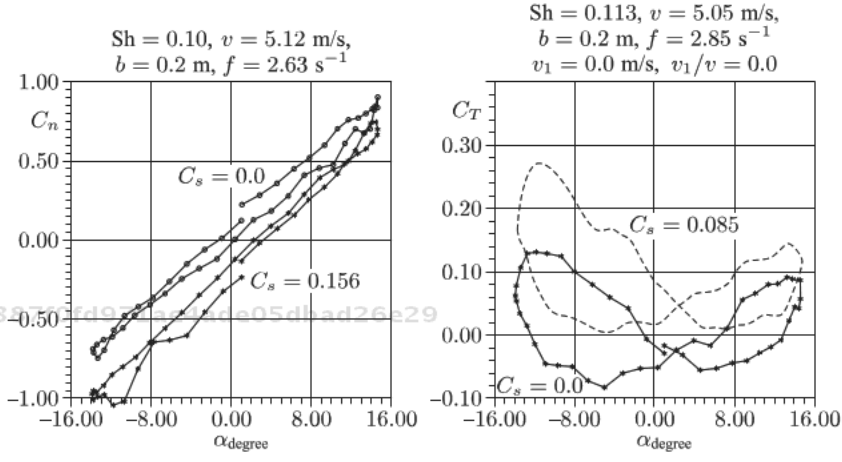

Figure 7.13 Jet influence at large numbers Strukhal.

– at a stream arrangement at the beginning or at the end of a profile giving of a stream increases the lifting and pulling forces of a profile, especially on big (subcritical) angles of attack in direct ratio to a jet impulse. At the maximum tested angle of attack 14.5° at a relative impulse of a jet 0.085–0.088 increase in carrying power made 60%, and increase in the pulling force – about 200% from the values of these sizes without the jet. The criterion influence Strukhal on this result was insignificant. Thus, for the cost of a jet, the capacity

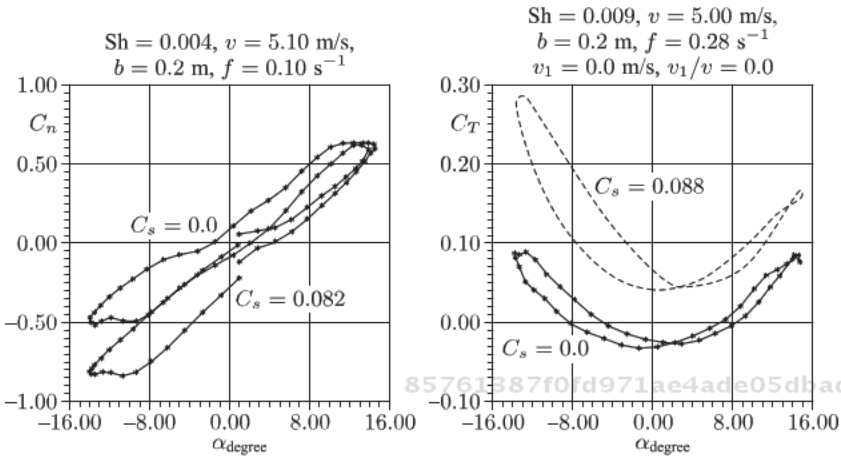

Figure 7.14 Option 2 – a jet at the beginning of a wing. Small numbers Strukhalya. At a stationary mode and an angle of attack -14.5° the coefficient of normal pressure is equal -0.5,-0.86 and -1.08 at an impulse 0, 0.082 and 0.15, the coefficient of pulling force is equal 0.09 and 0.29 at an impulse 0 and 0.086 respectively.

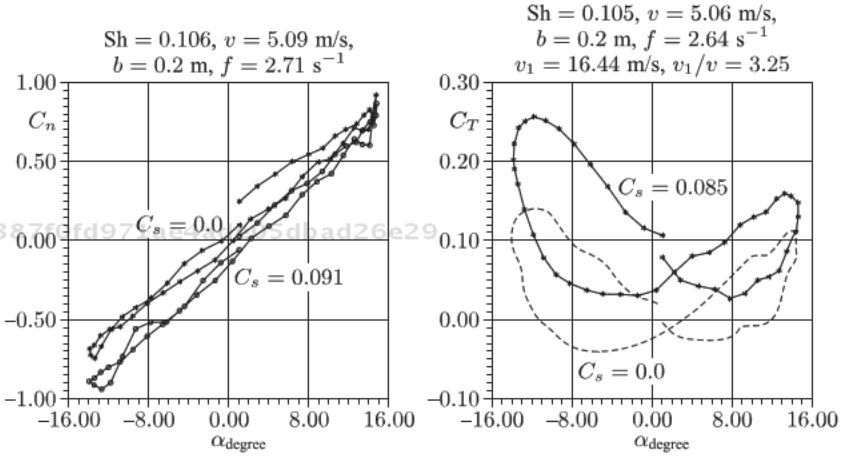

Figure 7.15 Option 2. Large numbers Strukhal. The jet on shady side of a profile considerably increases the lifting and pulling force of a wing.

of the turbine can be increased by almost 3 times, and the carrying power of the blade by more than 1.5 times.

There are published works stating that jet control of circulation on the blades of a model orthogonal windmill with a solidity ib/D= 0.1 can increase maximum efficiency of the C_p unit from 0.32 to

0.42 with reduction of optimum speed of rotation of a rotor from V/U = 5 to 4 [6].

The main ideas behind the turbine with operated circulation on the blades, providing any choice of the direction of the resultant force operating on the turbine as a whole, were checked on a large model of a fragment of the two-bladed unit (Figure 7.16, 7.17).

The turbine model has the hollow blades. The air through the distributive shaft is going to the blades. The shaft of the turbine was made in the dimensions shown in Figure 7.18.

The system of a suspension bracket of a model was made with two options – with the external electric drive in the form of a high-speed electric motor (Figure 7.19), and without it.

In the latter case, dispersal of the turbine is carried out at the expense of the reaction of the operating stream, which is let out on the external or internal parts of blades through cracks about 1 mm high(Figure 7.20).

In any option, the model was carefully balanced and hung out on electronic and mechanical scales (Figure 7.21).

Let's consider results of the experiments made without the external electric drive – the rotor rotated under the influence of the

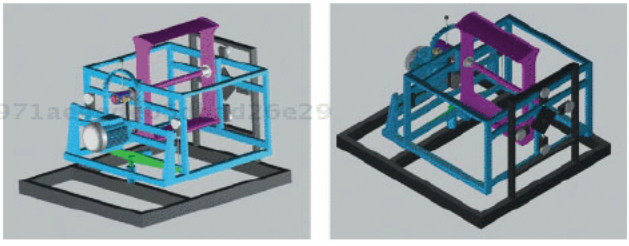

Figure 7.16 The model of a fragment of the two-bladed unit.

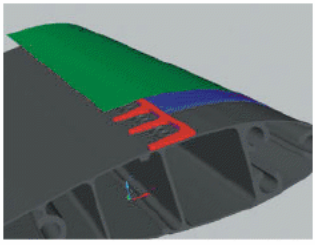

Figure 7.17 Scheme of giving of a stream. On the opposite side of the blade, the stream moves from the other channel in the blade.

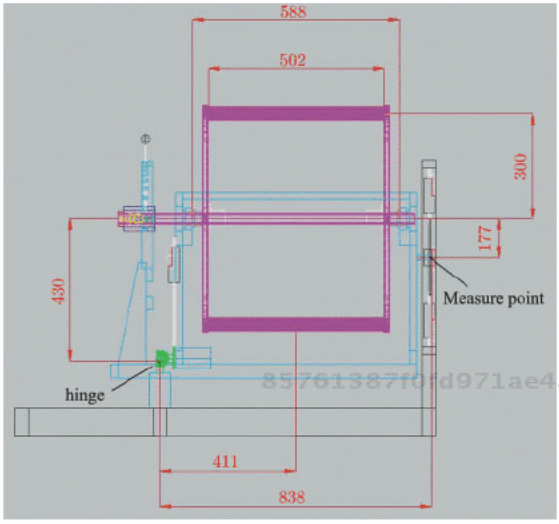

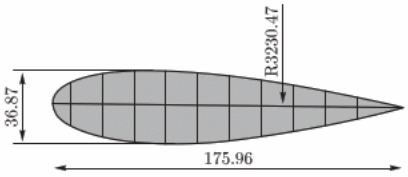

Figure 7.18 The turbine model with hollow blades and shaft.

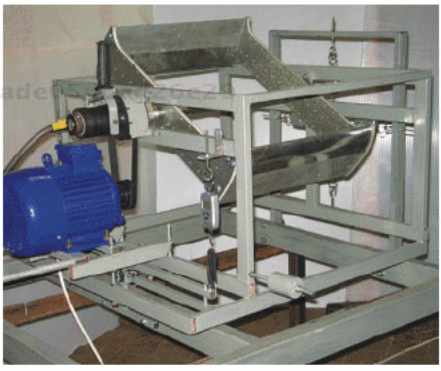

Figure 7.19 The model with electric motor to rotate the blades. In general test the motor did not use. The blades moved by impulse of jets.

reaction of the currents of air coming to the surfaces of blades during the periods when openings in the walls of an air-bringing pipe in the axis of a rotor coincided with entrance openings in channels inside a traverse, sending air into the internal cavities of the blades.

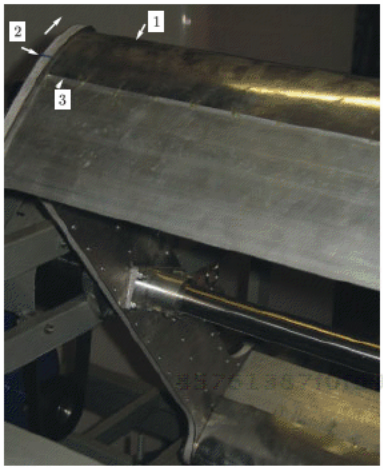

Figure 7.20 1 sock of the blade, 2 – an alignment of the greatest thickness of the blade, 3 – cracks for release of an operating current of air.

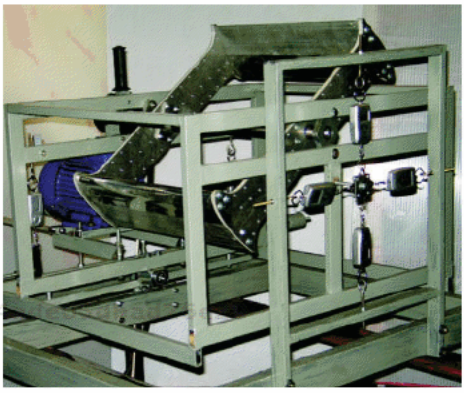

Figure 7.21 System for measuring forces.

The compressed air moved from a high-capacity receiver through a system of air ducts. The moment (phase) of the air supply in a cavity of blades and further – in a stream of management –was established by means of the rotary lever (a black core in Figure 7.21), rigidly connected with the hollow managing director of a shaft (air-giving pipe) in a turbine axis.

For high-rise power, plant the of particular interest is represented by these tests without the external electric drive, with the promotion of turbines under the influence of the reaction to a stream only. The primary results of these tests are presented in Figure 7.22 where the actually measured values, a component of the total force,

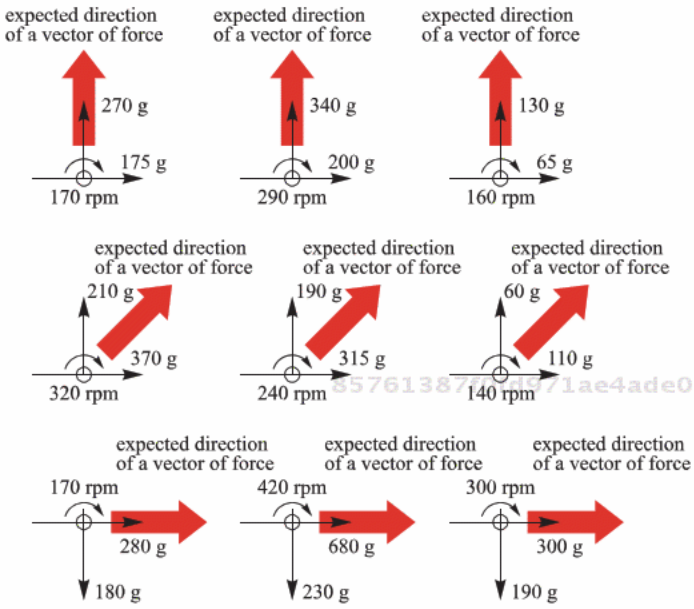

Figure 7.22 General results.

operating the turbine as a whole, are compared with the "theoretical" (expected) direction set by the position of the managing director of the channel in an axis of the turbine.

In Table 7.1 and in Figure 7.23 the module of force operating on the turbine (Newtons), carried to a square of frequency of rotation of the turbine n (rpm), is shown as the frequency of rotation of the

Table 7.1 The module of force operating on the turbine (Newtons), carried to a square of frequency of rotation of the turbine n (rpm).

170	1.1135
160	0.568
290	0.469
320	0.415
140	0.639
240	0.638
170	1.152
300	0.394
420	0.407

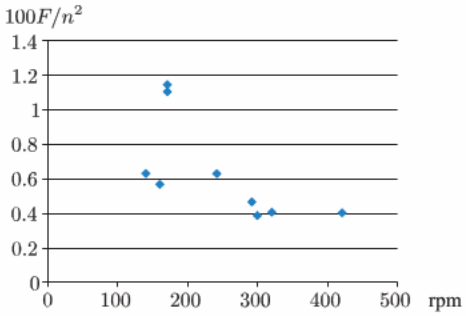

Figure 7.23 The module of force operating on the turbine (Newtons), carried to a square of frequency of rotation of the turbine n (rpm) the function of frequency of rotation of the turbine.

turbine. This parameter (frequency of rotation of the turbine) in the made experiments was the only characteristic of "entrance conditions" in the experiment which changed from experience to experience owing to a change of pressure in the air receiver feeding system.

According to the Table and Figure 7.23 the average values of the coefficient of the lifting force operating on the blade of the turbine, on the average for a turn of the turbine (Figure 7.24) are calculated:

$<C_L> = F/F_0$

$F_0 = \rho V^2 2bL/2 = 1.25\ (0.0314)^2\ 0.176\ 0.502\ n^2/2 = 6.16 \times 10^{-4}\ n^2$, N – the total force of the aero-speed pressure operating on two blades (R=0.3m, b=0.18m, L=0.45m)

$V = 0.30 \times 2\pi x n/60 = 0.0314$ n- module of speed of blades, m/s

The coefficient of the lifting force appeared within 0.08–0.18. Such a rather low value is explained by the fact that the operating force is averaged on the full period of rotation of the turbine, and actually the stream and carrying power on the blade is realized on a small site of the route when operating air gets on the blade.

Comparison of the expected and actual direction of the force (Figure 7.25 right) is very important.

It appears that the actual direction of force advances on the "expected" by 15–30 degrees. The dispersion is great at small speeds of rotation (small impulses of a stream). With a frequency of rotation, bigger than 300 rpm, the advancing corner doesn't exceed 18 degrees.

A scheme of this type – with a turning wing and a flap controlled by the traction from the center offset from the rotor axis – has been successfully applied in practice. The jet control system of the

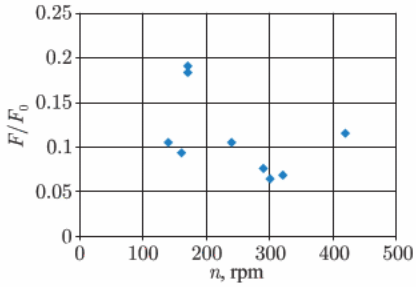

Figure 7.24 Average coefficient of lifting force of $<C_L>$, operating on the blade.

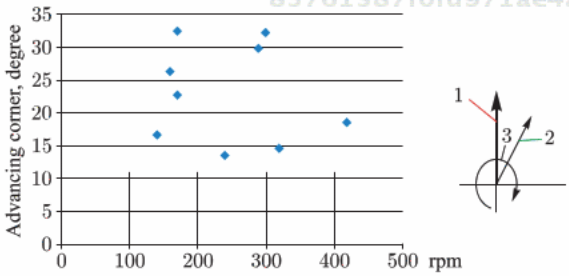

Figure 7.25 1-Theoretical (expected) direction of a vector of draft, 2- The measured direction of a vector of draft, 3- Advancing corner, degrees.

circulation on the wing in this case may be easier and more long-lived than the ordinary high-lift device system. The averaged value of the lifting force F acting upon the rotor per one revolution is a little greater

$$F = 1/6\, C_{Lmax} \rho \{(V + U)^2 + (V - U)^2\} \Omega_b \qquad (7.11)$$

in which V is the blade speed, U is the wind speed inside the rotor and Ω_b is the total surface of the rotor blades. For the designed wind speed U_0 =35 m/s, the wind speed inside the rotor will be

$$U = 0.8U_0 = 28 \text{ m/s} \qquad (7.12)$$

And averaged lifting force may be

$$F = 1/6\, C_{Lmax} 0.75\, \{(50+28)^2 + (50-28)^2\} 6{,}410 \text{ N}$$
$$= 5{,}262{,}610 C_{Lmax} = C_{Lmax} 526 \text{ (ton)} \qquad (7.13)$$

At the ground when a wind is absent, the averaged lifting force may be

$$F_0 = 1/6\, C_{Lmax} 1.23\, \{50^2 + 50^2\} 6{,}410\ N = C_{Lmax} 657(ton) \quad (7.14)$$

The orthogonal turbine is connected with the induction generator. It may be two variants – 3 or 6 turbines in the block (9 or 18 units in the plant).In variant 1 (3 turbines in block – Figure 7.4) the turbine diameter will be D= 40 m, and the frequency of rotation, n = 23.9 rpm. The weight of the generators with such a slow rotation will be too much. In the second variant (6 turbines in the block) the frequency of rotation will be 47.8 rpm, and the weight of the generators will be about 18 kg/KW. The total weight is 900 tons.

A contrrotor design may be used to decrease the weight of the generator when the rotor and "stator" of the generator are moving in opposite derivation (Figure 7.5). In this case, the total weight of the generators

with 3 couple turbines in the block will be the same – 900 tons. Using 6 couple turbines in the block,

the total weight of contrrotor generators decreases to 600 tons.

To choose the kind and number of rotors and generators we will compare the efficiency each variant.

In the first variant with 3 turbines in block, the overload on the blades by the inertial force ($2V^2/gD$) reaches 12.75; in the other variant (6 turbines) it may be twice as much –25.5.

In modern sea fighters (such as Sea Hawk or Sea Fury) the real overload reached 10.3 and more. For all aircrafts, the safety factor has to be 2 or more. This means that in turbine blade construction the overload, even 25.5, may be accepted.

In modern, large aircrafts with cantilever wing lengths up to 24 m, the mass of the wing reaches 29 to 35 kg per sq.m of the wing surface. The design load on the wing is 350 to 580 kg per sq.m. The real experience of constructing and testing the plastic blades for the orthogonal turbines with cantilever blade length 2.3 m has shown that the mass of the blades may be up to 12 kg per sq.m of blade with an overload of 26.5 and static loads up to 656 kg per sq.m.

In the proposed system, the blades surface is 6410 sq.m in total. The mass of the blades will be less than 225 metric tons, but really up to 77 tons. In variant with contrrotor generators, the total length of traverses will be 2160 m., its area – 4160 sq.m, and mass – 125 or 52 tons (more really). If the mass of the connected elements will

be 20% of the rotor mass the total mass of the flying power system will be

1020(755), t

Using plastic in the power construction we will be able to decrease the mass to 155+900=1055τ.

In variant with smaller turbines and contrrotor generators, the total mass will decrease at least on 300t reaches to 1020 (755)τ.

To lift the system from the ground in accordance with (14) needs

$$C_{Lmax} = 1.6 \div 2.0 \tag{7.15}$$

With control of the blade circulation that provides $C_{Lmax} = 2.4$ and more.

In the nominal operating position, the average lift force will be 1262t. This is more than the weight of system made by high strength plastic on the surplus vertical force

$$F_v = (207 \div 507), \text{ t} \tag{7.16}$$

The longitudinal force acted on the system in the nominal position is

$$F_x = C_x \rho U_0^2 A/2 \tag{7.17}$$

Here:A- swept area of the system, blowing by wind, C_x – drag factor of the system. For the design wind velocity $U_0 = 35$ m/s, blades speed $V = 50$ m/s and solidity$\sigma = 0.45$:

$$C_x < 0.5 \text{ and} F_x = 331\text{t}. \tag{7.18}$$

The power blocks are tethered by a hollow divided cable filled with hydrogen (or helium). This cable is made with kevlar. Kevlar is an Aramid fiber produced by the E.l. Dupont Company to offer a light-weight replacement for steel wire in products such as tires, conveyor belts and cables. KEVLAR's high strength and modulus, combined with ease of manufacturing, results in high efficiency at competitive costs. Ropes and cables using KEVLAR have excellent fatigue resistance and are non-corrosive, non-magnetic, and non-conductive, with low elongation, and have the highest combined specific strength and modulus. Specifically, KEVLAR cables are: stronger than steel (3X stronger than Nylon and Polyester),

Chart 2

Surplus lift force F_v, t	200	300	400	500
Total force acted on cable, t	387	447	519	600
Square section of Kevlar, sm^2	74	85	99	114
Mass of Kevlar per 1 m. of cable, kg	11.8	13.6	15.8	18.2
Cable length, km	11.6	8.94	7.79	7.2

withallowable cyclic stress of 5250 kg/sm^2 at least, at 1/5th the weight (density 1.6 g/ sm^3).

The cable consists of connected separate parts filled by hydrogen with a small surplus pressure. The cables' diameteris 6 m or more. The lift force acted on one meter of the length of the filled cable is 18.7 kg at the elevation of 6 km,andmuch more near the ground. Chart 7.2 shows the total force acted on the cable from the power unitswith different surplus vertical forces. In accordance with this total force we calculated the cross section of the kevlar cable, the mass of cable per one meter of length, and the total length of cable. The power blocks are located at6 km elevation in all variants.

The aluminium wires will be fixed on the surface of the cable to transmit power from the generators with the generator's voltage of 10 kV. If the density of current will be 4A/mm^2, the weight of these wires has to be 3.4 kg per one meter of the cable length.

Thus, if the cable diameter is 6 m, the surplus lift force cannot be more than 300 t, and the cable length has to be 8940 m. or more.

When the wind speed increases (more than 35 mps) the power system is designed to go down to the area with slower winds automatically. Conversely, when the wind speed decreases the power system will go up itself. Additional control would be achieved by changing the lift force acting on the power system. The needed length of the cable may be decreased by the choosing the fixed point on a high ground elevation (in the mountain area of California).

The surplus pressure of hydrogen in parts of the cable makes it to these parts by pumping through the individual pipes. If the losses of hydrogen will be about 0.8% per day, to keep the normal pressure, it will be necessary to use one unit of IMET-30 discharged 30 cub.m. of hydrogen per hour with the installed capacity of 200 kW.

The cabins may be moved to the outside of the cable surface to serve the power units and to go up to the tourist groups.

The lifting capacity would be sufficient to operate the plant in emergency situations and while lifting it from the ground. In

practice, circulation control is to be fulfilled automatically with the plant oriented by land-based radio beacons and the HAWPP gyroscope systems. In case of a cable breakdown, the revolution of the rotors and the smooth lowering of the plant to an assigned area would be fulfilled with the aid of the HAWPP electric accumulators and the operation of the HAWPP generators as engines. A similar routine is used while lifting the plant; the difference is that in this case, the supply line is employed.

The plant component being discussed is quite a complex structure and is the least developed one. Although its elaboration presents many difficulties, there is a practical solution of the problem. The comparison of a possible mass of the HAWPP and that of the cable shows that the HAWPP optimal unit power is about 70–100 or more MW, as the increase in the power plant capacity does not exert any significant influence on the cable mass, which makes the cost per unit of capacity drop. Preliminary calculations have shown that being production-run, the plants of the given capacity would require a specific capital investment of not more than 600 US dollars/kW.

It is advisable to accept an initial experimental plant capacity of not less than 50 MW, as a considerable share of the plant development and manufacture self-cost would fall on the gas-filled cable. Further on, as the plant capacity doubles, the cable self-cost will increase by not more than 20–30%, as most of the cable operation systems do not depend on the plant capacity. The first experimental model, with a 50 MW capacity, would cost approximately 1.2 thousand US dollars/kW, including all the design and research expenses and costs of the equipment manufacture and plant construction, installation, and commissioning. Taking into account the economic and ecological prospects of the proposed energy source, the above-stated cost of the first model should not be considered excessive.

The whole complex of work including the plant turnkey and simultaneous preparation of further line production of the plant can be completed within 2.5 years. The first step, including the check all ideas and numerals, in accordance with this applicant can be fulfilled within one year.

Further on, high-altitude wind power plants can be developed, which would have the capacity of 100-500 MW and annual production of 700–3,500 GW-hr, and cost 60–250 mln. dollars or less.

The combination of lower investment costs and extra yield bring the payback time back by a factor of 4, compared to traditional wind technologies. Due to this positive influence on investment costs, offshore wind energy can compete with traditional energy

production, such as a gas or coal fired power plant. Therefore, wind can play an important role in the renewable energy mix. It can even provide a solution for substitution of more conventional power plants.

The created demonstration windmill (model) has the same external form, as well as the future of a skilled electric power plant (Figure 7.4 right).

We accept following preliminary parameters of the model:

Chord-0.160 m

Diameter of a line of blades – 1.2 m

Number of blades in one circle – 2

Number of circles – 7

Length of the blade-0.6 m

Length of the turbine-4.2 m

Weight of the complete set of blades of one turbine-14 kg

Nominal frequency of rotation – 750 rpm

Settlement speed of blades (sliding 1.08) 50 m/s

The speed of a wind answering to the maximum capacity of 40 m/s

The speed of a wind answering to the beginning of delivery of capacity of 10 m/s

Power factor C_N=0.25

Efficiency of the turbine at an optimum mode (a wind of 23 m/s) $C_p = 0.43$ (see p.4).

Forces, the moments, the capacity, turbines operating on one store by calculation (length 0.6 m) are shown in Chart 3.

Chart 3

	Moment	Power	Forces, along, across on the blade		Radial	Tang
	Nm	kW	N		N	
Averaged	4.8	0.4	142	–45	–1.6	2.4
Max.	28.5	2.4	558	187	188	28.2
Minimum	–9	–0.8	–91	–276	–339	–6

The force of inertia operating on one blade of 375 kg

production, such as a gas or coal fired power plant. Therefore, wind can play an important role in the renewable energy mix. It can even provide a solution for substitution of more conventional power plants.

The created demonstration windmill (model) has the same external form, as well as the future of a skilled electric power plant (Figure 7.4 right).

We accept following preliminary parameters of the model:

Chord-0.160 m

Diameter of a line of blades – 1.2 m

Number of blades in one circle – 2

Number of circles – 7

Length of the blade-0.6 m

Length of the turbine-4.2 m

Weight of the complete set of blades of one turbine-14 kg

Nominal frequency of rotation – 750 rpm

Settlement speed of blades (sliding 1.08) 50 m/s

The speed of a wind answering to the maximum capacity of 40 m/s

The speed of a wind answering to the beginning of delivery of capacity of 10 m/s

Power factor C_N=0.25

Efficiency of the turbine at an optimum mode (a wind of 23 m/s) $C_p = 0.43$ (see p.4).

Forces, the moments, the capacity, turbines operating on one store by calculation (length 0.6 m) are shown in Chart 3.

Chart 3

	Moment	Power	Forces, along, across on the blade		Radial	Tang
	Nm	kW	N		N	
Averaged	4.8	0.4	142	–45	–1.6	2.4
Max.	28.5	2.4	558	187	188	28.2
Minimum	–9	–0.8	–91	–276	–339	–6

The force of inertia operating on one blade of 375 kg

The maximum averaged capacity of the turbine according to experiments:

$$7 \times 0.67 \times 0.25 \times 503 \times 2 \times 0.16 \times 0.6/2 = 14\text{kW}$$

Height over the earth, km	Parameters of a wind [7]			
	Season of year			
	Winter	Spring	Summer	Autumn
6 Average speeds of a wind, m/s	19.4	17.9	11.3	20.3
Energy stream, kW/m^2	3.8	2.7	1.8	4.3

Average temperature of air at minus 24°C, average density of air of 0.67 kg/

Capacity of power station (maximum) 126 kW

Capacity at an optimum mode (a wind of 23 m/s) 79 kW

Considering the high reloading ability of asynchronous generators, we accept for the model the engine-generator the AIR 132M2 with a weight of 54 kg, and an admissible overload of 3.5.

Management control jet.

Thickness of a jet, 2mm

Air density in jet, 1.25 kg/m^3

Speed of air in jet, 200 m/s

Relative impulse of a stream / forces $C_{L:}$

At 6 km, 0.75/2.0

At the earth, 0.40/1.6

Average carrying power on one turbine at the earth, at a stream speed of 200 m/s of 84 kg the expense of air is 16.8 litre/secAt the stream speed of about 120 kg the expense of air is 25 litre/sec

The capacity necessary for braking the station at the earth during 20 min. is 2–3 m^3 with air pressure of 10 bar. Such capacity is determined by dividing the constructive elements in width (3m) and height (0.15–0.25m)

The wind station is fixed on the earth through the hollow cable filled with helium. At a superfluous pressure of helium 0.5 bar superfluous carrying power makes 1 kg/m^3 at the earth and 0.4 kg/m^3 at height of 6 km.

The current strength from generators at voltage 660 v is 114 A.The section of copper wires nearby is 28 mm^2 with a weight of

249 g/ m of length. For maintenance of deduction of such weight it is necessary to increase the diameter of a cable with helium to 0.57 m at the earth, and to 1m at the height of 6 km.

The length of the cable will be defined by the superfluous carrying power which is formed both at the expense of the turbines and at the expense of the gliders between turbines. The minimum length of a cable is 6.5–7 km. The superfluous "buoyancy" of station is reached at the expense of an aerodynamic flow of turbines and dividing profiles, and also (if necessary) at the expense of filling vertical elements of a design with helium.

Each turbine has the open one-stage animator with transfer number 4 and the individual asynchronous generator with a shortly closed rotor and the nominal frequency of rotation of 3000 rpm. All the generators are also united by a uniform cable connected to a powerful electric network on the earth. In case of the breakage of a cable, generators are instantly switched to the battery of condensers through which the power supply of elements of the management located directly on the wind power model proceeds, and opening of valves for giving of operating streams, electric deduction of turbines from excessive dispersal, orientation of the model in space and its direction on an airfield is carried out.

Optimization of the design of the orthogonal unit is reached in a series of experiments with the orthogonal units having the form of a framework (p.4).

The turbine with operated jet circulation is as a project basis of "the flying car"[8].

All calculations and designs should be verified with the unsteady effects of the control of the jet. The experimental data on this subject the author is unknown.

References

1. V. M. Lyatkher., HIGH-RISE WIND POWER INSTALLATION, News of the Russian Academy of Sciences. Power, 2006, No. 4,p.47–57., V.M.Lyatkher, High-rise wind power installation, Patent RF 2240444, May05.2003. V.M.Lyatkher and V.L.Smirnov, High-rise wind power station, C.C. USSR 1765495, October 03. 1989.
2. Cristina L. Archer, and K. Caldeira, Global Assessment of High-Altitude Wind Power, *Energies* 2009, *2*, 307–319.

3. V.B Amfilokhiyev. hp Artyushkov, B.A.Barbanel, A.I.Korotkin. K.M.Mazayev. L.I.Maltsev, B. N. Semenov Current state of the theory of management of an interface. – St. Petersburg: Prod. SPMBM "Malachite", 2000. –415 pages 5. P.A.Bogdanov, P.G.Kozhukharov, L.I.Maltsev, V.I.Mikuta, V.Kh.Khadzhimikhalev, Underwater wing with jet management of its hydrodynamic characteristics, Sb. Liquid currents with free surfaces and polymeric additives, Novosibirsk, 1986, page 36–73.
4. V.B Amfilokhiyev. hp Artyushkov, B.A.Barbanel, A.I.Korotkin. K.M.Mazayev. L.I.Maltsev, B. N. Semenov Current state of the theory of management of an interface. – St. Petersburg: Prod. SPMBM "Malachite", 2000. –415 pages 5. P.A.Bogdanov, P.G.Kozhukharov, L.I.Maltsev, V.I.Mikuta, V.Kh.Khadzhimikhalev, Underwater wing with jet management of its hydrodynamic characteristics, Sb. Liquid currents with free surfaces and polymeric additives, Novosibirsk, 1986, page 36–73.
5. Research supervisors – V.P.Karlikov, A.N.Khomyakov, G.I.Sholomovich.
6. G.M.Angle II, F.A.Pertl, Mary Ann Clarke, J.E.Smith, Lift Augmentation for Vertical Axis Wind Turbines, International Journal of Engineering, vol.4, Issue5, pp.430–442, D.McGrain, G.M.Angle II ,J.P.Wilhelm, Circulation Control Applied to Wind Turbines, ASME 2009 3rd International Conference on Energy Sustainability, Volume 2, Paper no. ES2009–90076 pp. 905–910.
7. These numerals for Moscow region. The datum for different regions are in Cristina K.Archer and other articles (Energies, 2009, 2, pp. 307–319).
8. V.M.Lyatkher Power installation for the vehicle drive, Patent RF2327059, the Priority Dec. 14.2006.

Conclusion

Wind turbines in traditional execution, both collinear and orthogonal, can have the optimum capacity measured at best by tens, hundreds or the first thousand kilowatts.

The essential increase in single power wind turbines, improvement of the quality of developed energy and decrease in its cost is possible during the use of proposed new technical solutions, association in systems of the wind power plants located at distances, exceeding the radius of the correlation of streams of wind power, inclusion of wind power stations in complexes with hydro power plants or productions, and hydrogen storages.

In ground or water surface layers of the atmosphere, the wind units using the effects of turbulent vertical transfer (multi-blade power units of big diameter on electromagnetic subweight), and also power plants without external moving elements (Tormod system) can be especially effective.

The "soaring" power plants of new types transforming the energy of high-rise jet currents can make the greatest contribution to the balance of power supply systems of the developed countries of the world.

Author Index

Subject Index

Also of Interest

Check out these other related titles from Scrivener Publishing

Time to Shine: Applications of Solar Energy Technology, by Michael Grupp, ISBN 9781118016213. The perfect primer for the engineer, scientist, and layperson alike, for learning about the practical applications of solar energy technology and how it is being used today to heat homes, light city streets, and provide power worldwide. As solar energy becomes increasingly more important in all of our lives, it is more important to learn how it works and how it can be implemented. *NOW AVAILABLE!*

Biogas Production, Edited by Ackmez Mudhoo, ISBN 9781118062852. This volume covers the most cutting-edge pretreatment processes being used and studied today for the production of biogas during anaerobic digestion processes using different feedstocks, in the most efficient and economical methods possible. *NOW AVAILABLE!*

Bioremediation and Sustainability: Research and Applications, Edited by Romeela Mohee and Ackmez Mudhoo, ISBN 9781118062845. Bioremediation and Sustainability is an up-to-date and comprehensive treatment of research and applications for some of the most important low-cost, "green," emerging technologies in chemical and environmental engineering. *NOW AVAILABLE!*

Sustainable Energy Pricing, by Gary Zatzman, ISBN 9780470901632. In this controversial new volume, the author explores a new science of energy pricing and how it can be done in a way that is sustainable for the world's economy and environment. *NOW AVAILABLE!*

Green Chemistry and Environmental Remediation, Edited by Rashmi Sanghi and Vandana Singh, ISBN 9780470943083. Presents high quality research papers as well as in depth review articles on the